FOR INFORMATION

Doc. 19131/F-2.7.13

OT REPORT 76-97

SPECTRUM RESOURCE ASSESSMENT IN THE 2.7 TO 2.9 GHz BAND PHASE II: MEASUREMENTS AND MODEL VALIDATION (Report No. 1)

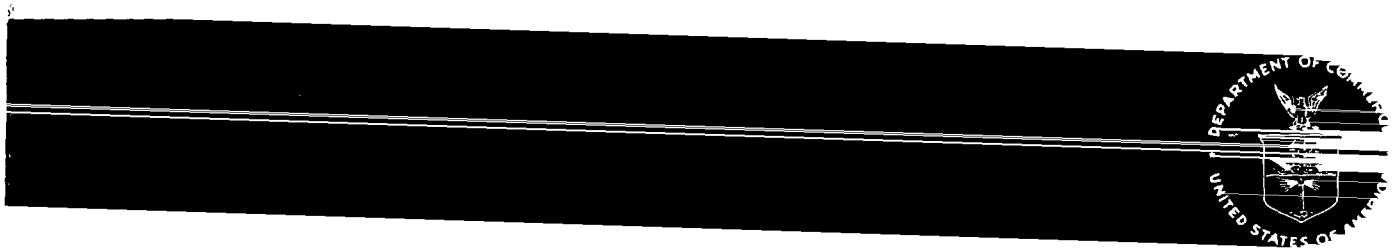

U.S. DEPARTMENT OF COMMERCE/Office of Telecommunications

OT REPORT 76-97

SPECTRUM RESOURCE ASSESSMENT IN THE 2.7 to 2.9 GHz BAND PHASE II: MEASUREMENTS AND MODEL VALIDATION (Report No. 1)

Robert L. Hinkle
Robert M. Pratt
Robert J. Matheson

U. S. DEPARTMENT OF COMMERCE
ELLIOT L. RICHARDSON, Secretary

BETSY ANCKER-JOHNSON, Ph.D.
Assistant Secretary for Science and Technology

OFFICE OF TELECOMMUNICATIONS
JOHN M. RICHARDSON
Director

August 1976

UNITED STATES DEPARTMENT OF COMMERCE
OFFICE OF TELECOMMUNICATIONS
STATEMENT OF MISSION

The mission of the Office of Telecommunications in the Department of Commerce is to assist the Department in fostering, serving, and promoting the nation's economic development and technological advancement by improving man's comprehension of telecommunication science and by assuring effective use and growth of the nation's telecommunication resources.

In carrying out this mission, the Office

- Conducts research needed in the evaluation and development of policy as required by the Department of Commerce
- Assists other government agencies in the use of telecommunications
- Conducts research, engineering, and analysis in the general field of telecommunication science to meet government needs
- Acquires, analyzes, synthesizes, and disseminates information for the efficient use of the nation's telecommunication resources.
- Performs analysis, engineering, and related administrative functions responsive to the needs of the Director of the Office of Telecommunications Policy, Executive Office of the President, in the performance of his responsibilities for the management of the radio spectrum
- Conducts research needed in the evaluation and development of telecommunication policy as required by the Office of Telecommunications Policy, pursuant to Executive Order 11556

PREFACE

This Measurement and Model Validation report has been prepared for the Office of Telecommunications (OT), Spectrum Management Support Division, as part of the 2.7 to 2.9 GHz Spectrum Resource Assessment. The report will be utilized as background information by the Office of Telecommunications Policy (OTP). The OTP has assigned Report Number 1/73-P2 to this memorandum.

ACKNOWLEDGEMENT

The completion of the Los Angeles and San Francisco area measurement program conducted in the 2.7-2.9 GHz band required the contribution of many individuals. In particular, without the able assistance and coordination provided by Mr. John P. Kemper (FAA Western Region Frequency Management Officer) and Mr. E. E. Angle (DOD Western Area Frequency Coordinator) and their staff, this investigation would not have been possible. The measurement program was also made possible by the generous cooperation provided by the FAA and DOD Air traffic control and radar maintenance personnel.

TABLE OF CONTENTS

TABLE OF CONTENTS (Continued)

TABLE OF CONTENTS (Continued)

LIST OF APPENDICES

TABLE OF CONTENTS (Continued)

LIST OF APPENDICES

TABLE OF CONTENTS (Continued)

LIST OF APPENDICES

APPENDIX D (Cont'd)

APPENDIX E

DETAILED MEASUREMENTS

TABLE OF CONTENTS (Continued)

LIST OF APPENDICES

TABLE OF CONTENTS (Continued)

LIST OF APPENDICES

TABLE OF CONTENTS (Continued)

LIST OF ILLUSTRATIONS

TABLE OF CONTENTS (Continued)

LIST OF ILLUSTRATIONS (Cont'd)

LIST OF ILLUSTRATIONS (Cont'd)

LIST OF ILLUSTRATIONS (Cont'd)

LIST OF ILLUSTRATIONS (Cont'd)

LIST OF ILLUSTRATIONS (Cont'd)

LIST OF ILLUSTRATIONS (Cont'd)

LIST OF ILLUSTRATIONS (Cont'd)

LIST OF ILLUSTRATIONS (Cont'd)

LIST OF ILLUSTRATIONS (Cont'd)

TABLE OF CONTENTS (Continued)

LIST OF TABLES

TABLE OF CONTENTS (Continued)

LIST OF TABLES (Cont'd)

ABSTRACT

The Office of Telecommunications (OT) undertook a detailed program to measure and analyze spectrum utilization in the 2.7 to 2.9 GHz band in the Los Angeles and San Francisco areas in support of an Office of Telecommunications Policy (OTP) Spectrum Resource Assessment task. The measurement program consisted of on-site visits to compare predicted and actual PPI interference patterns, and utilization of the Radio Spectrum Measurement System (RSMS) van to validate the component models used in predicting radar-to-radar interference.

From the measured data and a supporting literature search, it was concluded that ducting and man-made clutter (building attenuation) should be included in the propagation loss predictions in order to improve the prediction accuracy of radar-to-radar interference and radar frequency assignments. Even though potential multipath wave interference conditions can be identified, to account for this analytically would require an extremely complex antenna and terrain model. Due to modeling inaccuracies, the difference between the predicted and actual radar-to-radar Interference-to-Noise Ratio (INR) levels may be as large as 22 dB (2σ standard deviation region). However, INR errors of approximately 25 dB can still result in relatively accurate predictions of interference patterns on the victim PPI display for conditions where mainbeam-to-backlobe antenna coupling predominates. In summary, it was concluded that the analytical radar-to-radar interference techniques used in this investigation can be used to predict interference patterns on the victim radar PPI display with sufficient accuracy to allow assessment of radar band congestion, frequency assignment flexibility, and potential of the band to absorb new users.

KEY WORDS

Radar
Interference
Measurements
Model Validation

SECTION 1

INTRODUCTION

1.1 GENERAL BACKGROUND

The Office of Telecommunications Policy in accordance with Executive Order 11556 has tasked (Reference 1) the Spectrum Management Support Division of the Office of Telecommunications, U. S. Department of Commerce, to perform a number of spectrum resource assessments (References 2-5). The intent of these assessments is to provide a quantitative understanding of potential problems in each frequency band of concern as well as to identify options available to spectrum managers for dealing with these problems. One of the primary reasons for initiating these assessments is to ensure identification of problems during the early phases of design and planning rather than after-the-fact, i.e., after a system has been designed and hardware fabricated. By making these band assessments early, necessary actions can be taken to assure that appropriate communication channels are established between agencies whose systems are in potential conflict. This will enhance the early identification of solutions which are mutually satisfactory to all parties involved.

A multiphase approach to the solution of the 2.7 to 2.9 GHz Spectrum Resource Assessment task has been taken by OT.

Phase I: The first phase involves the identification of systems existing in and planned for the band in question, determination of available technical and operational data for each system, identification of the potential interactions between systems, and the generation of a plan that leads to an overall assessment of the bands' potential congestion. A Phase I report (Reference 6) for the 2.7-2.9 GHz Spectrum Resource Assessment has been completed.

Phase II: The second phase encompasses a quantitative analyses of potential interactions between existing and planned radar systems in eight designated congested areas. A measurement and model validation program, and radar processing circuitry investigation of existing and planned radars will be undertaken to assure that the Spectrum Resource Assessment will be based on the best available technical procedure. Findings from these investigations will be applied to assess the degree of congestion and spectrum-space utilization in the eight designated areas. Potential congested areas will be identified,

and alternatives for meeting the specified planned deployments will be provided either singularly or in combination.

Additional Phases: These phases would be conducted as required. Additional periodic assessments will take into account new inputs such as design or other system changes. They will continue until satisfactory solution to the problem is obtained or until the point where sufficient decisions have been made such that further assessment is unnecessary.

This report is the first in a series of Phase II reports related to the Spectrum Resource Assessment of the 2.7-2.9 GHz band. The nature of the 2.7-2.9 GHz spectrum resource problem requires that a rigorous measurement and model validation study be made in typical congested areas in order to accomplish the objectives of the task. This report contains measurements made in the 2.7-2.9 GHz band in the Los Angeles and San Francisco areas, and compares the measured data with radar-to-radar interference prediction models. Subsequent Phase II reports related to this Spectrum Resource Assessment will include:

a. Preliminary Signal Processing Study

b. Investigation of Congested Areas and Band Efficiency

c. Phase II Summary Report

1.2 2.7-2.9 GHz BACKGROUND

During the period of August 1971 through April 1973, the OTP/IRAC had under study the accommodation of DOD, FAA and Commerce radar operations in the band 2.7-2.9 GHz. A series of meetings were held between the agencies (Reference 7 and 8) to determine if the addition of new FAA air traffic control radars to the band could be accommodated without degrading their performance and what impact these radars would have on the performance of the existing radars in the band. An initial assessment of the problem (Reference 6) determined that the addition of new radars to the band could create a potential problem. To resolve the immediate problem of accommodating the new FAA air traffic control radars, the following actions were taken:

a. The band 3.5-3.7 GHz was reallocated to provide for co-equal primary Government use by both the Aeronautical Radionavigation and Radiolocation Services. A footnote was appended to the allocation table, reading as follows:

G110 - Government ground-based stations in the aeronautical radionavigation service may be authorized between 3.5-3.7 GHz where accommodation in the 2.7-2.9 GHz band is not technically and/or economically feasible.

Agencies were requested to cooperate to the maximum extent practicable to ensure on an area-by-area, case-by-case basis that the band 2.7-2.9 GHz is employed effectively.

b. The FAA has stated that they plan to develop their new dual frequency radars in the 2.7-2.9 GHz band and their "low cost" radars in the 3.5-3.7 GHz band. It is expected that compatibility problems may develop in certain geographical areas in the band 2.7-2.9 GHz as the FAA implements its new radar program.

c. The Spectrum Planning Subcommittee was tasked to develop a long-range plan for fixed radars with emphasis on the 2.7-2.9 GHz and 3.5-3.7 GHz bands. The SPS plan (Reference 9) has been completed and approved by the IRAC and forwarded to OT.

1.3 2.7-2.9 GHz OBJECTIVE

In order to promote effective use of the band, OT has been tasked to determine the electromagnetic compatibility of present and future radars planned for deployment in the 2.7-2.9 GHz band for the eight congested areas identified in Reference 9. The Phase I report (Reference 6) identifies the overall objectives of this task in detail. The first part of the Phase II program encompassed a detailed measurement and model validation study in the Los Angeles and San Francisco areas. The objectives of this extensive measurement program were to:

1. Determine the relative contribution of each input component model (i.e., propagation, emission spectrum, antenna pattern, and Frequency-Dependent-Rejection, FDR) to the total error in predicting radar-to-radar interference.

2. Verify predicted interference situations through on-site investigations to determine the accuracy of present radar-to-radar interference prediction techniques.

3. Assess the present potential radar-to-radar

interference situation in the Los Angeles and San Francisco areas.

The realization of these measurement objectives is directly related to the future task objectives of:

1. Developing engineering and management aids to assist the frequency manager in determining the effect of placing future assignments in the 2.7 to 2.9 GHz band in areas where the environment is already congested.

2. Determining if future radar deployments in the Los Angeles and San Francisco areas (and the six other designated congested areas) can be accommodated using present band sharing criteria.

3. Developing a recommended methodology for determining the spectrum-space utilization of the 2.7-2.9 GHz band in the eight designated congested areas.

1.4 APPROACH

In order to accomplish the objectives related to the measurement and model validation program in the Los Angeles and San Francisco areas, the following approach was taken:

1. Assemble environmental information and pertinent equipment characteristics on all radars within a 200 statute mile radius of the two locations. The environmental information and pertinent equipment characteristics were obtained from the GMF, FAA Western Region Frequency Coordinator and DOD Western Area Frequency Coordinator.

2. Select input component models (e.g., emission spectrum, antenna pattern satistics, propagation, and Frequency-Dependent-Rejection, FDR) based on the pertinent environmental information and equipment characteristics.

3. Establish a degradation criteria, and use the appropriate input component models and PPI simulation model to predict potential radar-to-radar interference situations in the 2.7-2.9 GHz band in the Los Angeles and San Francisco areas.

4. Make preliminary on-site measurements at several Los Angeles and San Francisco area radar sites to validate the accuracy of the predicted radar-to-radar interference situations. This involved making video tape recordings of the PPI scope at each radar site, and identifying the interferers by using a pulse train separator or by their respective bearing from the victim radar. A discussion of the measurement procedure and test plan for the preliminary site visits is given in Appendix F.

5. Based on the preliminary site visits, make detailed measurements at two radar sites in each area (one FAA ASR-X radar and one GCA radar site) using the Radio Spectrum Measurement System (RSMS). A discussion of the measurement plan and RSMS van measurement system is given in Appendices F and G, respectively.

6. Compare the data obtained from the detailed measurement program with the various input component models used to predict potential radar-to-radar interference to determine the error introduced by each component model, the deficiencies of the models and also possible use of alternative models.

7. Make closed system measurements on two radars: (1) ASR-5 analog radar, (2) ASR-7 digital radar. The purpose of these measurements is to determine the synchronous and non-synchronous pulse PPI MDS level and the effects of the radar signal processing on the interfering signal.

8. Use the information obtained in steps 4 through 7 to assess the present potential radar-to-radar interference electromagnetic environment in the 2.7-2.9 GHz band in the Los Angeles and San Francisco areas.

9. Make a literature search to support the findings resulting from the measurement program.

The findings and recommendations resulting from the Los Angeles and San Francisco area measurement and model validation study will be applied to develop engineering and management aids, spectrum-space utilization methodologies, and frequency assignment procedures for subsequent use in determining if future planned deployments can be accommodated in the eight designated congested areas. The results and findings of the Phase II program related to these areas will be given in subsequent reports.

SECTION 2

FINDINGS AND RECOMMENDATIONS

2.1 INTRODUCTION

The findings and recommendations resulting from the Los Angeles and San Francisco investigations have evolved from a combination of on-site observations of radar PPI displays, RSMS measurements, closed system measurements, and a literature search. The information obtained from the on-site radar PPI display observations was used to compare actual observed interference situations with predicted interference. The RSMS van measurements were used to determine the error introduced by the various component models used to predict potential interference situations. Closed system measurements were made to determine the non-synchronous pulse MDS level and the processing of interfering signals for the various radar operational modes.

2.2 FINDINGS

The measurement data and literature search information obtained during the Los Angeles and San Francisco area investigations were extensively analyzed. This led to the formulation of the following findings, which are discussed in detail in Sections 3 through 5 and Appendices A through E.

2.2.1 Los Angeles Environmental Observations

Ten of the eleven radar sites visited in the Los Angeles area had some interference from other radars in the band on their PPI display. The interference observed on the FAA radars was generally very light. One military GCA (Ground Control Approach) radar had very heavy interference on the PPI display. Also three of the military range surveillance radars at Point Mugu had very heavy interference on the PPI display. It should be noted that the measurements were made with the FAA radars operating on channels which resulted in minimum frequency separation, and therefore maximum potential for interference. Closed system measurements made during the Los Angeles investigation revealed that the integrators on the analog radars (ASR-4,5,6) do not suppress the level of interference. However, the ASR-7, digital radar, enhancer did suppress the level of interference. Considering all factors, it appears that frequency assignments for the 2.7 to 2.9 GHz band radars deployed in the Los Angeles area at the time of investigation have been engineered to the

extent possible to provide satisfactory air traffic control operating conditions.

Information on planned deployment changes by 1984 in the 2.7 to 2.9 GHz band in the Los Angeles area indicates that four radars are planned for removal from the band, six radars scheduled to be replaced, and three new radars added to the environment. A detailed outline of the planned band changes identifying which radars have frequency diversity capability is given in Table 4-5. Considering the degree of interference observed in the Los Angeles area during the measurement program, the present operational frequency assignments in the band, and the planned deployment changes by 1984, it is apparent that a detailed Spectrum Resource Assessment of the Los Angeles area will be required to determine if known planned deployment changes can be accommodated. The accommodation of planned future deployments in the Los Angeles area will be investigated and reported in a subsequent OT report.

2.2.2 San Francisco Environmental Observations

Interference was observed on the PPI display of all eight of the radar sites visited during the San Francisco area investigation. There was no consistent heavy interference observed; however, three of the FAA radars and one GCA radar were considered to have a moderate amount of interference on their PPI display. The frequency assignment of 2.7 to 2.9 GHz band radars in the San Francisco area (See Table 5-3) shows that all the radars in the San Francisco Bay are assigned to operate in the 2.7-2.8 GHz band, and all the radars in the Sacramento area are assigned to operate in the 2.8 to 2.9 GHz band. It is believed that the mountain range between the San Francisco Bay and Sacramento areas would reduce interference potential sufficiently to allow utilization of the whole 200 MHz band in each area. The present assignments do not take into consideration this factor. The significance of this factor will be investigated and reported in a subsequent report.

Information on planned deployment changes by 1984 in the 2.7 to 2.9 GHz band in the San Francisco area indicates that five radars are planned for removal from the band, two radars are scheduled to be replaced, and one new radar added to the environment. A detailed outline of the planned band changes identifying which radars have a frequency diversity capability is given in Table 5-5. Since the present frequency assignment of 2.7 to 2.9 GHz radars provides 100 MHz of unused band in the San Francisco Bay and Sacramento area, it is believed that known planned deployment changes by 1984 can be accommodated. A detailed study of known planned deployment changes in the

San Francisco area in the 2.7 to 2.9 GHz band will be given in a subsequent OT report.

2.2.3 Model Accuracies

One of the objectives of the Los Angeles and San Francisco measurement program was to determine the error introduced by each of the component models used to predict radar-to-radar interference. The following is a discussion of the measurements made with the RSMS van, and the findings relating to the accuracies of the models used to predict radar-to-radar interference.

2.2.3.1 Antenna Pattern Modeling

Limited measurements made during the Los Angeles and San Francisco area investigation and a literature search led to the formulation of the following findings related to antenna pattern modeling:

1.0 Because of the dynamic nature of radar antennas (i.e., rotating and nodding) and differences in radar site clutter conditions, a statistical description of radar antenna characteristics is the most realistic approach to radar antenna pattern modeling for predicting radar-to-radar interference.

2.0 Line-of-sight (free space) antenna pattern measurements made during the Los Angeles and San Francisco area investigations on cosecant squared elevation type antennas had an averaged median sidelobe (3° to 25° and 335° to 357°) level of -7.0 dBi and standard deviation of 3.3 dB. The average median backlobe (25° to 335°) level was found to be -12.8 dBi with a standard deviation of 3.1 dB. Considering the statistical antenna pattern data given in References 13 and 18, and the measured data resulting from the Los Angeles and San Francisco investigation, it is recommended that a median backlobe level of -13 dBi with a standard deviation of 4 dB be used to model the backlobe statistical characteristics of radionavigation radar antennas.

3.0 When predicting mainbeam-to-backlobe antenna coupling interference, the nominal radar antenna mainbeam gain should be adjusted to account for the reduction of mainbeam gain on the horizon due to the antenna tilt angle used to minimize clutter returns. Antenna tilt angles associated with radars in the Los Angeles and San Francisco areas varied from 2.75 degrees to

5.5 degrees, which results in mainbeam gain reduction of 5 to 12 dB.

4.0 Antenna patterns of potential interfering radars measured at the victim radar site revealed that line-of-sight (free space) antenna pattern models will not always result in realistic interferer pulse amplitude distributions at the victim radar RF input. Propagation related phenomena, such as multipath wave interference arising from multiple scattering and diffraction of the waves by mountains, buildings and other structures affect the interfering signal pulse amplitude distribution at the victim radar RF input. The effects of these propagation related pheomena are dependent on the azimuthal position and pattern of the victim and interfering radar antennas and, therefore, are difficult to realistically represent as separate models. Environmental antenna pattern measurements (interferer antenna pattern measured at the victim radar site) revealed the following antenna-propagation related phenomena:

A. Apparent reduction of sidelobe and backlobe radiation level relative to the mainbeam level occurred on two measured paths. This was believed to be caused by radar site foreground clutter attenuating the radiated spillover underneath and around the antenna reflector. This phenomena occurred when there were low buildings and trees between the radars, and no mountain ranges between the interfering and victim radars or in the vicinity. The apparent reduction in sidelobe and backlobe level for the paths measured was found to be approximately 6 dB.

B. Apparent broadening of the mainbeam and higher backlobe levels of the interferer antenna pattern, as seen by the victim radar. This propagation related phenomena was measured over four paths in the Los Angeles area where there were mountain ranges between the victim and interfering radar and also behind the interfering radar.

2.2.3.2 Emission Spectrum

Comparison of modeled emission spectra with measurements conducted in the Los Angeles and San Francisco investigation, and a literature search have led to the following findings related to emission spectrum modeling:

1.0 A statistical comparison between measured and modeled emission spectra indicated that the average absolute mean difference between measured and modeled emission spectra was 4.0 dB, and the standard deviation between measured and modeled emission spectra, 6.0 dB. The modeling accuracy varied depending on the pulse width category of the radar. The largest absolute mean (6 dB) and standard deviation (8 dB), between measured and modeled emissions, occurred for 0.5 μsec pulse width category radars. The smallest absolute mean (2.6 dB) and standard deviation (4.0 dB) occurred for the 0.8 μsec pulse width category which includes FAA ASR radars.

2.0 The difference between modeled and measured emission spectra of radars with the same pulse width are attributed to the following factors:

A. Magnetron Age
B. Modulating Pulse Shape
C. Magnetron Tube Type
D. Magnetron Anode Voltage and Current Setting
E. Magnetron Load

Since it is difficult to include the above factors into a magnetron emission spectra model, it is believed that the standard deviation of 6 dB between measured and modeled emission spectra may be the limit in obtainable accuracy of conventional magnetron emission spectra modeling.

2.2.3.3 FDR Modeling

A statistical comparison of FDR computed from modeled IF selectivities and emission spectra, and FDR computed from measured IF selectivities and emission spectra, led to the following findings:

1.0 Because of the slow fall-off rate of conventional magnetron emission spectra relative to normal radar receiver IF selectivity characteristics, the Frequency-Dependent-Rejection model accuracy is limited by emission spectrum modeling accuracy.

2.0 Radar frequency measurements in the Los Angeles and San Francisco area indicate that radars are not always operated exactly at their assigned frequency. The error contribution to FDR predictions due to the uncertainty

of frequency separation between transmitter (interferer) and receiver (victim) can be significant for frequency separations less than 10 MHz.

2.2.3.4 Propagation Modeling

Comparison of predicted and measured propagation loss over 20 paths in the Los Angeles and San Francisco area, supported by an extensive literature search, led to the following findings related to propagation loss predictions and measurements:

1.0 A statistical comparison of the point-to-point propagation model (Reference 14) loss predictions with measurements over 13 Los Angeles nonducting paths indicated that on the average, the measured losses were 10 dB higher than predicted. The average absolute difference between the predicted and measured propagation losses was 12 dB. Factors which are believed to have contributed to the differences are:

A. Increased attenuation due to buildings and man-made obstacles which were not included in the prediction model and terrain data base. Propagation loss measurements by researchers (Reference 34,35) in suburban and urban environments have ranged from 12 to 50 dB below free space, depending on the degree of building congestion. Measurements over suburban area paths, which constituted 80 percent of the type radar-to-radar paths encountered in this investigation, were reported to be 12 dB below free space loss.

B. Increased attenuation due to foliage is not included in the model and terrain data base. However, because the radar-to-radar paths over which loss measurements were made did not pass through heavy foliage, it is believed that the contribution of error between predicted and measured loss due to foliage was small relative to other factors.

C. The point-to-point propagation model considers only the terrain profile in the vertical plane that cuts through the great circle line between transmitter and receiver. Consequently, the model does not account for multipath propagation,

caused by mountain reflection and diffraction, which may result in less loss than the direct path. Even though potential multipath wave interference conditions can be identified, it is difficult to include this factor in the prediction process in other than a general way since multipathing is a function of the interferer and victim radar antenna azimuthal positions and the surrounding terrain. To account for this analytically would require an extremely complex terrain model.

2.0 The result of man-made clutter attenuation measurements by Turin (Reference 35) were incorporated into the San Francisco loss predictions. This involved identifying the degree of man-made clutter over the propagation path and adding the appropriate loss in dB to the point-to-point model loss prediction. However, for line-of-sight paths the loss for man-made clutter was simply added to the free space loss. The absolute mean difference between predicted and measured propagation was 7 dB which was a 5 dB improvement over Los Angeles area propagation loss predictions. The algebraic mean difference was -3 dB which was also an improvement (7 dB) over Los Angeles predictions.

3.0 Loss predictions by the area version of the propagation model were also statistically compared with measurements. The point-to-point version of the model had a lower average absolute prediction error and standard deviation than the area version.

4.0 Superrefraction (ducting) conditions were found to exist over one ocean path (from Miramar to Los Alamitos) in the Los Angeles area and two San Francisco Bay paths (from Oakland and Alameda to Mountain View). The measured loss for the first two paths were as much as 39 dB below the point-to-point predicted loss. The measured loss for the third path varied +25 dB relative to the predicted loss, indicating that both ducting and radio holes were likely present. Bean (Reference 54) reported that during the summer months at San Diego and Oakland, ducting occurs 50% of the time. Hitney (Reference 43) states that radar range enhancement occurs 30% of the time during the year in the offshore San Diego area.

5.0 The measured propagation loss as a function of antenna height decreased more at some radar sites than predicted. The degree of difference between measured and predicted antenna height gain depended on the density and proximity of clutter (trees and man-made obstacles) around the radar site. The measured propagation loss decreased 4 dB as the receiving antenna was raised 15 feet on the sparsely cluttered end of one path, and 11 dB on the densely cluttered end of the same path. These measurement results illustrated the importance of matching the receiving antenna height to the radar antenna in order to obtain accurate propagation loss measurements.

6.0 Propagation loss measurements revealed that moving the physical location of the receiving antenna by a few feet can result in received signal variations as great as 4.5 dB. For this reason, propagation loss measurements were conducted at more than one position at each radar site to average out the effect of signal level variation due to multipath.

7.0 It was evident from propagation loss measurement differences between using the RSMS omni, cavity back, and parabolic dish antennas, that measured propagation loss is affected by the antenna beamwidth in a multipath environment. Antennas with unlike patterns and beamwidth spatially weigh incident multipath signals differently, which affects the total power received by the antenna. This illustrates the importance of using the actual radar antenna, or at least a receiving antenna whose beamwidth approximates the radar antenna in the plane that multipathing is occurring.

2.2.4 Closed System Measurements

Closed system measurements were made on an FAA ASR-5 (analog) radar and FAA ASR-7 (digital) radar. The objective of these measurements was to determine the nonsynchronous pulse PPI display MDS level and the radar interfering signal processing characteristics. Both the radar PPI display and "A" scope were monitored during these closed system measurements while various radar modes and fixes were turned on and off. These measurements resulted in the following findings:

1.0 Analog radars similar to the FAA ASR-4, ASR-5 and ASR-6 have a nonsynchronous pulse PPI display

Minimum Discernible Signal (MDS) level at an INR of 10 dB for both the normal and MTI modes and in the integrated MTI mode. The 10 dB INR criterion is where the interference is clearly visible, not at the point when the interference is just causing speckling on the PPI display which occurs at an INR of approximately 4-6 dB for both normal and MTI modes.

2.0 The integrator on the FAA analog radars (ASR 4,5,6) does not significantly suppress nonsynchronous pulse interference. With the integrator on, approximately 1 or 2 dB more interfering signal power was required for the interference to become just visible on the PPI display. However, the interference was clearly visible with the integrator on at an INR of 10 dB. The analog integrator did enhance synchronous pulses by approximately 6 dB.

3.0 Closed system measurements made on a digital radar (ASR-7) indicated that nonsynchronous pulse interference was clearly visible on the PPI display at an INR of 10 dB for both the normal and MTI modes with the enhancer (integrator) off. With the enhancer on, the interference was significantly reduced. That is, for interfering signal levels as high as -60 dBm, pulse width range of .5 μsec to 30 μsec, and frequency separation of $\Delta F=0$ interference was significantly reduced on the PPI display. However, there were some interfering signal PRF's (not including synchronous PRF) which did result in light interference on the PPI display. The dependence of interference on PRF will be investigated in a subsequent report.

2.2.5 Frequency Assignment Factors

As a result of the 2.7 to 2.9 GHz band investigation conducted in the Los Angeles and San Francisco areas, factors were discovered which are not normally considered in making frequency assignments. These factors included: ducting, decreased magnetron lifetime when operating at the edges of the 2.7 to 2.9 GHz band, and building attenuation.

Discussions with the FAA Western Region Frequency Coordinator and measurements made with the RSMS van in the Los Angeles and San Francisco area confirm the necessity to include ducting phenomena, when appropriate, in determining frequency assignments.

As previously mentioned, ducting can cause as much as 39 dB less propagation loss than predicted by normal diffraction loss theory. The ducting phenomena motivated the FAA to assign frequencies to radars, within 20 miles of Los Angeles, 30 MHz above the San Diego area Miramar ASR-5 radar upper channel frequency of 2720 MHz.

Also, discussions with the FAA revealed that certain manufactured 5586 magnetron tubes have inherently short lifetimes when operated near the 2.7-2.9 GHz band edge, even though the manufactured tuning range is specified as 2.7-2.9 GHz. Consideration of this factor will be given in a subsequent OT report. The previous discussion on the finding and effects related to building attenuation amplifies the necessity to include a building attenuation factor in the predicted propagation path loss.

2.2.6 Interference Prediction Capability

The main objective of the Los Angeles and San Francisco area measurement program was to assess the ability to predict radar-to-radar interference. Measured data taken during the investigation indicates that the standard deviation between modeled and measured data was 4 dB for antenna pattern backlobe level, 6 dB for emission spectrum/FDR, and 8 dB for propagation loss incorporating a building attenuation factor. For these three component models used to predict radar-to-radar interference, an estimate of the total standard deviation (σ) would be 10.7 dB since the models are independent. The worst case limit that typically needs to be considered is the 2σ region which implies the predicted INR will not differ from the actual INR by more than 21.4 dB 96% of the time. Due to uncertainties in radar signal processing, plus the additional 10.7 dB standard deviation associated with antenna patterns, emission spectrum/FDR, and propagation loss, it appears that the interference pattern on the victim radar PPI display cannot always be accurately predicted. However, due to the inherent characteristics of the mutual antenna gain distribution, INR errors of approximately 25 dB can occur, but still result in relatively accurate predictions of interference patterns of the victim PPI display for conditions where mainbeam-to-backlobe antenna coupling predominates, which is the most common type of interference antenna coupling that occurs in a radar environment. (See Figure 3-1 and Table 3-1).

2.2.6.1 Los Angeles Area Investigation

For the 11 radar sites visited during the preliminary radar site measurements, there were 27 predicted interference cases

of mainbeam-to-backlobe coupling. The total number of actual observed interference cases during the preliminary site visits was 21. Of the 21 observed cases, there were 17 predicted and 4 unpredicted. Therefore, 63 percent of the predicted interferers were observed on the victim PPI display, and 19% of the observed interferers were unpredicted. The 4 unpredicted cases were due to multipath phenomena. Most of the predicted interference cases that were observed were not of the periodic nature that was predicted. Therefore, in general, most of the interference predictions were pessimistic when compared to the actually observed interference.

It was estimated that in most cases the predicted interfering signal power levels were approximately 10 to 20 dB too high. The difference between predicted and actual interference signal power level can be generally attributed to the statistical nature and biases associated with the antenna and propagation related variables that were not initially included in the models. Based on measurements made during the Los Angeles investigation and information obtained from a literature search, empirical modifications to the propagation model to include building attenuation and to the antenna model were made and incorporated in the interference prediction technique used in the San Francisco investigation.

2.2.6.2 San Francisco Area Investigation

For the eight radar sites visited during the San Francisco area preliminary radar site measurements, there were 13 predicted interference cases of mainbeam-to-backlobe antenna coupling. However, due to some of the radars being inoperative during the preliminary radar site measurement program, only 9 predicted interference cases could be verified. All 9 of the predicted interference cases that could be verified were observed during the preliminary site visits. There was also one case of unpredicted interference. Therefore, 100 percent of the predicted interferers were observed on the victim PPI display, and 10% of the observed interferers were unpredicted. In general, the predicted form of the interference on the PPI display was close to the actual observed interference with the exception of two cases where the interference was lighter than predicted, and one case where the interference was much heavier than predicted. The disagreement between observed and predicted interference for these three cases was attributed to the radars operating on frequencies other than their assigned frequency.

The San Francisco area investigation showed a significant improvement over the Los Anglees area investigation in the correlation between predicted and actual observed interference.

This improvement was attributed to empirical modifications to the interference prediction model.

2.2.6.3 Summary of Interference Prediction Capability

As a result of the extensive measurement program conducted in the Los Angeles and San Francisco areas, it was concluded that the statistical variations in antenna patterns, emission spectrum/FDR, propagation loss and signal processing parameters, that are inherently present, make it extremely difficult to make precise predictions of the interference on the PPI display. However, it is possible to provide a range of interference PPI display patterns, which for many cases may appear to have nearly identical operational impact. In effect, the analytical radar-to-radar interference techniques used in this investigation can be used to:

1. Assess congestion
2. Determine the EMC of new radar systems
3. Evaluate alternate assignment plans
4. Develop spectrum engineering and management aids
5. Develop a spectrum-space metric for determining band efficiency.

2.3 RECOMMENDATIONS

Considering the findings resulting from the Los Angeles and San Francisco area measurements, the literature search, and overall Spectrum Resource Assessment objectives, it is recommended that the following action be taken to improve radar-to-radar EMC prediction and analysis techniques, and procedures required for assessment of band efficiency and potential congestion:

1. Additional analysis or closed system measurements should be made to investigate interfering signal processing properties of existing and planned radar deployments in the 2.7 to 2.9 GHz band. This investigation should also include interfering signal processing characteristics of proposed new post processing equipment such as the RVD-4, ARTS-III Enhancement program and other new developments such as the Moving Target Detector (MTD) radar presently under consideration by the FAA. Findings from the analysis should then be incorporated in the various

radar-to-radar interference prediction models for improved prediction capability.

2. Additional analysis and measured data be obtained on emission spectra of ASR-8 radars which employ klystron output tubes, and height finding radars (AN/FPS 6 and 90), which reportedly will use tunable coaxial magnetrons.

3. Follow-up of the two on-going efforts* to establish controller performance keyed PPI degradation criteria to enable objective assessment of interference conditions.

Information obtained from the results of the above recommendations, and findings of the Los Angeles and San Francisco area investigations will be incorporated in the radar-to-radar interference prediction model(s) and techniques to assure that the overall Spectrum Resource Assessment of the 2.7 to 2.9 GHz band is based on sound technical procedures. The established technical procedure to predict potential radar-to-radar interference will then be applied in the eight designated congested areas to assess the accommodation of future radar deployments in the 2.7 to 2.9 GHz band, and as frequency management aids to assist OTP and other government agencies in achieving efficient spectrum management.

---

* Controller performance keyed PPI degradation studies are currently being conducted by the FAA at NAFEC and ECAC at CALSPAN.

SECTION 3

INTERFERENCE PREDICTION TECHNIQUE

3.1 INTRODUCTION

The following is a discussion of the method used to predict potential radar-to-radar interference during the 2.7 to 2.9 GHz band investigation conducted in the Los Angeles and San Francisco areas. The first step in predicting potential radar-to-radar interference situations involved calculating the interference-to-noise ratio (INR) at the victim radar receiver IF output. These predicted INR values were then used to determine the potential radar-to-radar interference conditions. Once potential radar-to-radar interference conditions were identified (INR 10 $\geq$dB), a PPI Simulation Program (Reference 12) was used to predict the pattern of the interference on the victim PPI display.

3.2 INR CALCULATION

The INR values were calculated for victim receiver mainbeam to interferer backlobe coupling conditions. That is, the interference should appear on the PPI display when the victim antenna is pointing in the direction of the potential interferer. A three-level victim and interferer antenna pattern model described in Appendix A was used to predict the interference. The emission spectrum, FDR and propagation loss models used to predict interference are discussed in Appendices B, C and D, respectively. The INR for each radar in the environment was calculated using the nominal characteristics of the victim and interfering radars and the following equation:

$$INR_{ij} = P_{T_i} + G_{T_i} + G_{r_j} - L_{P_{ij}} - FDR_{ij} - N_j \qquad (3\text{-}1)$$

Where:

P_{T_i} = The peak transmitter power of the i^{th} radar, in dBm

G_{T_i} = The interfering antenna median backlobe level of the i^{th} radar (-10 dBi, Reference 13)

G_{r_i} = The nominal mainbeam gain of the j^{th} radar minus correction factor for antenna tilt angle (mainbeam gain -5 to -12 dB), in dBi

$L_{P_{ij}}$ = Median propagation path loss exceeded 50% of the time. Determined using RAPIT point-to-point model (Reference 14), in dB

FDR = The frequency-dependent-rejection between the i^{th} transmitter and the j^{th} receiver, in dB

N_j = Victim receiver inherent noise level, in dBm.

Once potential radar-to-radar interference situations were identified (INR $\geq$ 10 dB), the PPI simulation model was used to predict the form which the interference would appear on the victim PPI scope. The interference-to-noise ratio criteria of 10 dB was obtained from Reference 47, and was used for both the Los Angeles and San Francisco investigation. During the Los Angeles investigation, closed system measurements on an analog radar (ASR-5) and a digital radar (ASR-7) were made to verify the interference threshold criteria. It was found that nonsynchronous interfering pulses were just perceptible on the PPI display at an INR of approximately 6 dB and clearly visible at an INR of 10 dB.

3.3 PPI SIMULATION MODEL

The concept of the PPI simulation program is that interference will appear on the victim PPI or RHI scope if the interfering signal level exceeds the victim receiver threshold criteria. One input parameter to the PPI simulation program is the required mutual antenna gain to exceed the interference criteria. This mutual antenna gain threshold level is given by:

$$G_{T_i} + G_{r_j} \geq - P_{T_i} + I_{MAX} + FDR_{ij} + L_{P_{ij}} + P_L \qquad (3\text{-}2)$$

Where,

$$I_{MAX} = \left(\frac{I}{N}\right) + N_j$$

and,

$G_{T_i} + G_{r_j}$ = Mutual antenna gain between victim and interference antennas, in dB relative to an isotropic antenna (dBi).

I_{MAX} = Maximum allowable interfering power at victim receiver input before the victim receiver interference criteria level is exceeded, in dBm.

$(\frac{I}{N})$ = Victim receiver interference criteria, 10 dB.

P_L = Peak power loss of interfering signal due to special radar signal processing circuitry, in dB.

Present PPI Simulation Program limitations are that the displays produced by the program are static in nature. That is, the model does not take into account the complete statistical variations in the victim and interferer antenna patterns since the program only displays the interference for one scan of the victim antenna. A similar PPI Simulation Program is being developed on the HP 8500 minicomputer which uses the graphics display to give a dynamic presentation of the interference as it would appear on an actual PPI display. The new PPI Simulation Program will use Monte Carlo techniques to simulate the antenna pattern of the victim and interferer radars. The antenna patterns used in the PPI Simulation Program for the Los Angeles and San Francisco investigation are shown in Figures A-21 and A-22 in Appendix A for the victim and interfering radars, respectively.

Figure 3-1 shows sample PPI Simulation Program runs for mutual antenna gain threshold ranges of +20.0 dBi to -18.8 dBi. These runs were made to determine the variations in degree of interference on the PPI display to parametric variations in predicted propagation loss and FDR. The victim and interfering radar parameters were held constant with only the mutual antenna gain threshold being varied. The relative bearing of the interferer from the victim is 97 degrees.

The calculated mutual antenna gain threshold (Equation 3-2) can be related to the mean percentage of the PPI scope covered by interference per scan. A mutual antenna gain probability distribution (Figure A-23) was calculated by convolving the victim and interfering antenna gain probability distributions shown in Tables A-2 and A-3 for the antenna patterns used in the PPI Simulation Program. Using the mutual antenna gain distribution shown in Figure A-23 for two of the Los Angeles area FAA radars, a mutual antenna gain of 5 dBi would indicate that the interference criterion would be exceeded approximately 3% of the time which implies that on the average 3% of the scope or 10.8° (.03 x 360°) of the PPI display would have interference. Table 3-1 shows a comparison of predicted percentage of PPI scope covered by interference using Figure A-23 and the PPI Simulation Program. The data taken from the mutual antenna gain distribution and the PPI Simulation Program are in close agreement considering the fact that the PPI simulation program is static in nature,

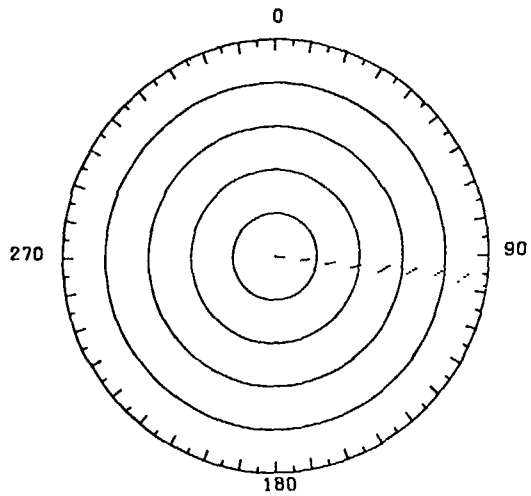

Figure 3-1A. Threshold=20 dBi

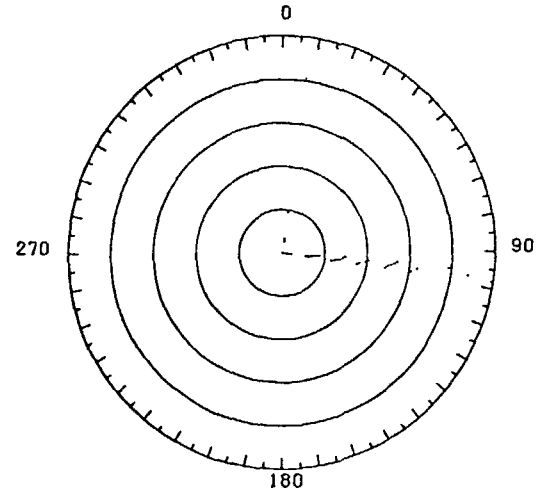

Figure 3-1B. Threshold=15 dBi

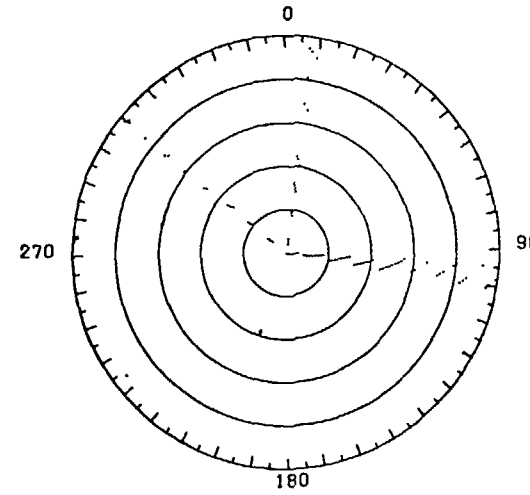

Figure 3-1C. Threshold=5 dBi

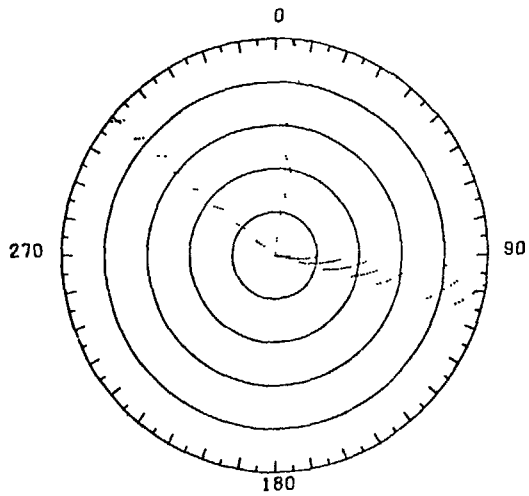

Figure 3-4D. Threshold=-5 dBi

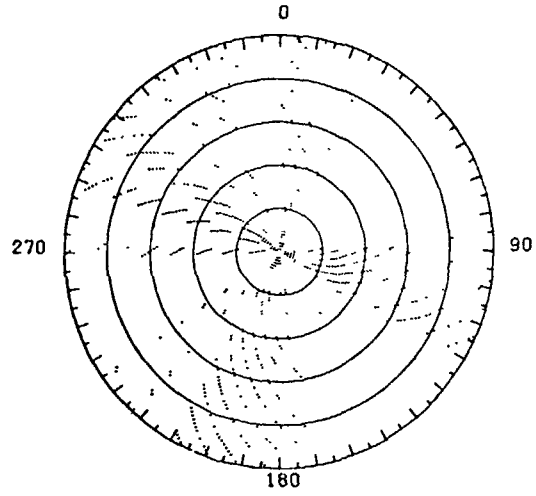

Figure 3-1E. Threshold=-15 dBi

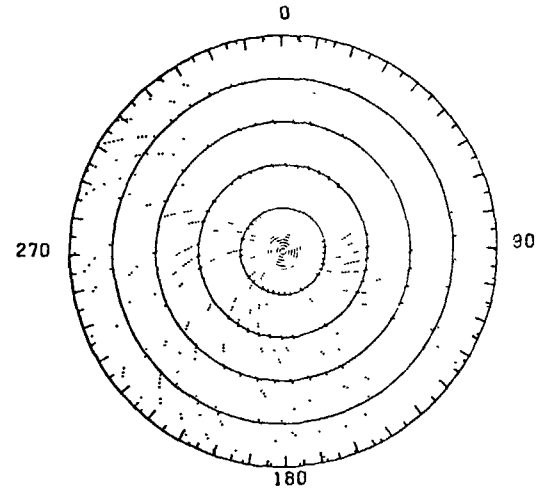

Figure 3-1F. Threshold=-18 dBi

Figure 3-1. PPI Display Interference Level as a Function of Mutual Antenna Gain Threshold

and does not perform a true convolution of the victim and interfering antenna patterns.

The mutual antenna gain threshold is a function of the propagation path loss between the victim and interfering radars and victim receiver Frequency-Dependent-Rejection (FDR). Therefore, changes in the mutual antenna gain threshold can be interpreted as representing variations in the prediction error of the propagation loss and FDR models. A study of Table 3-1 shows that the degree of interference on the PPI scope can be divided into several regions:

a. Region 1 (Mutual antenna gain threshold level between +30 dBi and +20 dBi): This region of mutual antenna gain threshold level can be defined as transition region 1 where the interference is very infrequent and random in nature and only occurs for mainbeam-to-major sidelobe coupling of the victim and interfering antennas.

b. Region 2 (Mutual antenna gain threshold level between +20 dBi and -5 dBi): In this region the interference is periodic in nature from scan to scan. The degree of interference on the PPI display is also approximately the same over the 25 dB range in mutual antenna gain threshold level. This mutual antenna gain threshold region occurs for mainbeam-to-backlobe coupling of the victim and interfering radars.

c. Region 3 (Mutual antenna gain threshold level between -5 dBi to -15 dBi): This region of mutual antenna gain threshold level is defined as transition region 3. In this region, the degree of interference changes from light strobes of interference to interference covering approximately 70% of the PPI display. This sharp change in degree of interference over a small mutual antenna gain threshold range is due to the threshold coupling level changing from mainbeam-to-backlobe coupling to backlobe-to-backlobe coupling.

d. Region 4 (Mutual antenna gain threshold level < -15 dBi): In this region the level of interference is approximately constant and covers a significant portion of the PPI display. This region is defined as the backlobe-to-backlobe coupling region.

TABLE 3-1

PERCENT OF PPI DISPLAY COVERED BY INTERFERENCE

MUTUAL ANTENNA GAIN THRESHOLD	% of Display Covered by Interference	
	Mutual Antenna Gain Distribution (Figure A-18)	PPI Simulation Program
25.0	0.1	0.0
20.0	0.5	1.0 (Figure 3-1A)
15.0	1.2	1.7 (Figure 3-1B)
5.0	2.4	3.5 (Figure 3-1C)
-5.0	6.0	6.3 (Figure 3-1D)
-15.0	40.0	34.7 (Figure 3-1E)
-18.8	61.7	60.5 (Figure 3-1F)

In summary, in predicting the form of the interference on the PPI display, a total error of approximately ± 10 dB in the propagation and FDR models can still result in a relatively accurate display of the interference if the predicted and actual mutual antenna gain threshold fall within the center of Regions 2 or 4. However, if the predicted and actual mutual antenna gain threshold level falls within the transition regions 1 or 3, a significant difference between predicted and actual observed interference can result due to the high sensitivity in these regions to errors in the propagation and FDR models.

The antenna patterns shown in Figures A-21 to A-22 are line-of-sight. In order to predict the actual degree of interference on the PPI display, the incorporation of environmental effects on the interferer's antenna pattern as seen by the victim radar is required in the mutual antenna gain distribution. These environmental effects are propagation related phenomenon, and are discussed in detail in Appendix A.

SECTION 4

LOS ANGELES AREA INVESTIGATION

4.1 INTRODUCTION

This section discusses the investigation and measurement program conducted by OT in the Los Angeles area to assess the capability and techniques used to predict radar-to-radar interference, and to make refinements to the prediction model. The investigation was made during the period of February to July 1975 with measurements being conducted from May 26 to June 8, 1975. The environment included all radar deployments in the 2.7 to 2.9 GHz band within 200 statute miles of Los Angeles. Included in this section is a comparison between predicted and actual observed interference at 11 radar sites visited in the Los Angeles area, and environmental observations. A detailed comparison of the measured data taken during the investigation with the various component models used to predict radar-to-radar interference is given in Appendices A through E.

4.2 ENVIRONMENT OF 2.7-2.9 GHz BAND

The environment for the Los Angeles area was determined from three sources: 1) Western Area DOD Frequency Coordinator (Reference 11), 2) Western Region FAA Frequency Manager (Reference 10), and 3) Government Master File (GMF). Comparison was made of the environmental lists received from the three sources, and differences resolved by contact with the area frequency coordinators. It was determined that there are a total of 23 radars within a 200 mile radius of Los Angeles operating in the 2.7-2.9 GHz band. Table 4-1 lists the location, nomenclature, and function of these radars. Figure 4-1 shows the location of these radars on a Los Angeles area map. The equipment characteristics of the radars are given in Table 4-2.

During this Los Angeles area investigation, the RSMS van was used to verify the frequency assignments obtained from the area coordinators. Most of the radars in the area were found to be operating within a few megahertz of their assigned frequency, with the exception of the following radars:

Radar #	Assigned Frequency (MHz)	Operating Frequency (MHz)
14 (San Nicolas Is.)	2866	2882.5
15 (Santa Cruz Is.)	2871	2883.1
16 (Laguna Pk.)	2880	2886.8

TABLE 4-1

LOCATION OF 2.7-2.9 GHz RADARS
IN LOS ANGELES AREA

RADAR NO.	CITY/BASE	NOMENCLATURE	LATITUDE:			LONGITUDE:		
	Present FAA	Airport Surveillance Radars						
1	Los Angeles Int.	ASR-4	33	57	12	118	24	00
2	Los Angeles Int.	ASR-7	33	55	57	118	24	23
3	Burbank	ASR-6	34	12	15	118	21	14
4	El Toro*	ASR-5	33	39	46	117	42	43
5	Ontario	ASR-5	34	03	15	117	35	41
6	Long Beach	ASR-5	33	49	09	118	08	16
7	Edwards AFB**	ASR-5	34	52	22	117	54	38
8	Miramar***	ASR-5	32	52	29	117	08	23
	Present Navy	Ground Control Approach Radars						
9	Lemoore	ASR-5	36	20	44	119	54	18
10	San Diego North Is.	CPN-4	32	41	48	117	12	45
11	San Clemente Is.	CPN-4	33	01	02	118	35	05
12	Los Alamitos	CPN-4	33	47	17	118	02	57
	Present Navy	Range Clearance Radars						
13	Point Mugu	ASR-7	34	07	06	119	07	25
14	San Nicolas Is.	APS-20	33	14	57	119	31	16
15	Santa Cruz Is.	APS-20	33	59	40	119	37	56
16	Laguna Peak	APS-20	34	06	28	119	03	51
	Present A.F.	GCA Radars						
17	Vandenberg AFB	MPN-14	34	43	42	120	34	31
18	Norton AFB	MPN-13	34	05	45	117	14	12
19	George AFB	MPN-14	34	35	54	117	23	02
20	March AFB	MPN-13	33	53	04	117	15	34
	Present A.F.	Tracking Radars						
21	Edwards AFB	MPS-19	34	56	43	117	54	45
	Present A.F.	Height Finding Radars						
22	Cambria	FPS-6	35	31	21	121	03	46
23	San Pedro Hill	FPS-90	33	44	48	118	20	09

*Joint FAA-MC use
**Joint FAA-AF use
***Joint FAA-N use

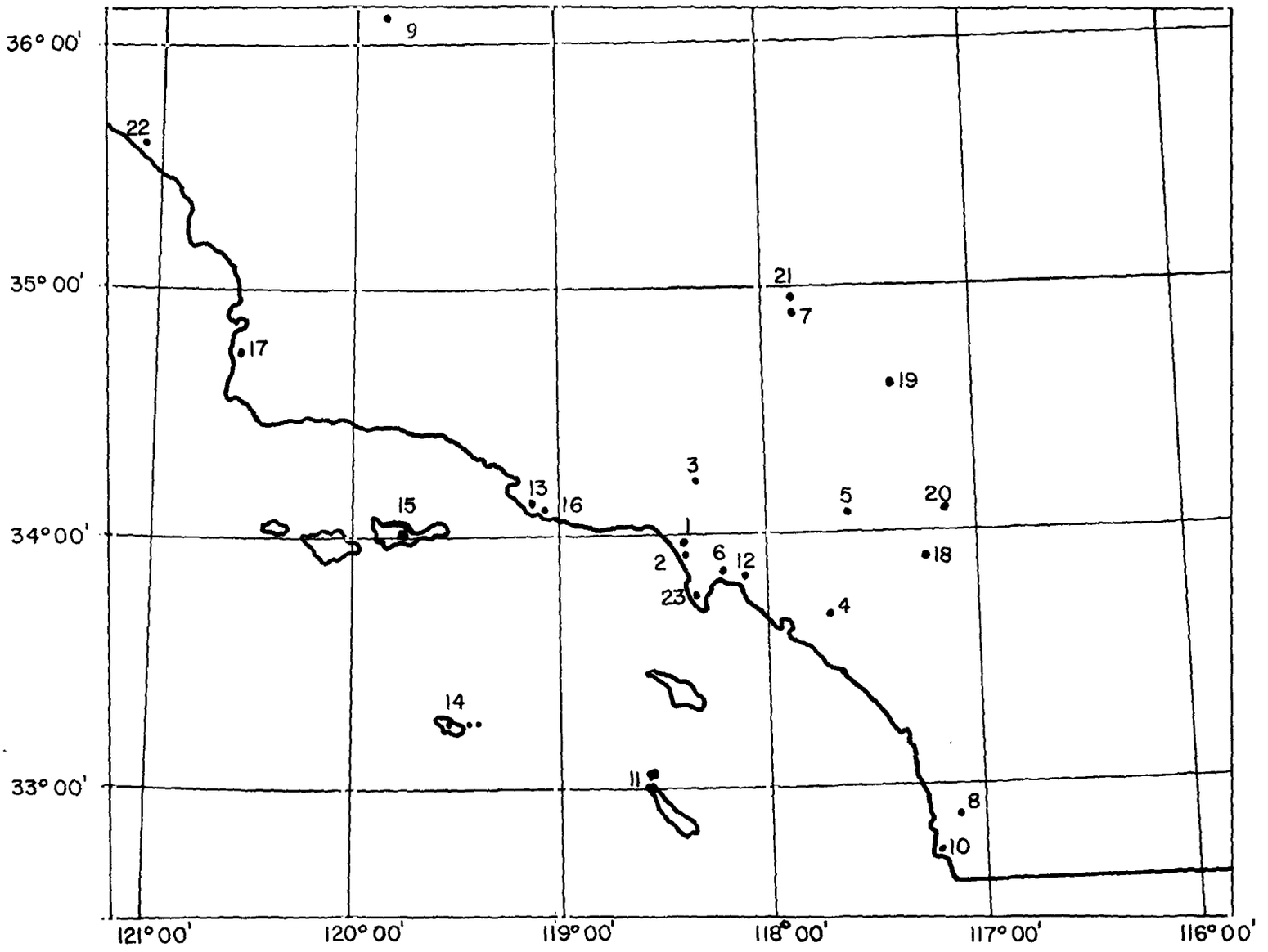

FIGURE 4-1 LOCATION OF RADARS IN THE 2.7-2.9 GHz BAND IN THE LOS ANGELES AREA

TABLE 4-2

CHARACTERISTICS OF 2.7-2.9 GHz RADARS IN LOS ANGELES AREA

RADAR NO.	CITY/BASE	EQUIPMENT NOMENCLATURE	ASSIGNED FREQUENCY (MHz)	PEAK POWER (kW)	OUTPUT TUBE TYPE	P.W. (μS)	PRF (PPS)	IF Bw (MHz)	NOISE LEVEL (dBm)	ANT. GAIN (dB)	ANT. HGT. (FT.)	ANT. TILT ANGLE	ANTENNA SCAN RATE (RPM)	SCOPE RANGE (NM)	SITE ELV. (FT.)
1	Los Angeles Int.	ASR-4	2750-2760	450	5586+	.833	810	2.4	-106	34	28	3.0°	13	60	116
2	Los Angeles Int	ASR-7	2850-2860	425	DX276	.833	Staggered 352	2.7,5*	-105	34	50	3.5°	15	60	115
3	Burbank	ASR-6	2785-2795	400	5586+	.833	1125	2.7,5*	-106	34	62	3.5°	10	60	703
4	El Toro	ASR-5	2730-2740	600	5586+	.833	780	2.7,5*	-106	34	44	3.5°	13	60	404
5	Ontario	ASR-5	2810-2820	600	5586+	.833	900	2.7,5*	-106	34	53	3.5°	13	60	995
	Long Beach	ASR-5	2770-2780	600	5586+	.833	820	2.7,5*	-106	34	26	3.75°	13	60	60
7	Edwards AFB	ASR-5	2870-2880	400	DX276+	.833	1140	2.7,5*	-106	34	26		15	60	2350
8	Miramar	ASR-5	2710-2720	400	5586+	.833	700	2.7,5*	-106	34	60		13	60	451
9	Pendora	ASR-5	2800-2810	400	5586	.833	700	2.7,5*	-106	34	35		13	60	235
10	San Diego North Is.	AN/CPN-4	2780	600	5586	.5	1500	2.25	-102	31	14	3.75°	20	30	24

* Normal and MTI IF Bw, respectively

+ FAA ASR radars may use 5586, DX276 or QK1643

TABLE 4-2 CONTINUED

CHARACTERISTICS OF 2.7-2.9 GHz RADARS IN LOS ANGELES AREA

RADAR NO.	CITY/BASE	EQUIPMENT NOMENCLATURE	ASSIGNED FREQUENCY (MHz)	PEAK POWER (kW)	OUTPUT TUBE TYPE	P.W. (μS)	PRF (PPS)	IF Bw (MHz)	NOISE LEVEL (dBm)	ANT. GAIN (dB)	ANT. HGT. (FT.)	ANTENNA TILT ANGLE	ANTENNA SCAN RATE (RPM)	SCOPE RANGE (NM)	SITE ELEV. (FT.)
11	San Clemente Is.	AN/CPN-4	2800	600	5586	.5	1500	2.25	-102	31	13		20	30	180
12	Los Alamitos	AN/CPN-4	2800	600	5586	.5	1200	2.25	-102	31	14	3.0°	20	30	35
13	Point Mugo	ASR-7	2862	400	DX276	.833	Stag-gered 1002	2.7,5*	-105	34	29	2.75°	15	60	13
14	San Nicolas Is.	AN/APS-20	2866	1000	4531	2.0	359	1.0	-111	30	28		10	200	500
15	Santa Cruz Is.	AN/APS-20	2871	1000	4531	2.0	309	1.0	-111	30	35		10	200	50
16	Laguna Peak	AN/APS-20	2880	1000	4531	2.0	311	1.0	-111	30	30	2.75°	10	200	20
17	Vandenberg AFB	AN/MPN-14	2793	750	5586	.7	1100	2.26	-106	32	14		15	30	1480
18	Norton AFB	AN/MPN-13	2797	750	8798	.7	1100	2.26	-106	32	18	4.25°	15	30	1105
19	George AFB	AN/MPN-14	2800	750	5586	.7	1100	2.26	-106	32	17	3.25°	15	30	2875
20	March AFB	AN/MPN-13	2802	750	8798	.7	1100	2.26	-106	32	16	5.5°	15	30	1507
21	Edwards AFB	AN/MPS-19	2801	325	5586	.8	2000	3.0	-105	37	26		0-20		2350
22	Cambria	AN/FPS-6	2785	5000	6410A	2.0	328	.8	-106	39	45	N.A.	7.5 RPM 20-30CPM	200	780
23	San Pedro Hill	AN/FPS-90	2835	5000	QK327A	2.0	370	.8	-105	39	45	N.A.	7.5 RPM 20-30CPM	200	1480

* Normal and MTI IF Bw respectively.

The airport surveillance radars are assigned to operate in a 10 MHz band. These dual-channel radars usually operate the "A" channel 1 or 2 MHz above the lower end of the 10 MHz band, and "B" channel 1 or 2 MHz below the upper end. The FAA standard procedure is to switch to alternate channels on a 24-hour rotational basis. As a result of operating procedure, both channels were analyzed separately for potential interference.

All the radars in the Los Angeles environment employ a conventional tunable magnetron output tube with the exception of radars 14, 15, 16 and 22 which employ fixed magnetron output tubes. Table 4-3 shows the operational frequency range, and the assigned frequency of the radars in the Los Angeles environment. Additional information on the magnetron tube employed in each radar, and the magnetron tuning range is discussed in Appendix B.

4.3 COMPARISON OF PREDICTED AND OBSERVED INTERFERENCE

The following is a comparison of the interference that was observed during the 2.7-2.9 GHz spectrum resource assessment measurement program in the Los Angeles area and predicted interference. The Los Angeles area measurement plan consisted of a two-phase investigation. The first phase involved preliminary radar site measurements which consisted of on-site verification of predicted interference. Potential interference situations were identified by using the parametric information listed in Table 4-2 and applying Equation 3-1. Table 4-4 shows predicted radar coupling situations where the calculated INR was greater than 0 dB. Only worst case (minimum frequency separation for dual channel radars) INR's are shown in the table for coupling with or between FAA ASR radars. Actual predicted interference situations are those cases listed in Table 4-4, where the INR $\geq$ 10 dB. For those cases where the INR was greater than 10 dB, the PPI Simulation Program was run to determine the form of the interference on the victim PPI scope.

The second phase involved detailed measurements using the RSMS van instrumentation to determine why predicted interference did not appear on the PPI display or why unpredicted interference appeared on the PPI display. The detailed measurements made are discussed in Appendices A through D. Appendix E gives a detailed discussion of the predicted and observed interference at two radar sites using the measured data discussed in Appendices A through D to explain the differences between predicted and observed interference. Appendix F gives a general outline of the Los Angeles area measurement plan, and Appendix G discusses the RSMS instrumentation used in the Los Angeles area radar measurements.

TABLE 4-3

FREQUENCY ASSIGNMENT INFORMATION OF 2.7-2.9 GHz RADARS IN LOS ANGELES AREA

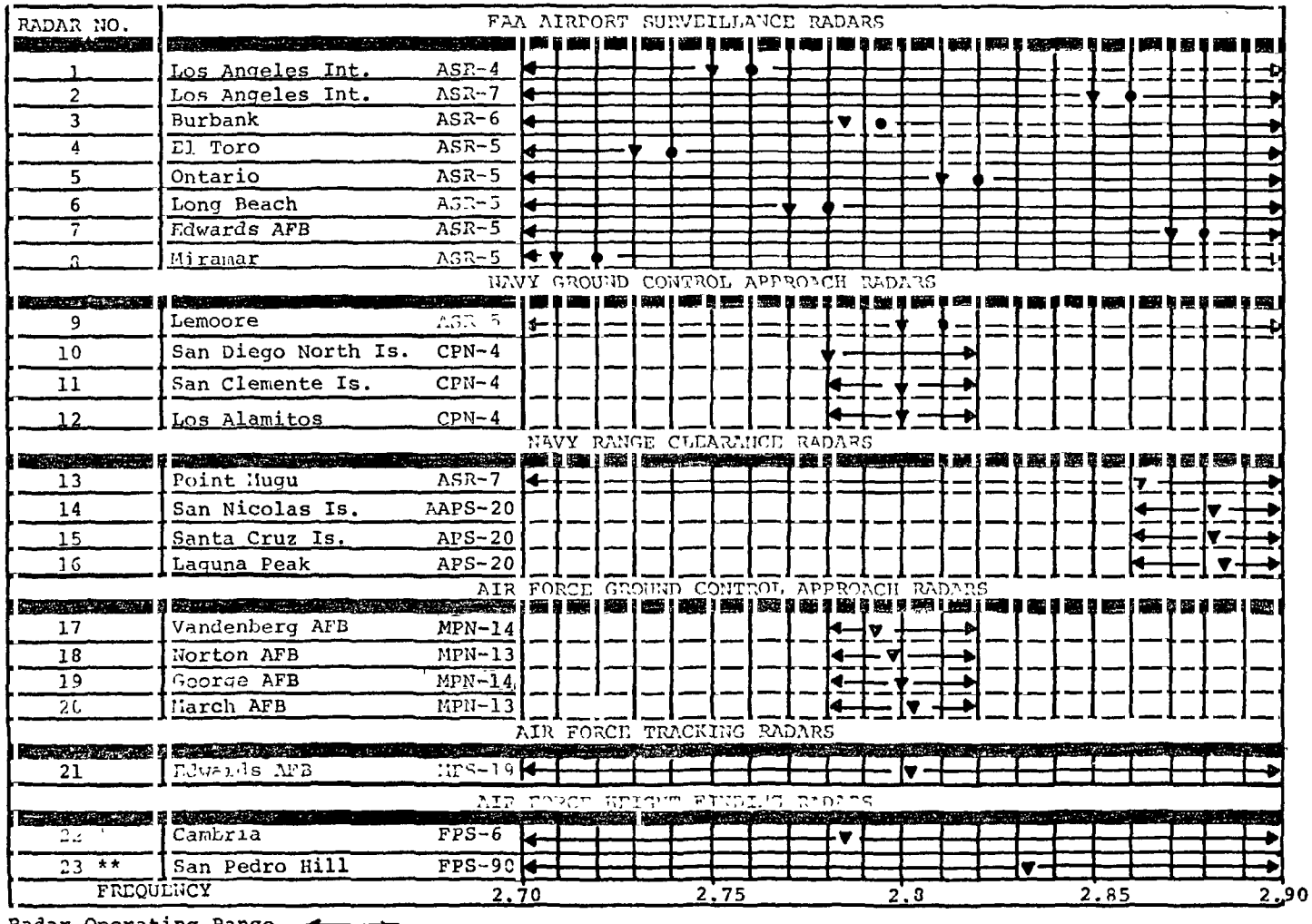

Radar Operating Range ◄——►
Assigned Frequency A ▼
Assigned Frequency B ●

* Magnitron Operating Range 2750-2860 MHz

** Magnitron Tuning Range 2700-2850 MHz

TABLE 4-4

INR For Victim Radar Mainbeam Coupling with the Interfering Radar Backlobe

VICTIM RECEIVER			INTERFERENCE RADAR			INR
RADAR NO.	CITY/BASE	NOMENCLATURE	RADAR NO.	CITY/BASE	NOMENCLATURE	
1	Los Angeles Int.	ASR-4	23	San Pedro	FPS-90	13.4
1	Los Angeles Int.	ASR-4	2	Los Angeles Int.	ASR-7	21.6
1	Los Angeles Int.	ASR-4	4	El Toro	ASR-5	9.4
1	Los Angeles Int.	ASR-4	6	Long Beach	ASR-5	12.3
2	Los Angeles Int.	ASR-7	1	Los Angeles Int.	ASR-4	21.9
2	Los Angeles Int.	ASR-7	15	Santa Cruz Is.	AN/APS-20	12.4
2	Los Angeles Int.	ASR-7	23	San Pedro Hill	AN/FPS-90	39.7
3	Burbank	ASR-6	14	El Toro	ASR-5	0.6
3	Burbank	ASR-6	6	Long Beach	ASR-5	8.7
3	Burbank	ASR-6	12	Los Alamitos	AN/CPN-4	8.5
4	El Toro	ASR-5	1	Los Angeles Int.	ASR-4	18.9
4	El Toro	ASR-5	3	Burbank	ASR-6	7.7
4	El Toro	ASR-5	6	Long Beach	ASR-5	4.8
4	El Toro	ASR-5	12	Los Alamitos	AN/CPN-4	14.7
4	El Toro	ASR-5	23	San Pedro Hill	AN/FPS-90	11.2
5	Ontario	ASR-5	18	Norton AFB	AN/MPN-15	12.2
5	Ontario	ASR-5	23	San Pedro Hill	AN/FPS-90	21.5
6	Long Beach	ASR-5	1	Los Angeles Int.	ASR-4	10.3
6	Long Beach	ASR-5	3	Burbank	ASR-6	11.8
6	Long Beach	ASR-5	4	El Toro	ASR-5	14.8
6	Long Beach	ASR-5	12	Los Alamitos	AN/CPN-4	50.7
6	Long Beach	ASR-5	23	San Pedro Hill	AN/FPS-90	27.1
7	Edwards AFB	ASR-5	21	Edwards AFB	AN/MPS-19	14.2
8	Miramar	ASR-5	4	El Toro	ASR-5	0.5
12	Los Alamitos	AN/CPN-4	6	Long Beach	ASR-5	25.5
12	Los Alamitos	AN/CPN-4	23	San Pedro Hill	AN/FPS-90	26.2
13	Point Mugu	ASR-7	15	Santa Cruz Is.	AN/APS-20	16.1
13	Point Mugu	ASR-7	16	Laguna Peak	AN/APS-20	50.8
14	San Nicolas Is.	AN/APS-20	15	Santa Cruz Is.	AN/APS-20	59.8
14	San Nicolas Is.	AN/APS-20	16	Laguna Peak	AN/APS-20	33.6
15	Santa Cruz Is.	AN/APS-20	14	San Nicolas Is.	AN/APS-20	57.8
15	Santa Cruz Is.	AN/APS-20	16	Laguna Peak	AN/APS-20	60.8

TABLE 4-4 Continued

INR For Victim Radar Mainbeam Coupling with the Interfering Radar Backlobe

VICTIM RECEIVER			INTERFERENCE RADAR			INR
RADAR NO.	CITY/BASE	NOMENCLATURE	RADAR NO.	CITY/BASE	NOMENCLATURE	
15	Santa Cruz Is.	AN/APS-20	23	San Pedro Hill	AN/FPS-90	0.8
16	Laguna Peak	AN/APS-20	13	Point Mugu	ASR-7	34.8
16	Laguna Peak	AN/APS-20	14	San Nicolas Is.	AN/APS-20	31.6
16	Laguna Peak	AN/APS-20	15	Santa Cruz Is.	AN/APS-20	50.8
17	Vandenberg AFB	AN/MPN-14	22	Cambria	AN/FPS-6	29.1
18	Norton AFB	AN/MPN-15	5	Ontario	ASR-5	19.4
20	March AFB	AN/MPN-13	5	Ontario	ASR-5	1.7
21	Edwards AFB	AN/MPS-6	7	Edwards AFB	ASR-5	21.4
21	Edwards AFB	AN/MPS-90	19	George AFB	AN/MPN-14	3.4
22	Cambria	AN/FPS-6	17	Vandenburg AFB	AN/MPN-14	29.9
23	San Pedro Hill	AN/FPS-90	2	Los Angeles Int.	ASR-7	19.3
23	San Pedro Hill	AN/FPS-90	5	Ontario	ASR-5	7.3
23	San Pedro Hill	AN/FPS-90	6	Long Beach	ASR-5	17.9
23	San Pedro Hill	AN/FPS-90	12	Los Alamitos	AN/CPN-4	21,6
23	San Pedro Hill	AN/FPS-90	15	Santa Cruz Is.	AN/APS-20	0.8

4.3.1 Preliminary Radar Site Measurements

The purpose of these measurements was to verify predicted interference situations to the extent that the live environment conditions and parameters used to predict the interference existed. This set of measurements was not comprehensive with the main objective to compare predicted interference with the live environment conditions for 11 victim radar sites. These measurements were made during normal operation of air traffic control.

During the preliminary radar site measurements, the victim radar's controls were set as follows:

MTI:	ON
NORMAL:	OFF
Stagger:	OFF
Integrator:	ON and OFF
Polarization:	Circular

FAA radars in the Los Angeles area operate in the MTI mode for full PPI scope range and with integrators on all the time. However, the radar receivers are generally aligned such that the integrator is used to enhance desired target returns, and not to suppress interference. Measurements made during the investigation show that radars with analog integrators (ASR-4, 5 and 6) did not suppress interference. However, the ASR-7 radar at Los Angeles International Airport, with a digital integrator, significantly suppressed the interference.

The following is a discussion of predicted and observed interference. The predicted interferers for each victim are listed in Table 4-4 with INR's $\geq$ 10 dB.

Los Angeles ASR-4 - Predicted interferers for the Los Angeles ASR-4 radar were:

Radar	Interferers Freq. (MHz)	Victim Freq. (MHz)	INR (dB)
San Pedro AN/FPS-90	2835	2758	13.4
Los Angeles ASR-7	2852	2758	21.6
Long Beach ASR-5	2772	2758	12.3

There was no identifiable interference from the Long Beach ASR-5 radar. However, interference was observed from the Los Angeles ASR-7 and San Pedro AN/FPS-90 radars at their respective bearings from the Los Angeles ASR-4. Interference from these two radars was infrequent and random, and was not periodic as predicted. The interfering strobes from the ASR-7 were approximately 5° wide. The interfering strobes from the AN/FPS-90 were 3° wide.

Los Angeles ASR-7 - Predicted interferers for the Los Angeles ASR-7 were:

Radar	Interferers Freq. (MHz)	Victim Freq. (MHz)	INR (dB)
Los Angeles ASR-4	2758	2852	21.9
San Pedro AN/FPS-90	2835	2858	39.7
Santa Cruz Is. AN/APS-20	2883	2858	12.4

Interference from the Los Angeles ASR-4 did appear on both channels of the ASR-7 at approximately the bearing of the Los Angeles ASR-4 radar. However, the interference was very infrequent and random in nature. Measurements made with the RSMS van indicate additional propagation loss due to building attenuation and also shielding of the backlobes of the ASR-4 antenna pattern due to foreground clutter, may be factors which contributed to the lack of predicted periodic interference. Interference was also observed on both channels from the San Pedro AN/FPS-90 radar. The interference was seen over sectors of 30° to 180° indicating that the interference was occurring when the height finder was nodding approximately in the direction of the Los Angeles ASR-7. Interference from the Santa Cruz Is. AN/APS-20 was not observed during the measurement period. It should also be noted that the ASR-7 is a digital radar which has the capability of suppressing interference when operating in the enhanced mode which is used 100% of the time on this radar.

Burbank ASR-6 - There were not any predicted interferers for the Burbank radar with an INR greater than 10 dB. However, frequent interference was observed from the San Pedro AN/FPS-90 radar (Predicted INR = -8.0 dB) when the Burbank radar was operating on both the low channel (2883 MHz) and the high channel (2893 MHz). The San Pedro radar is at a bearing of 182° from Burbank, but the interference was observed in a sector of 330° to 180°. Most of the interference from the

San Pedro radar occurred when the Burbank radar was pointing in the direction of a mountain range to the north and northeast of Burbank. This tended to indicate that the San Pedro signal was being reflected off the mountain range. Measurements were made with the RSMS van to verify this multipath phenomena and are discussed in Appendix D.

Ontario ASR-5 --Predicted interferers for the Ontario ASR-5 were:

Radar	Interferers Freq. (MHz)	Victim Freq. (MHz)	INR (dB)
Norton AN/MPN-13	2801	2810	12.5
San Pedro AN/FPS-90	2835	2818	21.5

A few interfering strobes were identified from the Norton AN/MPN-13 radar at approximately 66°, the bearing of the Norton radar, when the Ontario ASR-5 was operating on the low channel (2810 MHz). However, these strobes were infrequent and only occurred in a 2° sector. During these measurements, the San Pedro AN/FPS-90 radar was not operating. Therefore, potential interference from the AN/FPS-90 was not verified during these measurements.

Long Beach ASR-5 - Predicted interferers for the Long Beach ASR-5 were:

Radar	Interferers Freq. (MHz)	Victim Freq. (MHz)	INR (dB)
Los Angeles ASR-4	2758	2772	10.3
El Toro ASR-5	2738	2772	14.8
San Pedro AN/FPS-90	2835	2777	27.1
Burbank ASR-6	2788	2777	11.8
Los Alamitos AN/CPN-4	2801	2777	50.7

Identifiable interference from the Los Angeles ASR-4 and El Toro ASR-5 radars was not observed on the PPI display while the Long Beach radar was operating on the low channel. Interference from the San Pedro AN/FPS-90 was observed on both radar channels. The interference from the San Pedro AN/FPS-90 would appear over 30° sectors randomly over the PPI display and not always at the bearing of the height finder. These

30° sectors of interference were most likely occurring when the height finder was nodding in the direction of Long Beach. Interference from the Burbank ASR-6 was also observed at the bearing of the Burbank radar (319°) on both radar channels. The interference from the Burbank radar appeared on the PPI display approximately 1 out of 5 scans and covered approximately a 3° sector. Interference from Los Alamitos AN/CPN-4 radar was only observed on the Long Beach high channel and was infrequent. When the interference was observed, it appeared over a 10° sector. Interference to the Long Beach radar is discussed in more detail in Appendix E.

El Toro ASR-5 - Predicted interferers for the El Toro ASR-5 were:

Radar	Interferers Freq. (MHz)	Victim Freq. (MHz)	INR (dB)
Los Angeles ASR-4	2752	2738	18.9
Los Alamitos AN/CPN-4	2801	2738	14.8
San Pedro AN/FPS-90	2835	2738	11.2

The El Toro PPI display was observed for one hour during which there was no observed interference.

Los Alamitos AN/CPN-4 - Predicted interferers for the Los Alamitos AN/CPN-4 were:

Radar	Interferers Freq. (MHz)	Victim Freq. (MHz)	INR (dB)
San Pedro AN/FPS-90	2835	2801	25.5
Long Beach ASR-5	2777	2801	26.2

Interference was observed from the San Pedro AN/FPS-90. When the height finder was not nodding in the direction of Los Alamitos, the interference from the San Pedro AN/FPS-90 radar covered approximately a 5° sector. When the height finder was nodding in the direction of Los Alamitos, the interference covered approximately 3/4 of the PPI display. The interference from the San Pedro radar was of a periodic nature. During the measurements at Los Alamitos, interference from the Long Beach ASR-5 was not identified. However, interference was identified from three unpredicted radars: Ontario ASR-5, Norton AN/MPN-13,

and March AN/MPN-13. Interference from these radars was caused by multipathing of the interfering signal through a mountain range between the victim and interfering radars. The interference from these radars was frequent and appeared blurred on the PPI display due to the multipathing phenomena. Measurements documenting the multipath phenomena were made and are discussed in Appendix A. A more detailed discussion of the interference at this site is given in Appendix E.

San Nicolas Is. AN/APS-20 - Predicted interferers for the San Nicolas Is. AN/APS-20 radar were:

Radar	Interferers Freq. (MHz)	Victim Freq. (MHz)	INR (dB)
Santa Cruz Is. AN/APS-20	2883	2882	59.8
Laguna Peak AN/APS-20	2886	2882	33.6

Interference from the Santa Cruz and Laguna Peak AN/APS-20 radars was observed on the San Nicolas Is. AN/APS-20 PPI display. The interference from the two radars covered most of the PPI display as predicted. The AN/APS-20 radars are used at the Point Mugu NAS as missile range surveillance radars and DOD is able to perform their missions with heavy interference on the PPI display.

Santa Cruz.Is. AN/APS-20 - Predicted interferers for the Santa Cruz AN/APS-20 radar were:

Radar	Interferers Freq. (MHz)	Victim Freq. (MHz)	INR (dB)
San Nicolas Is. AN/APS-20	2882	2883	57.8
Laguna Peak AN/APS-20	2886	2883	60.8

Interference from the San Nicolas and Laguna Peak AN/APS-20 radars was observed on the Santa Cruz Is. AN/APS-20 PPI display. The interference from the two radars covered most of the PPI display as predicted.

Laguna Peak AN/APS-20 - Predicted interferers for the Laguna Peak AN/APS-20 radar were:

Radar	Interferers Freq. (MHz)	Victim Freq. (MHz)	INR (dB)
Point Mugu ASR-7	2862	2886	34.8
San Nicolas AN/APS-20	2862	2886	31.6
Santa Cruz AN/APS-20	2383	2886	50.8

Interference was observed from the three predicted interferers. The interference from each of the predicted interferers covered most of the PPI display as was predicted. The AN/APS-20 radars at Point Mugu will be replaced, by March 1976, with the AN/FPS-114 radar which operates in the 2890-3110 MHz band. The AN/FPS-114 radars most likely will not be operating in the 2.7-2.9 GHz band.

Norton MPN-13 - Predicted interferers for the Norton AFB AN/MPN-13 radar were:

Radar	Interferers Freq. (MHz)	Victim Freq. (MHz)	INR (dB)
Ontario ASR-5	2810	2800	19.4

Interference was observed from the Ontario ASR-5 radar. However, it was not at the bearing of the Ontario ASR-5 radar (246.6°). The interference came in at bearings from between 285° to 10° magnetic. It was not determined whether the interference randomly coupled in through the Norton AN/MPN-13 antenna backlobe from the Ontario ASR-5 mainbeam or was being coupled in by reflections off the San Bernadino Mountains. One factor which may have contributed to unpredicted random interference is that the Norton AN/MPN-13 antenna has a tilt angle of 4.25° which was assigned by the FAA. This increase in antenna tilt angle will cause about 3 dB decrease in mainbeam gain.

San Pedro AN/FPS-90 - Predicted interferers for the San Pedro AN/FPS-90 radar were:

Radar	Interferers Freq. (MHz)	Victim Freq. (MHz)	INR (dB)
Los Angeles ASR-7	2852	2835	19.3
Long Beach ASR-5	2777	2835	17.9
Los Alamitos AN/CPN-4	2801	2835	21.6

The AN/FPS-90 only has a dicke fix operating mode. Interference was observed from the Los Angeles ASR-7 when the height finder is nodding at bearings of 320°-345°. The interference appears on each nod at low elevation angles of the radar antenna. Interference from the Long Beach ASR-5 was not positively identified on the RHI display. However, an unidentified interference source was observed on one occasion. The preliminary site visit to the AN/FPS-90 was made on a Saturday when the Los Alamitos AN/CPN-4 radar is normally shut down. Therefore, potential interference from the Los Alamitos AN/CPN-4 could not be verified.

4.3.2 Summary of Observed and Predicted Interference

For the 11 radar sites visited during the preliminary radar site measurements, there were 27 predicted interference cases of mainbeam-to-backlobe coupling. The total number of actual observed interference cases during the preliminary site visits was 21. Of the 21 observed cases, there were 17 predicted and 4 unpredicted. Therefore, 63 percent of the predicted interferers were observed on the victim PPI display, and 19% of the observed interferers were unpredicted. The 4 unpredicted cases were due to multipath phenomena. Most of the predicted interference cases that were observed were not of the periodic nature that was predicted. Therefore, in general, most of the predicted interference was pessimistic when compared to the actually observed interference.

It was estimated that in most cases the predicted interfering signal power levels were approximately 10 to 20 dB too high. The difference between predicted and actual interference signal power level can be generally attributed to the statistical nature and bias associated with the antenna and propagation related variables not included in the models. Based on measurements made during the Los Angeles investigation and information obtained from a literature search, empirical modifications to the antenna and propagation model were made and incorporated in the interference prediction technique used in the San Francisco investigation. These empirical correction factors to the models are discussed in detail in Section 5 and Appendices A, B and D.

4.4 ENVIRONMENTAL OBSERVATIONS

It is difficult to make a quantitative assessment of the degree of congestion in the Los Angeles area without the establishment of controller performance-keyed PPI degradation criteria. PPI degradation test programs are currently being

conducted by ECAC at Calspan (Reference 15) and FAA at NAFEC (Reference 16). An informal working group consisting of OT, ECAC and the FAA has been established for this task. The fact that 10 of 11 radar sites visited had some form of interference on the PPI display indicates that potential congestion does exist. Considering all factors, it appears that frequency assignments for the 2.7-2.9 GHz band radars deployed in the Los Angeles area at the time of the investigation are engineered to the extent possible to provide satisfactory air traffic control operating conditions.

Information on planned deployment changes in the 2.7 to 2.9 GHz band in the Los Angeles area was obtained from the various government agencies (References 48 through 50), and is given in Table 4-5. The AN/APS-20 radars used as range clearance radars are planned for removal by March 1976. These range clearance radars are planned to be replaced by AN/FPS-114 radars which operate in the 2890-3100 MHz band, and most likely will not operate close to the 2.7-2.9 GHz band. There are three radars planned for replacement by AN/GPN-12 radars which are identical to an ASR-7. Also, there are three radars scheduled to be replaced by ASR-8 radars which have a dual frequency diversity capability. The ASR-5 radar planned for replacement at Long Beach by an ASR-8 will be relocated at Palm Springs. The height finding radars (AN/FPS-6, 90), planned for deployment in the area at Mt. Laguna and Paso Robles, are scheduled to be part of the joint FAA/DOD surveillance system. The height finding radar at Cambria is planned to be phased out once the joint FAA/DOD surveillance system becomes operational.

The FAA has indicated that due to ducting problems from the Miramar radar, the lower portion of the band cannot be utilized in the Los Angeles area. When assigning frequencies to the new dual frequency diversity radars (ASR-8) planned as replacement units at San Clemente Island and North Island, the ducting phenomena will also have to be taken into consideration. Another factor required for consideration in making frequency assignments is the reported decrease in conventional magnetron tube lifetime when the radars operate at the band edges of the 2.7-2.9 GHz band.

Taking into consideration the above frequency assignment factors needed to be considered, the information obtained during the measurement program, and the known planned environment changes listed in Table 4-5, it is apparent that a detailed Spectrum Resource Assessment of the 2.7 to 2.9 GHz band in the Los Angeles area is required. Accommodation of these planned deployments in the 2.7 to 2.9 GHz band in the Los Angeles area

TABLE 4-5

PLANNED ENVIRONMENT CHANGES IN THE LOS ANGELES AREA BY FY 84

CITY/BASE	LATITUDE/ LONGITUDE	AGENCY	ACTION	PRESENT RADAR	PLANNED RADAR	DATE
Long Beach	33 49 09 118 08 16	FAA	Replace	ASR-5	ASR-8 *	FY 76
Palm Springs	33 49 00 116 31 00	FAA	New	None	ASR-5	FY 76
San Nicolas Is.	33 14 59 119 31 16	Navy	Remove	AN/APS-20	None	FY 76
Santa Cruz Is.	33 59 40 119 37 56	Navy	Remove	AN/APS-20	None	FY 76
Laguna Peak	34 06 28 119 03 51	Navy	Remove	AN/APS-20	None	FY 76
San Clemente Is.	33 01 02 118 35 05	Navy	Replace	AN/CPN-4	ASR-8 *	FY 81
San Diego North Is.	32 41 48 117 12 45	Navy	Replace	AN/CPN-4	ASR-8 *	FY 78
George AFB	34 35 54 117 23 02	Air Force	Replace	AN/MPN-13	AN/GPN-12	FY 77
March AFB	33 53 04 117 15 34	Air Force	Replace	AN/MPN-13	AN/GPN-12	FY 77
Vandenberg AFB	34 43 42 120 34 31	Air Force	Replace	AN/MPN-13	AN/GPN-12	FY 78
Mt. Laguna	32 52 32 116 24 51	Air Force	New	None	AN/FPS-6,90	
Paso Robles	35 23 42 120 21 12	Air Force	New	None	AN/FPS-6,90	
Cambria	35 31 21 121 03 46	Air Force	Remove	AN/FPS-6	None	

* Frequency Diversity Capability

to assess potential congestion will be studied in detail in a subsequent OT report.

SECTION 5

SAN FRANCISCO AREA INVESTIGATION

5.1 INTRODUCTION

This section discusses the investigation and measurement program conducted by OT in the San Francisco area to assess the capability and techniques used to predict radar-to-radar interference, and to make refinements to the prediction model. The investigation was made during the period of August to December 1975 with measurements being conducted from November 3 to November 17, 1975. The environment included all radar deployments in the 2.7 to 2.9 GHz band within 200 statute miles of San Francisco. Included in this section is a comparison between predicted and actual observed interference at eight radar sites visited in the San Francisco area, and environmental observations. A detailed comparison of the measured data taken during the investigation with the various component models used to predict radar-to-radar interference is given in Appendices A through E.

5.2 ENVIRONMENT OF 2.7-2.9 GHz BAND

The environment for the San Francisco area was determined from two sources: 1) Western Region FAA Frequency Manager (Reference 51), and 2) Government Master File (GMF). Comparison was made of the environmental lists received from the two sources, and differences resolved by contact with the area frequency coordinator. It was determined that there are a total of 21 radars within a 200 mile radius of San Francisco operating in the 2.7 to 2.9 GHz band. Table 5-1 lists the location, nomenclature and function of these radars. Figure 5-1 shows the location of these radars on a San Francisco area map. The equipment characteristics of the radars are given in Table 5-2.

During this San Francisco area investigation, the RSMS van was used to verify the frequency assignments obtained from the area coordinators. All the radars in the area were found to be operating within a few megahertz of their assigned frequency. However, the operation of a radar not listed in the GMF or the FAA area coordinator list was discovered. An actual site visit verified the operation of an AN/FPS-90 at Mt. Tamalpais by the Air Force.

All the radars in the San Francisco environment employ a tunable conventional magnetron output tube with the exception

TABLE 5-1

LOCATION OF 2.7-2.9 GHz RADARS
IN SAN FRANCISCO AREA

RADAR NO.	CITY/BASE	NOMENCLATURE	LATITUDE	LONGITUDE
	Present FAA	Airport Surveillance Radars		
1	Monterey	ASR-3	36 35 16	121 50 09
2	Fresno	ASR-4	36 46 51	119 43 06
3	Sacramento *	ASR-4	38 39 56	121 24 14
4	Mountain View **	ASR-5	37 25 38	122 00 50
5	Marysville	ASR-5	39 07 49	121 27 35
6	Oakland	ASR-7	37 42 23	122 13 27
	Present	Navy Ground Control Approach Radars		
7	Lemoore	ASR-5	36 20 44	119 54 18
8	Vallejo	MPN-5	38 05 06	122 16 52
9	Alameda	MPN-11	37 47 23	122 19 20
	Present	Navy Tracking Radars		
10	Monterey	APS-20	36 35 52	121 52 25
	Present	AF GCA Radars		
11	Travis AFB	FPN-55	38 16 08	121 54 58
12	Castle AFB	FPN-47	37 22 34	120 33 03
13	Mather AFB	MPN-13	38 33 51	121 17 19
14	Beale AFB	MPN-15	39 08 12	121 26 00
15	Hayward ANG	MPN-13	37 40 00	122 07 00
	Present	AF Height Finding Radars		
16	Cambria	FPS-6	35 31 21	121 03 46
17	Almaden	MPS-14	37 09 38	121 53 47
18	Almaden	FPS-90	37 09 38	121 53 47
19	Point Arena	FPS-90	38 53 19	123 32 55
20	Mt. Tamalpais	FPS-90	37 55 45	122 35 20
	Present	NOAA Weather Radars		
21	Sacramento	WSR-57	38 35 00	121 29 00

* Joint FAA-AF use
** Joint FAA-N use

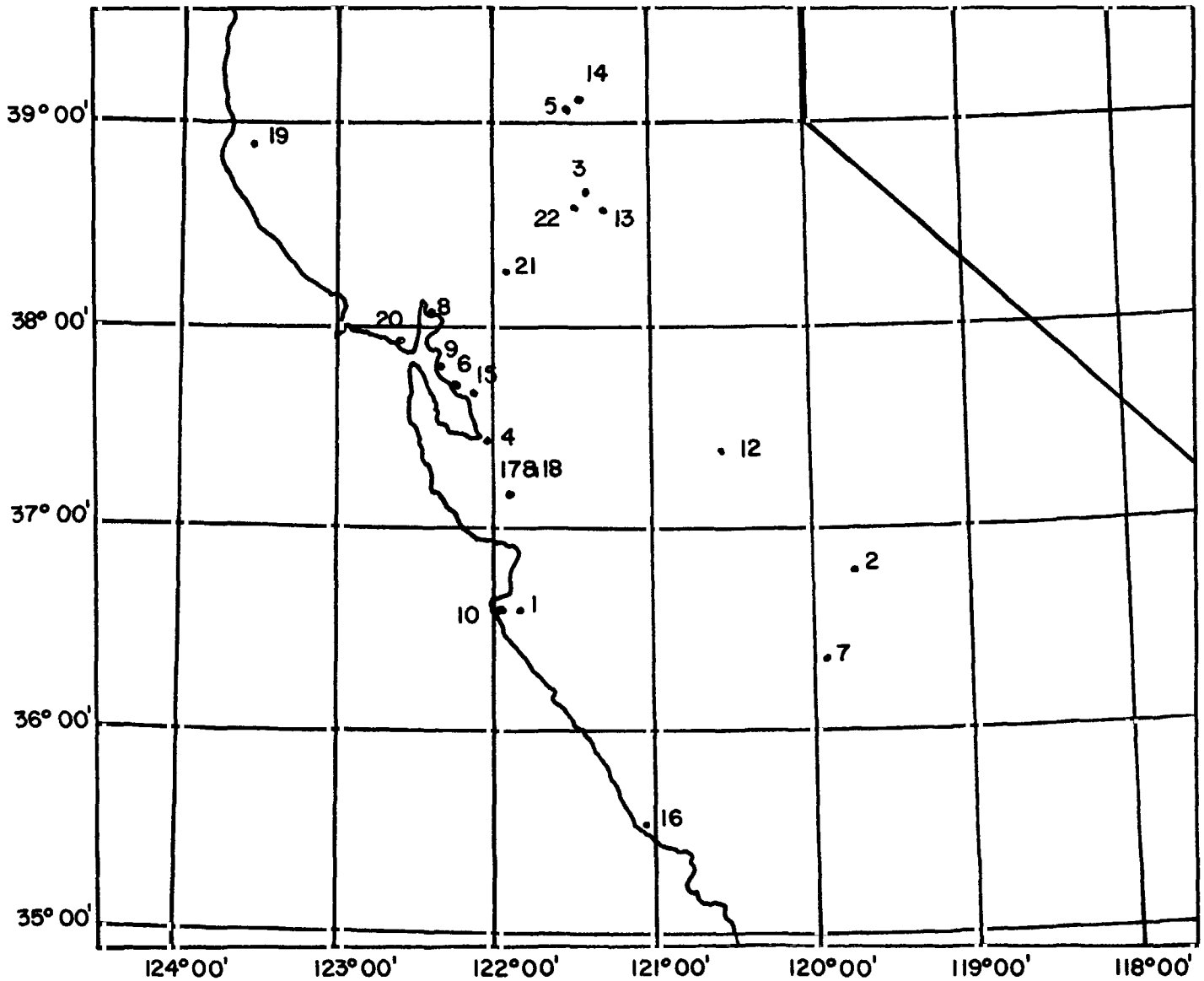

Figure 5-1. Location of Radars in the 2.7-2.9 GHz Band in the San Francisco Area

TABLE 5-2

CHARACTERISTICS OF 2.7-2.9 GHz RADARS IN SAN FRANCISCO AREA

RADAR NO.	CITY/BASE	EQUIPMENT NOMENCLATURE	ASSIGNED FREQUENCY (MHz)	PEAK POWER (KW)	OUTPUT TUBE TYPE	P.W. (μS)	PRF (PPS)	IF Bw (MHz)	NOISE LEVEL (dBm)	ANT. GAIN (dB)	ANT. HGT. (Ft.)	ANT. TILT ANGLE	ANTENNA SCAN RATE (RPM)	SCOPE RANGE (NM)	SITE ELV. (FT.)
1	Monterey	ASR-3	2850-2860	500	5586+	1.0	1185	2.0	-107	34	30		15	60	254
2	Fresno	ASR-4	2850-2860	425	5586+	.833	840	2.7,5*	-106	34	30		13	60	332
3	Sacramento	ASR-4	2860-2870	425	5586+	.833	810	2.7,5*	-106	34	26	3.0°	15	60	79
4	Mountain View	ASR-3	2750-2760	400	DX276+	.833	1125	2.7,5*	-106	34	26	3.0°	15	60	9
5	Marysville	ASR-5	2840-2850	400	5586+	.833	830	2.7,5*	-106	34	26		13	60	95
6	Oakland	ASR-7	2720-2730	400	DX276+	.833	stag-gered 1002	2.7,5*	-105	34	26	3.0°	15	60	9
7	Lemoore	ASR-5	2800-2810	400	5586	.833	700	2.7,5*	-106	34	35		13	60	235
8	Vallejo	AN/MPN-5	2800	350		.8	1100	1.5	-100	33	14		15 or 30	50	5
9	Alameda	AN/MPN-11	2800	600	5586	.5	1500	2.25	-102	33	14	3.5°	20	30	15
10	Monterey	AN/APS-20	2880	750		2.0	300	1.0	-111	30	30*		10	200	46

* Normal and MTI IF Bw, respectively

+ FAA ASR radars may use 5586, DX276 or QK1643

TABLE 5-2 Continued

CHARACTERISTICS OF 2.7-2.9 GHz RADARS IN SAN FRANCISCO AREA

RADAR NO.	CITY/BASE	EQUIPMENT NOMENCLATURE	ASSIGNED FREQUENCY (MHz)	PEAK POWER (KW)	OUTPUT TUBE TYPE	P.W. (μS)	PRF (PPS)	IF Bw (MHz)	NOISE LEVEL (dBm)	ANT. GAIN (dB)	ANT. HGT. (Ft.)	ANT. TILT ANGLE	ANTENNA SCAN RATE (RPM)	SCOPE RANGE (NM)	SITE ELV. (FT.)
11	Travis AFB	AN/FPN-55	2800	400	8798	.833	900	2.7,5*	-102	34	26	4.25°	13	60	68
12	Castle AFB	AN/FPN-47	2825	400	5586	.833	900	2.7,5*	-106	34	26	4.0°	15	60	130
13	Mather AFB	AN/MPN-13	2800	750	5586	.7	1100	2.26	-106	32	14	5.5°	15	30	70
14	Beale AFB	AN/MPN-15	2800	750		.7	1100	2.26	-106	32	14*	5.5°	15	30	98
15	Hayward ANG	AN/MPN-13	2800	750	8798	.7	1100	2.26	-106	32	14	3.75°	15	30	46
16	Cambria	AN/FPS-6	2785	5000	6410A	2.0	328	1.0	-106	39	45	N.A.	7.5 RP 20-30CI	200	790
17	Almaden	AN/MPS-14	2793	5000	QK327A	2.0	275	1.0	-106	39	50	N.A.	7.5 RP 20-30CI	200	3139
18	Almaden	AN/FPS-90	2780	5000	QK327A	2.0	275	1.0	-106	39	50	N.A.	7.5 RP 20-30CP	200	3539
19	Point Arena	AN/FPS-90	2805	5000	QK327A	2.0	328	1.0	-106	39	39	N.A.	7.5 RP 20-30CP	200	3379
20	Mt. Tamalpais	AN/FPS-90	2740	5000	QK327A	2.0	356	1.0	-106	39		N.A	7.5 RP 20-30CP	200	2604
21	Secramento	ASR-57	2890	500	QK729	0.5 4.0	545 164	4.5 0.75	-100 -108	36	258	N.A.	-5to45° Ely. C-5	250	20

* Normal and MTI IF Bw respectively.

of radars 10, 16 and 21 which employ fixed magnetron output tubes. Table 5-3 shows the operational frequency range, and the assigned frequency of the radars in the San Francisco environment. Additional information on the magnetron tube employed in each radar, and the magnetron tuning range is discussed in Appendix B.

5.3 COMPARISON OF PREDICTED AND OBSERVED INTERFERENCE

The following is a comparison of the interference that was observed during the 2.7-2.9 GHz spectrum resource assessment measurement program in the San Francisco area and predicted interference. The San Francisco area measurement plan consisted of a two-phase investigation similar to the investigation conducted in the Los Angeles area.

The first phase involved preliminary radar measurements which consisted of on-site verification of predicted interference. Potential interference situations in the San Francisco area were determined by calculating the INR at the victim radar receiver IF output using Equation 3-1 with the following empirical correction factors:

1. G_{T_i} = -13 dBi, based on measurements made in the Los Angeles investigation.

2. $L_{P_{ij}}$ = RAPIT point-to-point model plus correction factor for building and structure attenuation (discussed in Appendix D).

3. I_i = Insertion loss of both victim and interfering radar. A 2 dB insertion loss was used at both ends (Reference 31).

The above modifications to the INR calculation procedure are discussed in detail in Appendices A and D. Table 5-4 shows the predicted radar coupling situations in the San Francisco environment where the calculated INR was greater than 0 dB. For dual channel radars (FAA ASR radars), only worst case (minimum frequency separation for dual channel radars) INR's are shown in this Table. As in the Los Angeles investigation, the actual predicted interference situations are those cases listed in Table 5-4 when the INR > 10 dB. Also, as in the Los Angeles investigation, the PPI Simulation Program was run to determine the form of the interference on the victim PPI display.

The second phase of the San Francisco area investigation was similar to the Los Angeles area investigation. The RSMS

TABLE 5-3

FREQUENCY ASSIGNMENT INFORMATION OF 2.7-2.9 GHz RADARS IN SAN FRANCISCO AREA

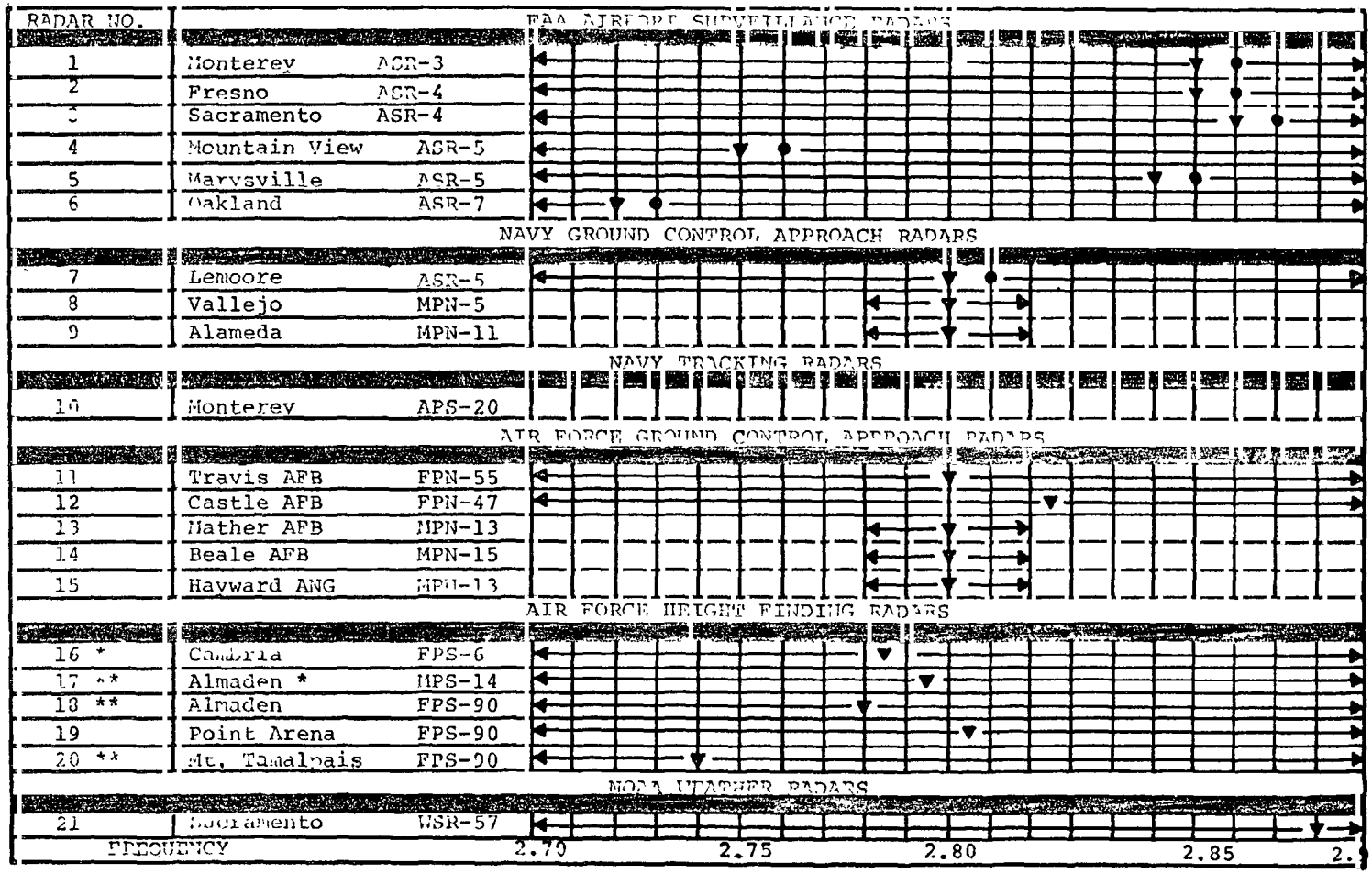

Radar Operating Range ←——→
Assigned Frequency A ▼
Assigned Frequency B ●

* Magnitron Operating Range 2750-2860 MHz

** Magnitron Tuning Range 2700-2850 MHz

TABLE 5-4

INR For Victim Radar Mainbeam Coupling with the Interfering Radar Backlobe

VICTIM RECEIVER			INTERFERENCE RADAR			INR
RADAR NO.	CITY/BASE	NOMENCLATURE	RADAR NO.	CITY/BASE	NOMENCLATURE	
1	Monterey	ASR-3	10	Monterey	AN/APS-20	18
3	Sacramento	ASR-4	21	Sacramento(.5μs)	WSR-57	30
3	Sacramento	ASR-4	21	Sacramento(4μs)	WSR-57	21
4	Mountain View	ASR-5	17	Almaden	AN/MPS-14	22
4	Mountain View	ASR-5	18	Almaden	AN/FPS-90	32
4	Mountain View	ASR-5	20	Mt. Tamalpais	AN/FPS-90	23
5	Marysville	ASR-5	14	Beale AFB	AN/MPN-15	30
6	Oakland	ASR-7	9	Alameda	AN/MPN-11	0
6	Oakland	ASR-7	20	Mt. Tamalpais	AN/FPS-90	38
8	Vallejo	AN/MPN-5	9	Alameda	AN/MPN-11	1
9	Alameda	AN/MPN-11	8	Vallejo	AN/MPN-5	7
9	Alameda	AN/MPN-11	15	Hayward	AN/MPN-13	33
9	Alameda	AN/MPN-11	17	Almaden	AN/MPS-14	21
9	Alameda	AN/MPN-11	18	Almaden	AN/FPS-90	9
10	Monterey	AN/APS-20	1	Monterey	ASR-3	22
11	Travis AFB	AN/FPN-55	8	Vallejo	AN/MPN-5	1
11	Travis AFB	AN/FPN-55	13	Mather AFB	AN/MPN-13	26
13	Mather AFB	AN/MPN-13	11	Travis AFB	AN/FPN-55	21
13	Mather AFB	AN/MPN-13	14	Beale AFB	AN/MPN-15	10
14	Beale AFB	AN/MPN-15	11	Travis AFB	AN/FPN-55	1
14	Beale AFB	AN/MPN-15	13	Mather AFB	AN/MPN-13	10
14	Beale AFB	AN/MPN-15	5	Marysville	ASR-5	30
15	Hayward ANG	AN/MPN-13	17	Almaden	AN/MPS-14	15
17	Almaden	AN/MPS-14	4	Mountain View	ASR-5	0
17	Almaden	AN/MPS-14	9	Alameda	AN/MPN-11	20
17	Almaden	AN/MPS-14	15	Hayward	AN/MPN-13	25
17	Almaden	AN/MPS-14	20	Mt. Tamalpais	AN/FPS-90	7
18	Almaden	AN/FPS-90	6	Oakland	ASR-7	4
18	Almaden	AN/FPS-90	15	Hayward ANG	AN/MPN-13	16
18	Almaden	AN/FPS-90	9	Alameda	AN/MPN-11	13
18	Almaden	AN/FPS-90	20	Mt. Tamalpais	AN/FPS-90	0

TABLE 5-4 (Continued)

INR For Victim Radar Mainbeam Coupling with the Interfering Radar Backlobe

VICTIM RECEIVER			INTERFERENCE RADAR			INR
RADAR NO.	CITY/BASE	NOMENCLATURE	RADAR NO.	CITY/BASE	NOMENCLATURE	
20	Mt. Tamalpais	AN/FPS-90	4	Mountain View	ASR-5	23
20	Mt. Tamalpais	AN/FPS-90	6	Oakland	ASR-7	14
20	Mt. Tamalpais	AN/FPS-90	17	Almaden	AN/MPS-14	11
20	Mt. Tamalpais	AN/FPS-90	18	Almaden	AN/FPS-90	17
21	Sacramento(4μs)	WSR-57	3	Sacramento	ASR-4	14
21	Sacramento(.5μs)	WSR-57	3	Sacramento	ASR-4	6

van instrumentation was used to determine why predicted interference did not appear on the victim PPI display or why unpredicted interference appeared on the PPI display. The detailed measurements made during the second phase of the measurement program are discussed in Appendices A through E. Appendix E gives a detailed discussion of the predicted and observed interference at two radar sites using the measured data discussed in Appendices A through D to explain the differences between predicted and observed interference. Appendix F gives a general outline of the measurement plan, and Appendix G discusses the RSMS instrumentation used in the San Francisco area radar measurements.

5.3.1 Preliminary Radar Site Measurements

The purpose of these measurements was to verify predicted interference situations to the extent that the live environment conditions and parameters used to predict the interference existed. This set of measurements was not comprehensive with the main objective to compare predicted interference with the live environment conditions for 8 victim radar sites. These measurements were made during normal operation of air traffic control.

During the preliminary radar site measurements, the victim radar's controls were set as follows:

MTI:	ON
NORMAL:	OFF
Stagger:	OFF
Integrator:	ON and OFF
Polarization:	Linear and Circular

FAA radars in the San Francisco area operate in the MTI mode for full PPI scope range and with integrators on all the time. The stagger was turned off on the victim radar so that the AS-330 pulse train separator could be used to identify the interfering radars by PRF. The following is a discussion of the predicted and observed interference. The predicted interferers for each victim are listed in Table 5-4 with INR's $\geq$ 10 dB.

Sacramento ASR-4 - Predicted interferers for the Sacramento ASR-4 radar were:

Radar	Interferer Freq. (MHz)	Victim Freq. (MHz)	INR (dB)
Sacramento WSR-57	2837	2868	30 * 21 **

* For .5 μsec mode of WSR-57
** For 4.0 μsec mode of WSR-57

With the WSR-57 antenna set at normal operating elevation (1 degree), interference from the Sacramento WSR-57 was observed on the Sacramento ASR-4 PPI display for both the 4.0 and 0.5 μsec pulse width operating modes of the WSR-57. The WSR-57 radar was located at a bearing of 200°. Interference from the WSR-57 radar was heavier for antenna coupling of the interferer mainbeam to the victim backlobe, than for antenna coupling of the victim mainbeam to the backlobe of the interferer. This was due to the higher antenna mainbeam gain of the WSR-57 radar than the ASR-4 radar; taking into consideration the antenna tilt angles, the mainbeam gains are 33 dBi and 27 dBi, respectively. Also, the much slower rotation rate of the WSR-57 antenna caused the interference to be heavier for antenna coupling of the mainbeam of the interfering radar with the backlobe of the victim radar. Because of the higher emission spectrum skirt levels of the WSR-57 radar when operating in the 0.5 μsec mode, the interference was greater when the WSR-57 was operating in the 0.5 μsec pulse width mode than in the 4.0 μsec pulse width mode. The 0.5 μsec pulse width mode of the WSR-57 radar caused interference wedges of 10° to 90°, and the 4.0 μsec pulse width mode caused interference wedges of 10° to 40°. The predicted and observed interference for 0.5 μsec pulse width mode of the WSR-57 radar is shown in Figure 5-2 and Figure 5-3, respectively. Figure 5-4 and Figure 5-5 show the predicted and observed interference for the 4.0 μsec pulse width mode of the WSR-57 radar.

Mountain View ASR-5 - Predicted interferers for the Mountain View ASR-5 radar were:

Radar	Interferer Freq. (MHz)	Victim Freq. (MHz)	INR (dB)
Almaden AN/FPS-90	2778	2758	32
Almaden AN/MPS-14	2793	2758	22
Mt. Tamalpais	2737	2754	23

Interference was observed from the Almaden and Mt. Tamalpais AN/FPS-90 radars on both channels of the Mountain View radar. Because of the alternating monthly operating procedure of the Almaden AN/MPS-14 and AN/FPS-90, potential interference from the AN/MPS-14 could not be verified. Interference from the Almaden AN/FPS-90 appeared on approximately every sweep of the victim radar at the interferer bearing of 144°. The interference from the Almaden radar usually appeared as a 3° to 40° wedge of interference. Interference from the Mt. Tamalpais

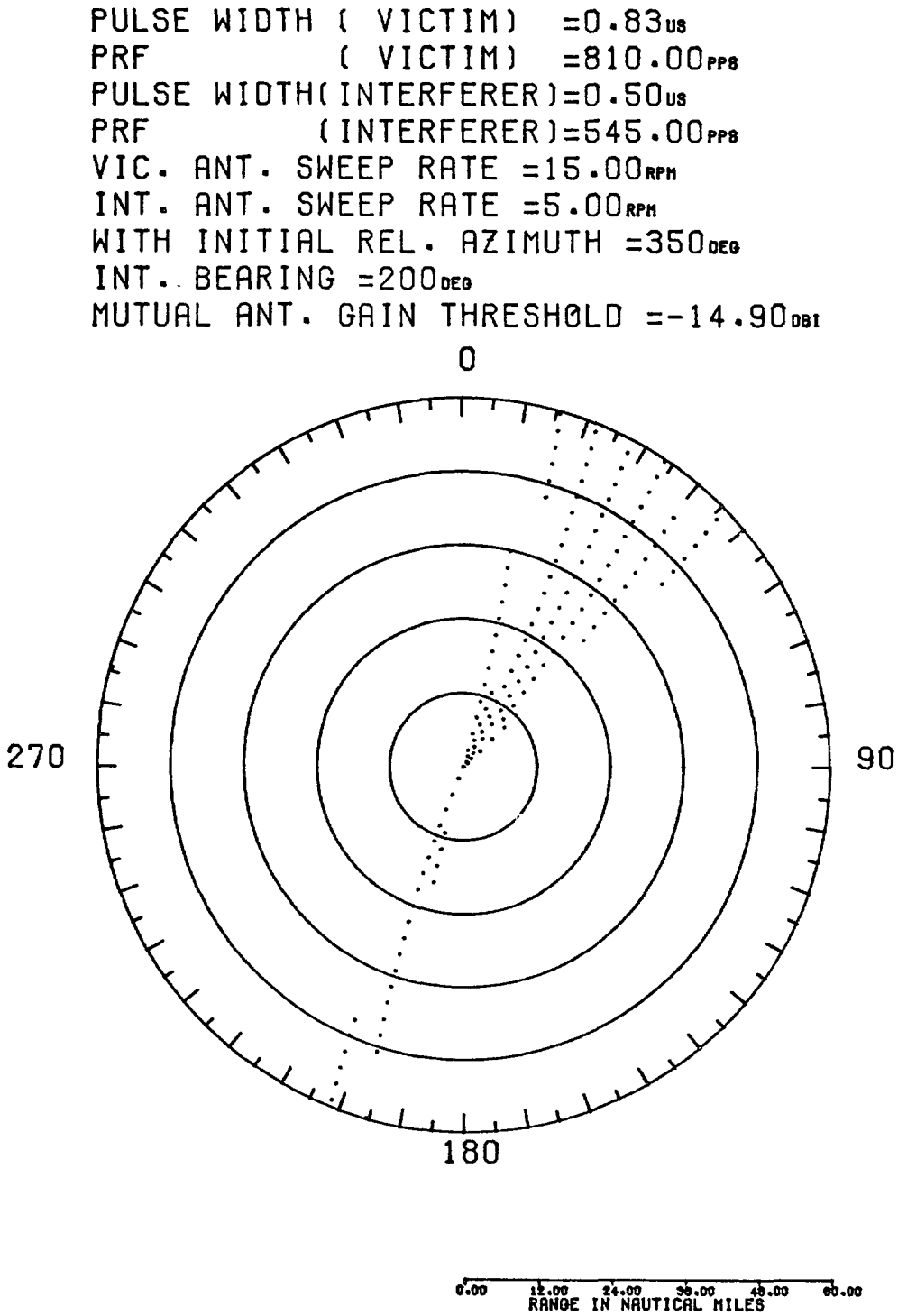

Figure 5-2. Simulated PPI display of Sacramento ASR-4 With Sacramento WSR-57 (0.5 μsec mode) Interference.

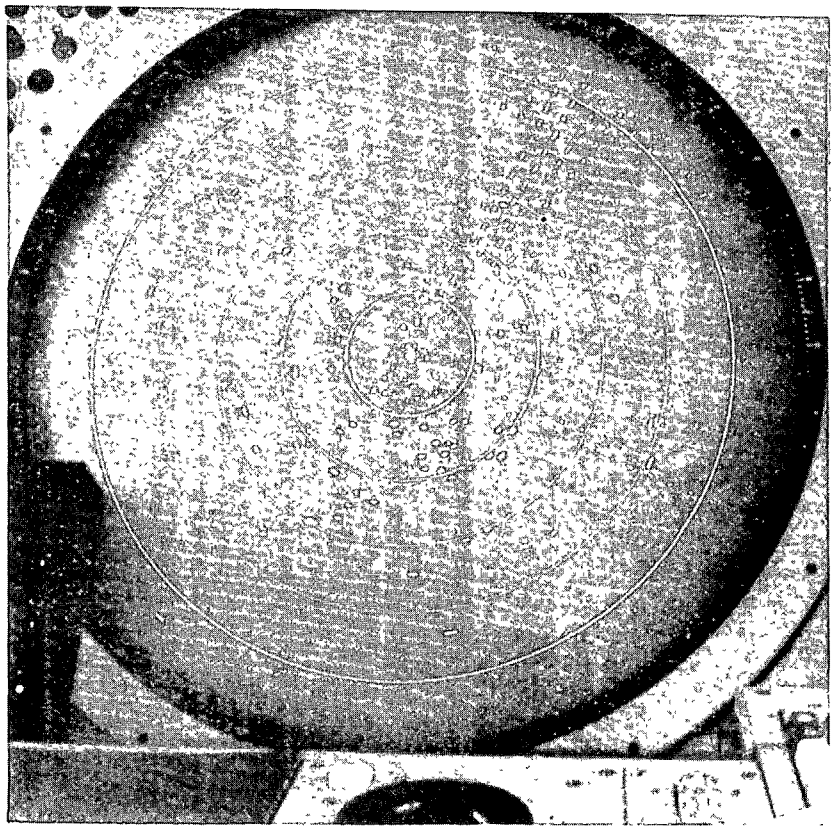

Figure 5-3. Photograph of Sacramento ASR-4 PPI Display with Sacramento WSR-57 (0.5 µsec mode) Interference

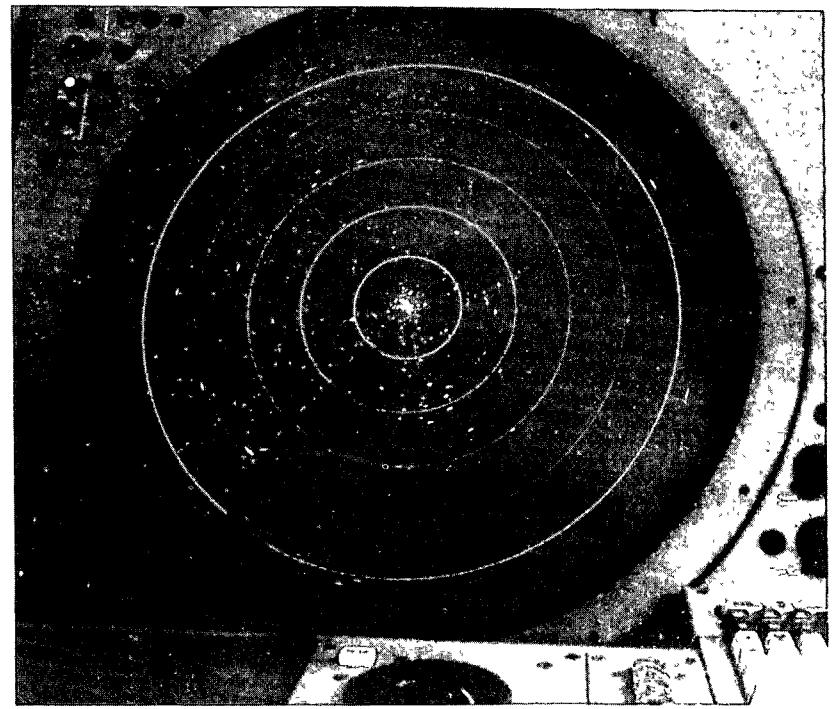

Figure 5-5. Photograph of Sacramento ASR-4 PPI Display with Sacramento WSR-57 (4.0 µsec mode) Interference

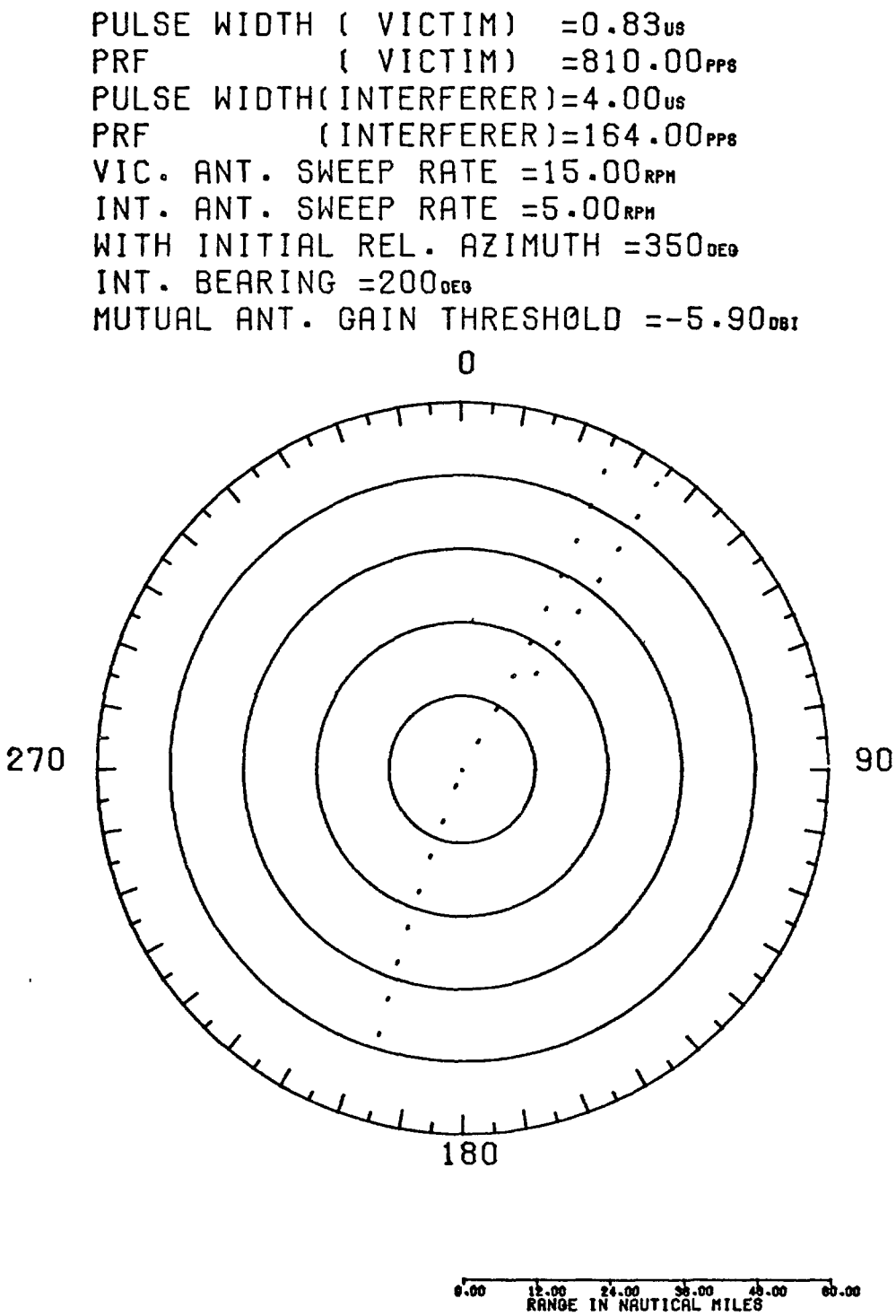

Figure 5-4. Simulated PPI Display of Sacramento ASR-4 With Sacramento WSR-57 (4.0 μsec mode) Interference.

AN/FPS-90 radar only appeared on the Mountain View ASR-5 PPI scope about one out of four scans of the victim radar. The interference from the Mt. Tamalpais AN/FPS-90 radar also appeared in wedges of 3° to 30° at a bearing of 300° to 360° on the victim PPI scope. The predicted and observed interference from the Almaden and Mt. Tamalpais AN/FPS-90 radars to the Mountain View ASR-5 radar is shown in Figure 5-6 and Figure 5-7, respectively. A more detailed discussion on interference to the Mountain View ASR-5 radar is discussed in Appendix E.

Oakland ASR-7 - Predicted interferers for the Oakland ASR-7 radar were:

Radar	Interferers Freq. (MHz)	Victim Freq. (MHz)	INR (dB)
Mt. Tamalpais AN/FPS-90	2737	2733	38

Heavy interference from the Mt. Tamalpais AN/FPS-90 radar was observed on the Oakland ASR-7 PPI display when the enhancer was off. With the enhancer off, the interference covered 360° of the victim PPI display. The interfering source was positively identified by having the Mt. Tamalpais AN/FPS-90 radar transmitter turned on and off.

The interference from the Mt. Tamalpais radar was heavier than predicted due to the fact that both the interferer and victim radars were not operating on their assigned frequency. The "B" channel of the Oakland ASR-7 radar is assigned to 2728 MHz, but was operating on 2733 MHz. Also, the Mt. Tamalpais AN/FPS-90 radar is assigned to 2740 MHz, but was operating at 2737 MHz. Therefore, there was only a frequency separation of 4 MHz between the interferer and victim radar. Using the Frequency-Dependent-Rejection (FDR) curve given in Appendix C (Figure C-13), the decreased frequency separation would result in a 10 dB increase in the INR.

When the victim radar enhancer was turned on, the interference from the Mt. Tamalpais radar was significantly reduced, and only appeared randomly on the victim PPI display at the bearing (291°) of the interfering radar as 5° to 20° interference wedges. When the enhancer and log FTC modes of the victim radar were used, the interference from the Mt. Tamalpais radar was eliminated. However, the FAA normally operates the Oakland ASR-7 radar in the enhanced MTI mode, and does not use the log FTC mode. The predicted and observed interference from the Mt. Tamalpais radar is shown in Figure 5-8 and Figure 5-9, respectively.

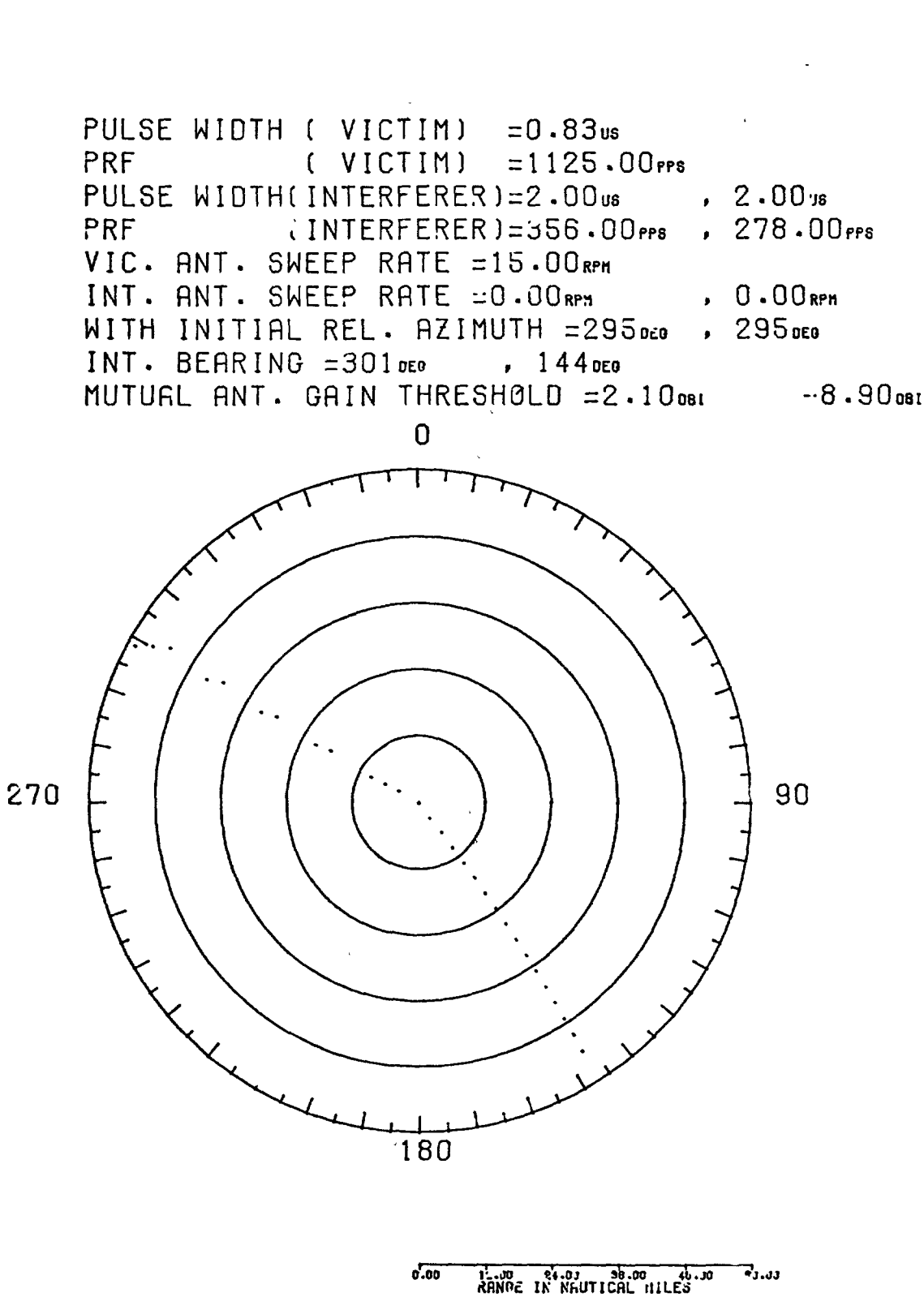

Figure 5-6. Simulated PPI Display of Mountain View ASR-5 With Alameda AN/FPS-90 (Bearing 144°) and Mt. Tamalpais AN/FPS-90 (Bearing 301°) Interference.

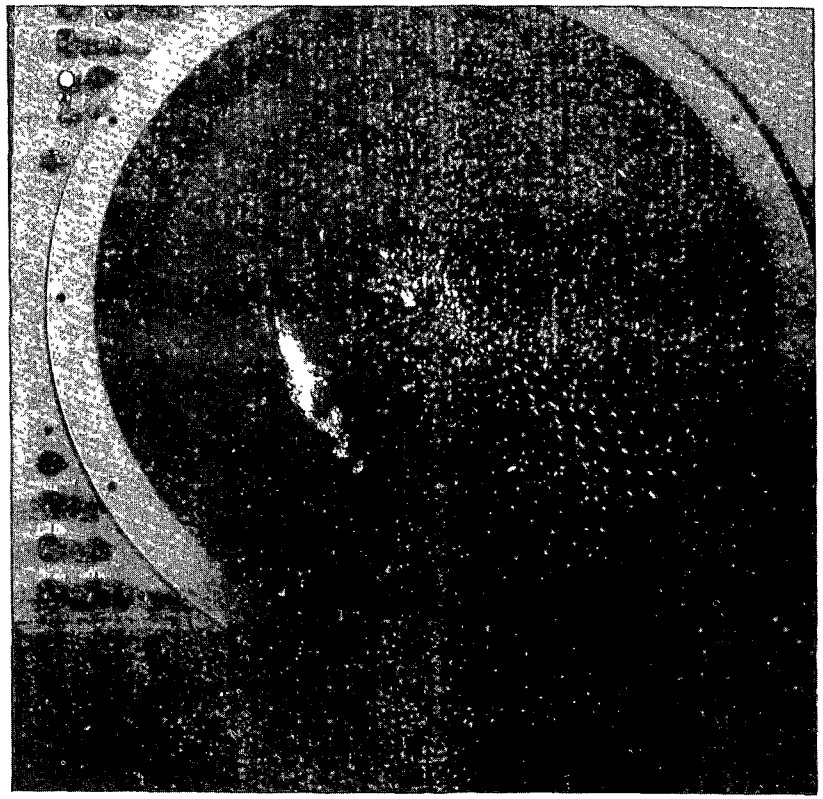

Figure 5-7. Photograph of Mountain View ASR-5 PPI Display with Alameda AN/FPS-90 and Mt. Tamalpais AN/FPS-90 Interference

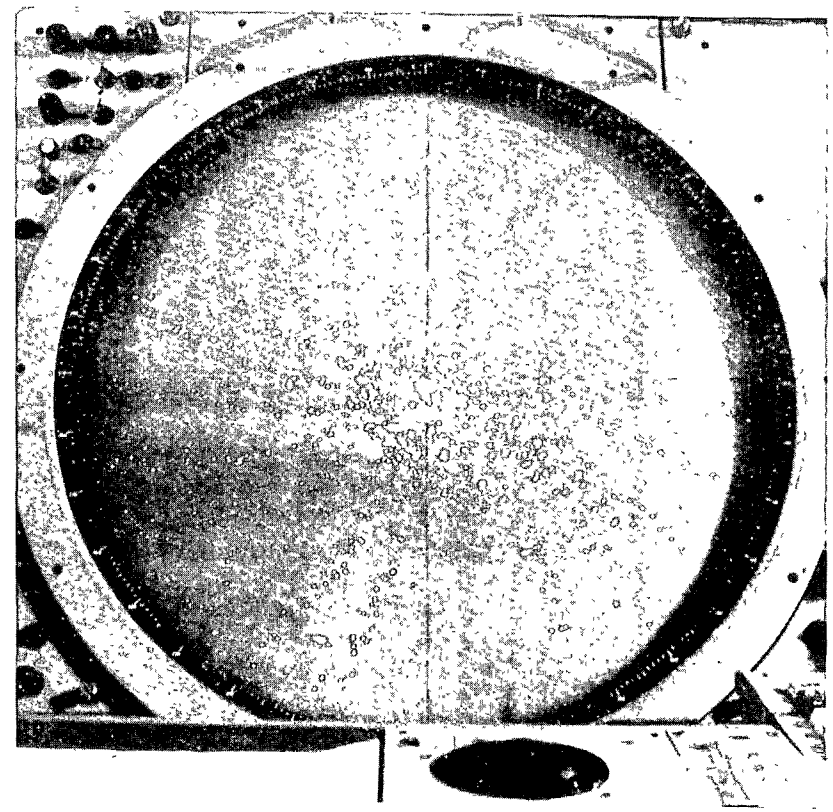

Figure 5-9. Photograph of Oakland ASR-7 PPI Display with Mt. Tamalpais AN/FPS-90 Interference

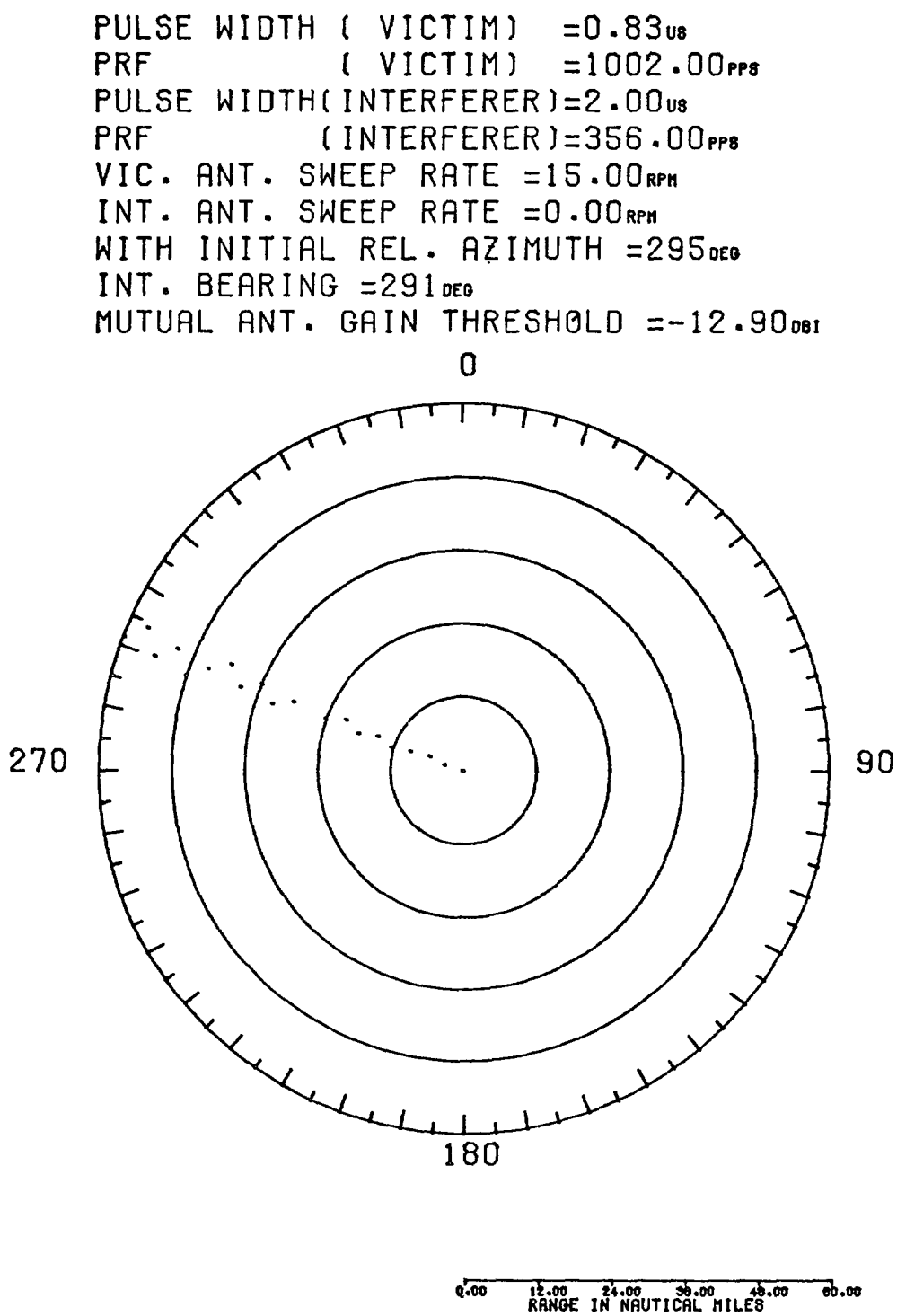

Figure 5-8. Simulated PPI Display of Oakland ASR-7 With Mt. Tamalpais AN/FPS-90 Interference.

Alameda AN/MPN-11 - Predicted interferers for the Alameda AN/MPN-11 were:

Radar	Interferers Freq. (MHz)	Victim Freq. (MHz)	INR (dB)
Hayward AN/MPN-13	2800	2800	33
Almaden AN/MPS-14	2793	2800	21

Interference from the Hayward AN/MPN-13 was observed on the Alameda AN/MPN-11 PPI display on approximately every scan of the victim radar. The interference from the Hayward radar was coupled in through the victim antenna mainbeam and backlobe, and resulted in interference wedges of 3° to 15°. Interference from the Almaden AN/MPS-14 radar could not be verified since the radar was not operating during the month of November. Interference from the Almaden and Mt. Tamalpais AN/FPS-90 radars was also observed, but only when the height finding radars were nodded directly at the Alameda AN/MPN-11 radar. Interference from these height finding radars was predicted, but is not listed in Table 5-4 since the Table is only for mainbeam of the victim radar coupling with the sidelobe of the interfering radar. Figure 5-10 shows the predicted form of the interference from the Hayward AN/MPN-11 radar and Almaden AN/MPS-14 radar on the Alameda NAS AN/MPN-11 PPI display. Photographs of the interference were not taken.

Travis AFB AN/FPN-55 - Predicted interferers for the Travis AFB AN/FPN-55 radar were:

Radar	Interferers Freq. (MHz)	Victim Freq. (MHz)	INR (dB)
Mather AN/MPN-13	2797	2801	26

Interference from the Mather AN/MPN-13 was only observed a few times during the video tape recordings, and was not periodic as predicted. The interference from the Mather AN/MPN-13 radar was observed at bearings of 290°-315° and around 20°. The Mather AN/MPN-13 radar is at a bearing of 42°. The occurrence of the interference on the victim PPI display at bearings other than the bearing of the Mather AFB radar was most likely due to coupling of the Mather AFB AN/MPN-13 radar antenna mainbeam with a high backlobe of the Travis AFB AN/FPN-55 radar antenna. Predicted interference to the

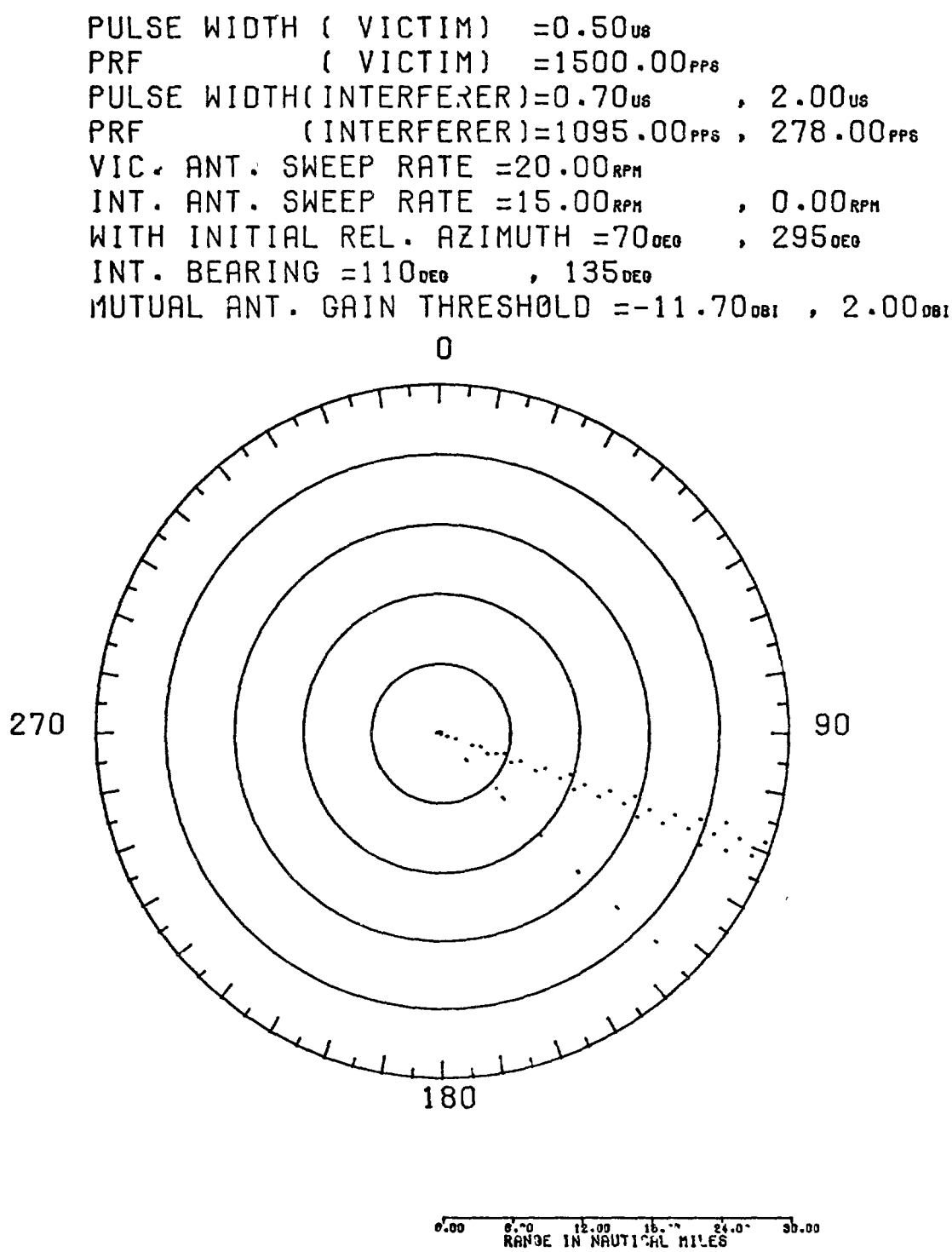

Figure 5-10. Simulated PPI Display of Alameda AN/MPN-11 With Hayward AN/MPN-13 (Bearing 110°) and Almaden AN/MPS-14 (Bearing 135°) Interference.

Travis AFB AN/FPN-55 radar from the Mather AFB AN/MPN-13 radar is shown in Figure 5-11. Because of the infrequency of the observed interference, the interference was not able to be photographed. Interference to the Travis AFB radar from the Mather AFB radar is discussed in more detail in Appendix E.

Mather AFB AN/MPN-13 - Predicted interferers for the Mather AFB AN/MPN-13 radar were:

Radar	Interferers Freq. (MHz)	Victim Freq. (MHz)	INR (dB)
Travis AN/FPN-55	2801	2797	23
Beale AN/MPN-15	2800	2797	10

Very light and intermittent interference was observed from the Travis AFB AN/FPN-55 radar. The interference from the Travis AFB AN/FPN-55 was only observed seven times over a fifteen-minute period, and resulted in a 5° interference wedge at a bearing of 220 to 260 degrees. The Travis AFB AN/FPN-55 radar is at a bearing of 223°. One reason the interference was lighter than predicted was that the antenna tilt angle for the Mather AN/MPN-13 was set at 5.5° instead of the nominal 3.5 degrees. The increased antenna tilt angle could result in a decrease of the Mather AFB AN/MPN-13 radar antenna mainbeam gain by 6 dB (Figure A-2). Also, both radars were assigned to operate at 2800 MHz. However, measurements made with the RSMS van showed a 4 MHz frequency separation between the operating frequency of the two radars. It is not known how much rejection of the interfering signal the 4 MHz frequency separation would account for since the tuned frequency of the victim radar receiver was not known. However, the Frequency-Dependent-Rejection (FDR) curve in Appendix C (Figure C-9) indicates that for a 4 MHz frequency separation, the rejection would be 17 dB. The Beale AFB AN/MPN-15 radar was operating intermittently during these tests and was not positively identified as an interferer. Figure 5-12 shows the predicted interference from the Travis AFB AN/FPN-55 radar to the Mather AFB AN/MPN-13 radar, and Figure 5-13 shows a photograph of the actual observed interference.

Almaden AN/MPS-14 - Predicted interferers for the Almaden AN/MPS-14 radar were:

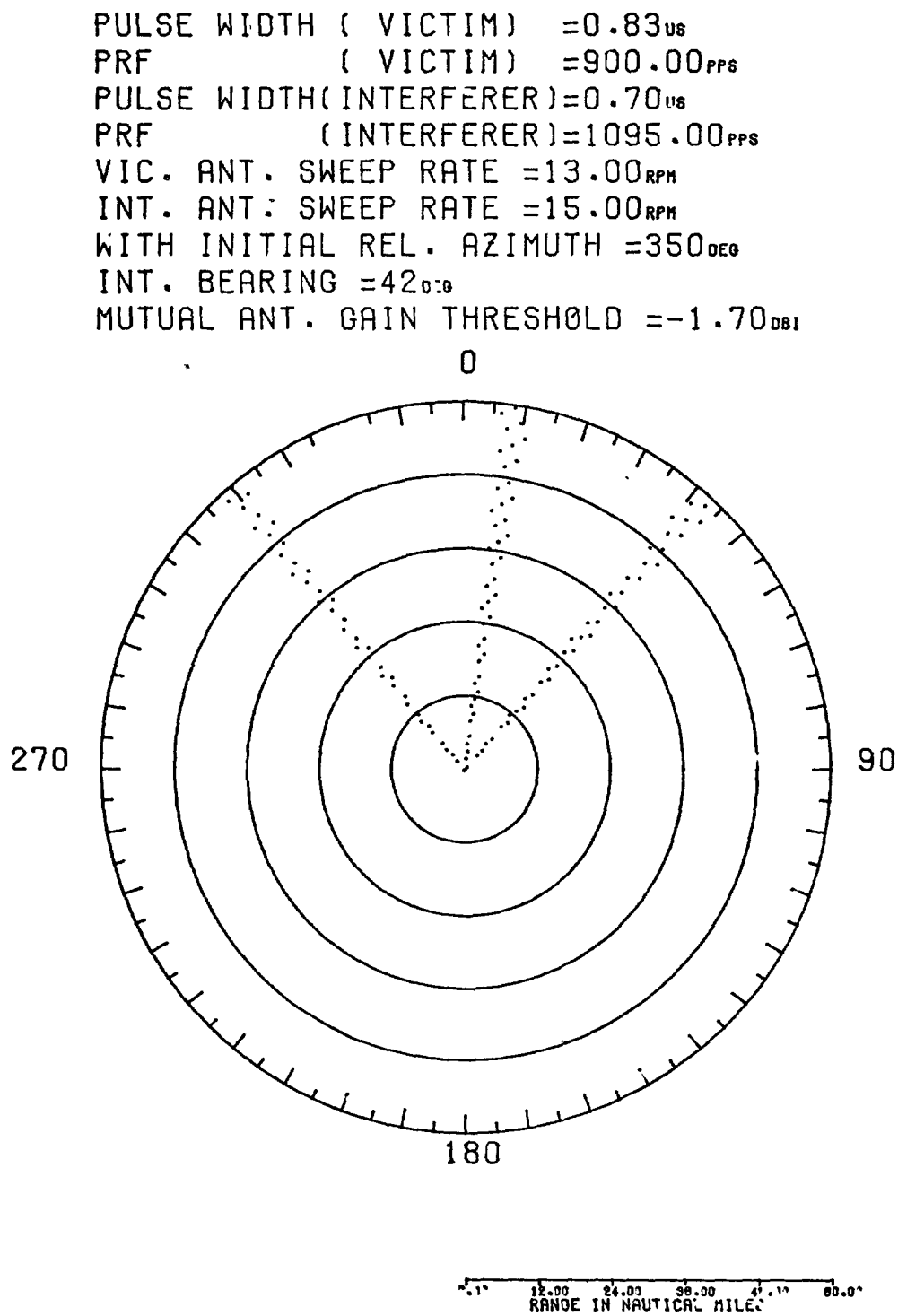

Figure 5-11. Simulated PPI Display of Travis AFB AN/FPN-55 With Mather AFB AN/MPN-13 Interference.

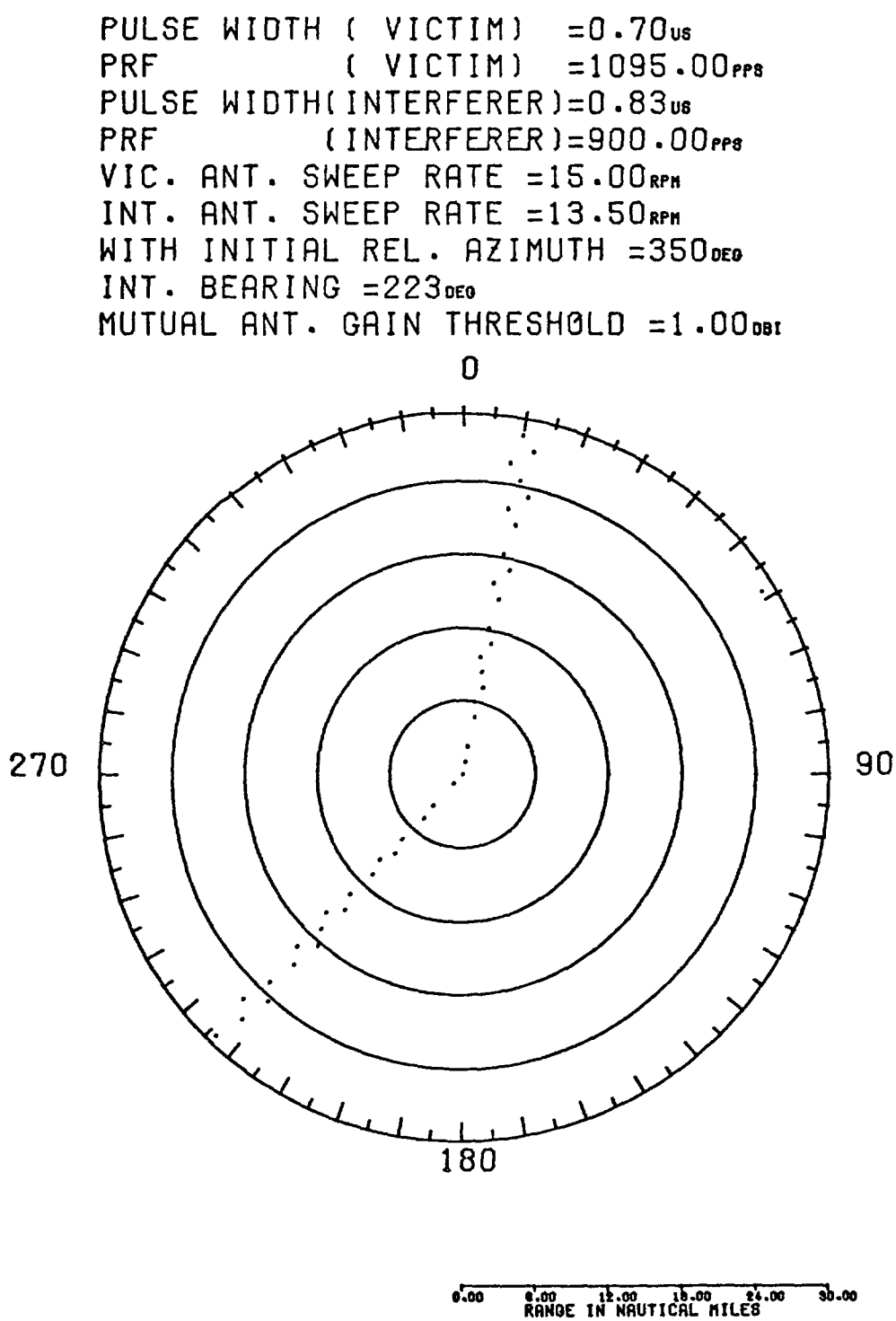

Figure 5-12. Simulated PPI Display of Mather AFB AN/MPN-13 with Travis AFB AN/FPN-55 Interference.

Radar	Interferers Freq. (MHz)	Victim Freq. (MHz)	INR (dB)
Alameda AN/MPN-11	2800	2793	20
Hayward AN/MPN-13	2800	2793	25

During the measurements at Almaden, the AN/FPS-90 radar was being actively used by the Air Force ADC, and could not be examined for verification of predicted interference. However, measurements were made on the AN/MPS-14 radar receiver. Interference was observed on the AN/MPS-14 RHI scope from the Alameda AN/MPN-11 radar. The interference appeared on the RHI scope when the height finding radar nodded in a 45° sector in the direction of the Alameda radar (bearing 321°). The Hayward AN/MPN-13 radar was unoperational during the measurement period, and therefore could not be confirmed as an interferer. Figure 5-14 shows observed interference from the Alameda AN/MPN-11 radar.

Sacramento WSR-57 - Predicted interferers for the Sacramento WSR-57 radar were:

Radar	Interferers Freq. (MHz)	Victim Freq. (MHz)	INR (dB)
Sacramento ASR-4	2868	2887	14

Interference from the Sacramento ASR-4 radar was observed on almost every scan of the victim radar when the WSR-57 was operating in the 4.0 μsec mode. The interference from the ASR-4 radar appeared only at the bearing of the interfering radar (37°), and covered approximately a 5° sector on the victim PPI display. When the WSR-57 was operating in the 0.5 μsec mode, no interference from the Sacramento ASR-4 radar was observed. The reason the interference of the ASR-4 radar was not observed when the WSR-57 was operating in the 0.5 μsec mode was that the inherent noise level in the victim radar receiver is increased by 8 dB due to a wider IF bandwidth. Unpredicted interference at a bearing of 97° was also observed from the Mather AFB AN/MPN-13 radar. The predicted INR from the Mather radar was -1 dB. The interference from the Mather AFB AN/MPN-13 radar was observed on approximately one out of seven scans of the victim radar. It is believed that the slow antenna rotation rate (4 rpm) relative to the antenna rotation rate of the AN/MPN-13 (15 rpm)

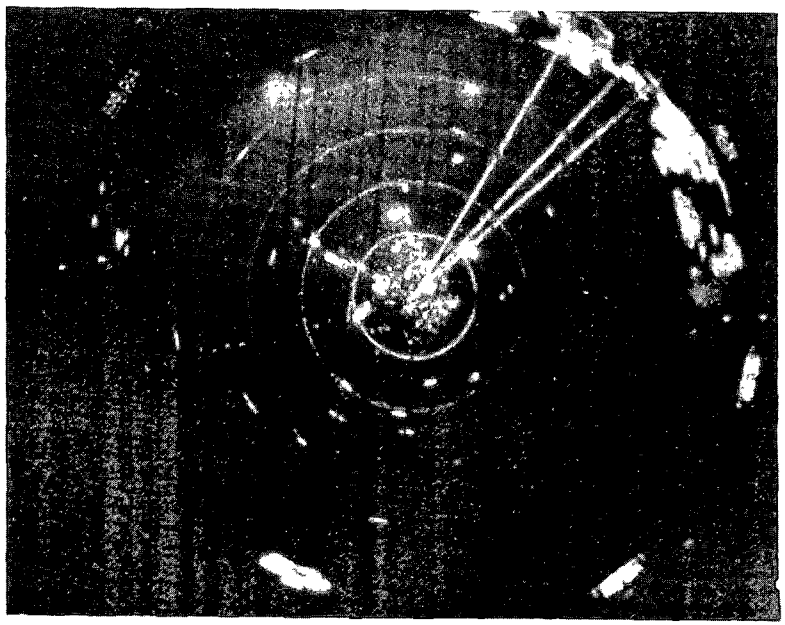

Figure 5-13. Photograph of Mather AFB AN/MPN-13 PPI Display with Travis AN/FPN-55 Interference

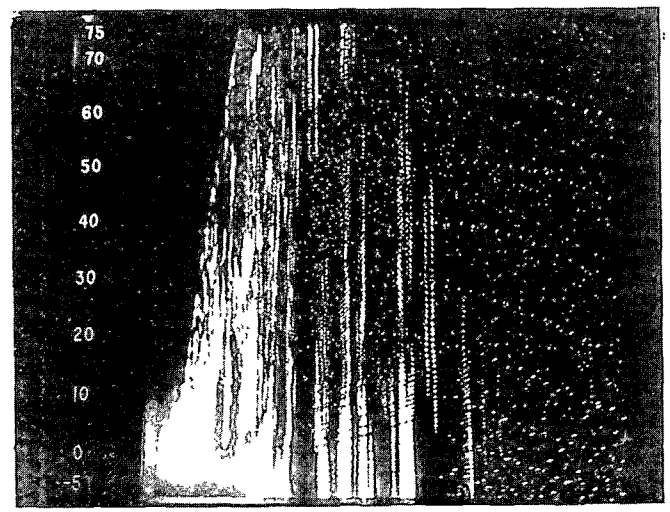

Figure 5-14. Photograph of Almaden AN/MPS-14 RHI Display with Alameda AN/MPN-11 Interference

caused occasional coupling of the victim antenna mainbeam with the interferer antenna mainbeam or major sidelobe. The interference from the Mather AFB AN/MPN-13 radar covered approximately a 10° sector at the bearing of the Mather AFB radar (110°). Interference was also observed from the Mt. Tamalpais AN/FPS-90 radar at a bearing of 217° when it was coordinated to have the Mt. Tamalpais radar nodding in the direction of the WSR-57 radar. The interference from the Mt. Tamalpais radar caused an interference wedge of 3° on the victim PPI scope. The form of the predicted interference to the Sacramento WSR-57 radar when operating in the 4 μsec pulse width mode from the Sacramento ASR-4 radar is shown in Figure 5-15. Figure 5-16 shows observed interference to the Sacramento WSR-57 radar from the Sacramento ASR-4 radar, Mather AFB AN/MPN-13 radar and Mt. Tamalpais AN/FPS-90 radar.

5.3.2 Summary of Observed and Predicted Interference

For the eight radar sites visited during the preliminary radar site measurements, there were 13 predicted interference cases of mainbeam-to-backlobe antenna coupling. However, due to some of the radars being inoperative during the preliminary radar site measurement program, only 10 predicted interference cases could be verified. All 10 of the predicted interference cases that could be verified were observed during the preliminary site visits. In general, the predicted form of the interference on the PPI display was close to the actual observed interference with the exception of three cases: 1) Mt. Tamalpais AN/FPS-90 interference to the Oakland ASR-7 radar, 2) Mather AFB AN/MPN-13 interference to Travis AFB AN/FPN-55 radar, and 3) Travis AFB AN/FPN-55 interference to Mather AFB AN/MPN-13 radar. There was also one case of unpredicted interference that was observed (Mather AFB AN/MPN-13 radar interference to the Sacramento WSR-57 radar). However, it appeared that the interference from the Mather radar was due to coupling of the victim antenna mainbeam to the interferer antenna mainbeam or major sidelobe, and not victim antenna mainbeam coupling with the interferer antenna backlobes which was the coupling mechanism used to predict interference.

The San Francisco area investigation showed a significant improvement over the Los Angeles area investigation in the correlation between predicted and actual observed interference. It is believed that this improvement in interference prediction capability was a result of:

1) incorporating empirical propagation loss factors for buildings and man-made obstacles into the overall propagation path loss (see Appendix D).

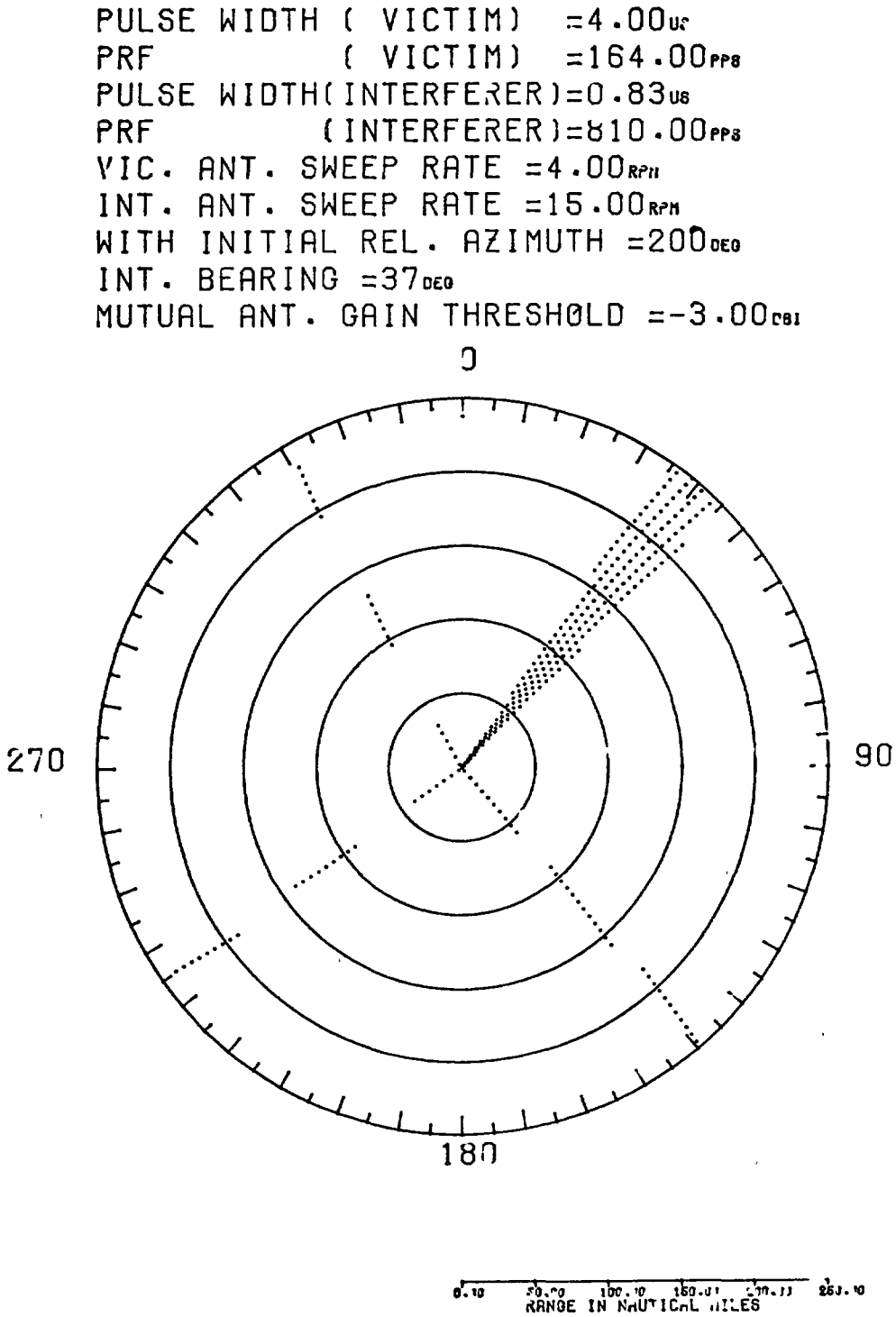

Figure 5-15. Simulated PPI Display of Sacramento WSR-57 with Sacramento ASR-5 Interference.

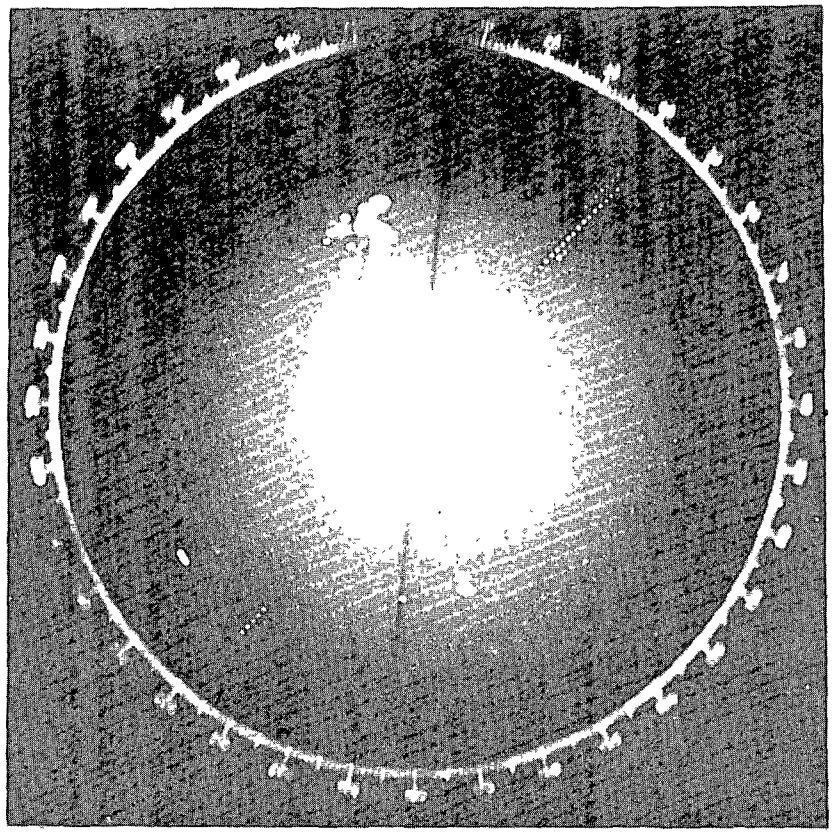

Figure 5-16. Photograph of Sacramento WSR-57 PPI Display with Sacramento ASR-4, Mather AFB AN/MPN-13 and Mt. Tamalpais AN/FPS-90 Interference

2) changing the median antenna backlobe level from -10 dBi to -13 dBi.

3) including transmission line insertion loss of the victim and interferer radars.

5.4 ENVIRONMENTAL OBSERVATIONS

Interference was observed at all eight of the radar sites visited in the San Francisco area investigation. Three of the FAA radars (Sacramento ASR-4, Mountain View ASR-5, and Oakland ASR-7) and one GCA radar (Alameda AN/MPN-11) were considered to have a moderate amount of interference on their PPI display. A look at Table 5-3 shows that all the radars in the San Francisco Bay are assigned to operate in the 2.7 to 2.8 GHz band, and all the radars in the Sacramento area are assigned to operate in the 2.8 to 2.9 GHz band. It is believed, that if the whole 200 MHz band was utilized in the San Francisco Bay area and the Sacramento area, interference between the radars in these areas would be significantly reduced. The present radar frequency assignment distribution in the San Francisco and Sacramento areas is due to past history frequency assignments, and removal of radars from the environment.

Information on planned deployment changes in the 2.7 to 2.9 GHz band in the San Francisco area was obtained from the various government agencies (References 48 through 50), and is given in Table 5-5. The only known planned dual frequency radar for the area is the Alameda NAS ASR-8 scheduled to replace the AN/MPN-11 radar. Due to known ducting problems in the bay area (see Appendix D), consideration of the ducting phenomena must be given in determining frequency assignments for the new Alameda ASR-8 radar. A height finding radar (AN/FPS-6,90) is scheduled for Half Moon Bay as part of the joint FAA/DOD surveillance system. The height finding radars at Cambria, Almaden and Mt. Tamalpais will eventually be phased out once the joint FAA/DOD surveillance system becomes operational. The Monterey AN/APS-20 radar has been removed from the band. The Beale AFB AN/MPN-15 radar will be removed in FY 78 after an ILS is installed. A detailed investigation on the accommodation of planned future radar deployments in the 2.7 to 2.9 GHz band in the San Francisco area will be given in a subsequent OT report.

TABLE 5-5

PLANNED ENVIRONMENT CHANGES IN THE SAN FRANCISCO AREA BY FY 84

CITY/BASE	LATITUDE/ LONGITUDE	AGENCY	ACTION	PRESENT RADAR	PLANNED RADAR	DATE
Alameda NAS	37 47 00 122 19 00	Navy	Replace	AN/MPN-11	ASR-8 *	FY 80
Mather AFB	38 33 51 121 17 19	Air Force	Replace	AN/MPN-13	AN/GPN-12	FY 77
Beale AFB	39 08 12 121 26 00	Air Force	Remove	AN/MPN-15	Use FAA ASR info.	FY 78
Half Moon Bay	37 31 43 122 25 35	Air Force	New	None	AN/FPS-6,90	
Cambria	35 31 21 121 03 46	Air Force	Remove	AN/FPS-6	None	
Almaden	37 09 38 121 53 47	Air Force	Remove	AN/MPS-14 AN/FPS-90	None	
Mt. Tamalpais	37 55 45 122 35 20	Air Force	Remove	AN/FPS-90	None	
Monterey	36 35 52 121 52 25	Navy	Remove	AN/APS-20	None	CY 75

* Frequency Diversity Capability

APPENDIX A

ANTENNA CHARACTERISTIC MODELING

INTRODUCTION

The subject matter discussed in this appendix includes the antenna model used to predict interference in the Los Angeles and San Francisco investigations, and the antenna radiation pattern measurements of radars in the Los Angeles and San Francisco areas. The measured data was compared with previous measured data and existing models. Also discussed in this section is a mutual antenna gain model and the interrelationship between antennas and environment propagation phenomena which determine the interfering power level seen by the victim radar. A discussion of the RSMS van system hardware and software used to measure the radar antenna pattern characteristics is given in Appendix G.

Since antennas are the means by which an interfering signal is radiated and coupled into the victim receiver, an adequate antenna model is an essential component in the capability of predicting radar-to-radar interference. Because of the dynamic nature of radar antennas (i.e., rotating and nodding) and differences in site conditions, a statistical description of the radar antenna radiation and reception characteristics is a more realistic approach. The statistical model may be represented in terms of a three level pattern consisting of a mainbeam gain region, median sidelobe level, and a median backlobe level; or in terms of the likelihood that any particular level will be equaled or exceeded using the cumulative gain distribution of the antenna characteristics.

THREE-LEVEL ANTENNA PATTERN MODEL

A three-level antenna pattern statistical model for an average clutter area was used to predict interference in the Los Angeles and San Francisco investigations (Reference 13 and measurements). Figure A-1 shows a pictorial representation of the three-level pattern with the mainbeam, sidelobe, and backlobe region. The statistical median antenna gain and degrees for each of the three regions used in the Los Angeles investigation were:

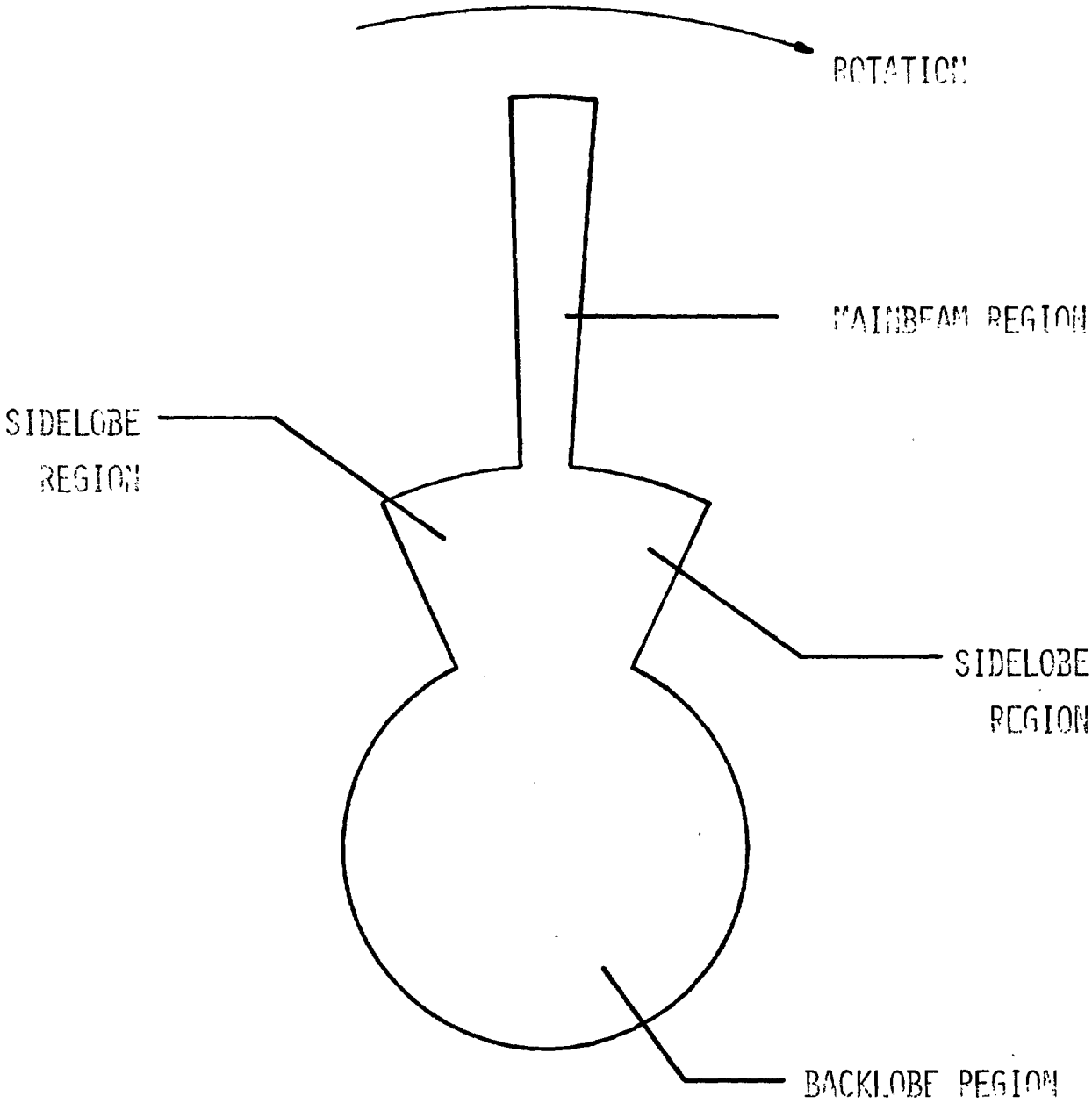

Figure A-1. Three Level Antenna Pattern Representation

Mainbeam Region:	Gain:	Nominal mainbeam gain minus correction for antenna tilt angle
	Degrees:	357° to 3°
Sidelobe Region:	Gain:	-4 dBi
	Degrees:	3° to 25° and 335° to 357°
Backlobe Region:	Gain:	-10 dBi
	Degrees:	25° to 335°

Airport surveillance radars with cosecant squared elevation antenna patterns normally tilt the mainbeam of the radar above the horizon to reduce ground clutter; therefore, the energy radiated at an elevation angle of zero degrees may be typically 5 to 12 dB below the actual mainbeam gain. Based on a statiscal analysis of the line-of-sight antenna radiation patterns measured in the Los Angeles investigation, an antenna gain level of -13 dBi in the backlobe region was used in the San Francisco investigation.

LINE-OF-SIGHT ANTENNA PATTERN MEASUREMENTS

During the Los Angeles and San Francisco investigations, several line-of-sight antenna radiation patterns were measured. These measurements were made at the radar site and include the environmental and clutter effects of the area which cause extraneous reflections of the transmitted signal. When possible, care was taken to minimize surface and obstacle reflections. Methods outlined in Reference 17 were used to determine the optimum measurement distance to minimize the environmental clutter effect. All the measurements were made at distances slightly greater than the far field distance of D^2/λ, where D is the size of the aperture and λ is the wavelength.

All the measurements were made with reference to absolute power received or relative to the mainbeam gain. However, for EMC application, the antenna radiation characteristics need to be referenced relative to an isotropic radiator. In order to convert the measured antenna pattern data relative to an isotropic radiator, the antenna elevation radiation pattern characteristics were required in order to adjust the antenna nominal mainbeam gain by the electrical and mechanical tilt angle of the antenna and the measurement angle (angle of the measurement van antenna and radar feed horn relative to

the horizon). Figure A-2 shows a measured antenna elevation pattern for the FAA ASR antenna that was used to adjust the nominal mainbeam gain. The antenna specifications for the ASR-4 through ASR-7 radars are the same with the ASR-4, ASR-5 and ASR-7 antennas being manufactured by the same company. The ASR antenna elevation pattern was also used to adjust the mainbeam gain for the GCA radars.

Figures A-3 through A-10 show the measured data of several airport surveillance radar antenna radiation patterns. The figures show the antenna radiation pattern from -20° to +380°, where the angles are relative to the mainbeam occurrence. The plot covers -20° before the occurrence of the first mainbeam and continues 20° past the occurrence of the second mainbeam giving a coverage of 400° (40° overlap) to permit full mainbeam observation. The radar frequency, antenna scan period, peak received power in dBm, and antenna statistical information are shown at the top of the figure.

Table A-1 summarizes the antenna measurements shown in Figures A-3 through A-10 for three-level statistical representation of the antenna radiation pattern characteristics relative to isotropic. The following statistical data for each measured antenna radiation pattern is contained in the table:

1. The median antenna pattern level between 0° and 360°.

2. Peak sidelobe antenna pattern level between 3° and 25° on either side of the mainbeam.

3. Median sidelobe antenna pattern level between 3° and 25° on either side of the mainbeam.

4. Peak backlobe antenna pattern level between 25° and 335°.

5. Median backlobe antenna pattern level between 25° and 335°.

Also shown in Table A-1 are the mean and standard deviation taken across the eight measured samples for the above five categories. The mean of the median antenna pattern levels shown in the Table A-1 was found to be -11.8 dBi with a standard deviation of 2.8 dB. Reference 18 states that the mean of sampled median antenna pattern levels for an uncluttered site was -12.1 dBi with standard deviation of 6.2 dB. The mean of the median sidelobe levels shown in Table A-1 was found to be -7.1 dBi with a standard deviation of 3.3 dB.

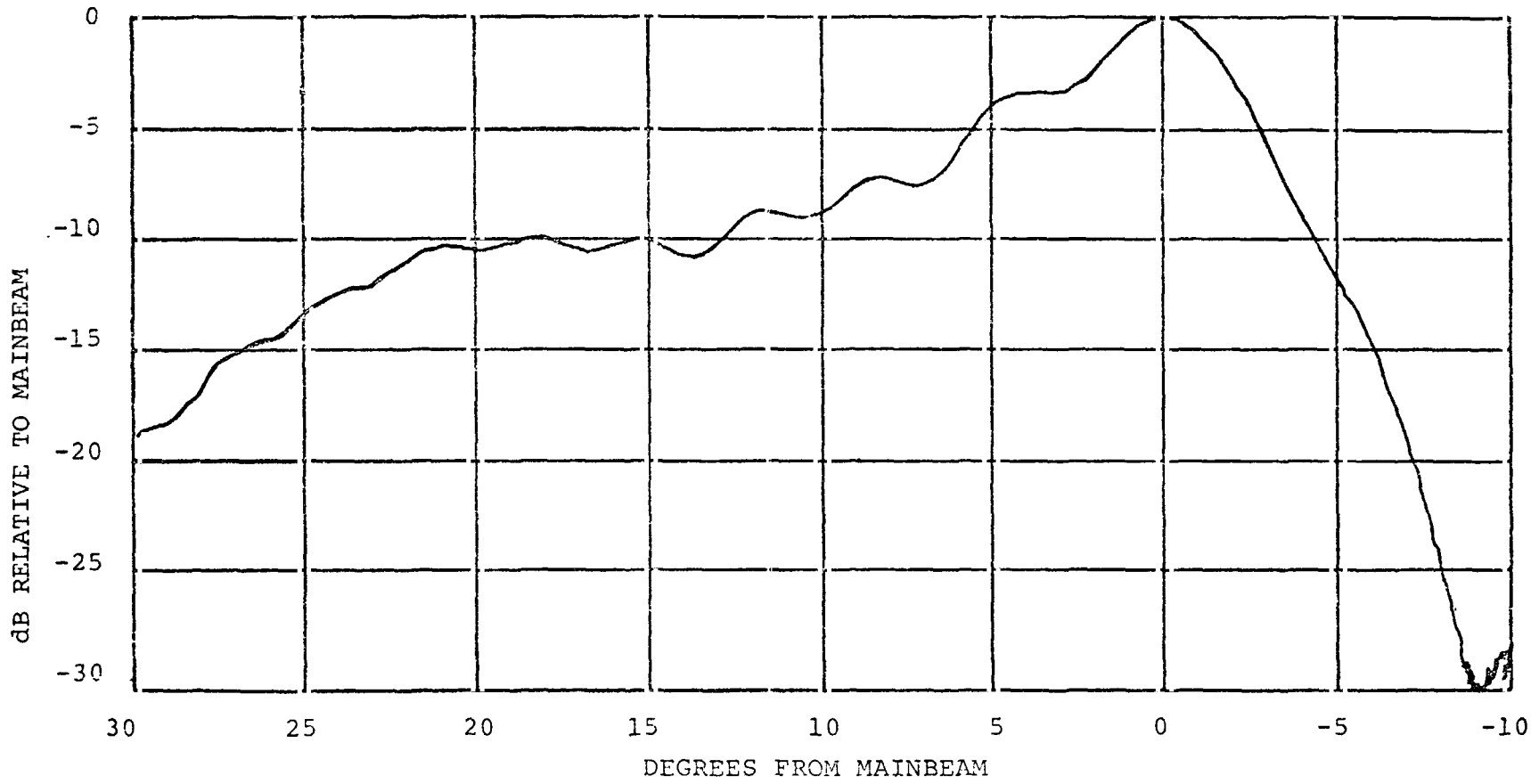

Figure A-2. Measured Elevation Antenna Radiation Pattern of ASR Radar

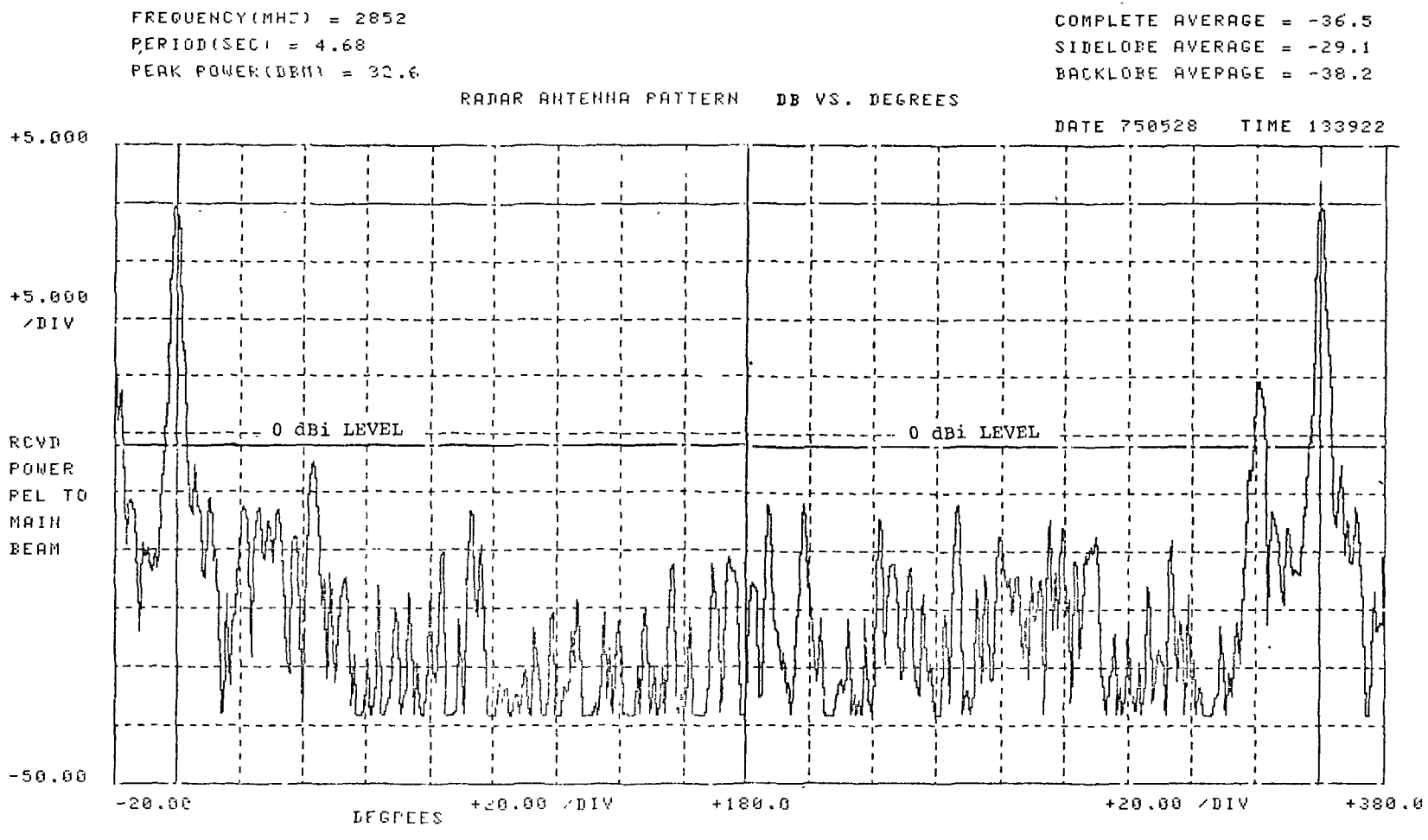

Figure A-3. Measured Antenna Radiation Pattern of Los Angeles ASR-7

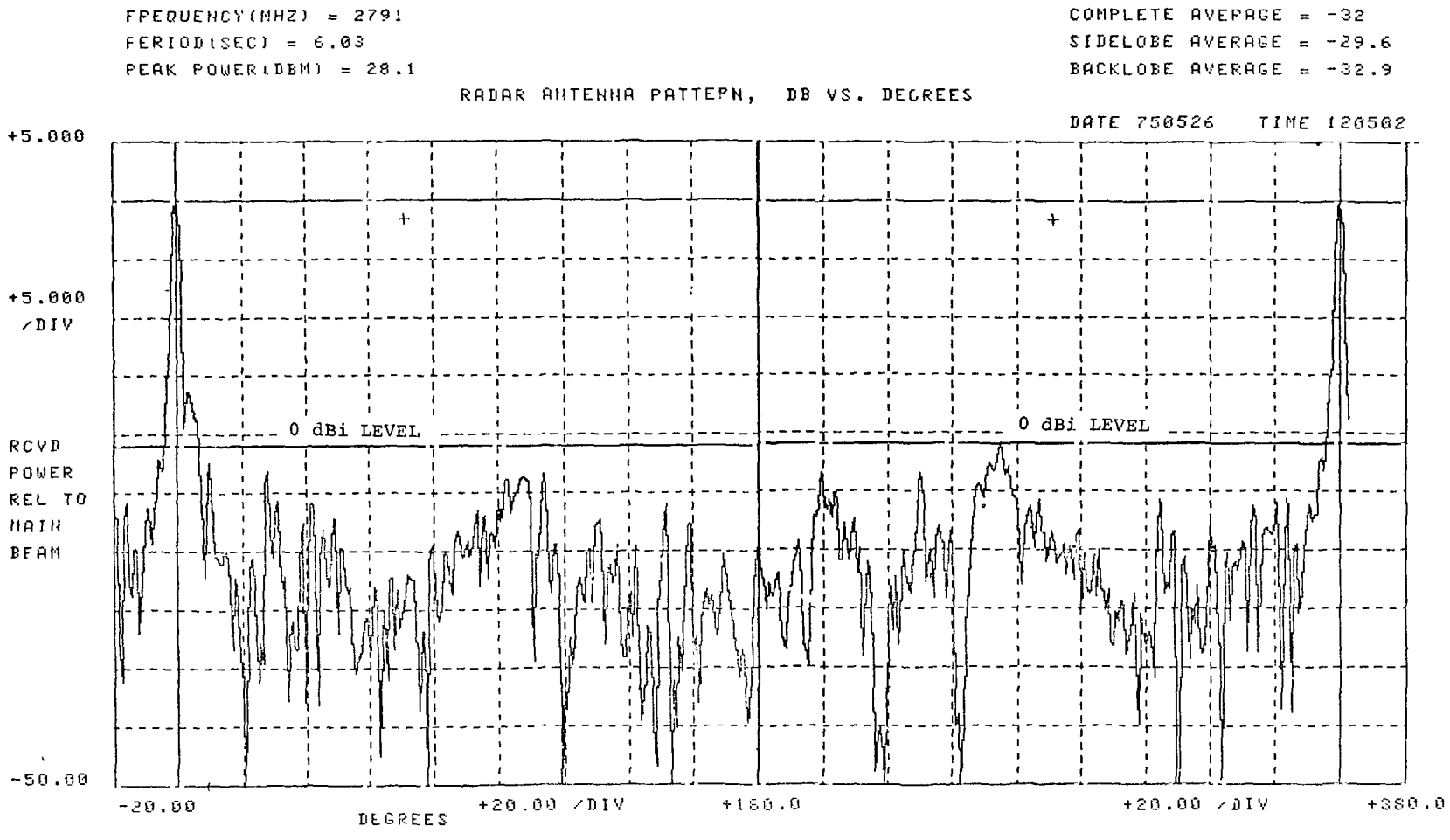

Figure A-4. Measured Antenna Radiation Pattern of Burbank ASR-6

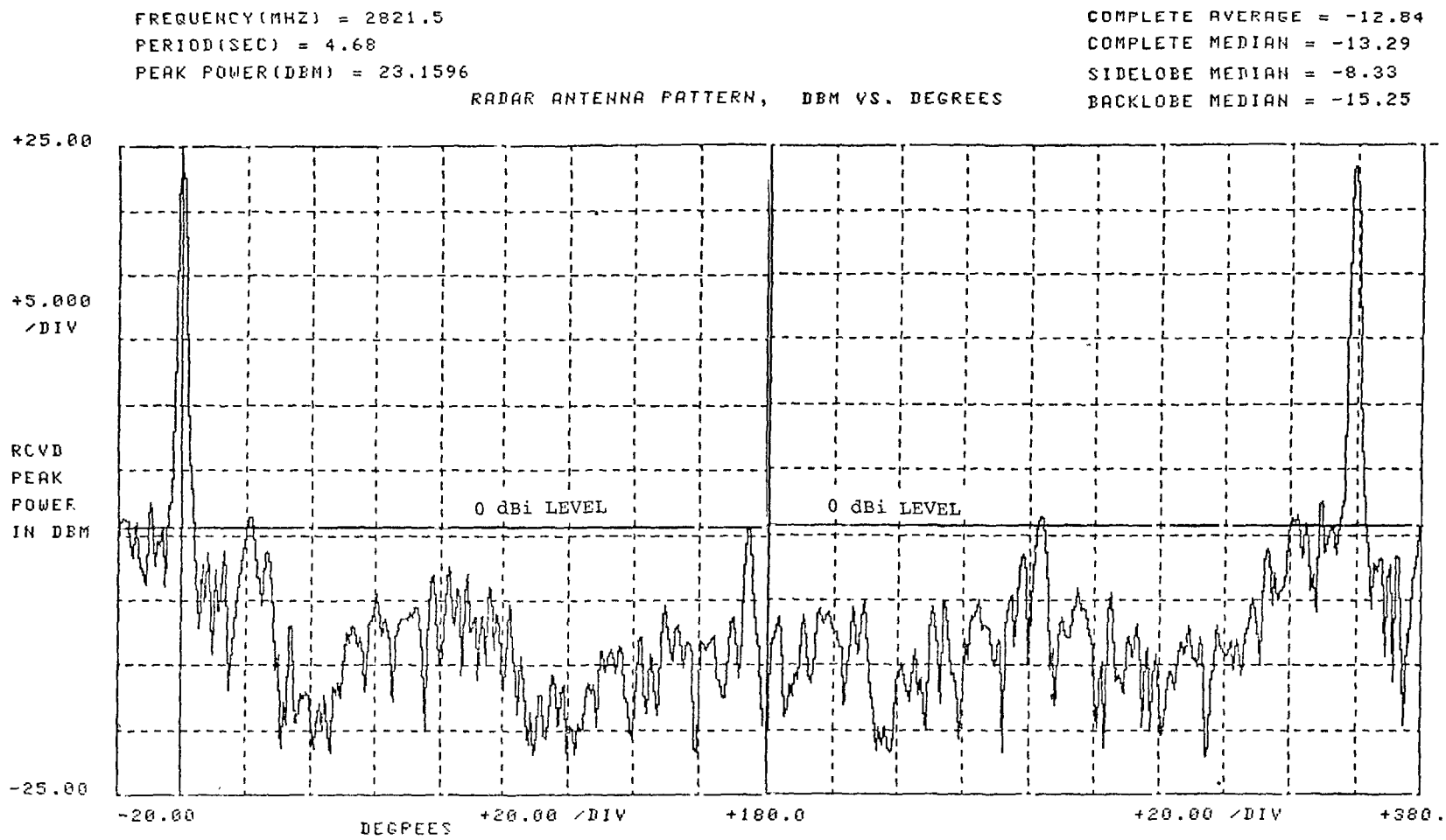

Figure A-5. Measured Antenna Radiation Pattern of Ontario ASR-5

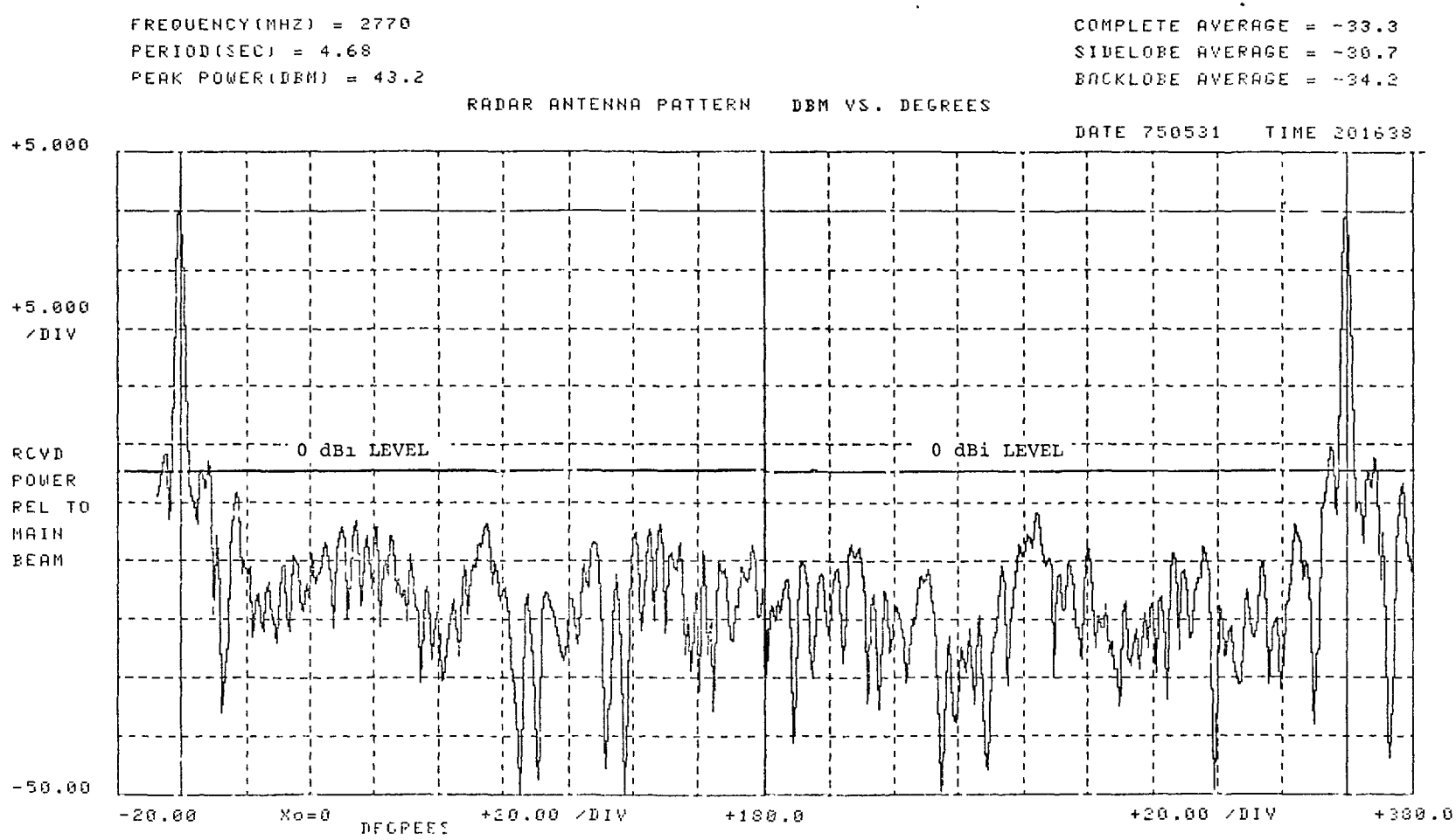

Figure A-6. Measured Antenna Radiation Pattern of Long Beach ASR-5

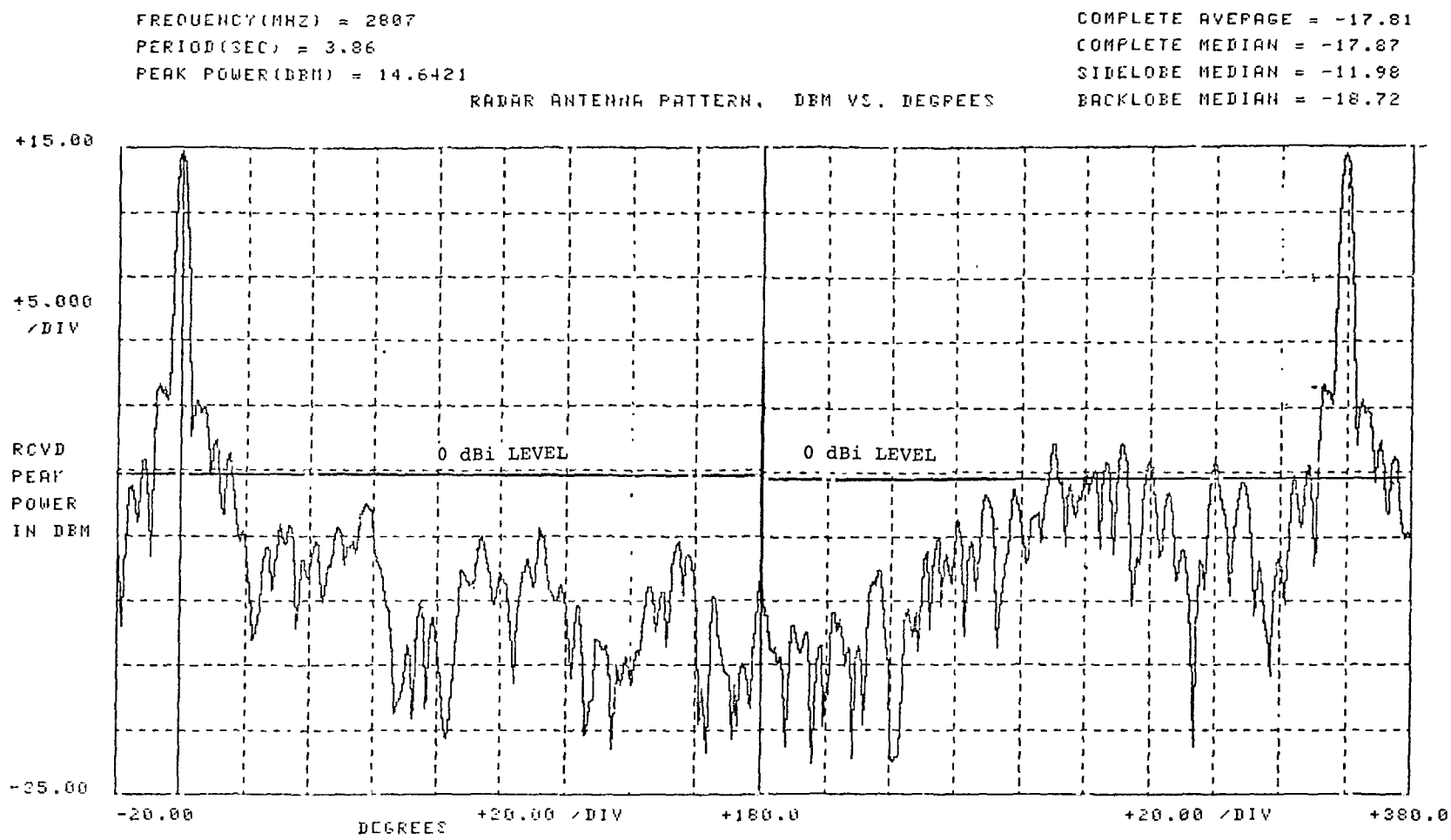

Figure A-7. Measured Antenna Radiation Pattern of Los Alamitos AN/CPN-4

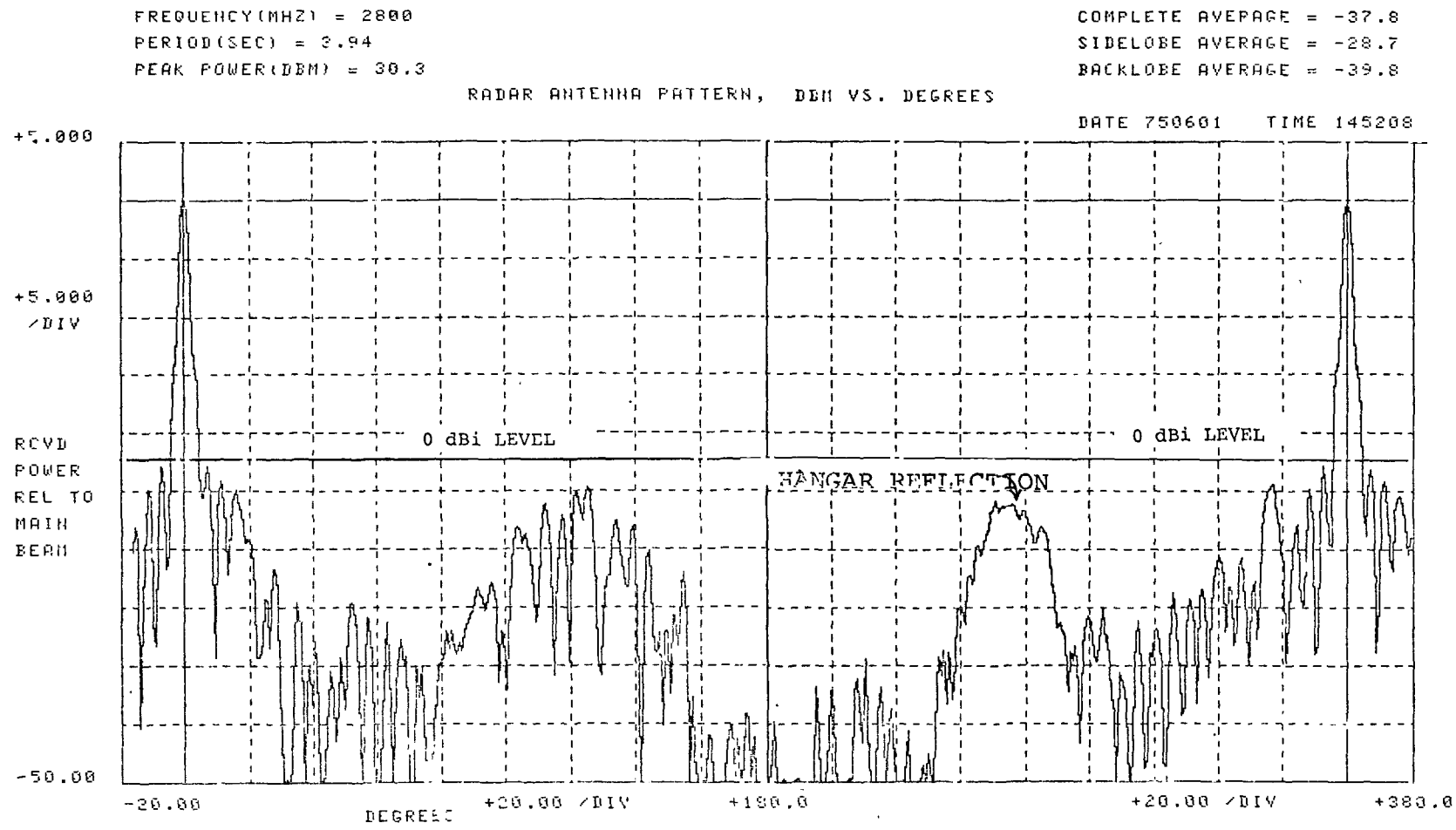

Figure A-8. Measured Antenna Radiation Pattern of Norton AN/MPN-13

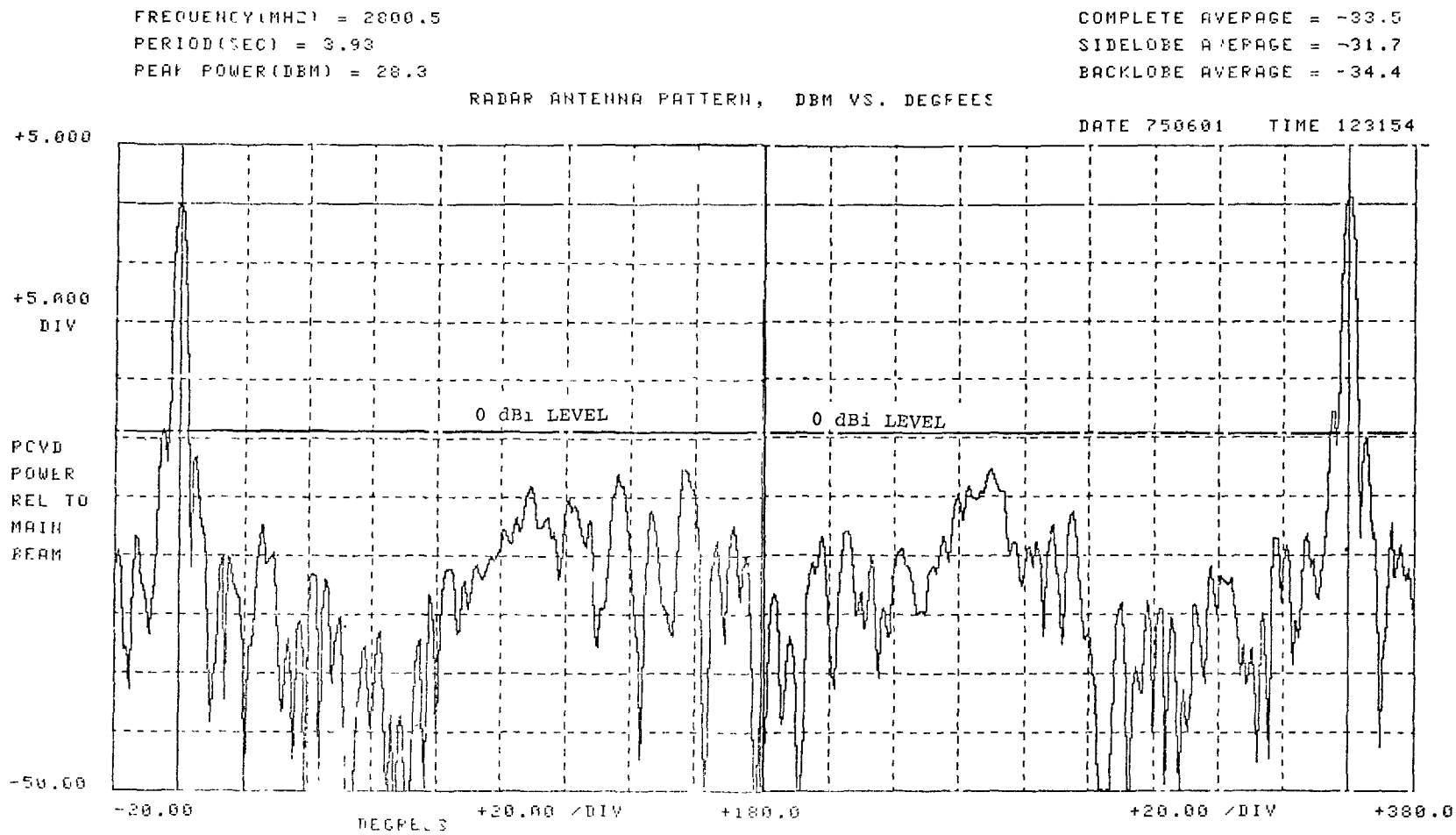

Figure A-9. Measured Antenna Radiation Pattern of March AN/MPN-13

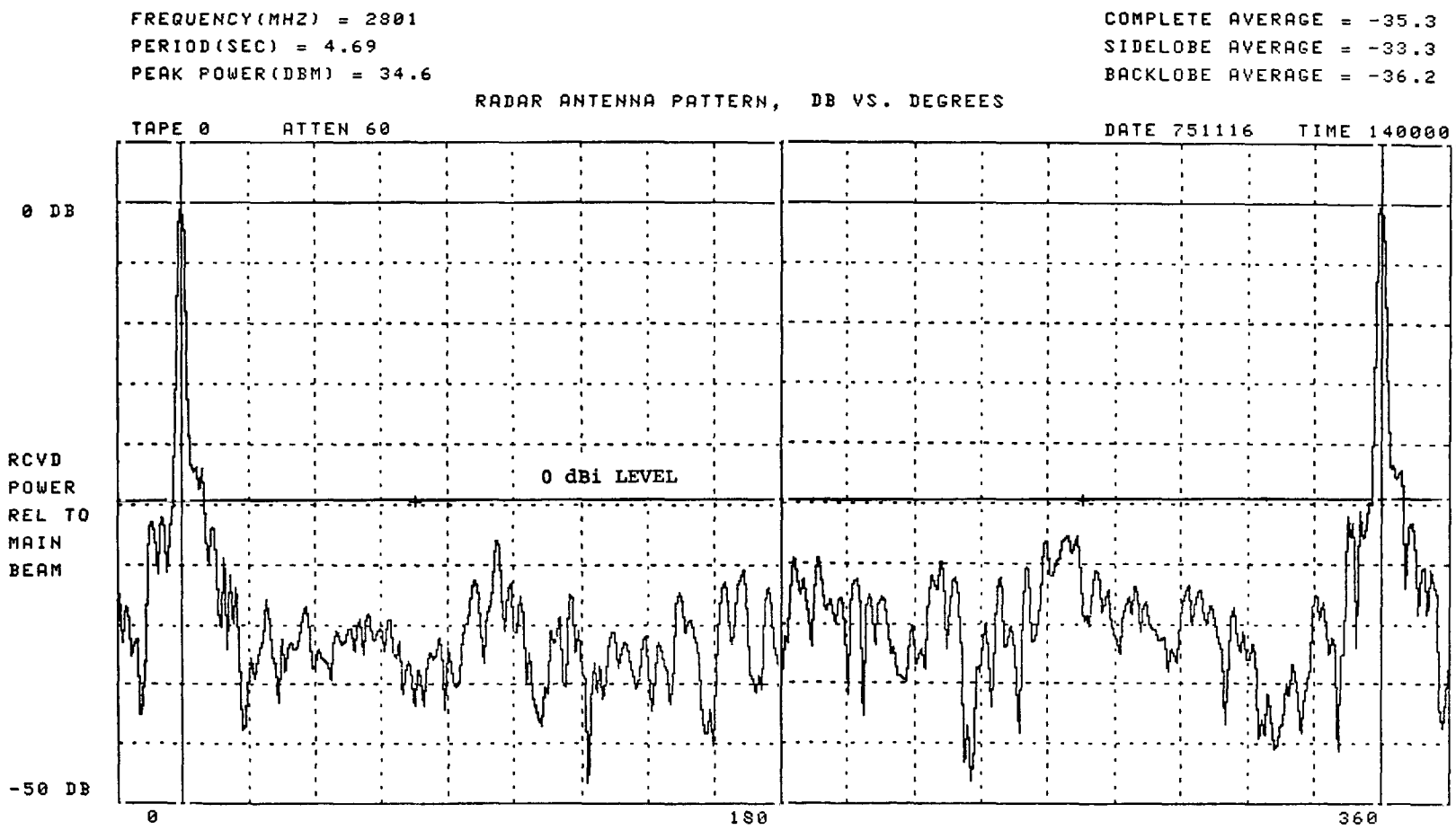

Figure A-10. Measured Antenna Radiation Pattern of Travis AFB AN/FPN-55

TABLE A-1

ANTENNA PATTERN STATISTICS OF 2.7-2.9 GHz RADARS

CITY/BASE	EQUIPMENT NOMENCLATURE	NOMINAL MAINBEAM GAIN (dBi)	ANTENNA TILT ANGLE (DEGREES)	ADJUSTED MAINBEAM GAIN (dBi)	MEDIAN ANTENNA PATTERN LEVEL (dBi)	SIDELOBE PEAK LEVEL (dBi)	SIDELOBE MEDIAN LEVEL (dBi)	BACKLOBE PEAK LEVEL (dBi)	BACKLOBE MEDIAN LEVEL (dBi)
LOS ANGELES	ASR-7	34	3.5	21*	-15.5	+5.0	-8.1	-2.0	-17.2
BURBANK	ASR-6	34	3.5	21.0*	-11.0	+4.0	-8.6	0.0	-11.9
ONTARIO	ASR-5	34	3.5	27*	-10.0	+0.8	-3.8	+0.3	-10.5
LONG BEACH	ASR-5	34	3.75	22.6*	-10.7	+1.6	-8.1	-3.4	-11.8
LOS ALIMITOS	CPN-4	31	3.0	25**	-7.5	+7.36	-1.6	+2.8	-8.4
NORTON	MPN-15	32	4.25°	22.5**	-15.3	-0.5	-5.3	-2.5	-17.3
MARCH	MPN-13	32	5.5°	19.5**	-14.0	-0.5	-12.2	-3.0	-14.0
TRAVIS	FPN-55	34	4.25°	24.5	-10.8	+2.1	-8.8	-3.0	-11.7
					μ=-11.85 σ=2.8	μ=2.48 σ=2.77	μ=-7.06 σ=3.32	μ=-1.35 σ=2.17	μ=-12.85 σ=3.13

* Includes Adjusted Mainbeam Gain for Tilt Angle Plus Measurement Angle

** Estimated Adjusted Mainbeam Gain

The mean of the median backlobe levels for the sample shown in Table A-1 was found to be -12.8 dBi with a standard deviation of 3.1 dB. Reference 13 states that the median backlobe level for an average-siting condition should be -10.0 dBi. with a standard deviation of 6.0 dB. Therefore, the measured antenna radiation pattern statistics for airport surveillance radars taken during the Los Angeles and San Francisco investigations is in close agreement with previous measured data.

Line-of-sight antenna radiation pattern measurements were also made on the Sacramento WSR-57 radar which has a parabolic dish type antenna. The weather radar has the capability to tilt in elevation the parabolic dish at angles between -5° to +45° with the horizon. The WSR-57 at Sacramento is normally operated with the antenna tilted in the elevation plan +1° with respect to the horizon. The WSR-57 radar antenna has a nominal mainbeam gain of +36 dBi, and a 3 dB beamwidth of two degrees. Figures A-11 through A-13 show measured antenna radiation patterns for tilt angles of zero, one, and two degrees, respectively. The statistics in Figure A-11 show an average backlobe level of approximately -7.2 dBi for the parabolic dish. A comparison of Figures A-11 through A-13 illustrates the reduction in mainbeam gain due to the narrow beamwidth of the pencil beam antenna for only a small change in the elevation tilt angle of the antenna. This indicates that the normal operating antenna tilt angle of weather radars must be considered in predicting interference to and from weather radars.

CUMULATIVE DISTRIBUTION MODEL

Figures A-14 through A-19 show the cumulative antenna radiation pattern distribution of several radars listed in Table A-1. The dotted line on the graph shows the 0 to 10 percent probability of exceeding a specified antenna gain level. The solid line shows the 0 to 100 percent probability of exceeding a specified gain level. Figure A-20 shows the mean and 2σ cumulative distribution taken from Figures A-14 through A-16, A-18, and A-19. Figure A-17 was not included in the averaged statistics because of the unusally high backlobe level due to hangar reflections. An examination of Figure A-20 shows the standard deviation is decreasing as the percentage of time exceeded is increasing from 80% to 100%. In theory, this should not be true due to variations in site clutter. This indicates that the measurements have been biased due to insufficient dynamic range of the measurement receiver. This is discussed in Appendix G.

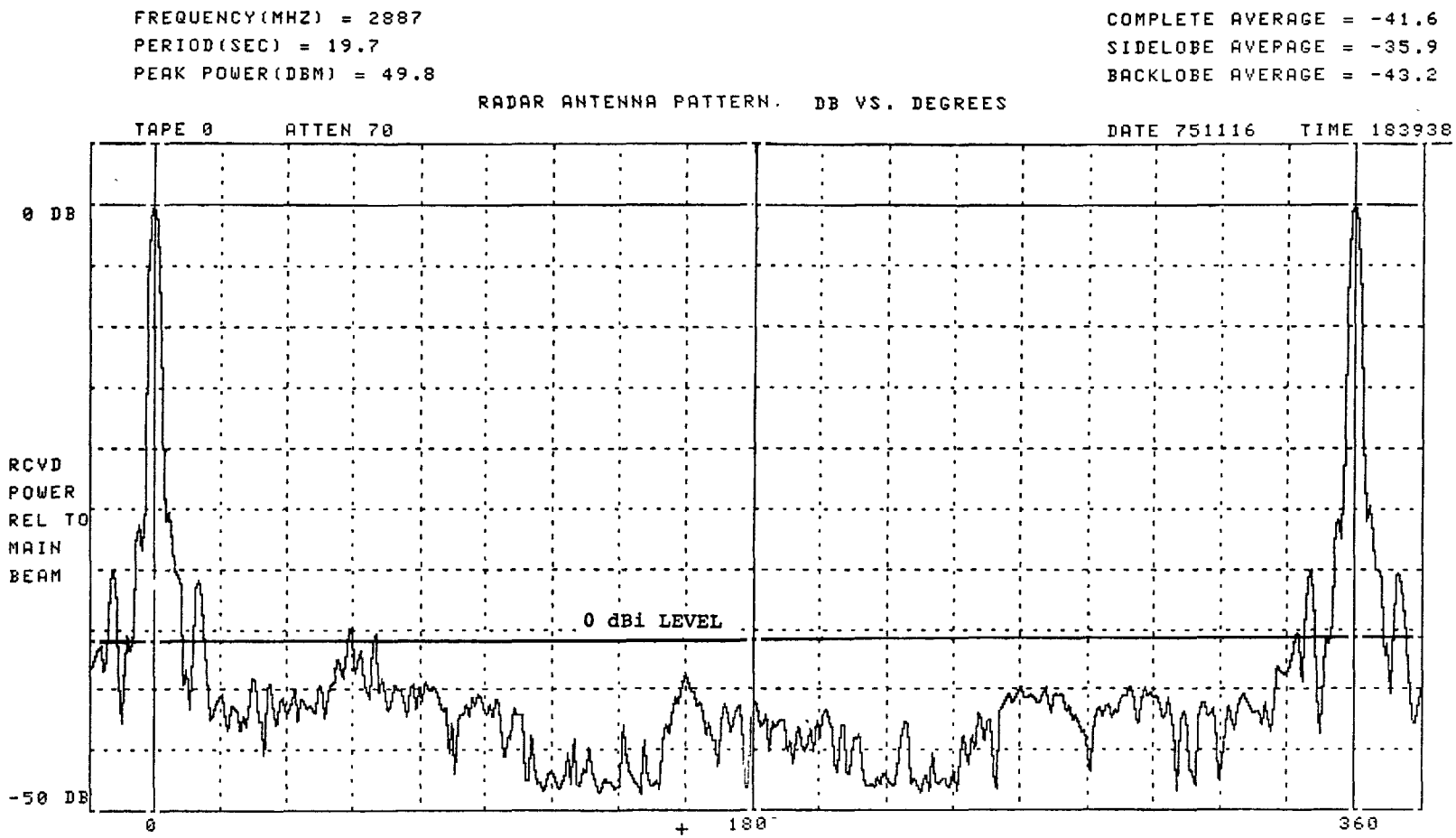

Figure A-11. Measured Antenna Radiation Pattern of Sacramento WSR-57 for Antenna Tilt of 0°

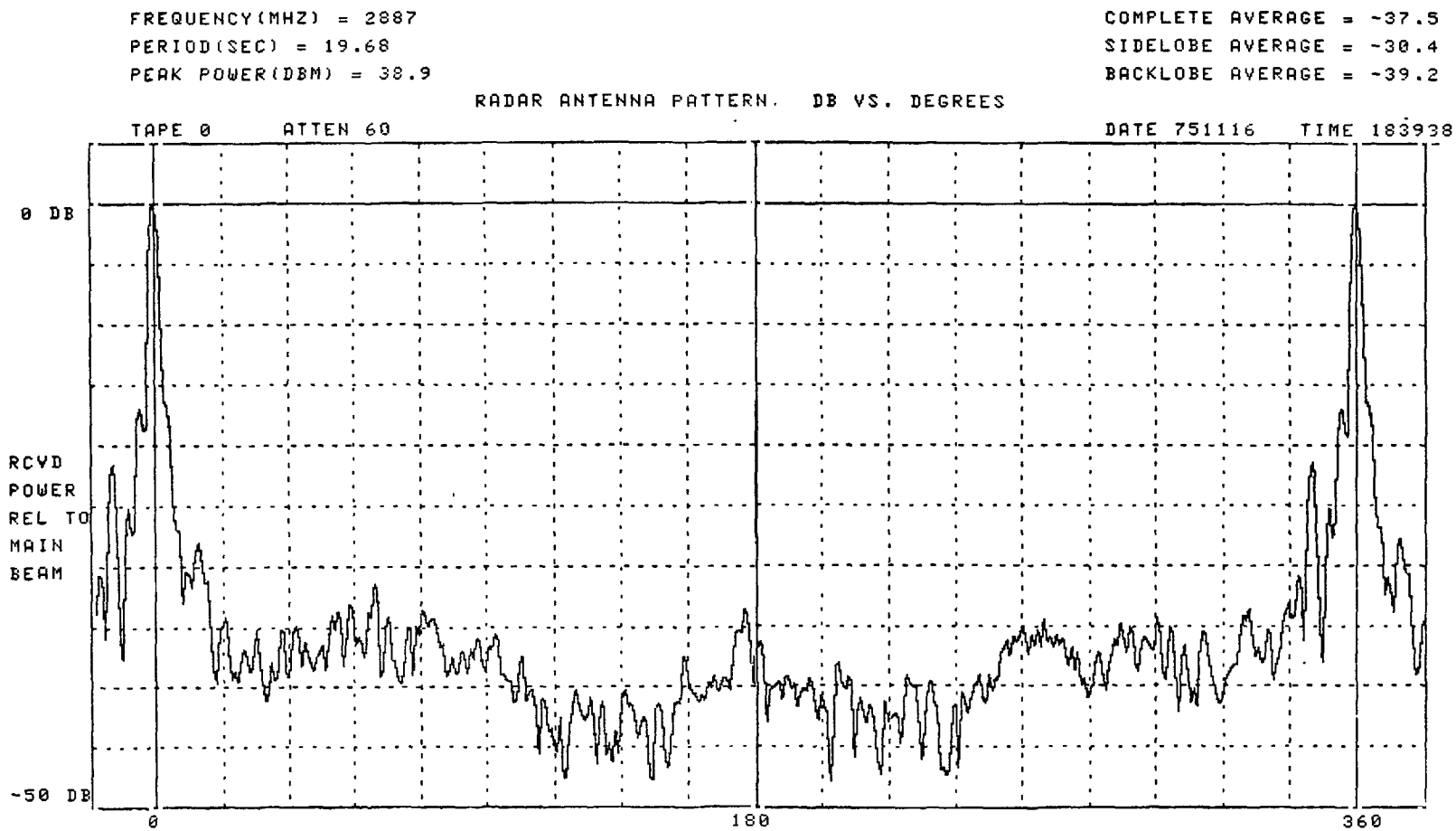

Figure A-12. Measured Antenna Radiation Pattern of Sacramento WSR-57 for Antenna Tilt of 1°

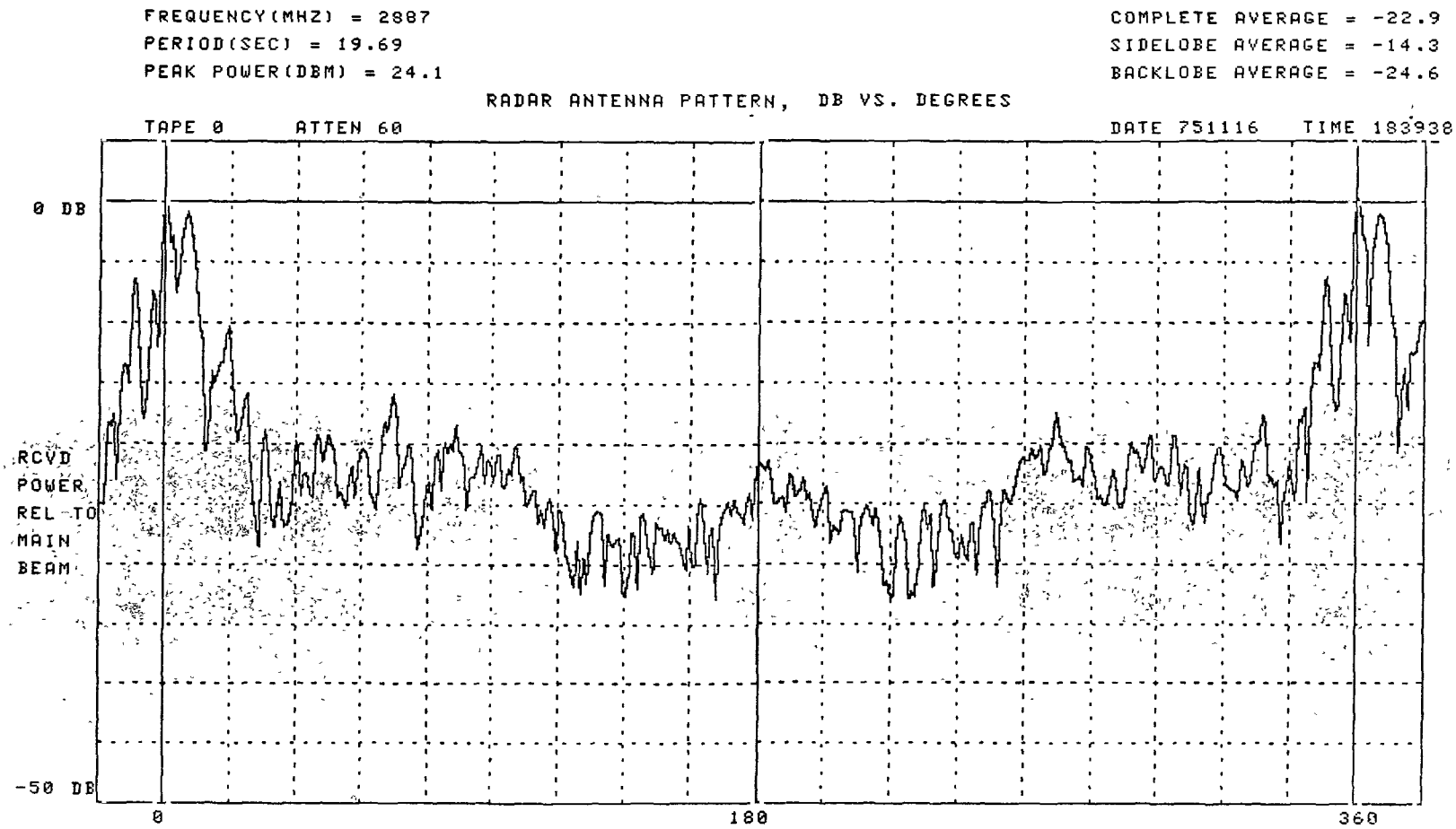

Figure A-13. Measured Antenna Radiation Pattern of Sacramento WSR-57 for Antenna Tilt of 2^{o}

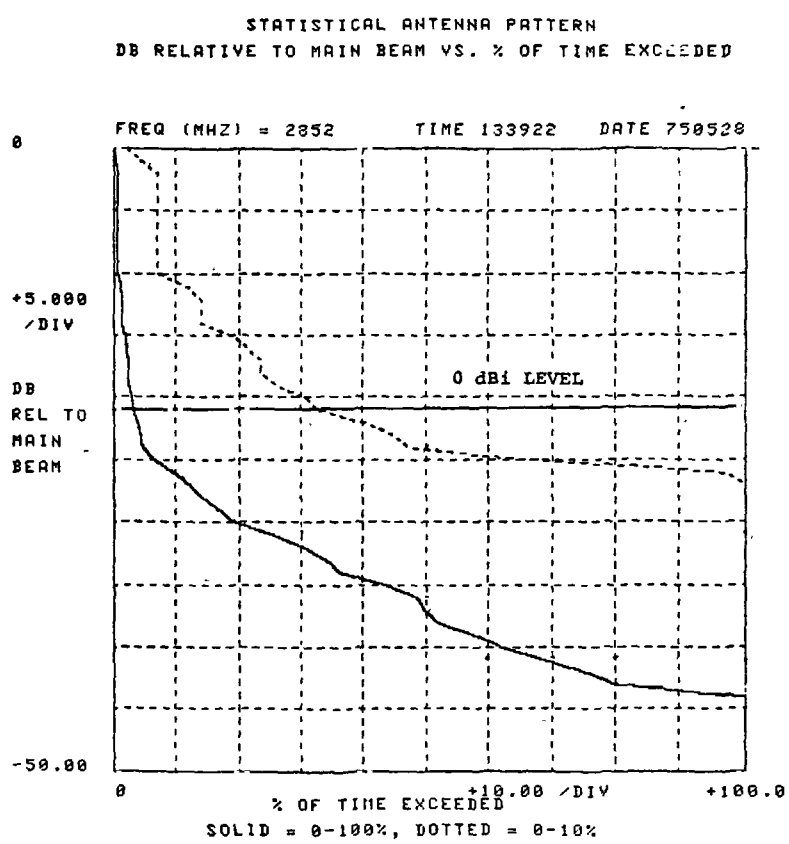

Figure A-14. Cumulative Distribution of Los Angeles ASR-7 Antenna Radiation Pattern

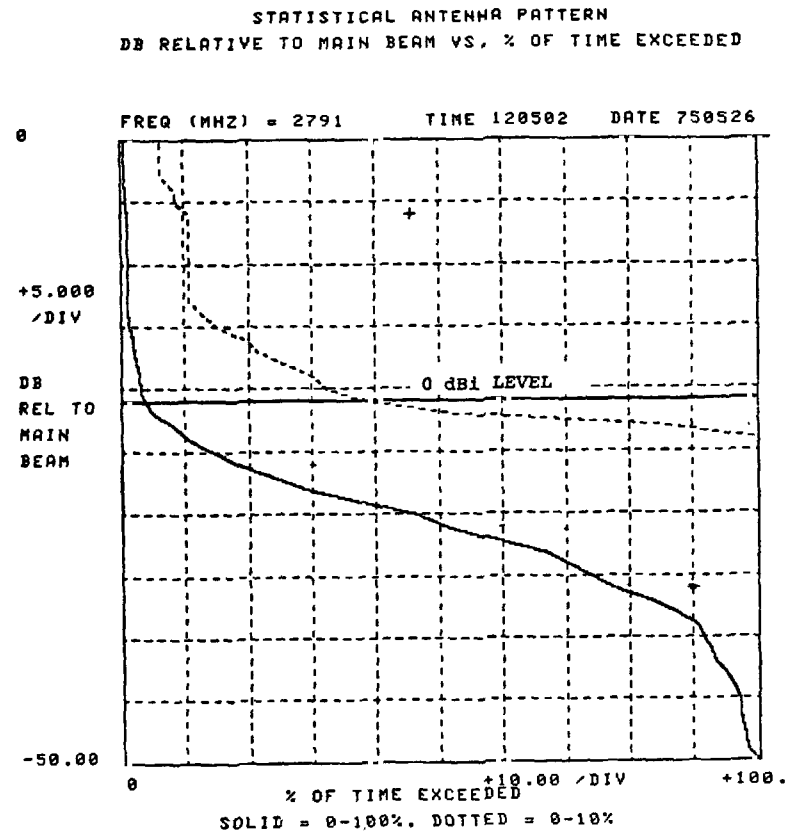

Figure A-15. Cumulative Distribution of Burbank ASR-6 Antenna Radiation Pattern

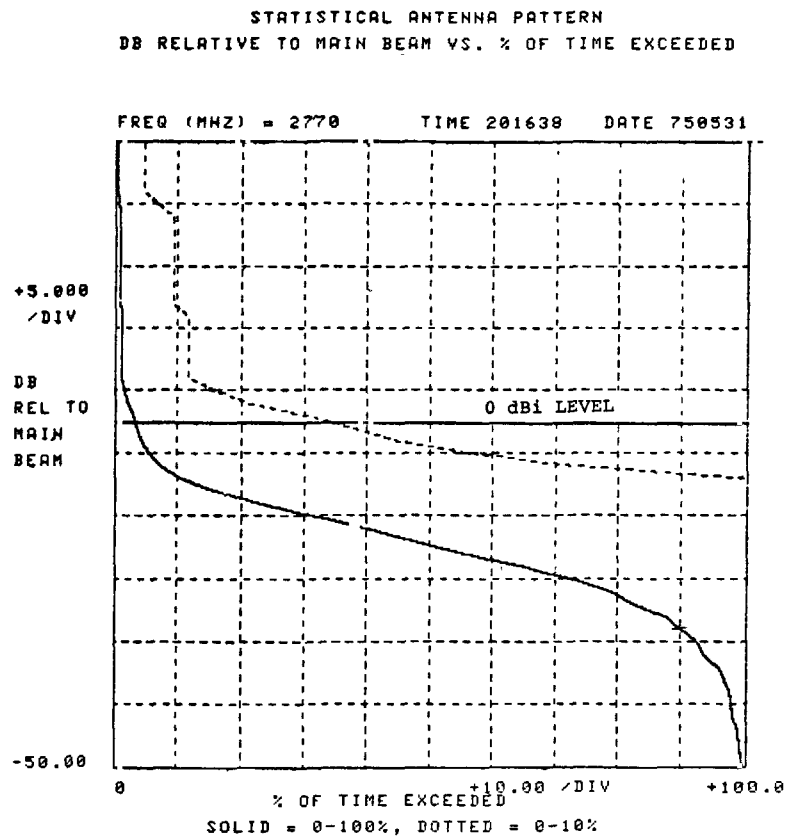

Figure A-16. Cumulative Distribution of Long Beach ASR-5 Antenna Radiation Pattern

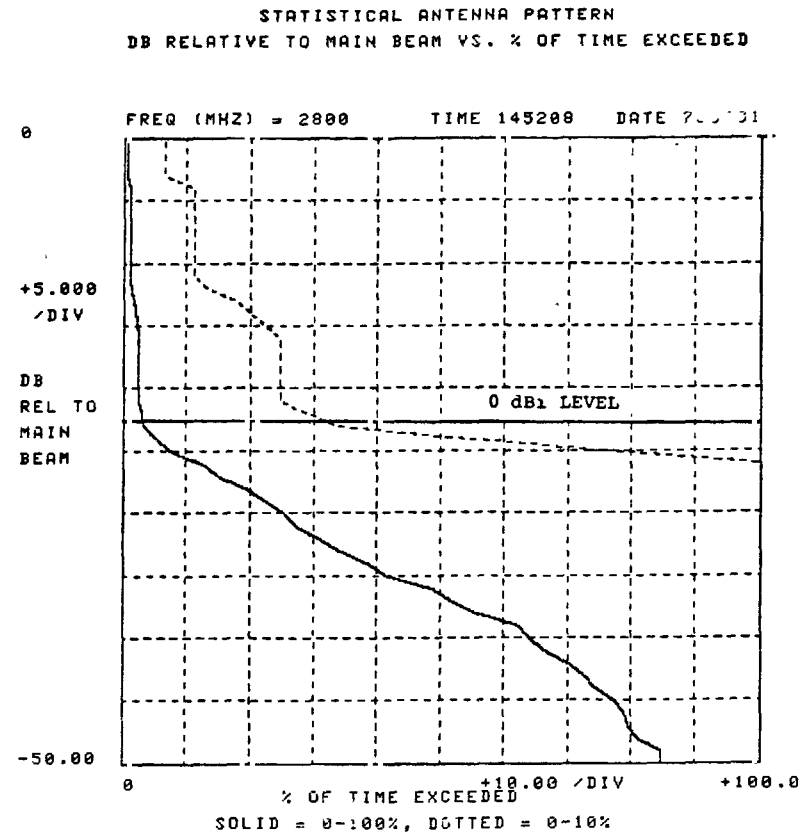

Figure A-17. Cumulative Distribution of Norton AN/MPN-13 Antenna Radiation Pattern

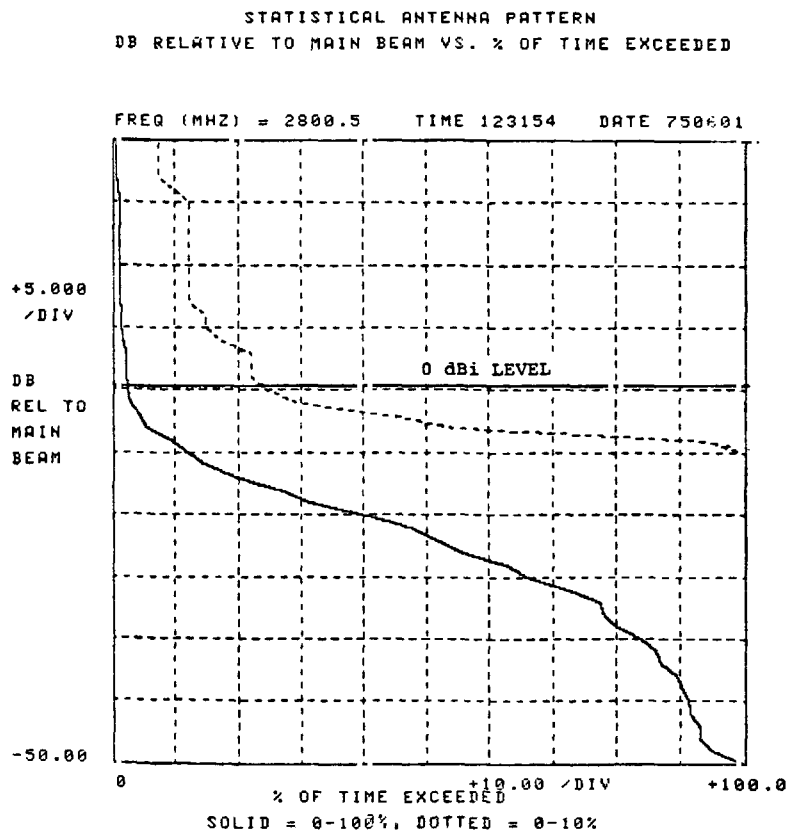

Figure A-18. Cumulative Distribution of March AN/MPN-13 Antenna Radiation Pattern

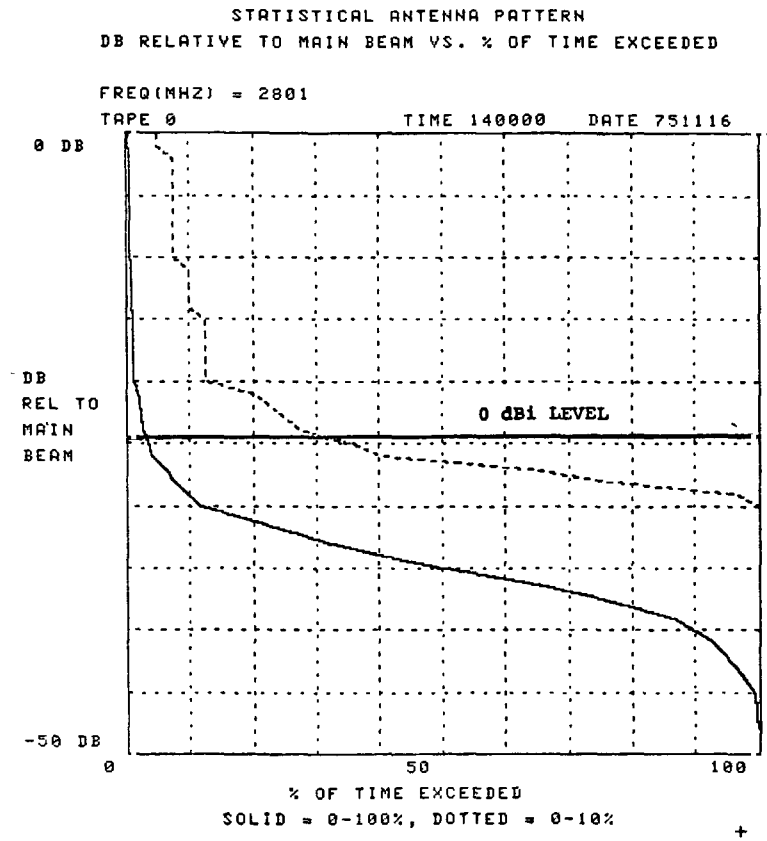

Figure A-19. Cumulative Distribution of Travis AFB AN/FPN-55 Antenna Radiation Pattern

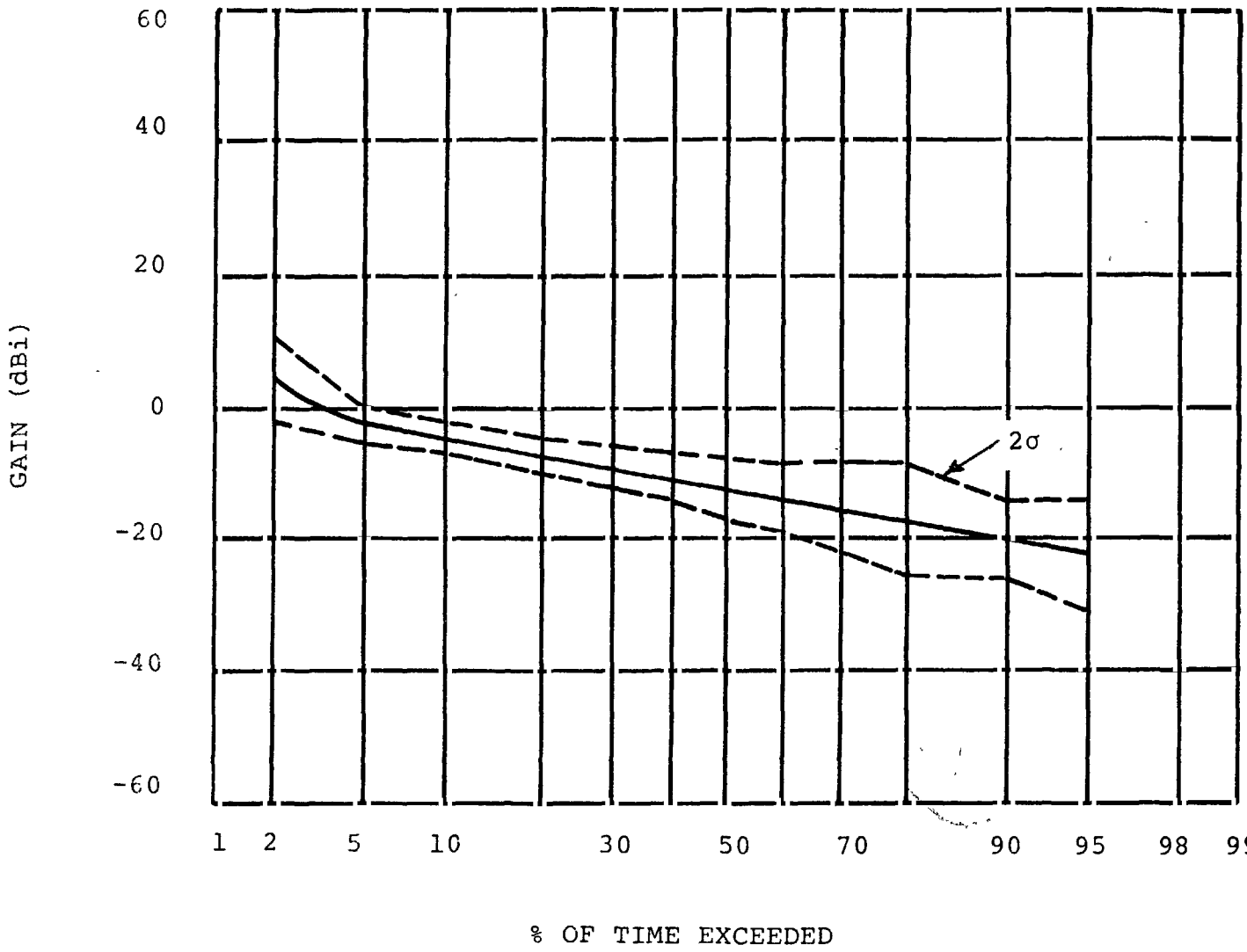

Figure A-20. Averaged Cumulative Antenna Gain Distribution of 2.7-2.9 GHz Radars

MUTUAL ANTENNA GAIN MODEL

Previous discussions in this appendix dealt with statistical models of single antennas. However, since both the victim and interfering antennas are rotating and both the antennas determine the level of interference coupled into the victim receiver, it is appropriate to determine a statistical distribution of the mutual antenna gain of both antennas. Since the probability distribution of the victim and interfering antenna radiation pattern are independent, the mutual antenna gain can be obtained by taking the convolution of the distributions of the victim and interfering antenna radiation patterns.

Figures A-21 and A-22 show the antenna radiation pattern of the Ontario ASR-5 radar and Burbank ASR-6 radar respectively measured by the FAA. Tables A-2 and A-3 show the probability distribution and cumulative distribution of both radars respectively. The mutual antenna gain distribution can be obtained by forming a random variable, G_m, (Reference 19).

$$G_m = G1 + G2 \qquad \text{(A-1)}$$

Where the probability of a specific mutual antenna gain level (G_m) is given by:

$$P(G1_i+G2_j = G_{mr}) = \Sigma\, a_i b_j$$

Where: $\Sigma\, a_i b_j$ = the sum of all mutually exclusive events where $G1_i + G2_j = G_{mr}$

a_i = Probability of $G1_i$

b_j = Probability of $G2_j$

Figure A-23 shows the mutual antenna gain probability distribution of the two patterns shown in Figures A-21 and A-22. The straight line of the mutual antenna gain distribution between -8 dBi and -40 dBi indicates that the mutual antenna gain distribution in this region is gaussian distributed.

Even though the statistical mutual antenna gain model described in this section takes into account the line-of-sight azimuthal radiation patterns of the victim and interfering radars, the model is not a realistic statistical model which can be used to predict the interfering power level received

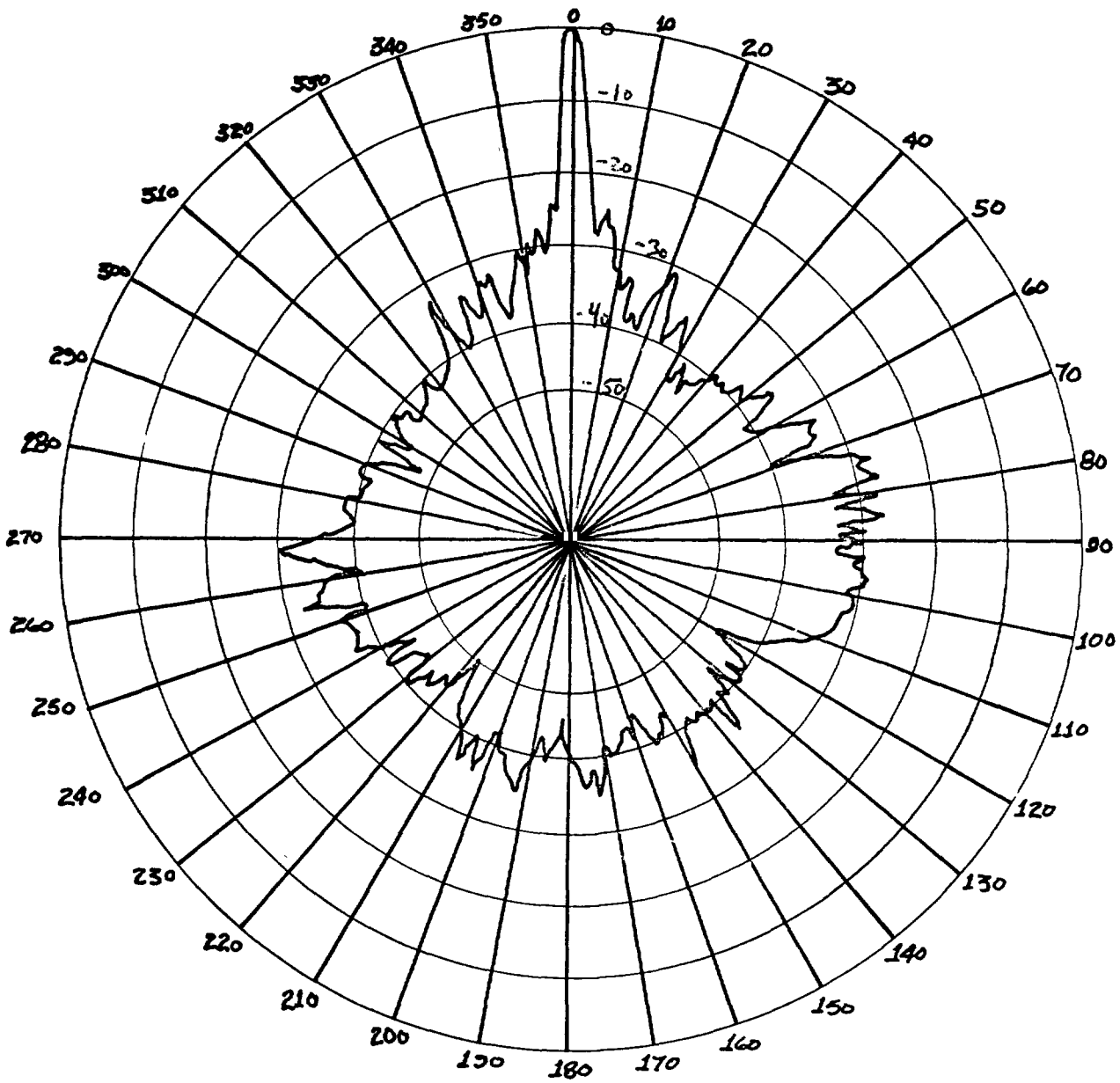

Figure A-21. Antenna Radiation Pattern of Ontario ASR-5 Radar Measured by the FAA

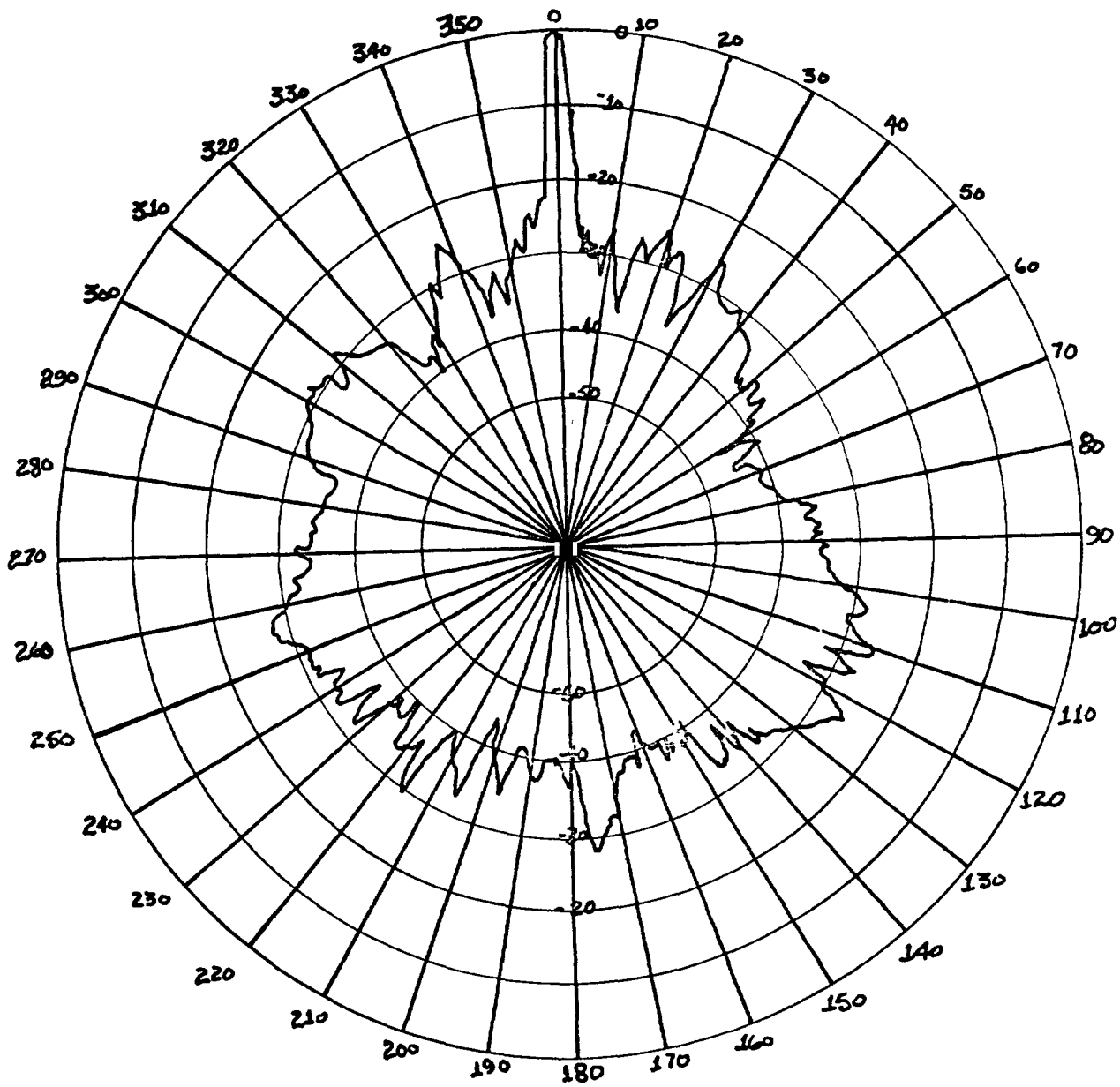

Figure A-22. Antenna Radiation Pattern of Burbank ASR-6 Radar Measured by the FAA

TABLE A-2

ANTENNA RADIATION PATTERN STATISTICS
OF ONTARIO ASR-5 RADAR

GAIN IN dBi (Gl_i)	BIN COUNT	CUMULATIVE SUM	CUMULATIVE PROBABILITY	PROBABILITY DISTRIBUTION (a_i)
27	1	1	.28	.28
25	1	2	.56	.28
24	1	3	.83	.28
23	1	4	1.11	.28
17	1	5	1.39	.28
9	1	6	1.67	.28
3	2	8	2.22	.55
2	1	9	2.50	.28
1	2	11	3.06	.56
0	4	15	4.17	1.11
-1	3	18	5.00	.83
-2	4	22	6.11	1.11
-3	16	38	10.56	4.45
-4	13	51	14.17	3.61
-5	8	59	16.39	2.22
-6	9	68	18.89	2.50
-7	17	85	23.61	4.72
-8	11	96	26.67	3.06
-9	27	123	34.17	7.50
-10	11	134	37.22	3.05
-11	35	169	46.94	9.72
-12	19	188	52.22	5.28
-13	51	239	66.39	14.17
-14	29	268	74.44	8.05
-15	32	300	83.33	8.89
-16	16	316	87.78	4.45
-17	25	341	94.72	6.94
-18	9	350	97.22	2.50
-19	6	356	98.89	1.67
-20	1	357	99.17	.28
-21	2	359	99.72	.55
-23	1	360	100.00	.28

TABLE A-3

ANTENNA RADIATION PATTERN STATISTICS
OF BURBANK ASR-6 RADAR

GAIN IN dBi ($G2_j$)	BIN COUNT	CUMULATIVE SUM	CUMULATIVE PROBABILITY	PROBABILITY DISTRIBUTION (b_j)
27	1	1	.28	.28
20	1	2	.56	.28
25	1	3	.83	.28
15	1	4	1.11	.28
7	1	5	1.39	.28
4	1	6	1.67	.28
2	2	8	2.22	.55
1	9	17	4.72	2.50
0	7	24	6.67	1.95
-1	15	39	10.83	4.16
-2	17	56	15.56	4.73
-3	39	95	26.39	10.83
-4	15	110	30.56	4.17
-5	45	155	43.06	12.50
-6	30	185	51.39	8.33
-7	30	215	59.72	8.33
-8	16	231	64.17	4.45
-9	31	262	72.78	8.61
-10	14	276	76.67	3.89
-11	30	306	85.00	8.33
-12	6	312	86.67	1.67
-13	17	329	91.39	4.72
-14	11	340	94.44	3.05
-15	11	351	97.50	3.06
-16	4	355	98.61	1.11
-17	3	358	99.44	.83
-18	1	359	99.72	.28
-19	1	360	100.00	.28

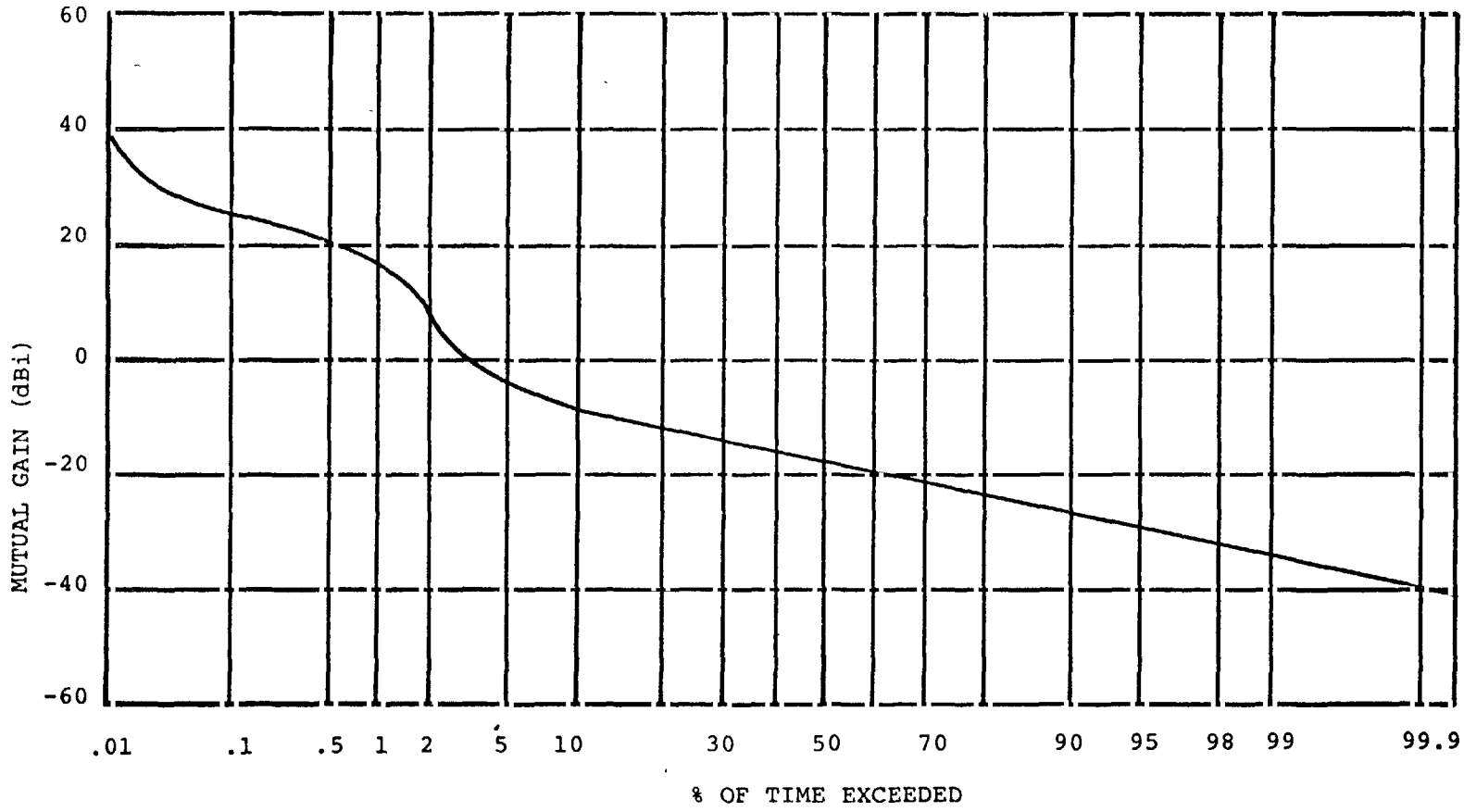

Figure A-23. Mutual Antenna Gain Distribution of Ontario ASR-5 and Burbank ASR-6 Radars.

as a function of the azimuth orientation of the victim and interfering antennas. Other parameters which contribute to the power level received as a function of the azimuth orientation of the victim and interfering radar are discussed in the next section.

ENVIRONMENTAL ANTENNA PATTERN MEASUREMENTS

In addition to line-of-sight antenna patterns at the victim and interferer radar sites, environmental modified antenna patterns of interfering radars were measured at the victim radar site during the Los Angeles and San Francisco area investigations. The main objective of these measurements was to determine if the environment was altering the received interfering power level as a function of azimuth orientation of the victim and interfering antennas in addition to the variation due to free-space antenna coupling. Measurements made during the Los Angeles-San Francisco area investigations revealed several cases where multipath wave interference, arising from multiple scattering of the waves by mountains, buildings and other structures, was occurring which significantly changed the statistical distribution of the interfering power level at the victim receiver RF input resulting in unpredicted interference.

From an electromagnetic theory viewpoint, the multipathing (terrain and building reflections) of the interfering signal is a propagation phenomena. However, the effect of these propagation phenomena is to alter the received interfering power level as a function of the azimuth orientation of the victim and interfering antennas. Actually, the multipathing of interfering signals and the antenna pattern characteristics of the victim and interferer antennas are statistical parameters which are very difficult to separate in the real environment. Therefore, from a modeling aspect of the multipathing phenomena, it appears that it would be more practical to incorporate the modeling of multipathing with the mutual antenna gain distribution model.

The following is a discussion of the environmental modified antenna patterns of potential interfering radars made at the victim radar sites. Because of differences in antenna heights and antenna patterns of the victim radar antenna and RSMS van dish antenna, extreme care was required in extrapolating data measured with the RSMS van dish antenna to what the victim radar antenna would see. Also, in some cases, due to low received interfering power level, a complete interfering antenna pattern could not be measured. These

measurements were made with the measurement antenna stationary and the interferer antenna rotating.

Some measurements were also made of the peak power received from interfering radars while rotating the RSMS van dish. These measurements were made to document the multipath reflections of the environment and are discussed in the propagation Appendix D.

Los Alamitos

Measurements of interferer environmental antenna patterns were made at the Los Alamitos AN/CPN-4 radar site using both the RSMS van dish and the antenna of the AN/CPN-4 radar. The RSMS van dish was approximately the same height (14 ft.) as the antenna of the AN/CPN-4 radar. The following is a brief discussion of interferer environmental antenna patterns measured at the Los Alamitos radar site.

Long Beach ASR-5 - Figure A-24 shows the Long Beach ASR-5 environmental antenna pattern measured at the Los Alamitos radar site using the RSMS van dish. A comparison of Figure A-24 with Figure A-6 (Line-of-sight-measurement) indicates that multipath reflections were occurring from the environment. Also the average backlobe level of the antenna pattern measured at Los Alamitos is 5.6 dB lower. This tends to indicate that the backlobe level is being attenuated more than the mainbeam due to foreground clutter at the Long Beach site. This was one of the factors contributing to not being able to observe the predicted interference from the Long Beach ASR-5 radar.

Ontario ASR-5 - Figures A-25 and A-26 show the Ontario ASR-5 environmental antenna pattern measured at the Los Alamitos radar site with the RSMS van dish pointed at 35° and 40° respectively. The Ontario ASR-5 radar is at a bearing of 40°. A comparison of these figures with Figure A-5 shows that there is a significant amount of multipathing occurring. The multipathing was caused by Chino Hills between Los Alamitos and Ontario with elevations over 2000 feet. Figure A-27 shows the Ontario ASR-5 antenna pattern measured at Los Alamitos using the AN/CPN-4 radar antenna pointing at 40° magnetic. One can easily see that there is a significant difference between Figures A-26 and A-27. The reason for this difference is that the AN/CPN-4 antenna has only a 1.5° azimuth beamwidth as compared to the 8 degree azimuth beamwidth of the RSMS van dish resulting in a different spatial weighting of the multipathing signal. However, during this set of measurements, the AN/CPN-4 antenna was aimed between 30° - 50° magnetic with very little change in peak

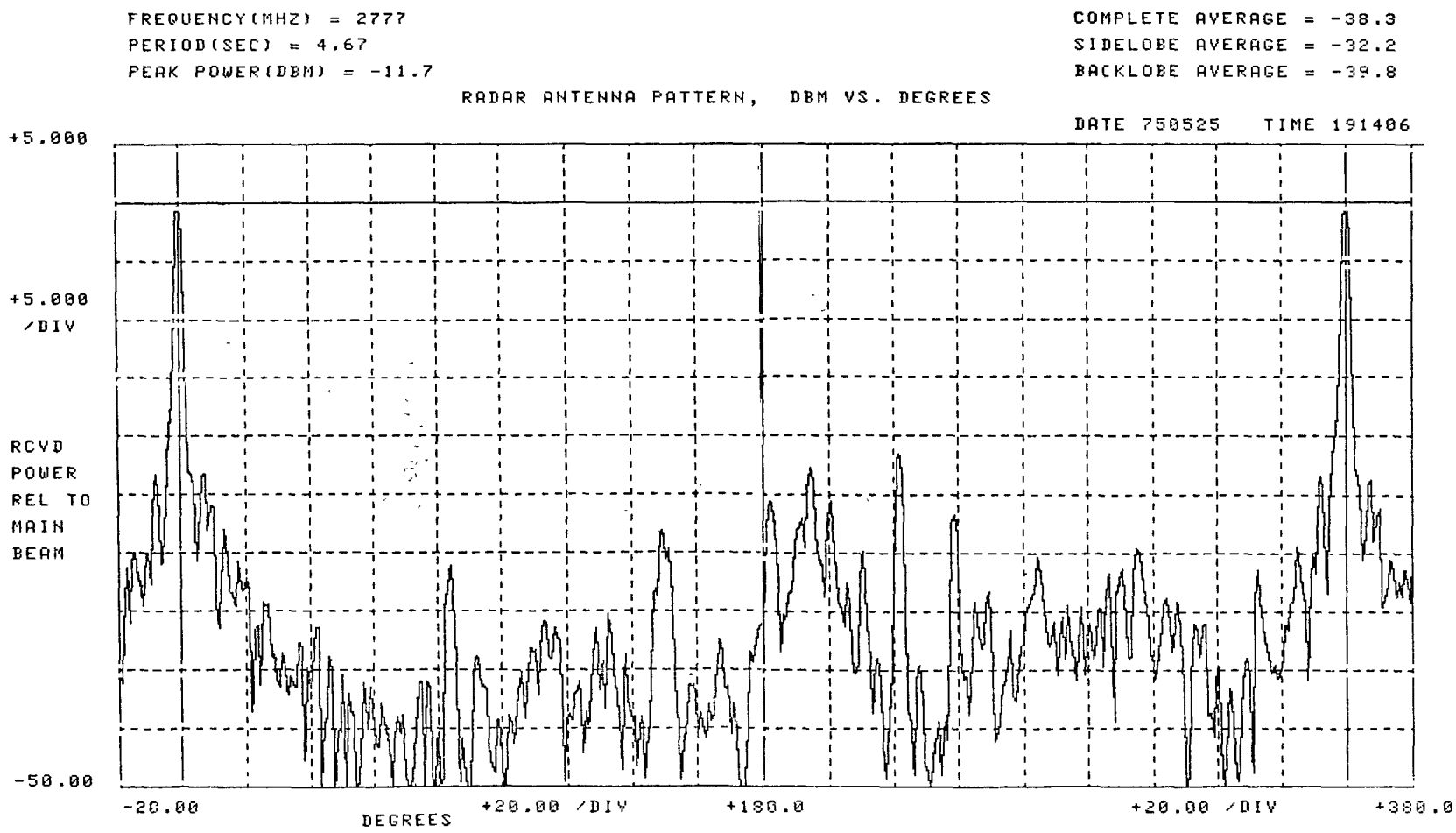

Figure A-24. Long Beach ASR-5 Antenna Pattern Measured at Los Alamitos Using RSMS Van Dish Pointing at 278° Magnetic

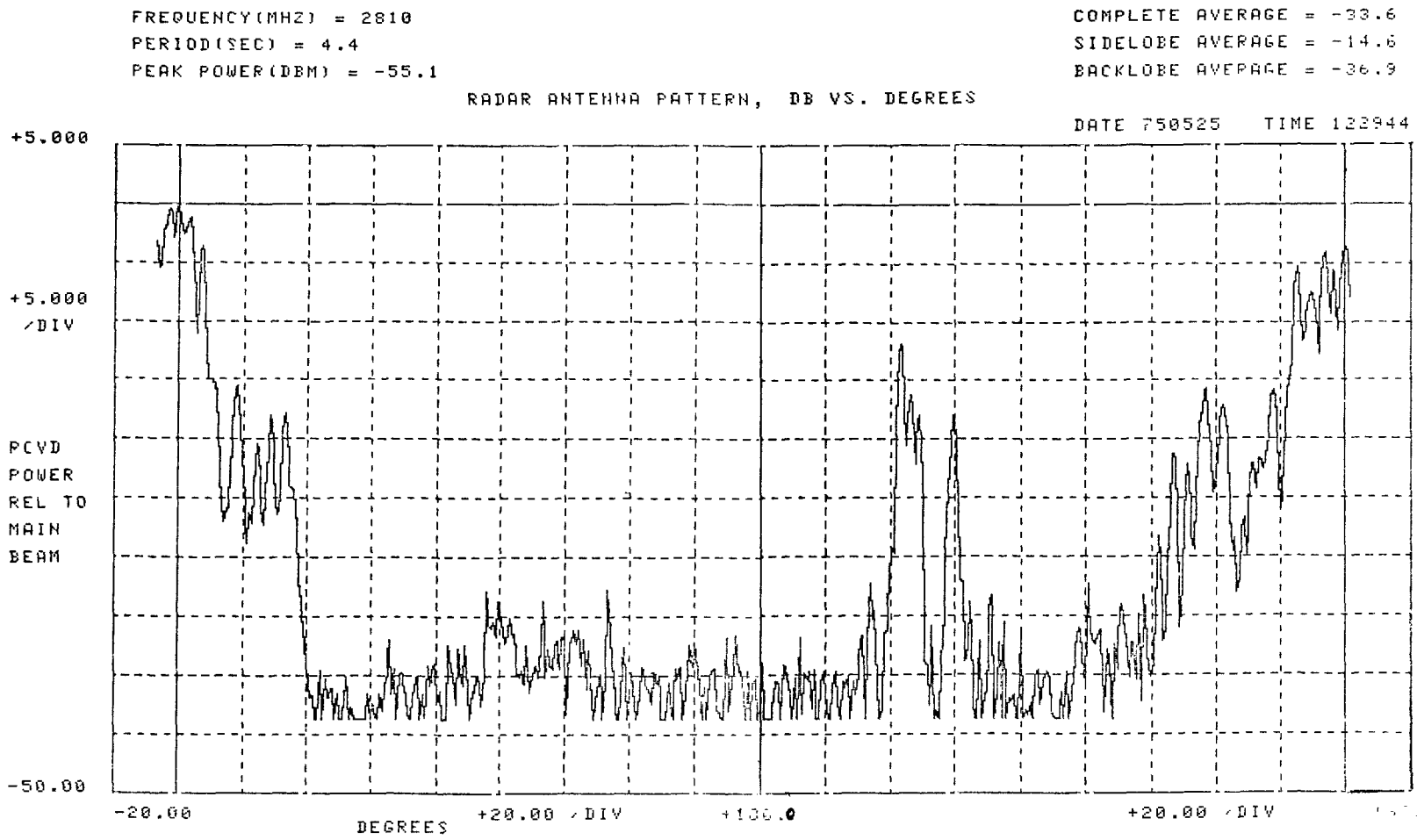

Figure A-25. Ontario ASR-5 Antenna Pattern Measured at Los Alamitos Using RSMS Van Dish Pointed at 35° Magnetic

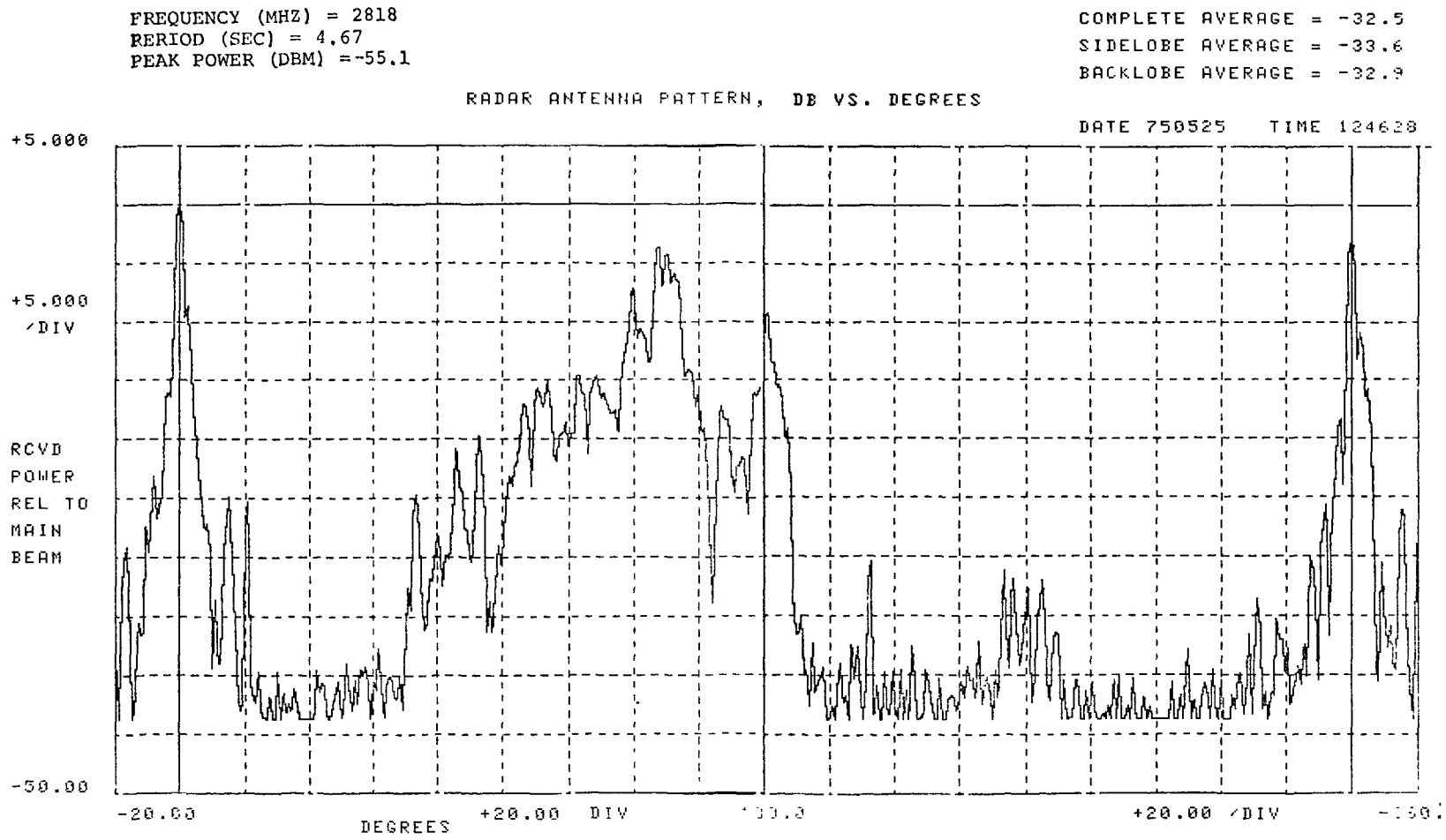

Figure A-26. Ontario ASR-5 Antenna Pattern Measured at Los Alamitos Using Van Dish Pointed at 40° Magnetic

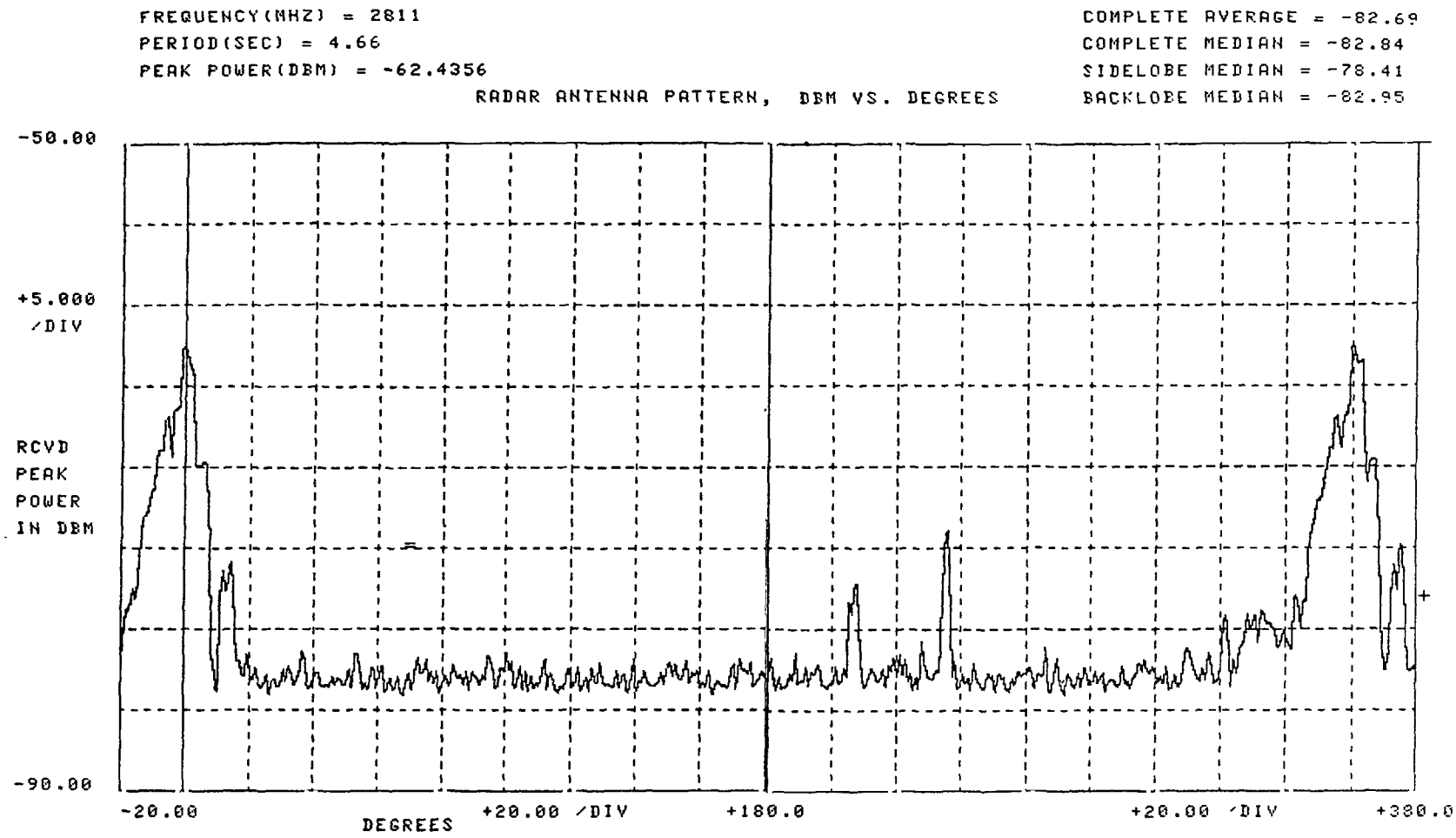

Figure A-27. Ontario ASR-5 Antenna Pattern Measured at Los Alamitos Using AN/CPN-4 Antenna Pointed at 40° Magnetic

received power measured on the 8580 spectrum analyzer. Also during these measurements the oscilloscope on the van was observed, and the pulses from the Ontario ASR-5 radar were stretched out to approximately 100 μsec.

Norton AN/MPN-13 - Figure A-28 shows the Norton AFB AN/MPN-13 environmental antenna pattern measured at the Los Alamitos radar site with the AN/CPN-4 antenna pointed at 56.5° magnetic. The pulse train separator AS-330 was used to discriminate between the Norton AFB AN/MPN-13 and the March AFB AN/MPN-13 since both radars operate at approximately 2800 MHz. The Norton radar was requested to operate on three stagger (3x365 = 1095) PRF, and the March radar with stagger off (1095 PRF). When Figure A-8 is compared with Figure A-28, the environmental antenna pattern shows the multipathing caused by the Chino Hills located between Los Alamitos NAS and the Norton AFB.

Long Beach

Measurements of interferer environmental antenna patterns were also made at the Long Beach ASR-5 radar site using both the RSMS van dish antenna and the antenna of the ASR-5 radar. The RSMS van dish antenna height is 14 feet, and the ASR-5 antenna height is 26 feet. The following is a discussion of the environmental antenna patterns measured at the Long Beach radar site.

Los Alamitos AN/CPN-4 - Figure A-29 shows the Los Alamitos AN/CPN-4 environmental antenna pattern measured at the Long Beach radar site with the RSMS van dish pointed at 97.4° magnetic. A comparison of Figure A-29 with Figure A-7 (Line-of-sight measurement) shows that the average backlobe level is 9.7 dB lower at Long Beach indicating that the environment is attenuating the backlobe more than the mainbeam due to foreground clutter.

Figure A-30 shows the Los Alamitos antenna pattern measured using the Long Beach ASR-5 antenna operating in the right-hand circular polarization mode (same as RSMS van dish). The mainbeam to average backlobe level using the ASR-5 antenna is only 33 dB as compared to 43 dB (Figure A-29) using the RSMS van dish. It is difficult to resolve this difference in mainbeam to average backlobe ratio in a multipath environment since it is not known whether the difference in atenna height between the RSMS van dish and the radar may have changed the average backlobe level or the differences in the radar and van antenna patterns caused the change of average backlobe level.

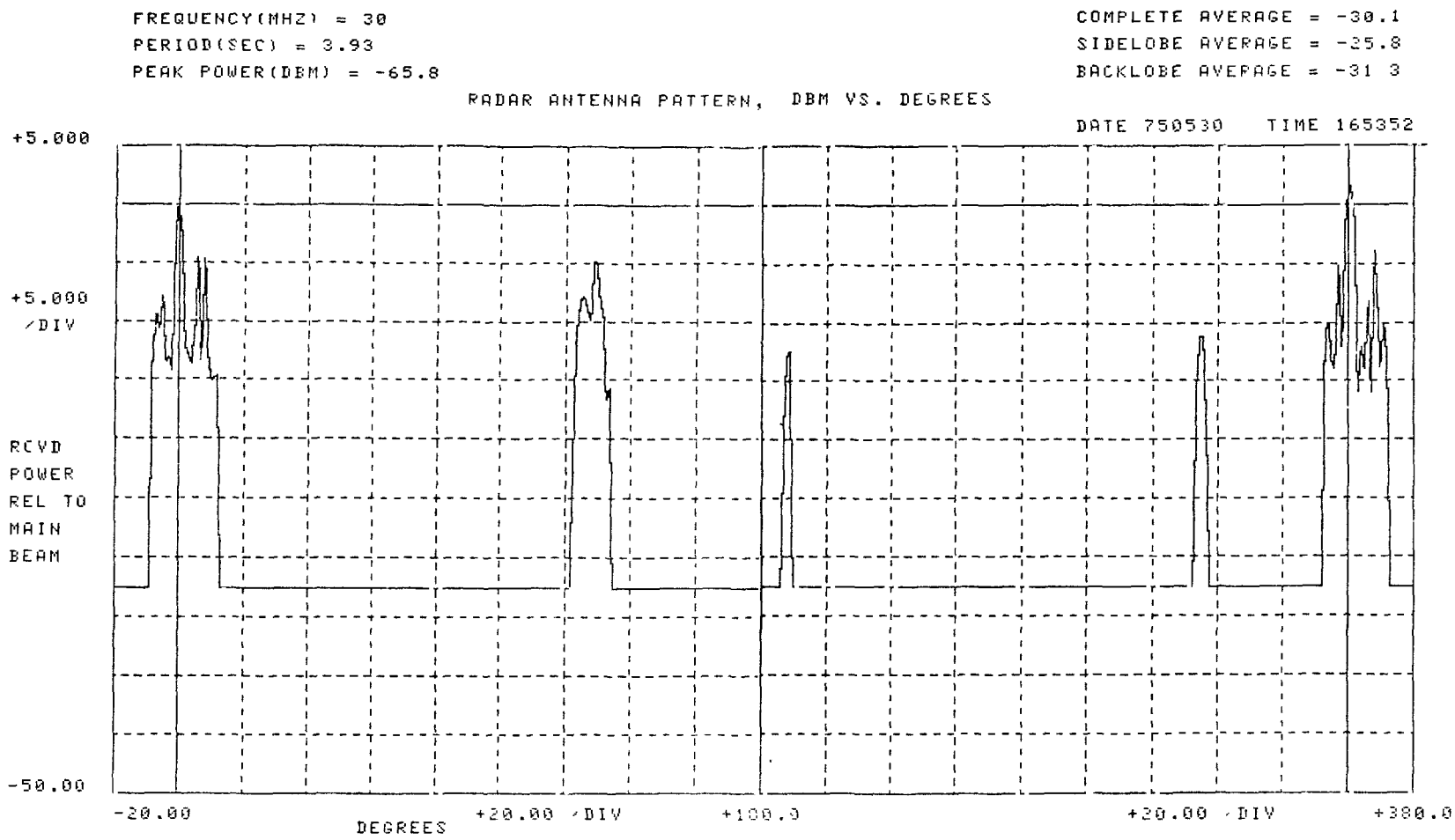

Figure A-28. Norton AN/MPN-13 Antenna Pattern Measured at Los Alamitos Using AN/CPN-4 Antenna Pointed at 56.5° Magnetic and Pulse Train Separator On

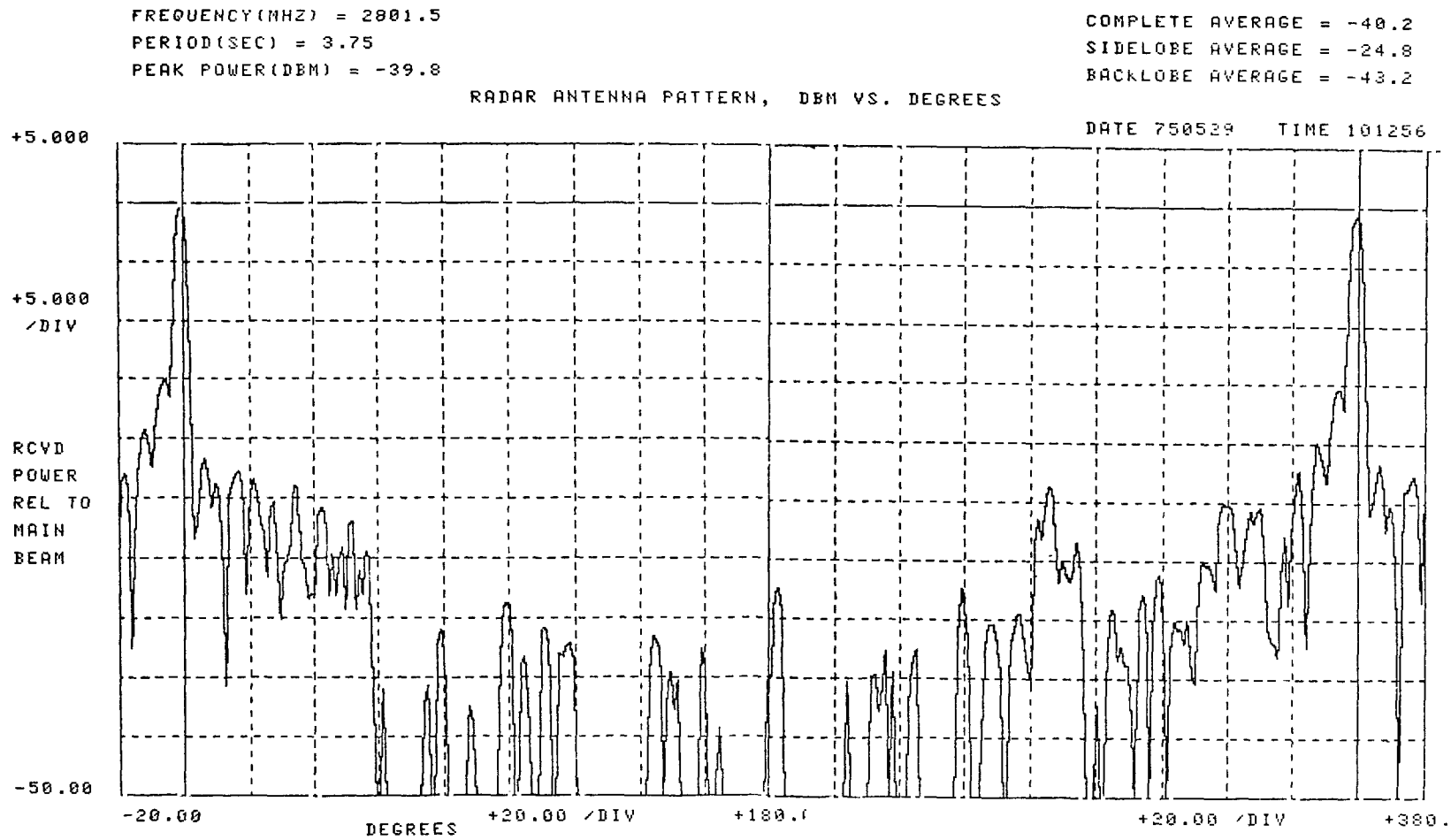

Figure A-29. Los Alamitos AN/CPN-4 Antenna Pattern Measured at Long Beach Using RSMS Van Dish Pointed at 97.4° Magnetic

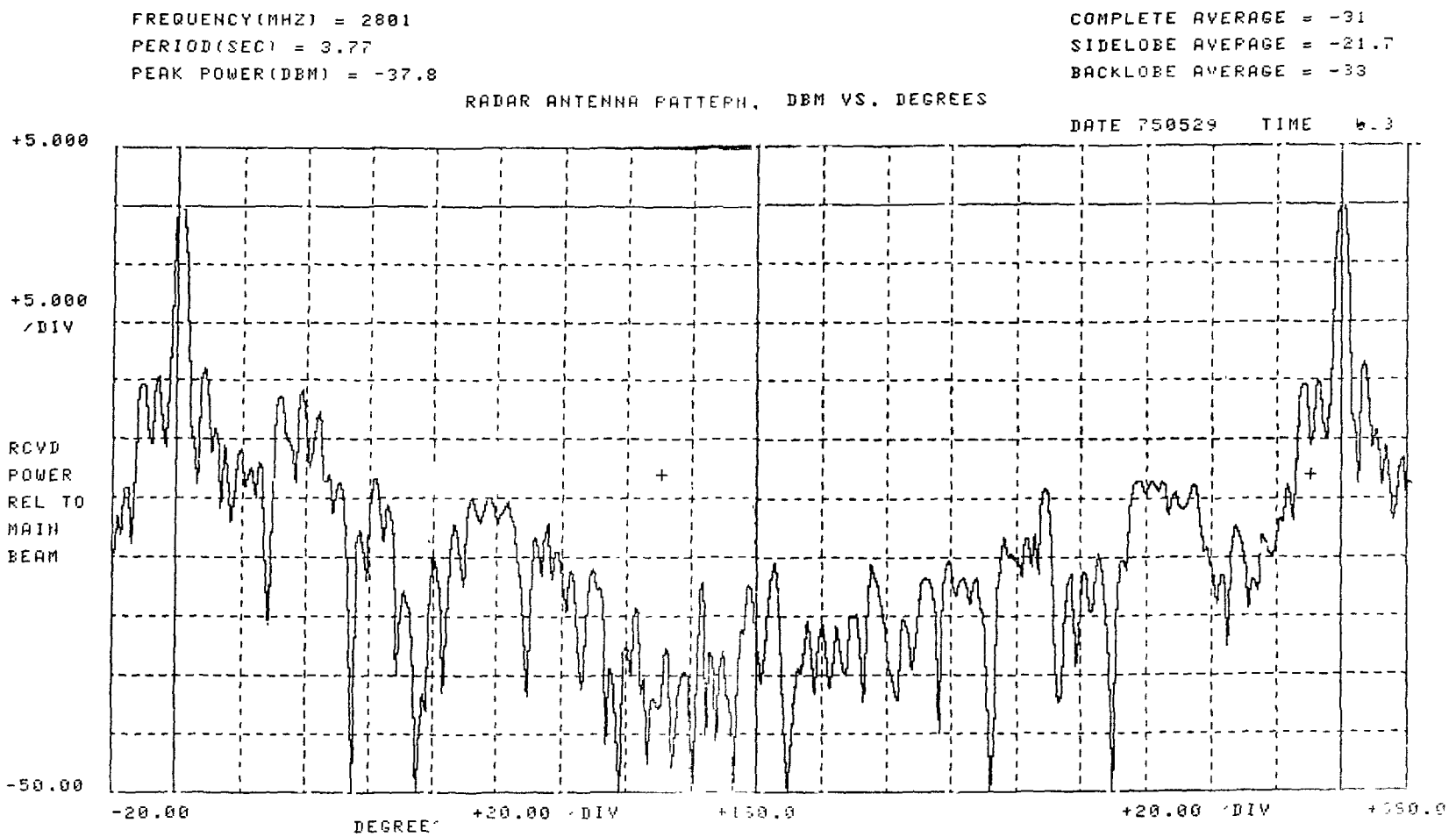

Figure A-30. Los Alamitos AN/CPN-4 Antenna Pattern Measured at Long Beach Using ASR-5 Radar Antenna in Circular Polarization and Pointed at 97.4° Magnetic

Figure A-31 shows the Los Alamitos antenna pattern measured using the Long Beach ASR-5 antenna operating in the vertical polarization mode. A comparison of Figure A-30 and A-31 shows that the mainbeam level has been attenuated by 6.2 dB (44 dBm - 37.8 dBm). The reason for this attenuation is due to the radar antenna polarization (Long Beach operating vertical and Los Alamitos operating horizontal). Also, a comparison of Figures A-25 and A-26, for the two different polarizations, shows that the average backlobe level is -71 dBm. This is expected since the polarization of the backlobes of a radar antenna are random.

Burbank ASR-6 - Figure A-32 shows the Burbank ASR-6 environmental antenna pattern measured at Long Beach with the RSMS van dish pointed at 319.6° magnetic. The pulse train separator, AS-330, was used to discriminate against the Long Beach signal. A comparison of Figure A-32 with Figure A-4 shows that there is a significant amount of multipathing caused by the Santa Monica mountain range, with Griffith Peak (altitude 1821 feet), which is between the two radars. The multipathing occurring between 270° and 300° is due to reflection off the San Gabriel mountain range with altitudes of up to 4000 feet.

Mountain View

Measurements of environmental antenna patterns of other radars were also made at the Mountain View ASR-5 radar site using both the RSMS van dish antenna and the antenna of the ASR-5 radar. The RSMS van dish antenna height is 14 feet, and the ASR-5 antenna height is 26 feet. The following is a discussion of the environmental antenna patterns measured at the Mountain View radar site.

Oakland ASR-7 - Figure A-33 shows the Oakland ASR-7 antenna pattern measured at the Mountain View radar site using the RSMS van dish pointed at 312° magnetic. A line-of-sight antenna pattern of the Oakland radar was not measured. Taking into consideration the tilt angle (3°) of the Oakland ASR-7 antenna, the mainbeam gain at zero degrees elevation is approximately 29 dBi (34 dBi -5 dB) using Figure A-2. Therefore, the mean backlobe level is -9.6 dBi which is close to the average median backlobe level (-12.85 dBi) given in Table A-1 for line-of-sight antenna radiation patterns. Thus the environmental antenna pattern of the Oakland ASR-7 radar measured at Mountain View was not significantly altered by propagation related phenomena, and, therefore, has statistical characteristics similar to typical line-of-sight antenna

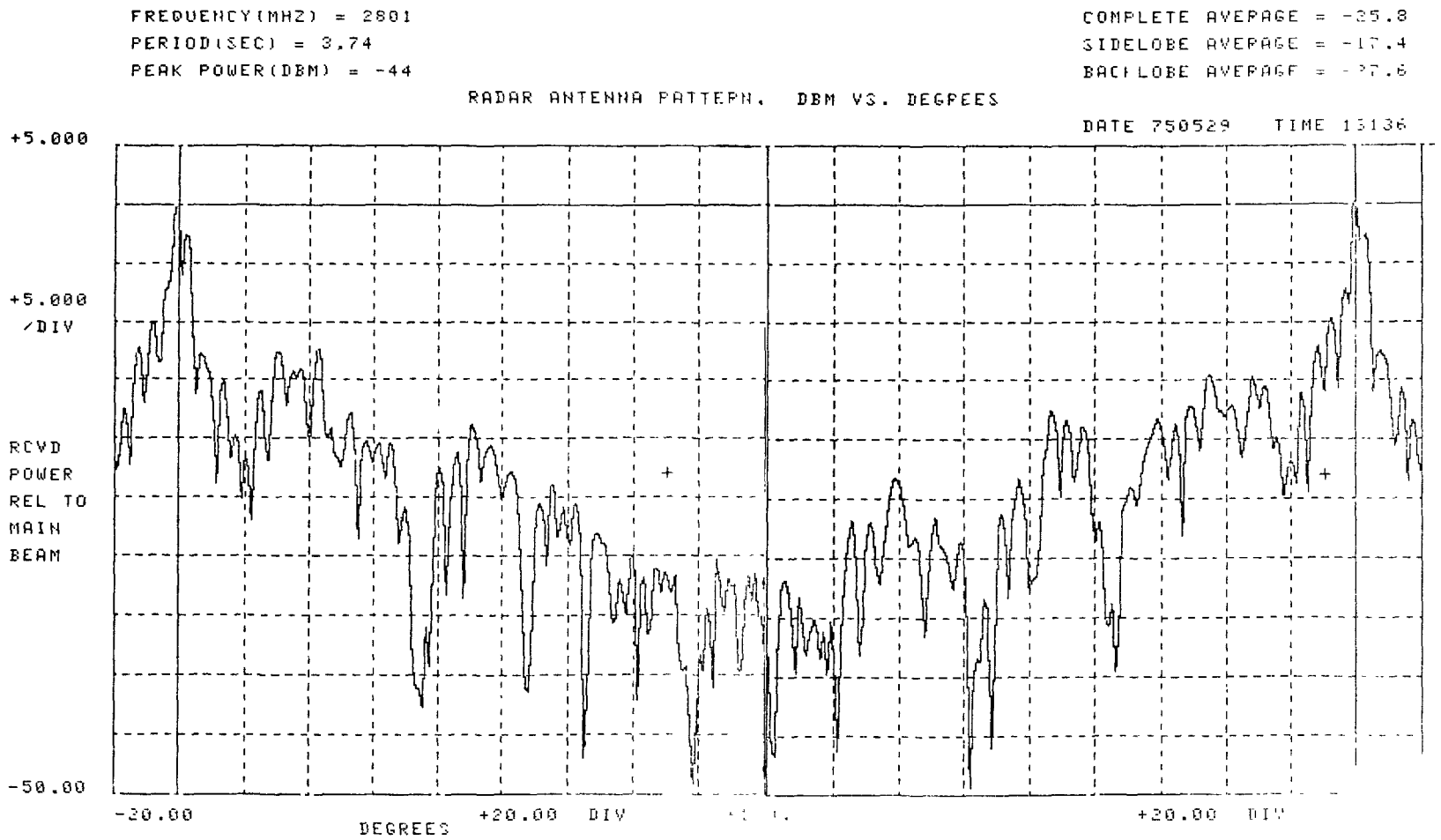

Figure A-31. Los Alamitos AN/CPN-4 Antenna Pattern Measured at Long Beach Using ASR-5 Radar Antenna in Vertical Polarization and Pointed at 97.4° Magnetic

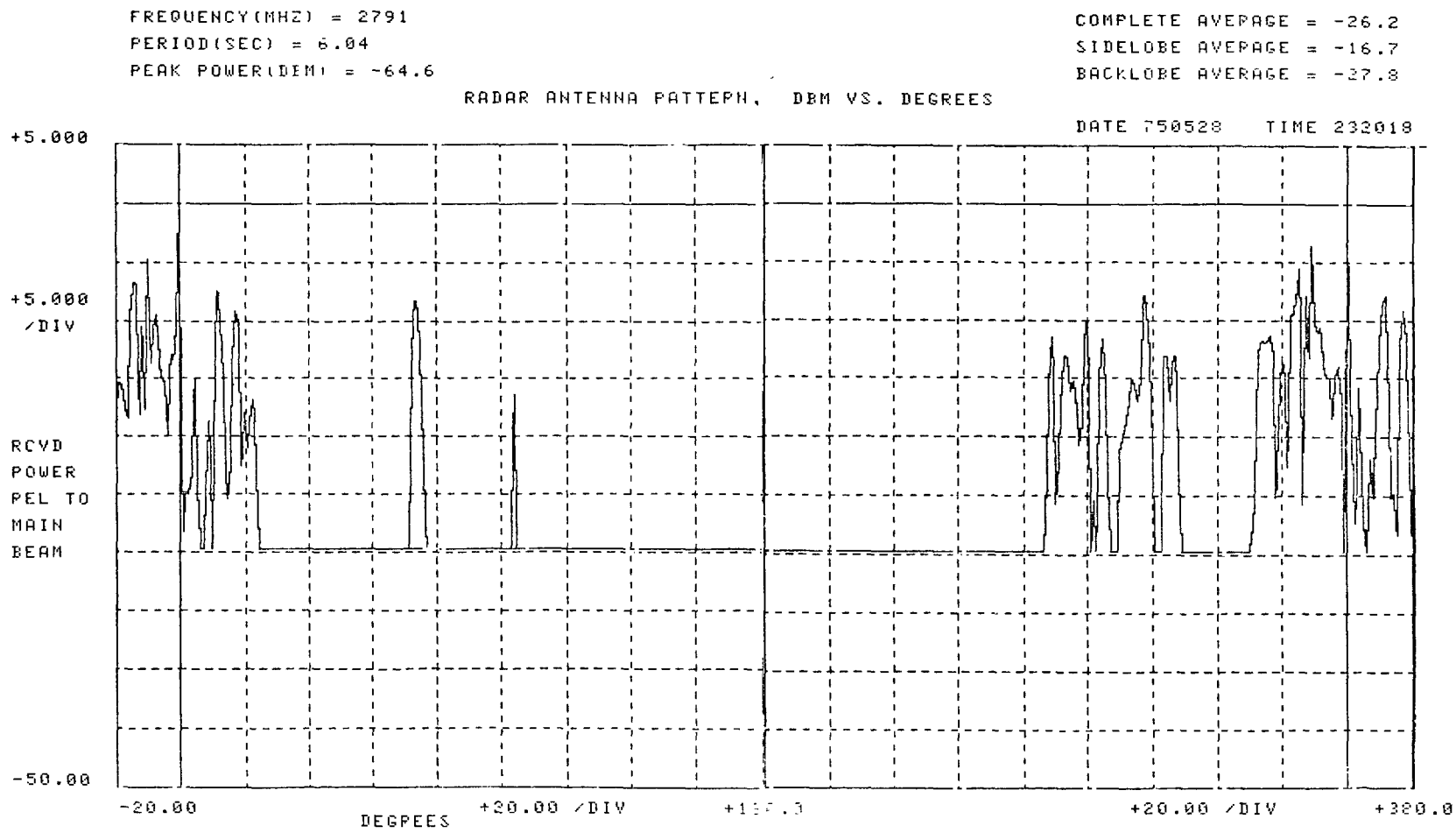

Figure A-32. Burbank ASR-6 Antenna Pattern Measured at Long Beach Using RSMS Van Dish Pointed at 319.6° Magnetic

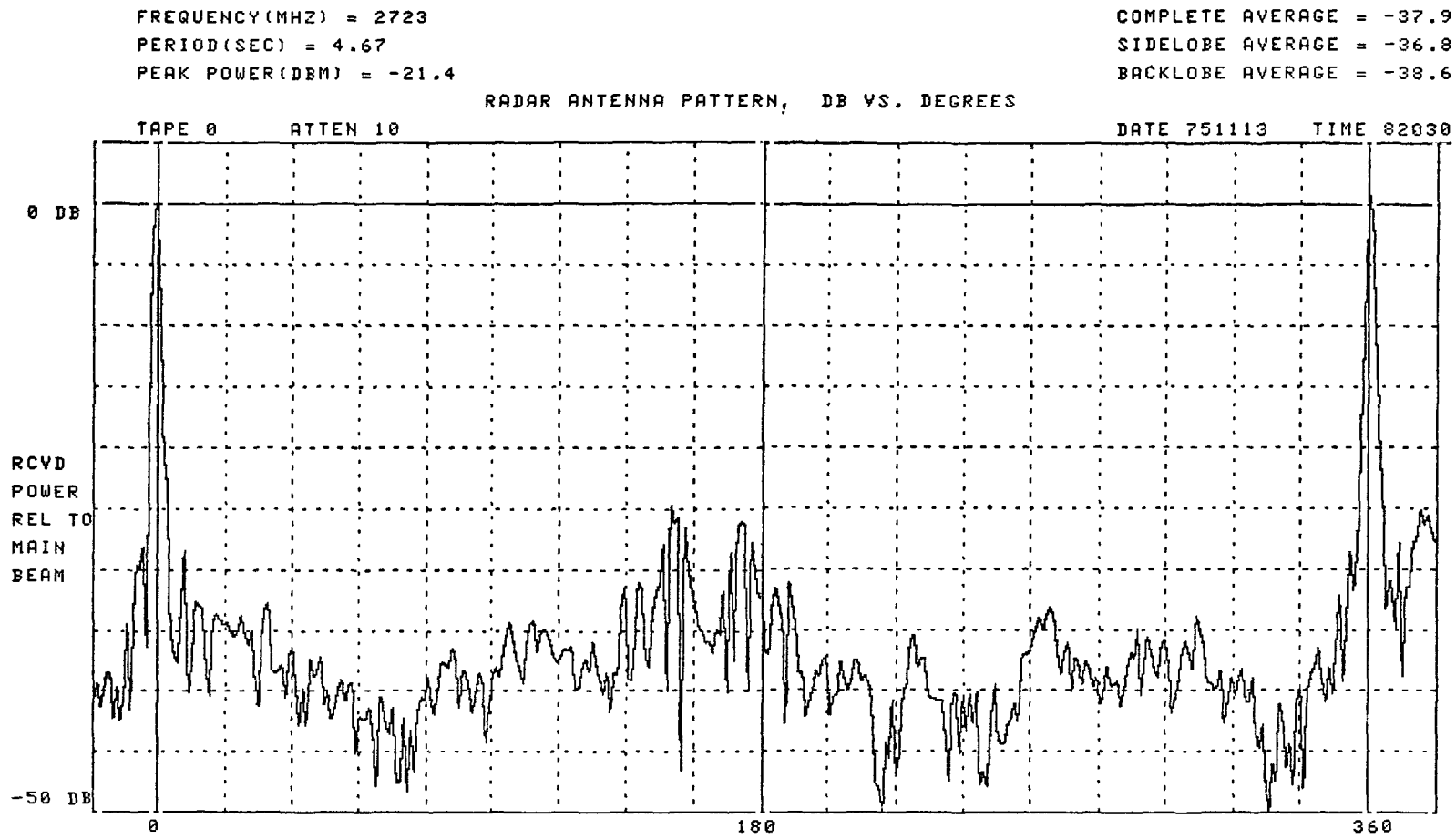

Figure A-33. Oakland ASR-7 Antenna Pattern Measured at Mountain View Using RSMS Van Dish Pointing at 312° Magnetic.

radiation patterns.

Alameda NAS AN/MPN-11 - Figures A-34 and A-35 show the Alameda AN/MPN-11 antenna pattern measured at the Mountain View radar site using the RSMS van dish and ASR-5 radar antenna, respectively. The antennas were pointed at 309° magnetic. A line-of-sight antenna pattern of the Alameda AN/MPN-11 radar was not measured. The tilt angle on the Alameda AN/MPN-11 radar antenna is 3.5 degrees. Therefore, the mainbeam gain at zero degrees elevation is approximately 26 dBi using Figure A-2. With a mainbeam gain of approximately 26 dBi, the statistics shown in Figures A-34 and A-35 indicate an average backlobe level of -5.9 dBi and -7.5 dBi, respectively. The high backlobe level of the Alameda AN/MPN-11 environmental antenna pattern measured at Mountain View may be due to the high clutter in the vicinity of the Alameda NAS. The NAS had numerous hangars in the area, and the San Francisco skyscrapers and the San Francisco and Oakland bay bridge were within line-of-sight. It is believed that the two high spikes in Figure A-34 and the one spike in Figure A-35 around 180° are due to reflections off the San Francisco-Oakland bay bridge.

Alameda NAS

Measurements of environmental antenna patterns of other radars were also made at the Alameda NAS AN/MPN-11 radar site using the RSMS van dish antenna. The RSMS van dish antenna height (14.0 feet) was approximately the same height as the antenna on the AN/MPN-11 radar.

Oakland ASR-7 - Figure A-36 shows the Oakland ASR-7 antenna pattern measured at the Alameda NAS radar site using the RSMS van dish antenna pointed at 120° magnetic. For a mainbeam gain of approximately 29 dBi at zero degrees elevation, the statistics in Figure A-36 show a median backlobe level of approximately -10.3 dBi (+29 dBi - 39.3 dB) which is relatively close to the -12.85 dBi average median backlobe level given in Table A-1.

Mountain View ASR-5 - Figure A-37 shows the Mountain View ASR-5 antenna pattern measured at the Alameda NAS radar site using the RSMS van dish antenna pointed at 129° magnetic. A line-of-sight antenna pattern of the Mountain View ASR-5 antenna pattern was not measured. The tilt angle on the Mountain View ASR-5 radar antenna is three degrees. Therefore, the mainbeam gain at zero degrees elevation is approximately 29 dBi using Figure A-2. With a mainbeam gain of approximately 29 dBi, the statistics shown in Figure A-37

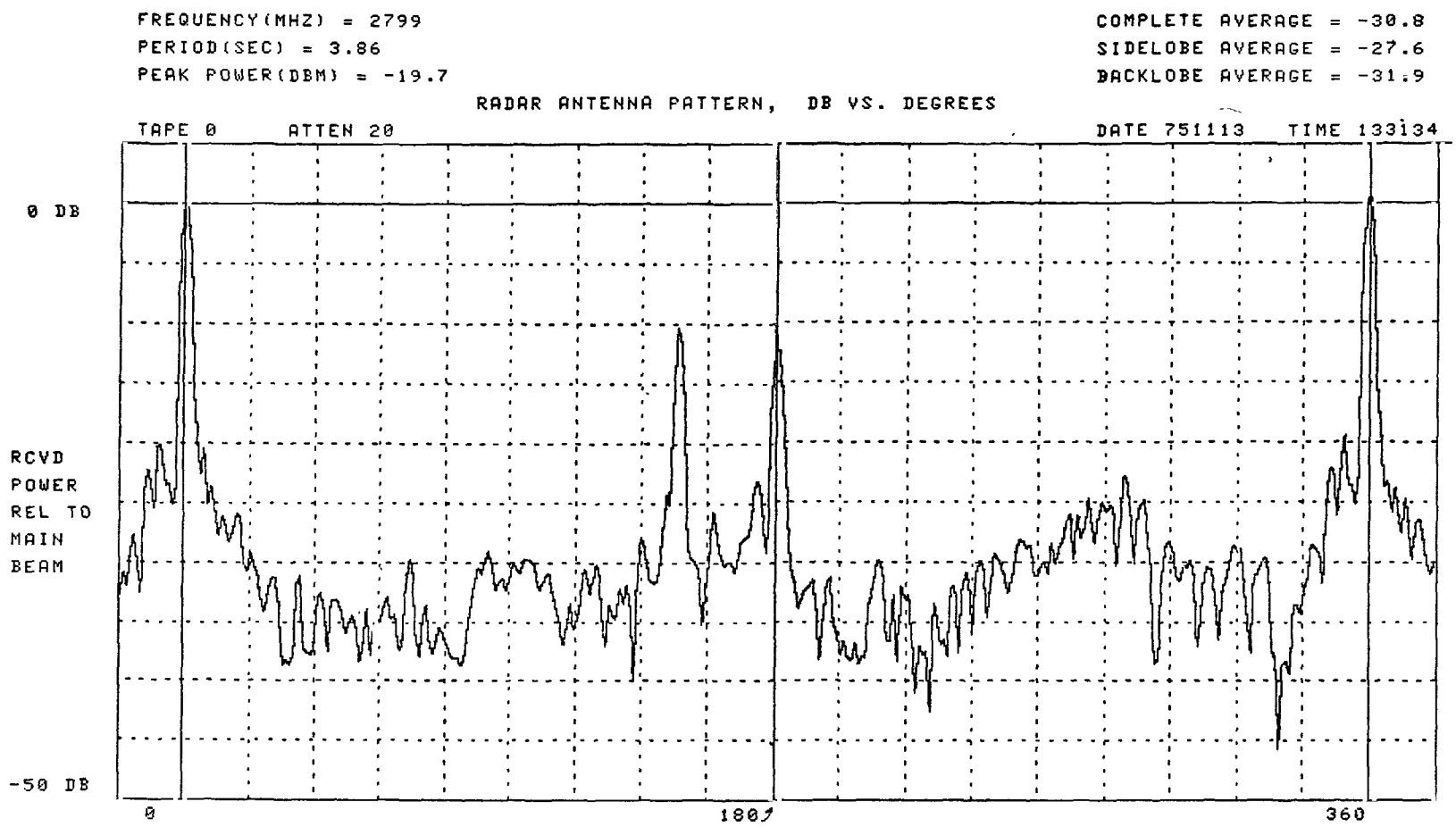

Figure A-34. Alameda AN/MPN-11 Antenna Pattern Measured at Mountain View Using RSMS Van Dish Pointed at 309° Magnetic.

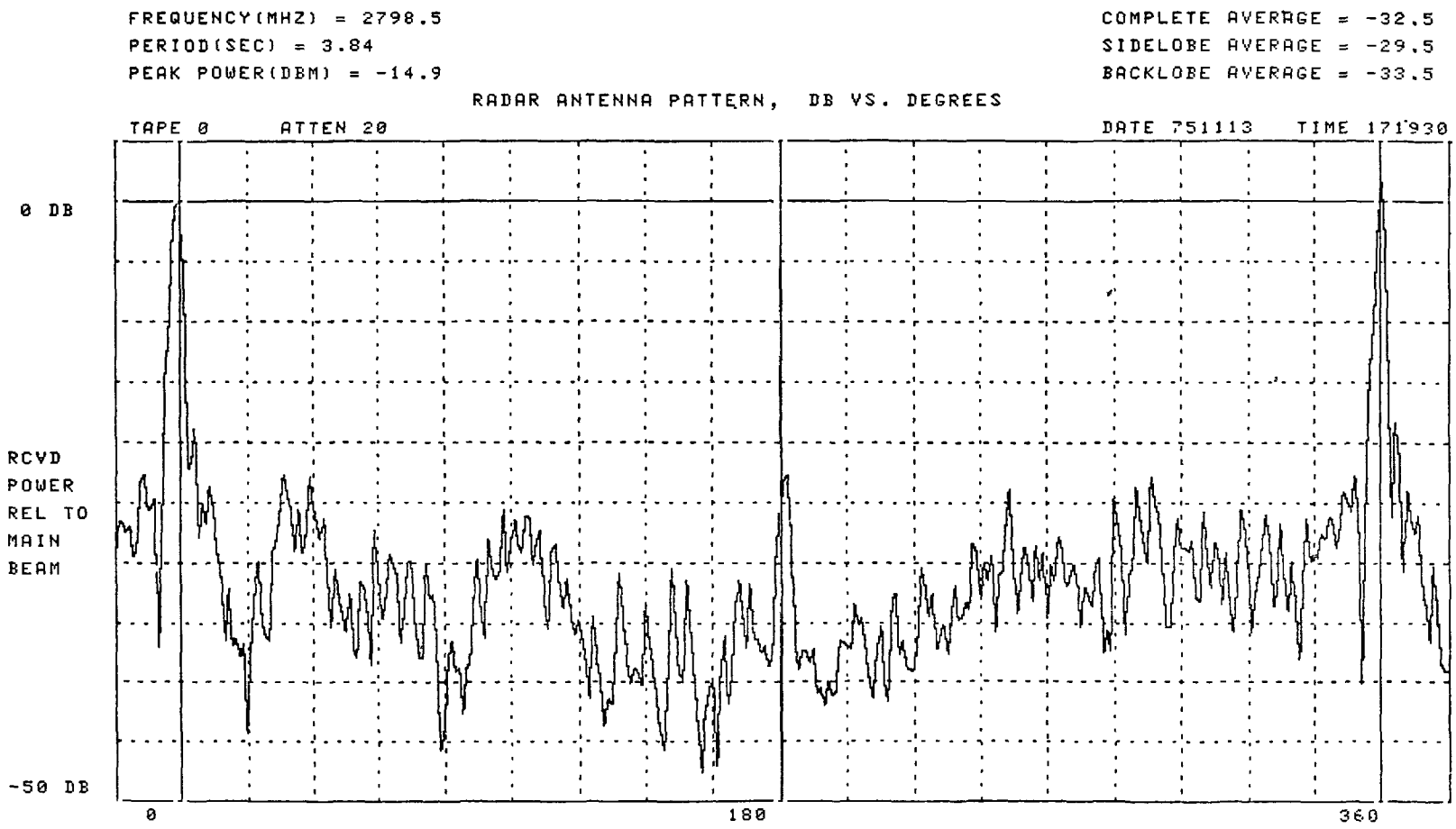

Figure A-35. Alameda AN/MPN-11 Antenna Pattern Measured at Mountain View Using Mountain View Radar Antenna Pointed at 309° Magnetic.

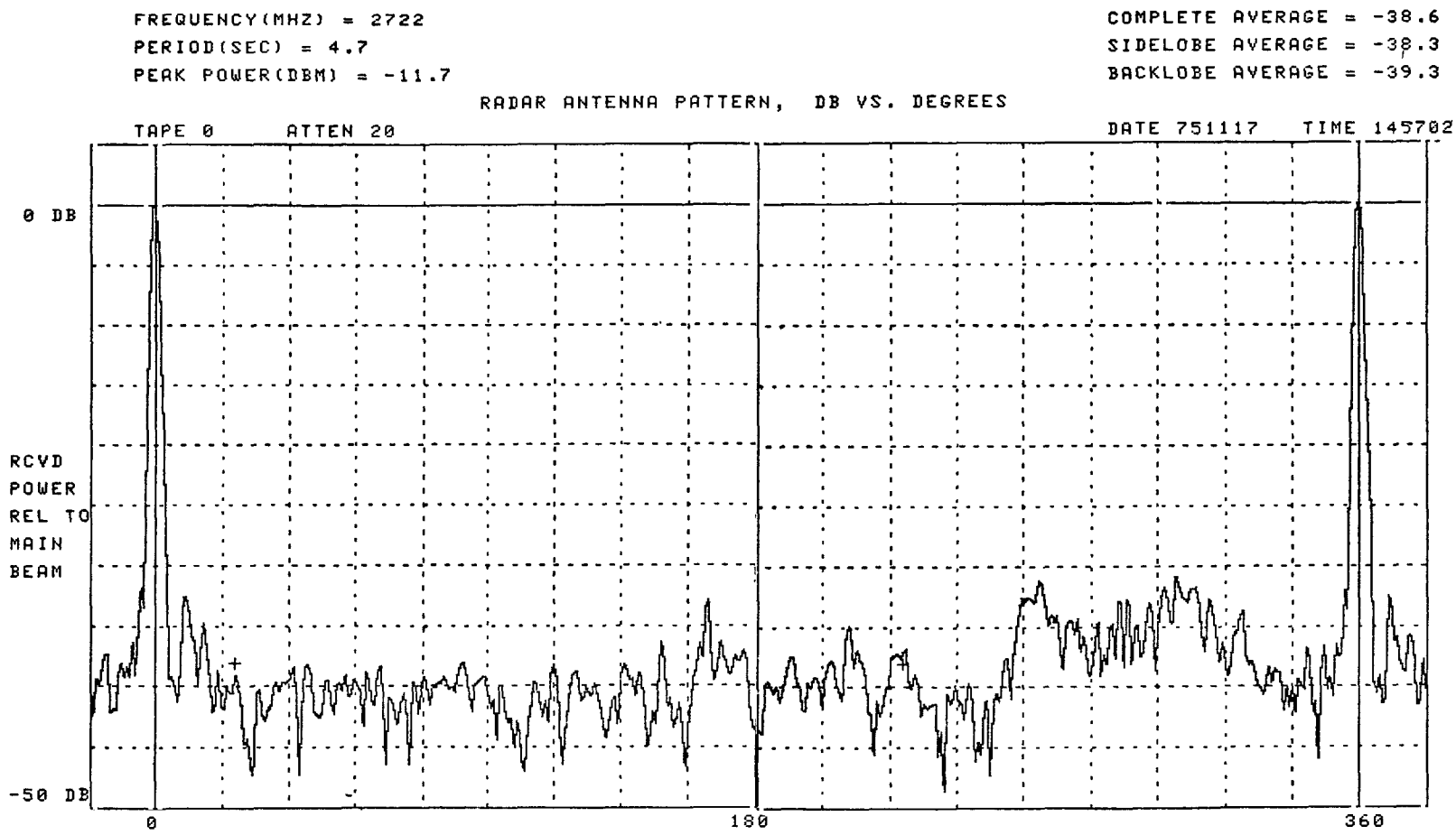

Figure A-36. Oakland ASR-7 Antenna Pattern Measured at Alameda NAS Using RSMS Van Dish Pointed at 120° Magnetic.

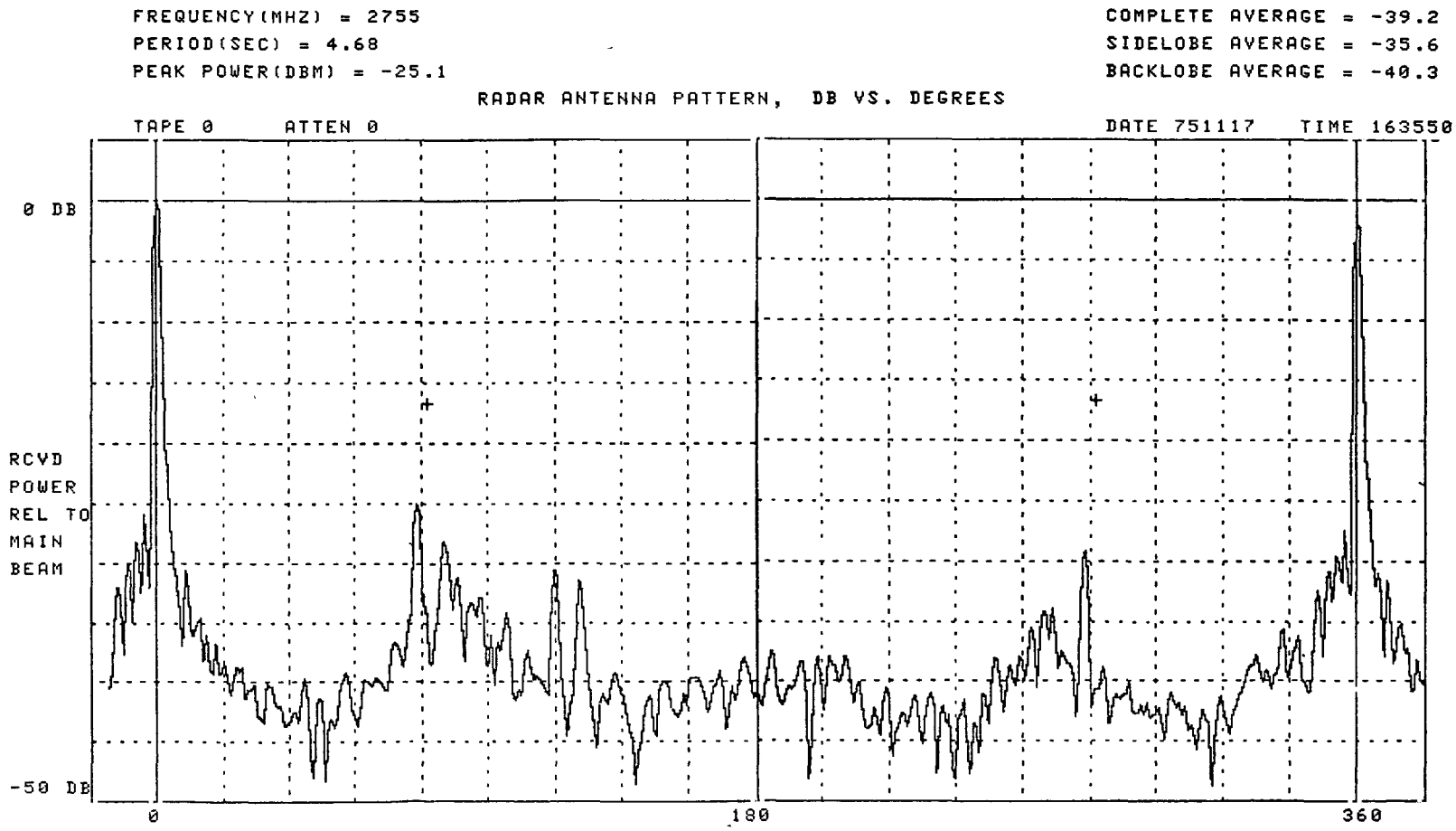

Figure A-37. Mountain View ASR-5 Antenna Pattern Measured at Alameda NAS Using RSMS Van Dish Pointed at 129° Magnetic.

indicate a median backlobe level of -11.3 dBi (29 dBi - 40.3 dB) for the environmental antenna pattern of the Mountain View ASR-5 radar measured at Alameda. The median backlobe level of -11.3 is close to the -12.85 dBi averaged median backlobe level of measured line-of-sight antenna radiation patterns given in Table A-1.

SUMMARY OF ANTENNA PATTERN MODELING

Line-of-sight (free space) antenna pattern measurements made during the Los Angeles and San Francisco area investigations on cosecant squared elevation type antenna had an averaged median sidelobe (3° to 25° and 335° to 357°) level of -7.0 dBi and standard deviation of 3.3 dB. The average median backlobe (25° to 335°) level was found to be -12.8 dBi with a standard deviation of 3.1 dB. Considering the statistical antenna pattern models given in References 13 and 18, and the measured data resulting from the Los Angeles and San Francisco measurements, it is recommended that a median backlobe level of -13 dBi with a standard deviation of 4 dB be used to predict radar-to-radar interference.

Environmental antenna pattern measurements of potential interfering radars made at the victim radar site revealed that line-of-sight (free space) antenna pattern models will not result in realistic pulse amplitude distributions at the victim radar RF input. There are propagation related phenomena, such as multipath wave interference arising from multiple scattering of the waves by mountains, buildings, and other structures which affect the interfering signal pulse amplitude distribution. Also in some cases, there is more attenuation of sidelobe and backlobe levels than the mainbeam due to foreground clutter at the radar site. The effects of these propagation related phenomena are dependent on the antenna positions and antenna patterns of the victim and interfering radar antennas. Since the multipathing and foreground clutter attenuation of the interfering signal and the antenna pattern characteristics of the victim and interferer antennas are statistical parameters which are difficult to separate in the real environment, it appears that the free-space antenna patterns could be modified to incorporate these propagation phenomena. One particular advantage of this approach is that it can more readily be incorporated in the present PPI simulation program.

As a result of the Los Angeles area investigation, it appears that potential multipathing through mountain ranges may be identified. However, the effect of multipathing on

the interfering signal pulse amplitude distribution would be very difficult to predict. Also, the effect of multipathing due to buildings and other structures would be difficult to predict and very subjective. One approach to modeling these propagation phenomena would be to develop an empirical mutual environmental antenna gain model which would incorporate the statistical pulse amplitude distribution of these propagation related phenomena. This could be done by classifying the environment into several categories, such as:

1. Free-space coupling environment.

2. Free-space with foreground clutter.

3. Moderate multipath coupling.

4. Heavy multipath coupling.

The major drawback to the empirical approach is that numerous additional measurements would be required to determine what the mutual environmental antenna gain model distribution should be for each category. Even if empirical models were developed, the actual implementation of the models would still be subjective. Since multipathing of interfering signals through mountain ranges only occurred on a few paths, it appears that a measurement program would not be practical. However, it is apparent that without incorporating these propagation related phenomena into the radar-to-radar interference prediction model, realistic prediction of the interference on the PPI display cannot be achieved.

APPRENDIX B

EMISSION SPECTRUM MODELING AND MEASUREMENTS

INTRODUCTION

Modeling transmitter emission spectra is an essential step in performing an EMC analysis. This appendix discusses factors that affect emission spectrum characteristics, and the model selected for predicting emission spectrum. Modeled emission spectra for particular radar characteristics and transmitter output tubes are presented, and compared with measurements made during the Los Angeles and San Francisco area investigation. A discussion of the RSMS van system hardware and software used to measure radar emission spectra is given in Appendix G.

FACTORS AFFECTING EMISSION SPECTRUM CHARACTERISTICS

The emission spectrum of a pulse radar is determined by the modulating pulse shape and width, transmitter RF tube, and RF output tube load. The transmission waveguide, rotary couplers, and antennas also affect the emission spectra but to a much less degree.

Magnetron Characteristics

All the 2.7 to 2.9 GHz band radars operating in the Los Angeles and San Francisco areas currently employ conventional magnetron tubes. The magnetron tube types employed by each radar in the Los Angeles and San Francisco area are indicated in Tables 4-2 and 5-2. The tuning range and nominal operating characteristics of the employed magnetron tube types are indicated in Table B-1. The inherent wideband asymmetrical emission characteristics of conventional magnetrons are exhibited by these tubes. The wide emission spectrum is due to the low Q of the tubes resonant cavity. The operating frequency of the tube increases with modulating voltage amplitude, which results in a lower tube operating frequency during the rise time of the modulating pulse. This instability causes an asymmetrical spectrum with greater power on the low side of the carrier frequency. In addition, conventional magnetrons emit high levels of both harmonic and nonharmonic spurious emissions. These outputs result from the excitation of cavity modes, in addition to the desired Π mode, during the rise time of the modulating pulse. The frequency of the undesired modes

depend on the resonant cavity structure of the particular type tube and rise time of the modulating pulse.

The tube parameters listed in Table B-1 are typical operating values specified by the manufacturer and differ from those used by government users. For example, it was observed that the magnetron peak power of FAA ASR and military GCA radars were typically set at 25 to 50 percent lower than the values listed in Table B-1 to increase tube life. On the other hand, the magnetron peak power of military range clearance and height finding radars were set about 20 percent higher to maximize range. The peak power of a magnetron is set by adjusting the tubes peak anode voltage and current. This adjustment affects the modulating pulse ability to excite resonant cavity modes and consequently alters the tubes emission spectrum. The magnitude and direction of the emission spectrum change as a function of magnetron peak power setting has not been tested by manufacturers. However, it is a known fact that, if the anode voltage and current are not in the range specified by the manufacturer, spurious modes and poor emission will result.

Modulating Pulse

A clean emission spectrum will be realized only if the modulation circuitry provides a voltage pulse shape that is within the tolerance (Reference 22) specified by the manufacturer. Exciting the proper mode requires a specific rate of voltage rise between the 60 to 80 percent amplitude levels of the pulse. This rate of voltage rise must be long enough to permit oscillations to start in the desired π mode, but not so slow that undesired modes are excited. The tolerance of this voltage rate increase depends on the excitation time of the tube and how close the modes are in frequency. Once the oscillations are started in the desired π mode, the modulating voltage should increase to the maximum pulse amplitude value as rapidly as possible to prevent excitation of other modes. The voltage should remain constant over the duration of the pulse to prevent spectrum broadening. It is also important that the modulating pulse drop to zero as rapidly as possible, because inverse and post-pulse voltages can result in undesirable noise radiation. For the above reasons, different radar types employing the same model magnetron at identical peak power settings and pulse widths, can have different emission spectrums due to the adjustment and design of the modulating pulse shaping circuitry.

TABLE B-1
MAGNETRON TUBE TYPES

TUBE* TYPE	FREQ. RANGE IN MHz	TUNABLE	PEAK POWER (KW/dBM)	PEAK CURRENT (A)	PEAK VOLTAGE (KV)	PULSE WIDTH (sec)	DUTY CYCLE
5586	2700-2900	YES	800/89.0	70	29.5	1.0	.0005
8789 (QK1463)	2700-2900	YES	450/86.5	70	30	1.0	.001
4J31	2860-2900	NO	800/89.0	70	28	1.0	.0005
6410A (QK338A)	2750-2860	NO	4500/96.5	130	70	2.0	.001
7529 (QK327A)	2700-2800	YES	3500/95.4	115	62	2.0	.0007
(DX276)	2700-2900	YES	450/86.5	50	32	1.5	.001
(QK729)	2860-2900	NO	480/86.8	50	26	4.0	.0007

*Tube types listed in brackets are manufacturer designators. Those tube types not listed in brackets are Joint Electron Device Engineering Council (JEDEC) designators.

Magnetron Load

The magnetron in a typical radar is loaded by an electrically long transmission line that is terminated by an ATR (anti-transmit-receive) gas discharge tube. At the start of a pulse, the ATR is unfired and presents an open circuit to the transmission line which results in a voltage standing wave on the line. Under these conditions, the impedance that the magnetron output sees depends on the electrical length of the line in wavelengths and the magnetron's oscillating frequency. The impedance that the magnetron sees influences its frequency mode starting characteristics and consequently the radars emission spectrum. The transmission line electrical length is normally optimized during the radar design and in modern radars ferrite isolators are employed to isolate the reflected wave and ATR tube input impedance from the magnetron. However, when a magnetron is being replaced by a different model than the radar was originally designed for, to prevent emission spectrum spreading, it is necessary that the replacement tube operate over the transmission line lengths and VSWR (voltage standing wave ratio) limits specified by the manufacturer.

The impedance that the magnetron sees changes with magnetron operating frequency, since the electrical length of the transmission line changes with frequency. If the VSWR magnitude on the line is large, tuning of the magnetron will result in broadening of the spectrum. At some frequencies, there will be periodic holes in the tuning curve where the magnetron will not oscillate. This was confirmed by conversations with Air Force personnel who stated that some frequencies in the tuning range of AN/MPN-13 radars result in poor emission spectrum. Therefore, the magnetron tuning ranges listed in Table B-1 do not necessarily imply that the radar emission spectrum will be satisfactory at all frequencies over this range.

MODELING

Several models (References 23, 24) were considered for predicting the emission spectrum envelope of conventional magnetron for this investigation. The model by Newhouse (Reference 24) was chosen because it takes into account the frequency shift characteristics of the conventional magnetron.

Conventional Magnetron Model

The conventional magnetron model used in this investigation consists of emission envelope segments defined by the following equation:

$$\frac{K_1}{(f-f_c)^2} = \frac{P}{[\pi(f-f_c)]^2} \qquad \text{(B-1)}$$

$$\frac{K_2}{(f-f_c)^4} = \frac{P}{16\delta_r^2[\pi(f-f_c)]^4} \qquad \text{(B-2)}$$

$$\frac{K_3}{[f-(f_c-B_t/2)]^4} = \frac{P}{4\delta_r^2[f-(f_c-B_t/2)]^4} \qquad \text{(B-3)}$$

Where the emission peak power is given by

$$P = \left[\tau + \frac{\delta_f}{2B_t}^{1/2}\right]^2 \qquad \text{(B-4)}$$

and

K_1, K_2, K_3 are constants

f_c = carrier frequency of pulse (Hz)

P = Peak power of emission spectrum (watts)

δ_r, δ_f = Pulse rise and fall times (sec)

τ = transmitter pulse width (sec)

f = frequency (Hz)

B_t = total amount of frequency deviation during the rise and fall times of modulating pulse (Hz)

The portion of the emission spectrum that equation B-1 through B-4 depict, and the relationship between the modulating pulse amplitude and magnetron frequency shift are shown in Figure B-1.

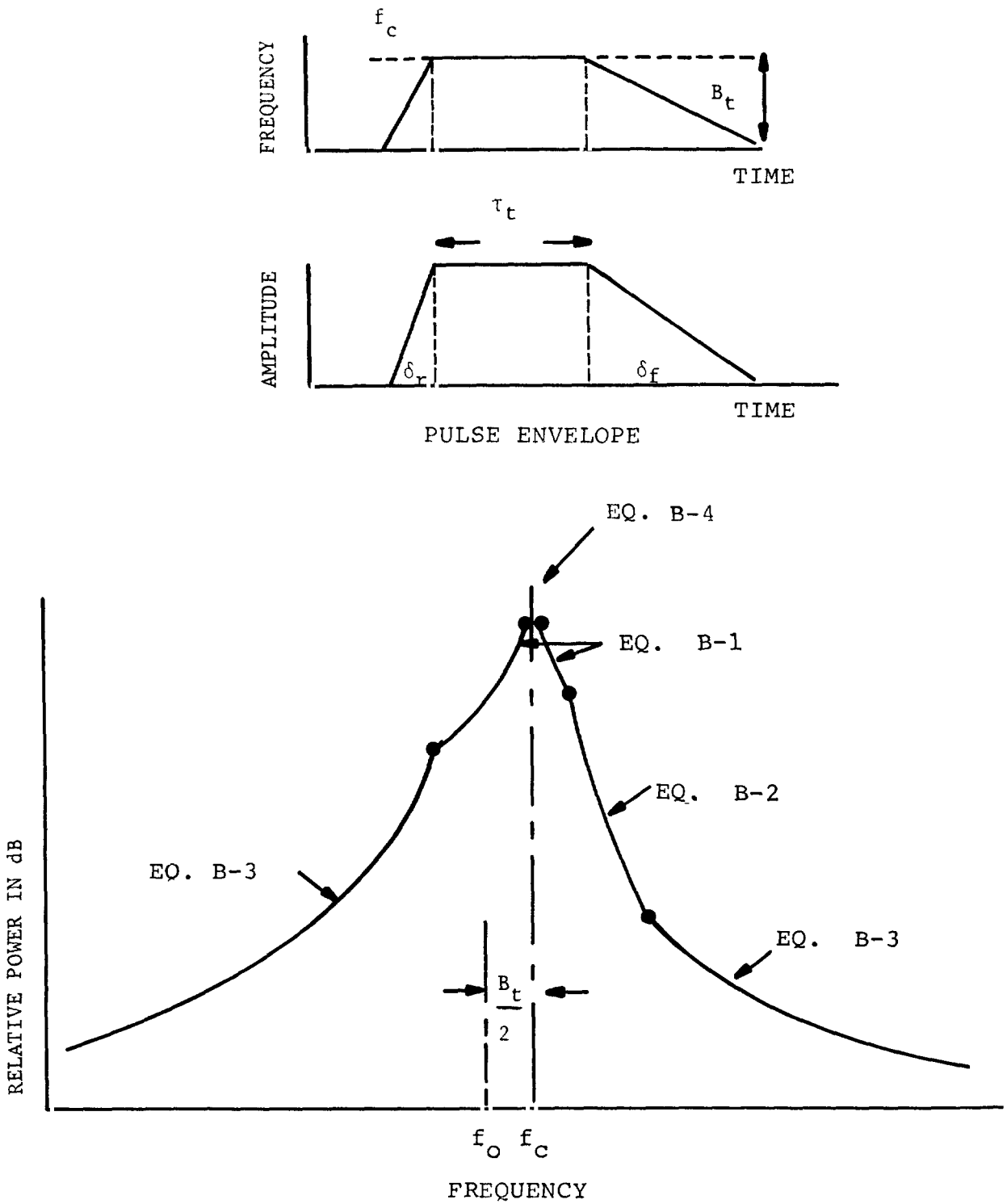

Figure B-1. Emission Spectrum Model for Radar With Conventional Magnetron

The magnetron model does not include the high level of harmonic and nonharmonic spurious emissions that occur with conventional magnetrons. Conversations with several experts concerning magnetron spurious emissions (References 45 and 46) indicated that it is difficult to analytically predict the frequency and amplitude of magnetron spurious emissions. A practical approach is to use an empirical model for the spectrum skirts. This is usually accomplished by increasing the lower level skirts of the model emission skirts by a fixed number of dB for $|\Delta F| > 100$ MHz. The adjusted skirt level should be based on spurious emission measurement data on the particular radar type being modeled. The measured radar emission spectra in this investigation confirmed that refinement to the magnetron model for spurious emissions was not necessary for $|\Delta F| < 100$ MHz. Since this frequency range covered the 2.7 to 2.9 GHz band of interest, in most cases, the spurious emission refinement to the magnetron model was not employed in this investigation.

Emission Spectrum Model Categories

To simplify the calculations of radar emission spectra, radars operating in the Los Angeles and San Francisco areas were categorized by pulse width in the manner indicated in Table B-2. The asterisks identify weather radars with two operational pulse widths. The computed emission spectra, for the various category radars are shown in Figures B-2 through B-5. The parameters used to compute the emission model are indicated in the upper right hand corner of each figure.

MEASURED EMISSION SPECTRA

Radiated emission spectra of the Los Angeles and San Francisco area radars were measured intermittently over 1975. The results of these measurements are presented in Figures B-6 and B-8 through B-20. The AN/CPN-4 emission spectrum shown in Figure B-7 was measured at the Norfolk, Virginia Naval Air Station in June 1974.

These emission spectra were measured with the test receiving antenna positioned in the far field and in line-of-sight of the radar antenna. When possible, the emissions were measured no further from the radar than necessary to be in the radar antenna far field.

This procedure reduced the chance of error contribution by frequency selective multipath and short term propagation fading.

TABLE B-2
EMISSION SPECTRUM CATEGORIES

PULSE WIDTH CATEGORY	RADAR NEMENCLATURE	PULSE WIDTH (μ SEC)
1 (0.5 μsec)	AN/CPN-4 AN/FPS-41* AN/MPN-11 WSR-57*	.5 .5 .5 .5
2 (0.83 μsec)	AN/MPN-13, 14, 15 AN/MPN-5 AN/MPS-19 AN/FPN-47, 55 ASR-4,5,6,7 ASR-3	.7 .8 .8 .833 .833 1.0
3 (2.0 μsec)	AN/APS-20 AN/FPS-6,90 AN/MPS-14	2.0 2.0 2.0
4 (4.0 μsec)	AN/FPS-41* WSR-57*	4.0 4.0

*Weather Radars which have two operational pulse widths.

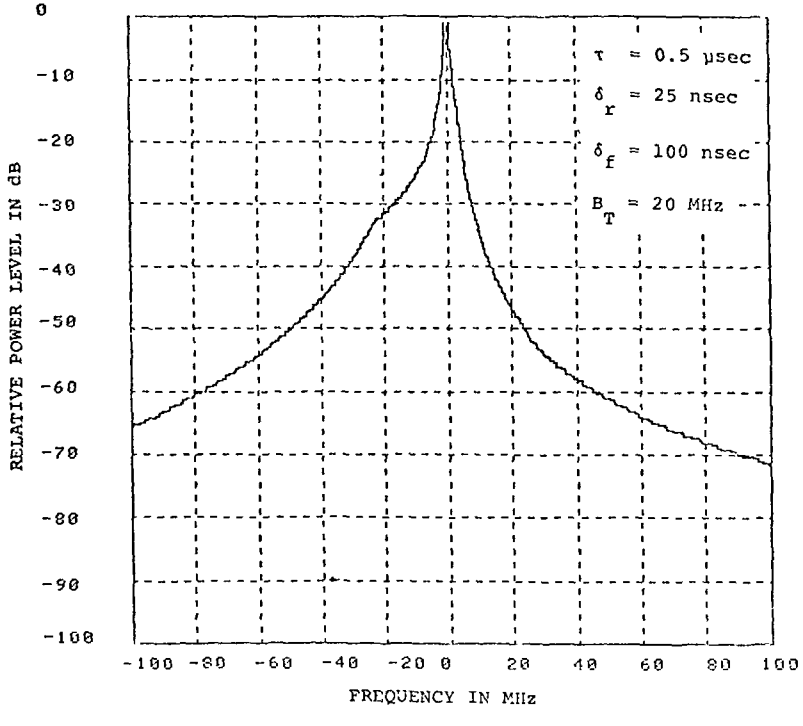

Figure B-2. Modeled Emission Spectrum For Category 1 Radars With Conventional Magnetrons

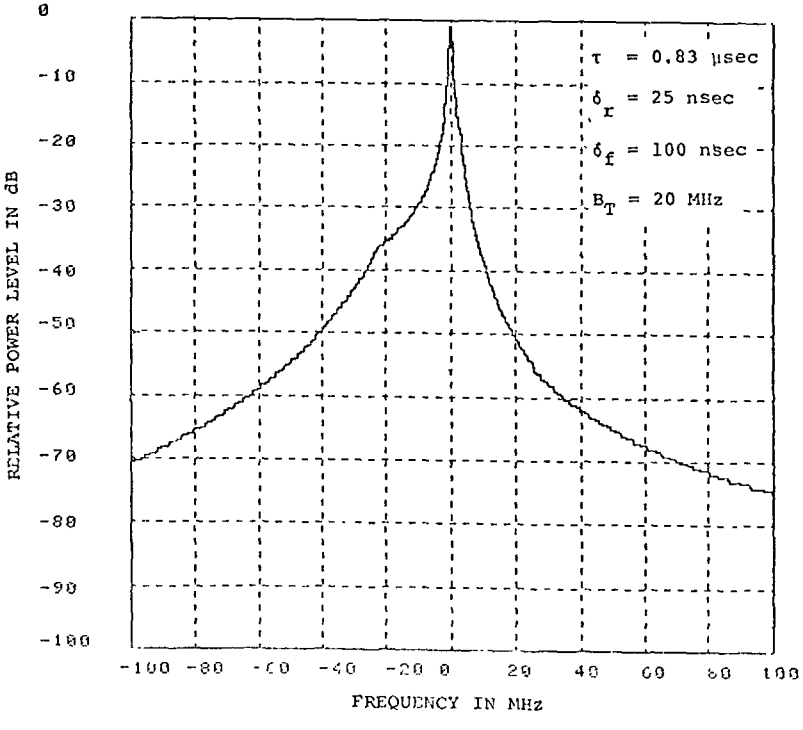

Figure B-3. Modeled Emission Spectrum For Category 2 Radars With Conventional Magnetrons

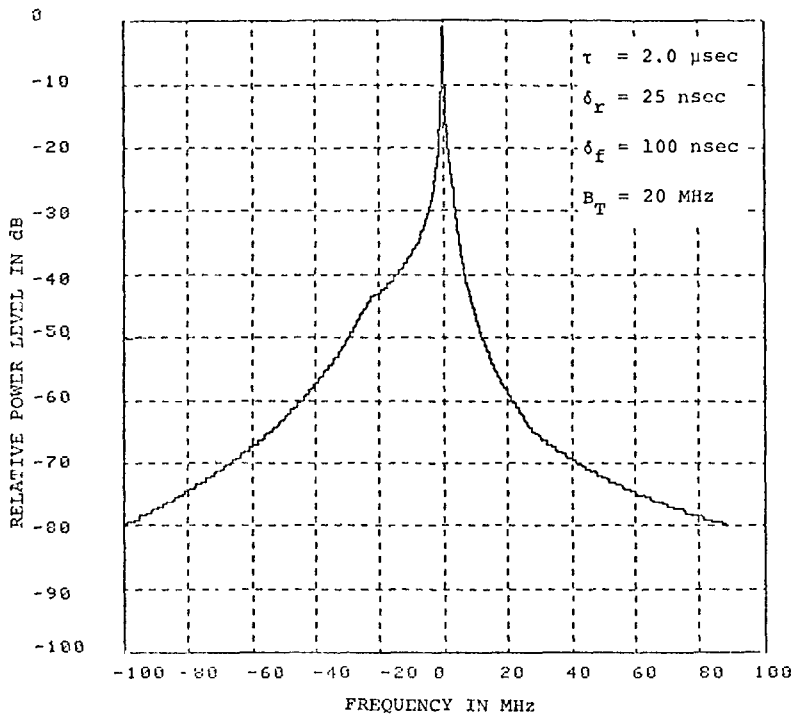

Figure B-4. Modeled Emission Spectrum for Category 3 Radars With Conventional Magnetrons

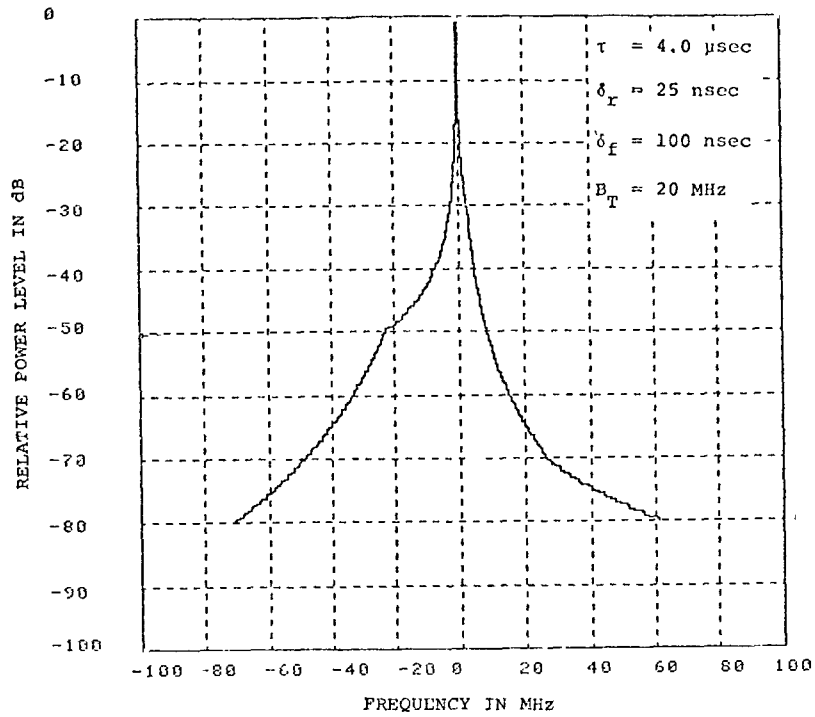

Figure B-5. Modeled Emission Spectrum For Category 4 Radars With Conventional Magnetrons

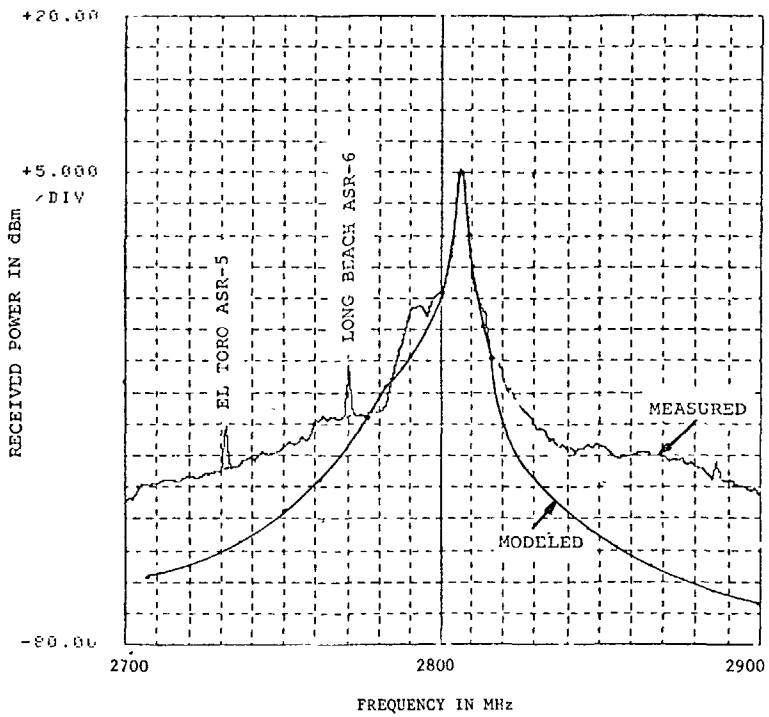

Figure B-6. Measured and Modeled Emission Spectrum of Los Alamitos AN/CPN-4 Radar

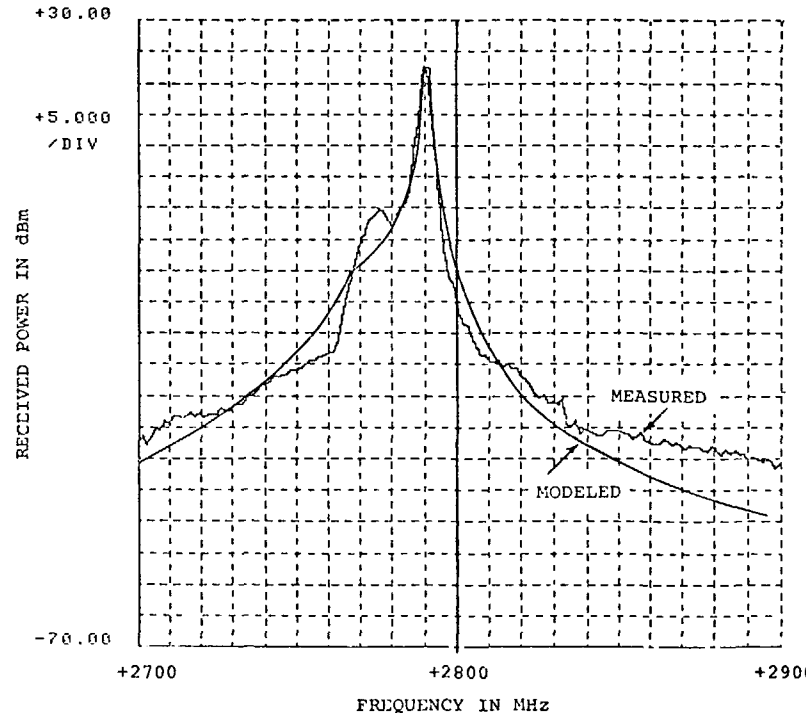

Figure B-7. Measured and Modeled Emission Spectrum of Norfolk AN/CPN-4 Radar

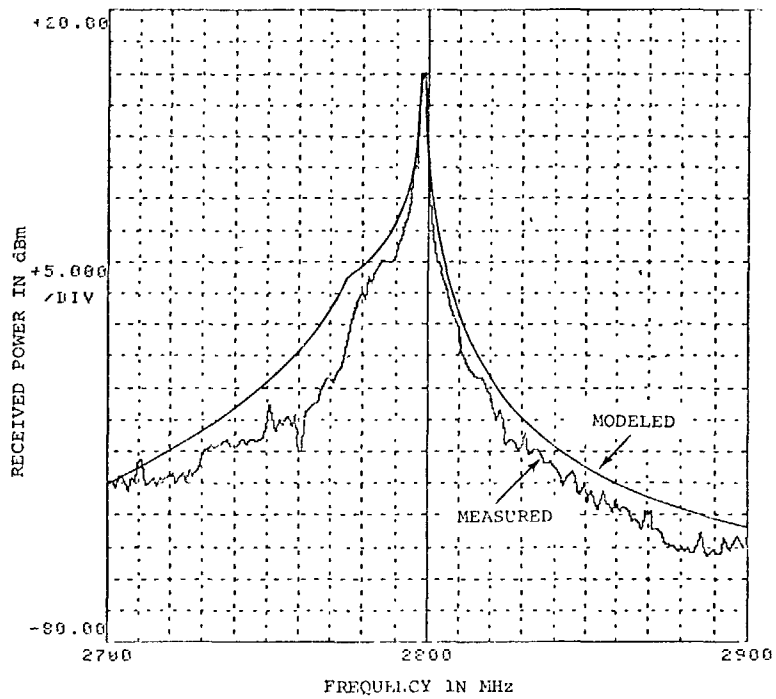

Figure B-8. Measured and Modeled Emission Spectrum of Alameda AN/MPN-11 Radar

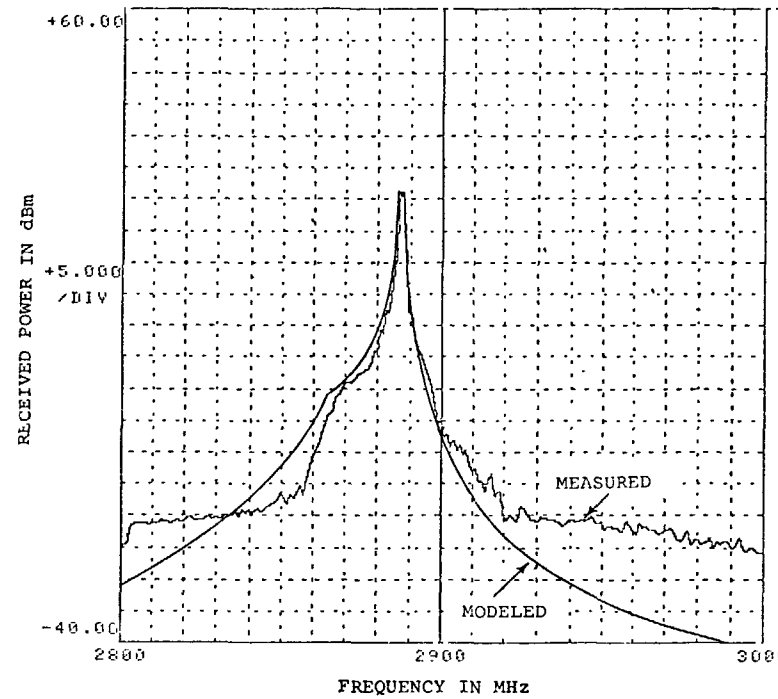

Figure B-9. Measured and Modeled Emission Spectrum of Sacramento WSR-57 Radar (0.5 μsec Pulse Width Mode)

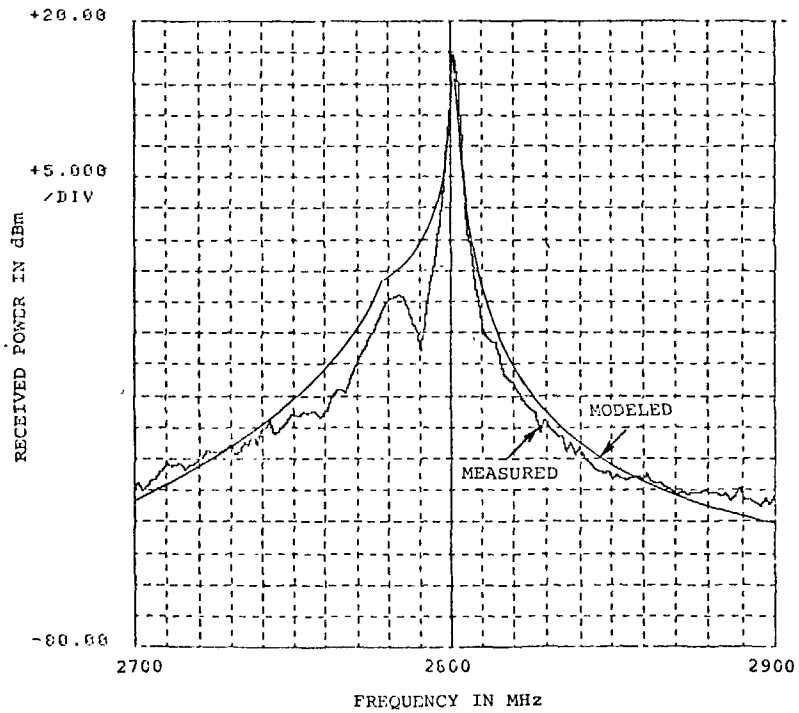

Figure B-10. Measured and Modeled Emission Spectrum of March AFB AN/MPN-13 Radar

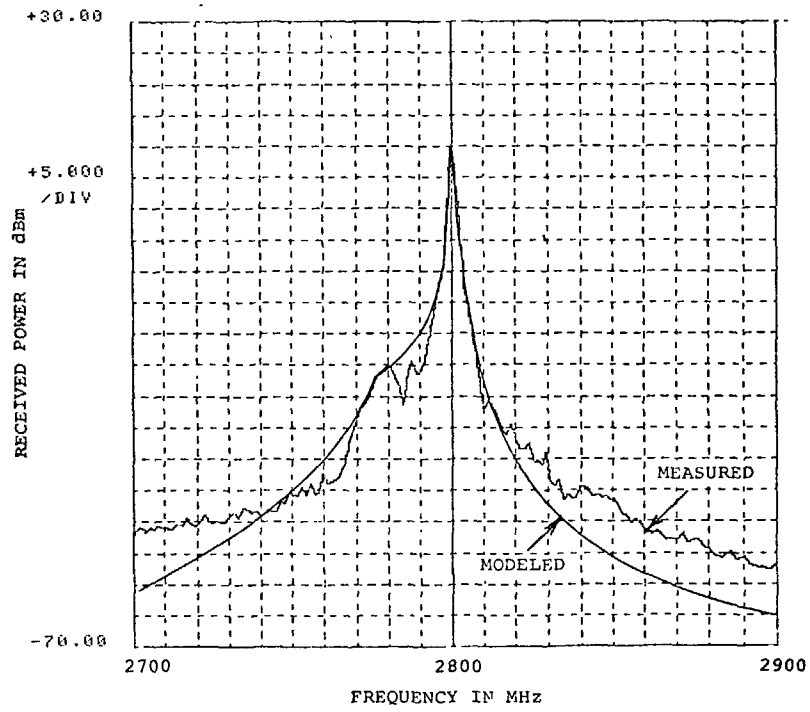

Figure B-11. Measured and Modeled Emission Spectrum of Norton AFB AN/MPN-13 Radar

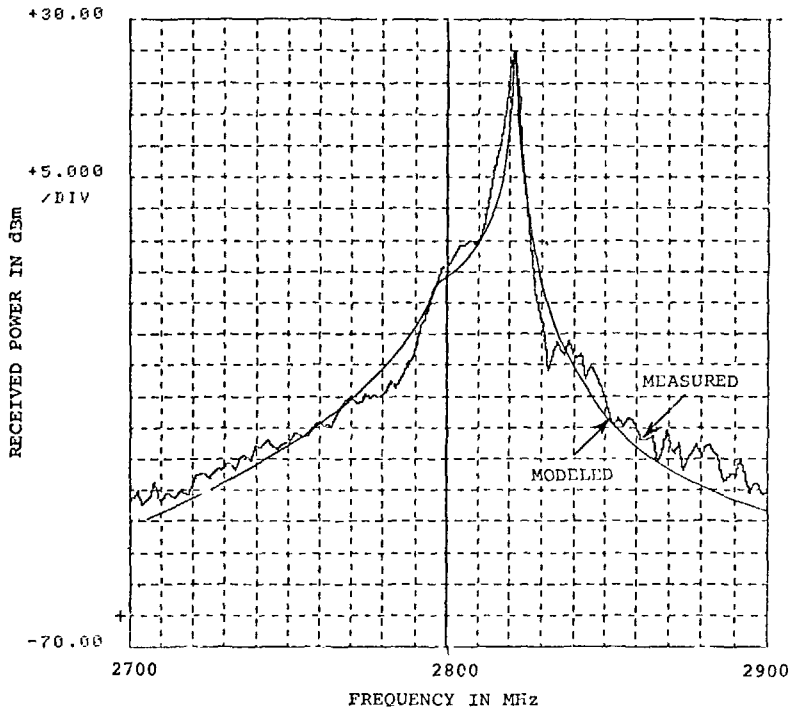

Figure B-12. *Measured and Modeled Emission Spectrum of Ontario ASR-5 Radar.*

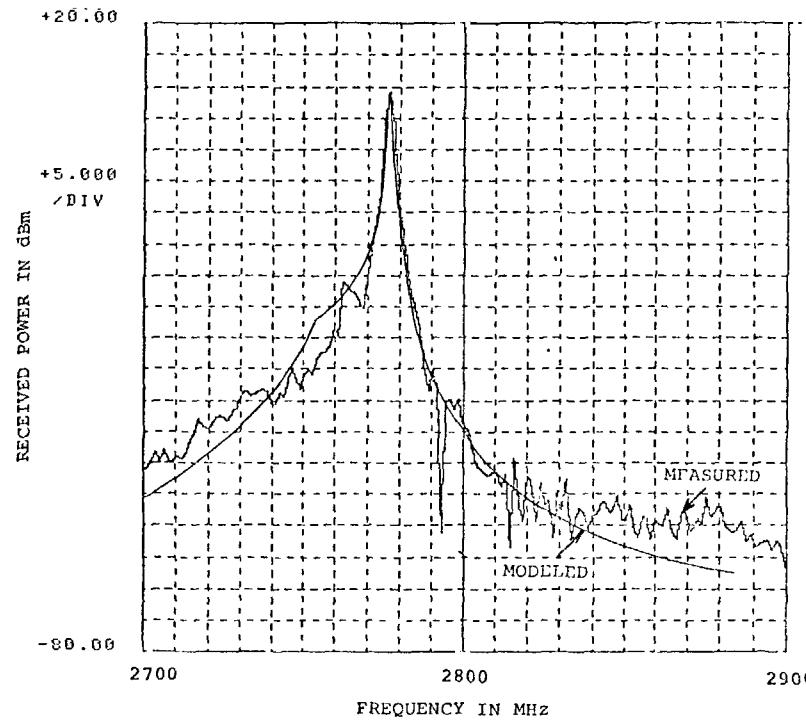

Figure B-13. Measured and Modeled Emission Spectrum of Long Beach ASR-5 Radar

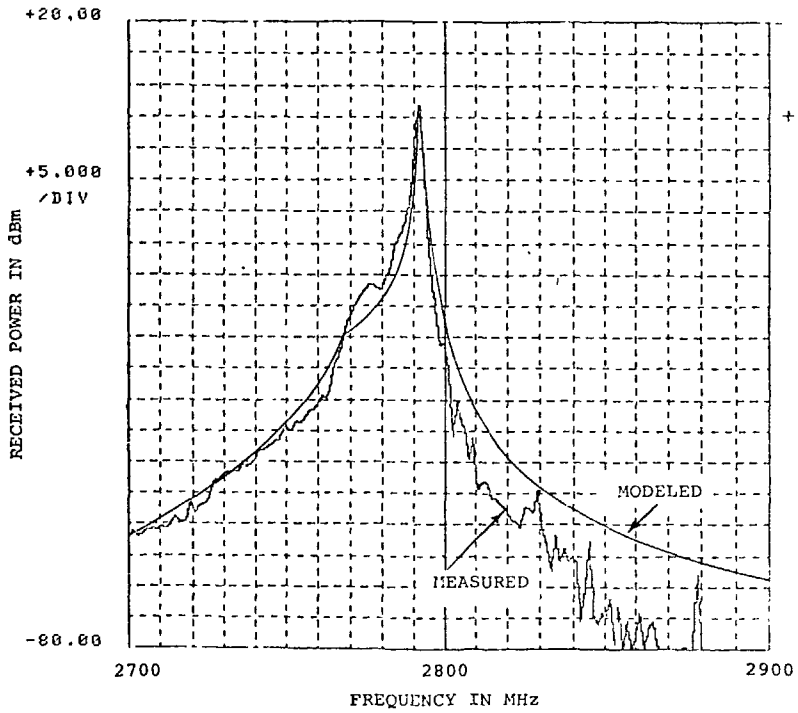

Figure B-14. Measured and Modeled Emission Spectrum of Burbank ASR-6 Radar

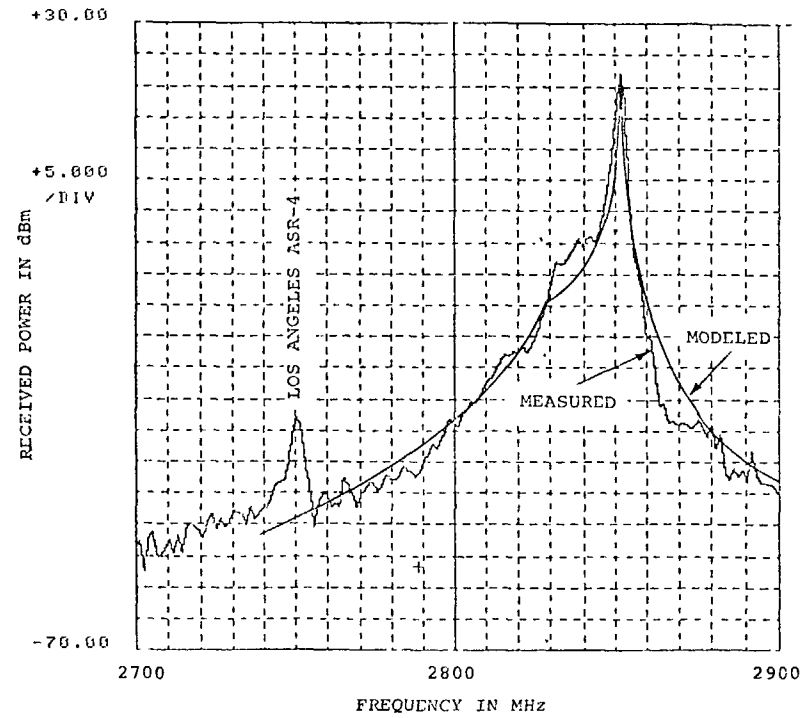

Figure B-15. Measured and Modeled Emission Spectrum of Los Angeles ASR-7 Radar

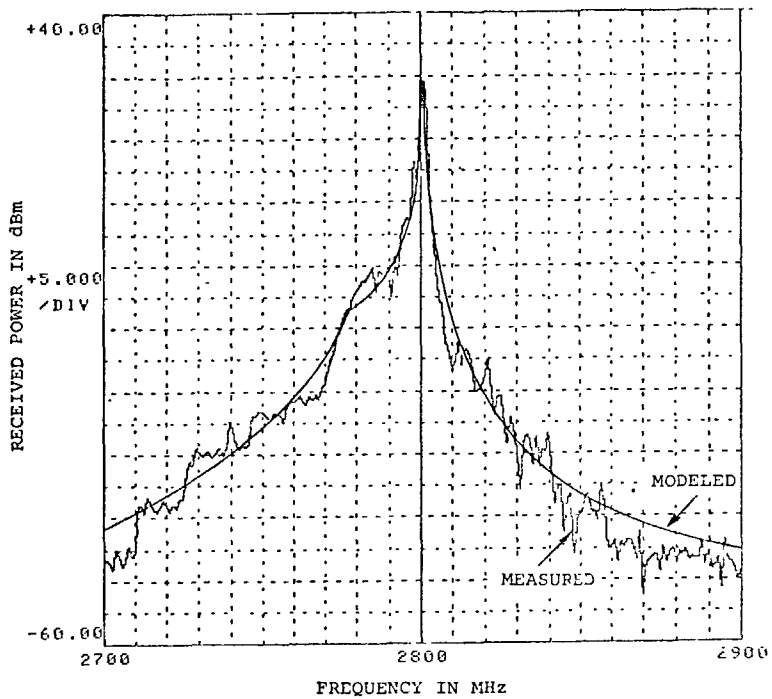

Figure B-16. Measured and Modeled Emission Spectrum of Travis AFB AN/FPN-55 Radar

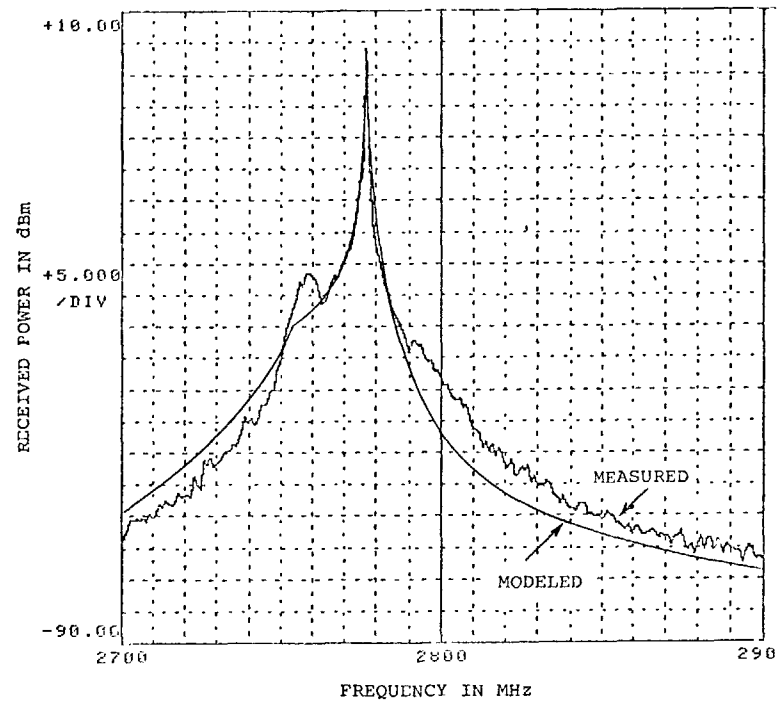

Figure B-17. Measured and Modeled Emission Spectrum of Almaden AN/FPS-90 Radar

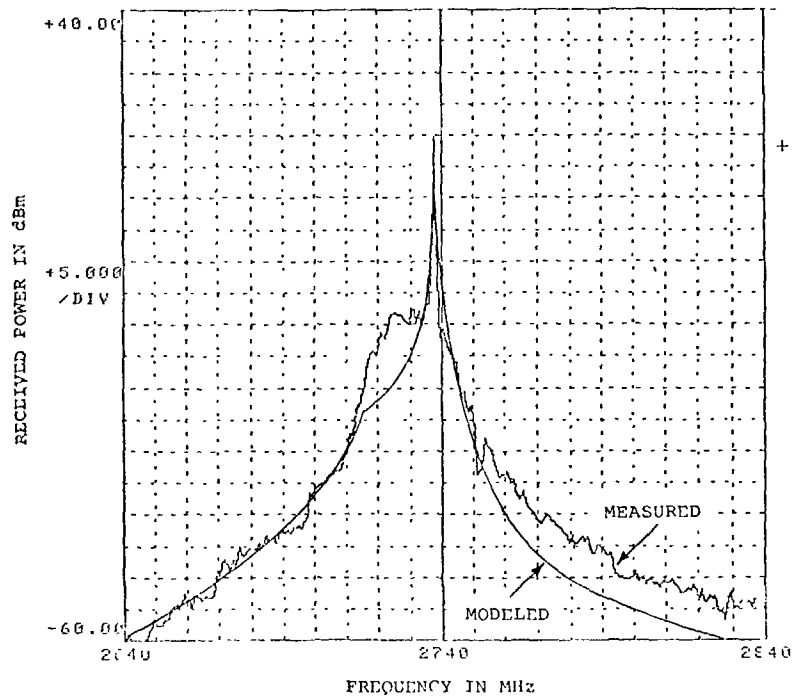

Figure B-18. Measured and Modeled Emission Spectrum of Mt. Tamalpais AN/FPS-90 Radar

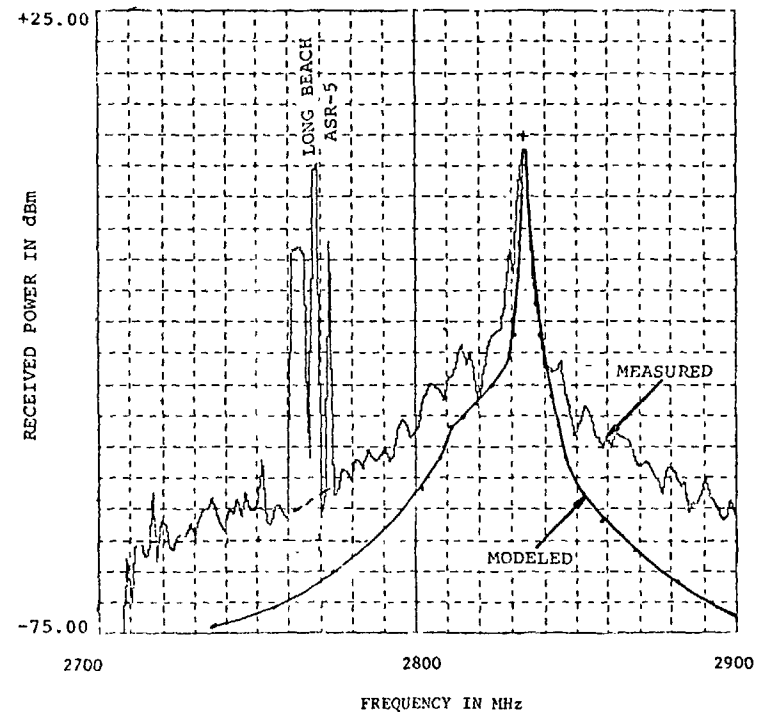

Figure B-19. Measured and Modeled Emission Spectrum of San Pedro Hill AN/FPS-90 Radar

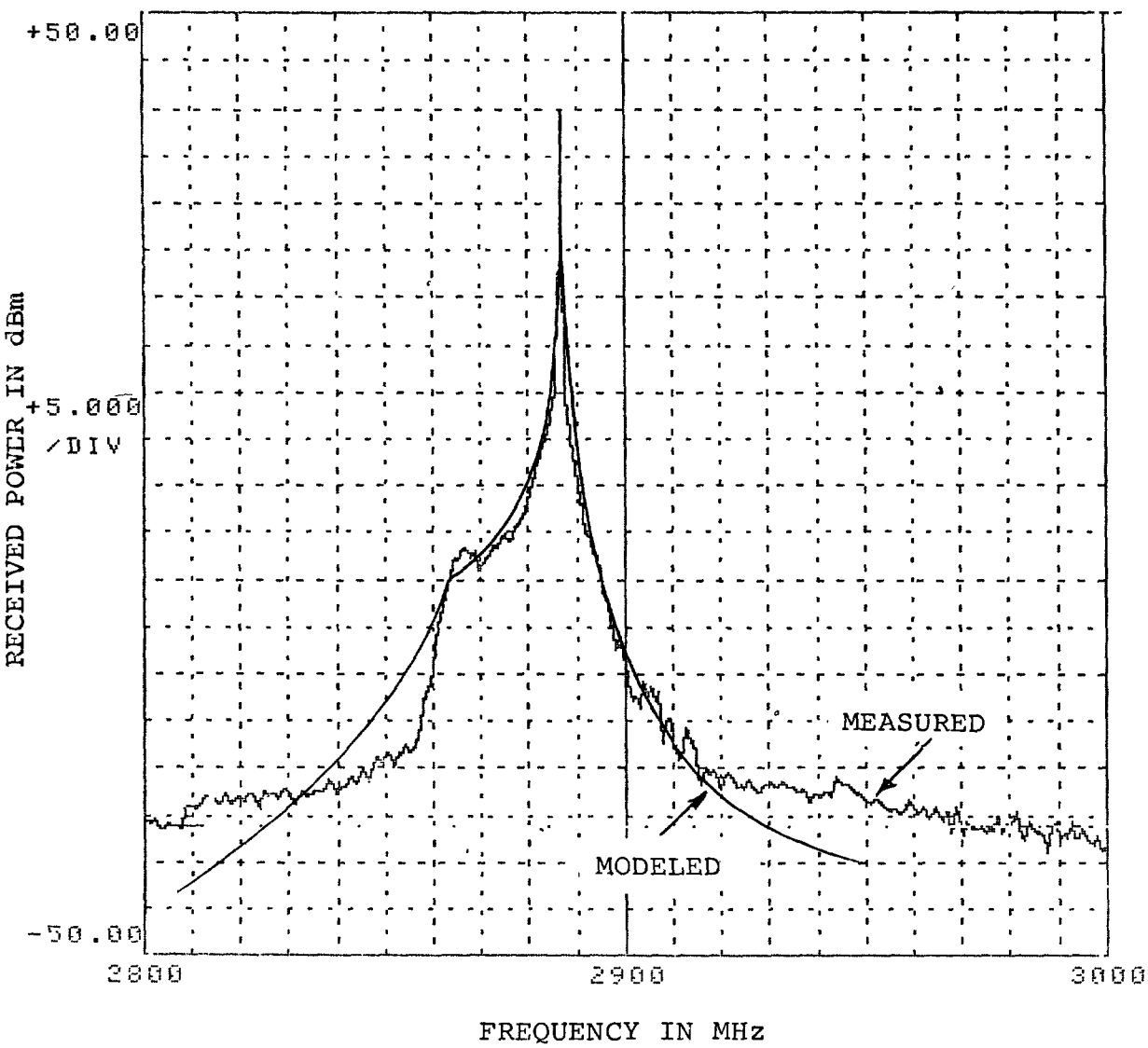

Figure B-20. Measured and Modeled Emission Spectrum of Sacramento WSR-57 Radar (4.0 μsec Pulse Width Mode)

The RSMS van does not have the capability in all measurement situations to completely eliminate undesired radar signals from interfering with emission spectrum measurements. An example of this interference appears at 2752 MHz on the measured emission spectrum of the Los Angeles ASR-7 radar in Figure B-15. This frequency corresponds to the Los Angeles ASR-4 radar and is, in fact, a low level emission spectrum of the ASR-4. The frequency location of the interfering radars are noted on the measured emission spectra.

COMPARISON OF MODELED AND MEASURED EMISSION SPECTRUMS

The modeled emission spectra are shown superimposed on the measured emission spectra in Figures B-6 through B-20.

Category 1 Emission Spectra

The measured and modeled emission spectra for 0.5 μsec pulse width radars are shown in Figures B-6 through B-9. The measured Los Alamitos AN/CPN-4 emission spectrum skirts (Figure B-6) are 10 to 20 dB above the model. However, the measured emission skirts of the Norfolk AN/CPN-4 (Figure B-7) and Alameda AN/MPN-11 (Figure B-8) agree with the model to within 10 dB. The AN/MPN-11 radar is electronically identical to the AN/CPN-4 radars. The radars at the above locations all employ the same model, 5586, magnetron tubes. There are two possible reasons why the measured emission spectrum skirts of the Los Alamitos radar were 10 dB greater than the measured emission spectrum skirts of the two other electronically identical radars. When the magnetron tube begins to fail the level of the emission skirts tend to increase. Second, the magnetron modulation pulse shape must be maintained within manufacturer specifications for a clean emission spectrum.

The measured emission spectrum of the Sacramento WSR-57 radar for 0.5 μsec pulse width setting (Figure B-9) was as much as 15 dB greater than the model; however, for the 4.0 μsec pulse width setting (Figure B-20), the measured emission spectrum agrees with the model to within 10 dB. The same Ratheon model QKH729 is used for both pulse width transmissions of the WSR-57 radar. The manufacturers catalog rates the tube for 4.0 μsec operation. However, the manufacturer has stated that the tube will operate with a clean emission at 0.5 μsec pulse width. Therefore, the high emission spectrum is attributed to the difficulty of achieving and maintaining required pulse rise time for narrow pulse widths.

Category 2 Emission Spectra

The measured and modeled emission spectrums for radars with pulse widths between 0.7 to 1.0 μsec are shown in Figures B-10 through B-16. In general, the measured FAA ASR radar emission spectra agreed closer (within 5 dB) with the model than the military AN/MPN-13 radars. The measured emission spectrum of the Travis AN/FPN-55 radar (Figure B-16) agreed closely with the modeled emission spectrum. However, the AN/FPN-55, with the exception of the antenna subsystem, is a military version of the ASR-5 radar.

The measured emission spectrum of the Burbank ASR-6 radar (Figure B-14) on the $+\Delta F$ side was as much as 15 dB less than the model. Comparison of this emission spectrum with the other 3 ASR emission spectra indicates that this fast roll-off is untypical of ASR radars.

Category 3 Emission Spectra

The measured and modeled emission spectra for 2.0 μsec pulse width radars are shown in Figure B-17 through B-19. The greatest difference between measured and modeled emission spectra occurred for the San Pedro AN/FPS-90 radar (Figure B-19), with differences as great as 20 dB at some frequencies. However, some of this difference is believed to be due to measurement error. The San Pedro radar spectrum was measured from the Long Beach ASR-5 radar site, located about 20 KM away. The signal level variation introduced to the emission spectra due to propagation short term fading is estimated, based on half hour propagation loss measurement over this distance, to be less than 2.5 dB. In addition, the low grazing angle of this line of sight path barely cleared the trees and building tops surrounding the measurement location. This is believed to have introduced selective multipathing error to the measured emission spectrum. For the above reasons, the San Pedro emission spectrum was not used in the statistical comparison between modeled and measured emissions.

Category 4 Emission Spectra

The measured emission spectrum of the Sacramento WSR-57 radar with 4.0 μsec pulse width setting is shown in Figure B-20. The category 4 (4.0 μsec) modeled emission spectrum agrees well with the model down to the -75 dB level from the peak. The measured emission spectrum appears to flatten rather abruptly beyond this point.

Statistical Comparison of Measured and Modeled Emission Spectra

Statistical techniques were employed to gauge the disagreement between the measured and modeled emission spectra for the four radar pulse width categories. This was accomplished by computing the difference between the modeled and measured emission spectra (EP-EM) at every 10 MHz increment over the measured emission spectra indicated in Figures B-6 through B-18 and B-20. The differences, EP-EM, were used to compute the statistics indicated in Table B-3. Statistical comparisons were made for the negative ($-\Delta F$) and positive ($+\Delta F$) side of the emission spectra for each pulse width category.

The absolute mean of the difference between modeled and measured emissions, and the standard deviation of the predicted (modeled) about the measured emissions are indicators of the overall agreement between measured and modeled emissions. The smallest values of these indicators occurred for the category 2 radars.

The increase in the category 2 absolute mean from 1.4 to 3.8 dB, from $-\Delta F$ to ΔF respectively, was primarily due to the fast emission spectrum roll-off of the Burbank radar (Figure B-14) which seems to be untypical for FAA radars. The largest absolute mean and standard deviation of the modeled about the measured emissions occurred for category 1 radars. The greatest contributors to this disagreement were the Los Alamitos AN/CPN-4 and Sacramento WSR-57 radar emission spectra indicated in Figures B-6 and B-9, respectively.

The negative algebraic means, $\overline{X}$, for the category 1, 2 and 3 radar emission spectrums indicates that the modeled emission tended to be lower than measured emissions for these radars by 2 to 5 dB.

The standard deviation, $\sigma_{\overline{x}}$, is a measure of the variation or repeatability of the absolute difference between modeled and measured emissions. The σ of 7 dB for category 1 radars is about 2 dB greater than other category radars. This is because the difference between modeled and measured emission spectra varied from radar-to-radar the most for category 1 radars.

SUMMARY OF EMISSION SPECTRUM MODELING

Radars with 0.83 μsec pulse widths, particularly FAA ASR type radars, can be modeled with an average absolute error of

TABLE B-3

COMPARISON OF MEASURED AND
MODELED EMISSION SPECTRA

STATISTICAL COMPARISON CRITERIA \ PULSE WIDTH CATEGORY	1 (.5 μsec)		2 (.83 μsec)		3 (2.0 μsec)		4 (4.0 μsec)	
	$-\Delta F$	$+\Delta F$	$-\Delta F$	$+\Delta F$	$-\Delta F$	$+\Delta F$	$-\Delta F$	$+\Delta F$
MEAN $\bar{X} = \frac{\Sigma(EP-EM)}{N}$ (dB)	-1.6	-5.5	0.6	1.5	0.4	-3.6	-1.4	-3.2
STANDARD DEV. ABOUT MEAN, $\sigma_{\bar{X}} = \left[\frac{\Sigma(EP-EM-\bar{X})^2}{N}\right]^{1/2}$ (dB)	7.0	7.3	3.0	5.1	3.5	2.9	5.2	4.6
EXTREMES OF DIFFERENCES BETWEEN PREDICTED AND MEASURED (dB)	-13.0 to 15.0	-18.0 to 6.0	-10.0 to 15.0	-10.0 to 15.0	-7 to 5	-7 to 5	-10 to 6	-8 to 6
ABSOLUTE MEAN $\frac{\Sigma\lvert EP-EM\rvert}{N}$ (dB)	5.4	7.2	1.4	3.8	2.5	4.0	3.9	4.6
STANDARD DEV. BETWEEN PRED. AND MEASURED $\left[\frac{\Sigma(EP-EM)^2}{N}\right]^{1/2}$ (dB)	7.1	9.1	3.0	5.3	3.5	4.6	5.2	5.5

EP = Predicted or Modeled Emission Level at Particular Frequency
EM = Measured Emission Level at Particular Frequency
N = Total Number of Comparisons (Frequency Point) for Each Category

of about 3.0 dB. Radars with pulse widths of 0.5, 2 and 4 μsec, which included all military radars with the exception of one WSR-57 weather radar, had a mean absolute difference between predicted and measured that ranged from 3 to 7 dB. For these cases, the modeled emission level was on the average 2 to 4 dB less than the measured emission level.

The greatest absolute mean difference (6 dB) between modeled and meausred emission occurred for 0.5 μsec pulse width category radars. The measured emission skirt level varied the most (maximum 15 dB) between individual radars in the 0.5 μsec pulse width category.

This large variation even occurred between electrically identical, including type magnetron, AN/CPN-4 and AN/MPN-11 radars. The most likely explanation for this paradox are the radar-to-radar differences in the magnetron age and calibration of the pulse shaping circuitry that controls the magnetron.

The following factors are believed to have caused the radar-to-radar variations of the differences between measured and modeled emissions:

1. Magnetron age
2. Modulating pulse shape
3. Magnetron Type
4. Magnetron Anode Voltage and Current (peak power) setting
5. Magnetron Load

The factors are listed in their suspected order of significance. Only the first two factors are believed to have caused the large difference in measured emission spectrum levels for AN/CPN-4 and AN/MPN-11 radars since these radars are electrically identical, including the type magnetron employed, and were operated at the same peak power setting. The degree that a conventional magnetron emission spectrum increases with age depends on the tube type. The shape of the pulse that modulates the magnetron must be calibrated and maintained within the manufacturer specifications to insure a clean emission spectrum. Frequent calibration of the pulse rise time on narrow 0.5 μsec pulse width radars is particularly critical.

It is difficult to analytically include the above factors into the emission spectrum model. Because the standard deviation of the differences between predicted and measured emissions were significantly greater than the absolute mean, an

empirical correction to the magnetron emission model, based on the algebraic mean, is not recommended. It is believed that the overall standard deviation between modeled and measured emission spectrum of 6 dB may be the limit in obtainable accuracy for conventional magnetron emission modeling.

APPENDIX C

FREQUENCY-DEPENDENT-REJECTION

INTRODUCTION

The Frequency-Dependent-Rejection (FDR) model accounts for the energy coupling loss of an undesired signal in a victim receiver due to Off-Frequency Rejection (OFR) and On-Tune Rejection (OTR) of the undesired signal, and is therefore a necessary component in predicting radar-to-radar interference levels. The factors which affect the FDR of a victim radar are the undesired signal emission spectrum, victim receiver IF selectivity characteristics, and the frequency separation between the interfering and victim radar. This appendix discusses the techniques used to model the radar IF selectivity, and presents the method and program used to compute the FDR factor. FDR curves computed from the modeled IF selectivities and emission spectrums, and used in Los Angeles and San Francisco area investigations are also presented.

IF SELECTIVITY

Since the victim receiver frequency selectivity is the principal means by which the receiver discriminates agains undesired signals, it is an important input parameter to the FDR program.

Receiver spurious responses must also be considered when determining the FDR of a victim radar to an undesired signal. Spurious responses occur when the undesired signal is at a frequency such that it mixes with the local oscillator to produce an output at the receiver IF frequency. Since most radars have mixers, only image responses were investigated. The local oscillator frequency of most radars are tuned to 30 MHz above the receiver RF tuned frequencies in order to obtain an IF frequency of 30 MHz. An RF undesired signal that is 30 MHz above the local oscillator frequency (60 MHz above RF receiver center tuned frequency) will also be down-converted to the 30 MHz IF frequency. Modern radars normally employ an image-rejection mixer or a notch filter at the radar input to suppress image responses. The image response of the AN/CPN-4 and AN/MPN-13 radars are generally only 15 dB down from their center-tuned response, the ASR-4, 5 and 6 47 dB down, and the remainder of the radars greater than 50 dB down. Reduced FDR due to receiver image response was not incorporated in the FDR model, but was considered in an independent FDR calculation.

The selectivity of a receiver is the composite selectivity of all the tuned circuitry in the receiver prior to detection; however, in a superheterodyne receiver, the selectivity is determined by the IF stages because the preceding mixer and RF circuits are relatively broadar band. This is because the required filter characteristics are more physically relaizable and less expensive to build at the lower IF frequency.

IF Selectivity Modeling

The radars in the 2.7 to 2.9 GHz band generally employ a combination of synchronously-tuned, stagger-tuned triplets, and stagger-tuned doublet stages of IF amplification. The frequency response function (Reference 26) for the number and type of tuned IF stages employed in most radars indicated that an 80 dB/decade slope beyond the -3 dB points is the best choice for the IF selectivity model. This fall-off slope agrees with measured IF selectivities of the 2.7 to 2.9 GHz band radars that appear in Reference 27. Although some radars may have a steeper selectivity skirt, this will not significantly affect the frequency-dependent-rejection since the 20 and 40 dB/decade fall-off of conventional magnetron emission spectrum (see emission spectrum modeling equations B-1 through B-3 in Appendix B) governs the shape of the FDR curve.

To simplify the modeling effort, radars with nearly identical IF selectivities and bandwidths were grouped into the categories indicated in Table C-1. The modeled IF selectivities for the categories listed in the Table are plotted in Figure C-1.

FDR CALCULATIONS

FDR is the sum of attenuation of the undesired signal due to OFF-Frequency-Rejection (OFR) and the On-Tuned-Rejection (OTR) in dB.

$$FDR(dB) = OFR(dB) + OTR(dB) \qquad \text{EQ. C-1}$$

Off-Frequency Rejection (OFR) is defined in Reference 28 as:

$$OFR = \frac{\int \frac{P(F)}{G(F+\Delta F)}\, dF}{\int \frac{P(F)}{G(F)}\, dF} \qquad \text{EQ. C-2}$$

TABLE C-1

RADAR IF BANDWIDTH CATEGORIES

CATEGORY	RADAR	BANDWIDTH (MHz)
A (1.0 MHz BANDWIDTH)	AN/APS-20	1.0
	AN/FPS-6	0.8
	AN/FPS-90	0.8
	AN/MPS-14	0.8
	WSR-57*	0.75
B (2.25 MHz BANDWIDTH)	AN/CPN-4	2.25
	AN/MPN-11	2.25
	AN/MPN-13,14,15	2.26
	AN/MPS-19	3.00
C (5.0 MHz BANDWIDTH)	AN/FPN-47	5.0 ***
	AN/FPN-55	5.0 ***
	ASR-4,5,6,7	5.0 ***
	WSR-57 **	4.5

* (4.0 μsec pulse width mode)
** (0.5 sec pulse width mode)
*** (MTI Mode Bandwidth)

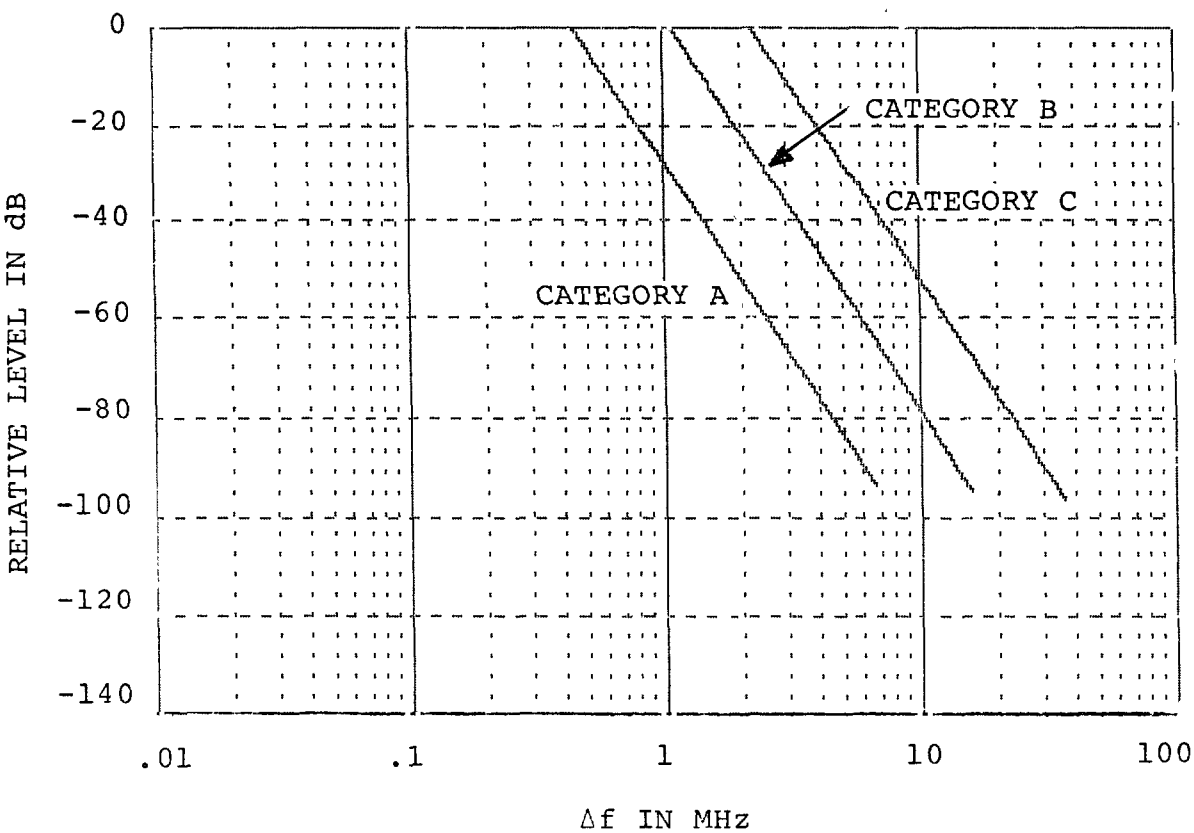

Figure C-1. Modeled Radar Category IF Selectivities

Where $P(F)$ = transmitter relative power density (normalized) to be ≤ 1)

$G(F)$ = relative receiver selectivity (normalized to be ≥ 1)

ΔF = frequency separation (transmitter minus receiver frequency)

Absolute transmitter power and receiver sensitivity does not enter into the caluclation because FDR depends only on the shape of the victim receiver IF selectivity and undesired signal emission spectrum.

Since the undesired signal emission spectrum and victim receiver selectivity curves are usually given in dB units, a more practical form of equation C-2 in dB is:

$$OFR_{dB} = 10 \log \int 10^{[P_{dB}(F)-G_{dB}(F+\Delta F)]/10} dF - 10 \log \int 10^{[P_{dB}(F)-G_{dB}(F)]/10} dF \qquad \text{EQ. C-3}$$

Where

$P_{dB}(F)$ = emission spectrum, in dB

$G_{dB}(F)$ = selectivity curve, in dB

The On-Tuned-Rejection (OTR) factor is derived in Reference 30, In summary, the OTR factor can be obtained by considering the Laplace transforms of a single pulse of amplitude "A" and width τ:

$$\mathcal{L}\left[\begin{matrix}\text{SINGLE}\\ \text{PULSE}\end{matrix}\right] = A\tau \frac{\sin \pi F\tau}{\pi F\tau} e^{-j\pi F\tau} \qquad \text{EQ. C-4}$$

Where the Laplace transform parameter, S, has been replaced by $j2\pi F$. The phase given by the exponential factor indicates that when the receiver bandwidth B_R is less than the emission bandwidth $B_T = 1/\tau$, the phase variation over the receiver bandwidth is small. This means that the voltage must be summed first and then squared instead of summing the square of the

voltages as many documents imply. For a relatively constant emission spectrum over the IF pass band, the received peak power is therefore proportional to the ratio of the receiver to transmitter bandwidths and the OTR factor in dB is given by:

$$OTR = \begin{cases} 20 \log_{10} B_R/B_T & B_R < B_T \\ 0 & B_R > B_T \end{cases} \qquad \text{EQ. C-5}$$

Where

B_R = receiver 3 dB bandwidth

B_T = emission 3 dB bandwidth

OFRCAL Program and its Validation

A computer program called OFRCAL (Reference 29) was employed to evaluate equation C-3 numerically by the trapezoidal method. Input to the program consisted of amplitude (dB) and frequency data point pairs of the undesired signal emission spectrum and victim receiver IF selectivity curves.

The OFRCAL program accuracy was validated by experiment. This involved using the measured IF selectivity (Figure C-2) of the RSMS spectrum Analyzer and the measured emission spectrum output (Figure C-3) of a RF pulse generator as inputs to the OFRCAL routine. The FDR curve computed by the routine was then compared with the measured FDR curve as shown in Figure C-4. The measured FDR was obtained by using the RF pulse generator as an input source to the RSMS spectrum analyzer and tuning the spectrum analyzer across the RF pulse emission spectrum. The measured and computed FDR curves agreed within 2 dB of each other at all ΔF frequencies.

Computed FDR's for Radar-to-Radar Interference Predictions

The computed FDR curves used in the Los Angeles and San Francisco area radar-to-radar interference investigations are presented in Figures C-5 through C-16. The FDR curves are computed for combinations of the emission spectrum categories listed in Table B-2 and the receiver IF bandwidth categories listed in Table C-1.

The OFRCAL routine used to compute the FDR performs the integration relative to the receiver tuned frequency.

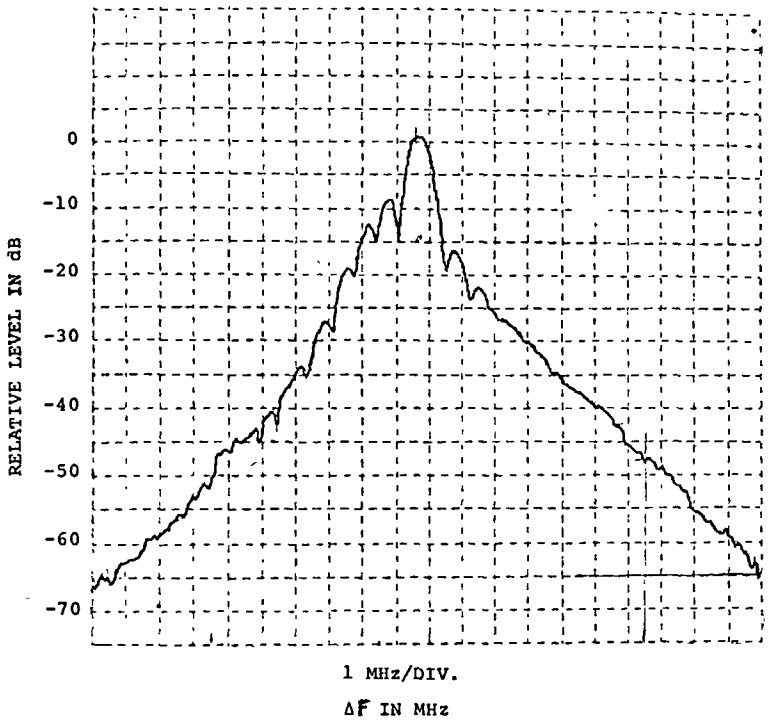

Figure C-2. Measured Selectivity of RSMS Spectrum Analyzer.

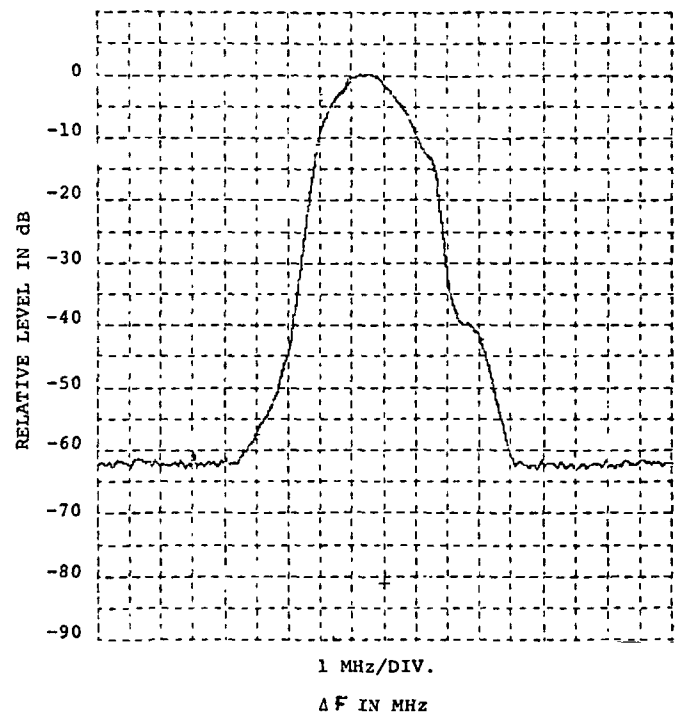

Figure C-3. Measured Emission Spectrum of Generator RF Pulse.

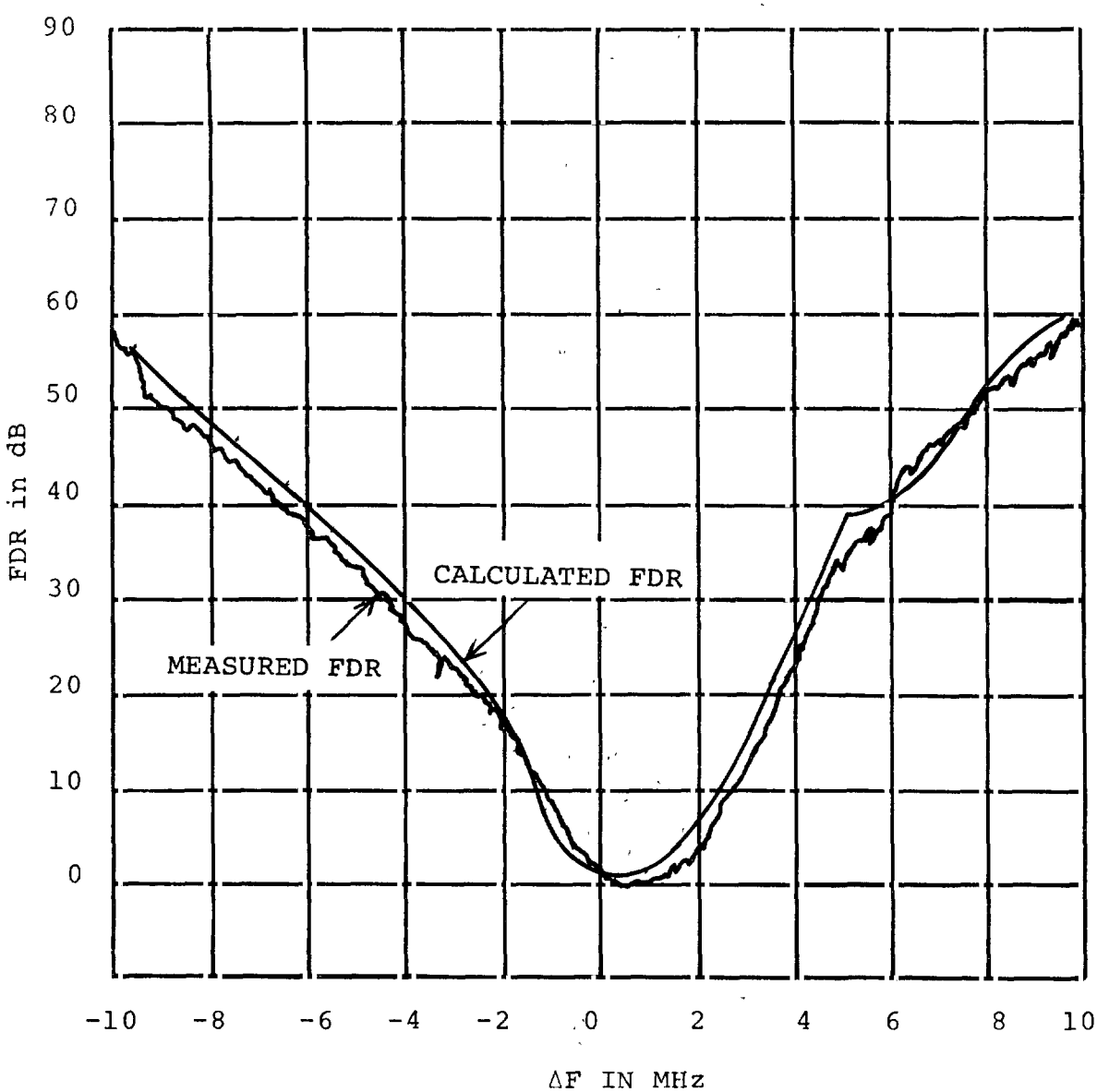

Figure C-4. Comparison of Measured and Calculated FDR

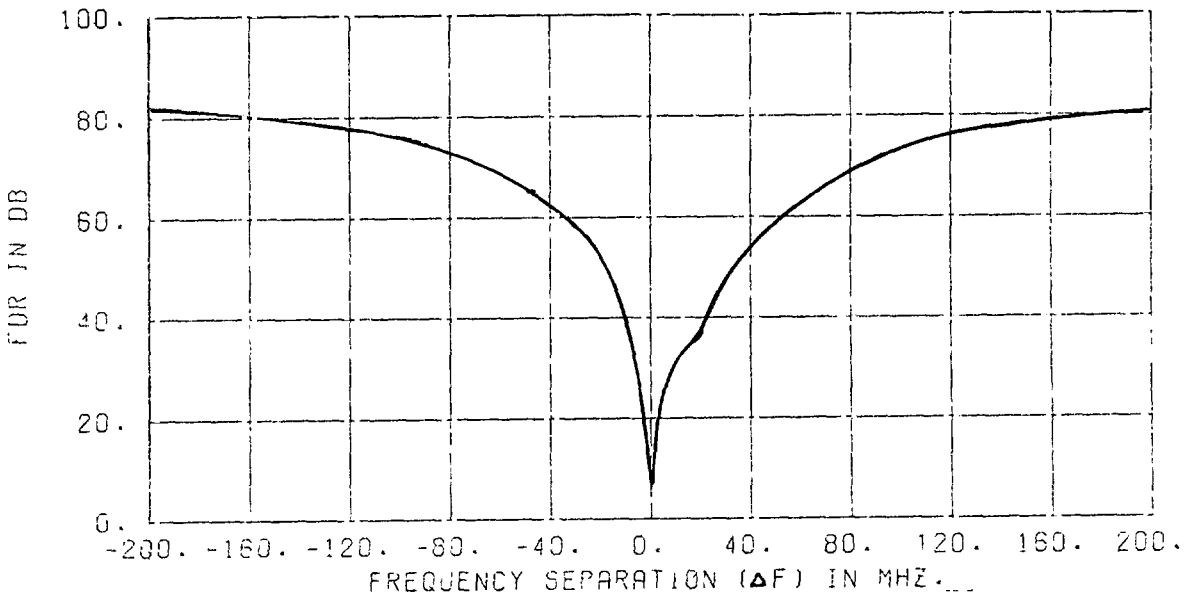

Figure C-5. FDR for Category 1 Transmitter Vs. Category A Receiver

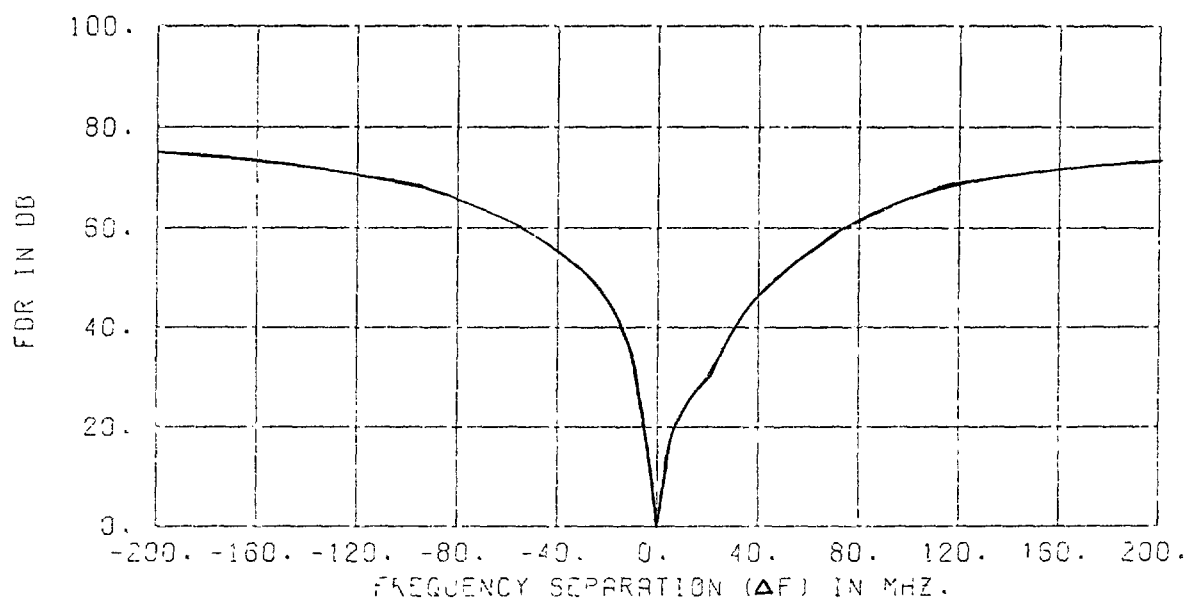

Figure C-6. FDR for Category 1 Transmitter Vs. Category B Receiver.

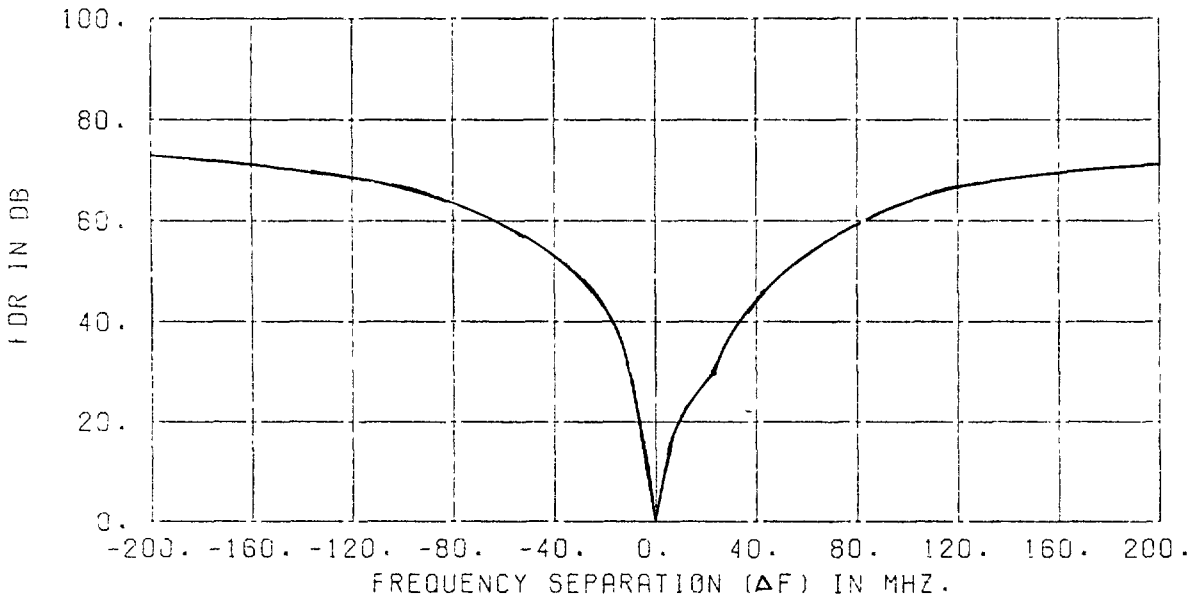

Figure C-7. FDR for Category 1 Transmitter Vs. Category C Receiver

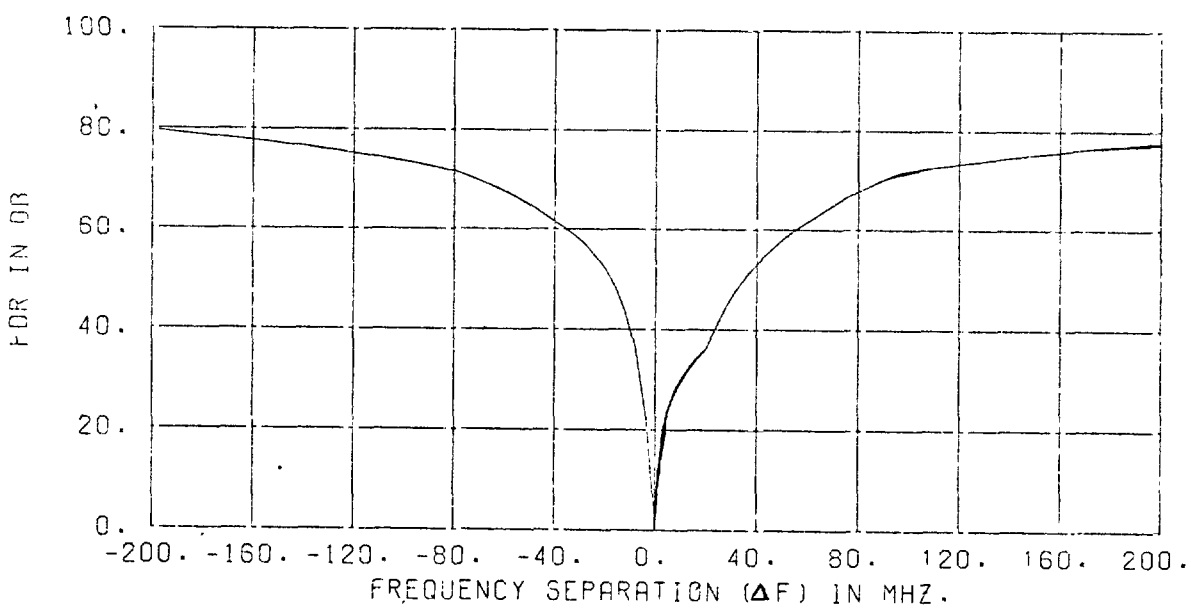

Figure C-8. FDR for Category 2 Transmitter Vs. Category A Receiver.

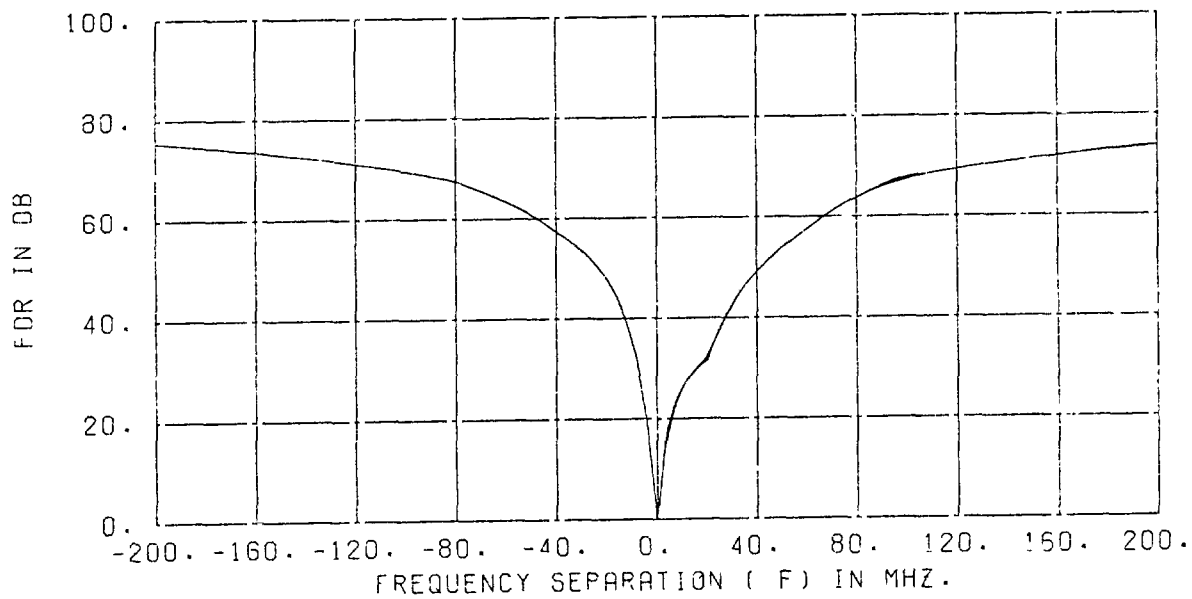

Figure C-9. FDR for Category 2 Transmitter Vs. Category B Receiver.

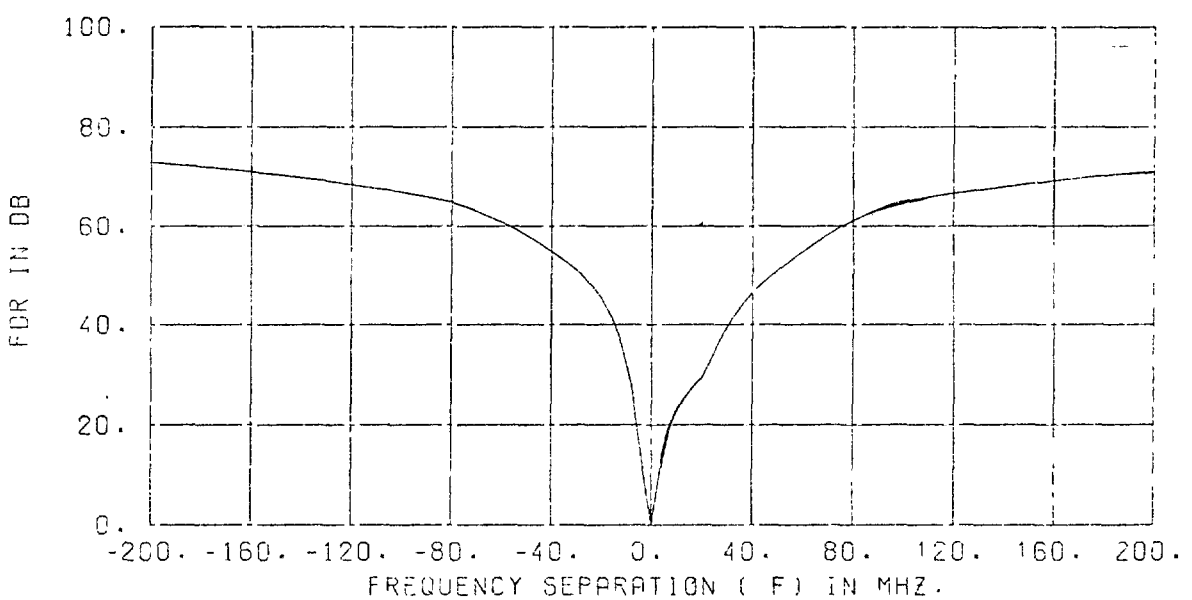

Figure C-10. FDR for Category 2 Transmitter Vs. Category C Receiver.

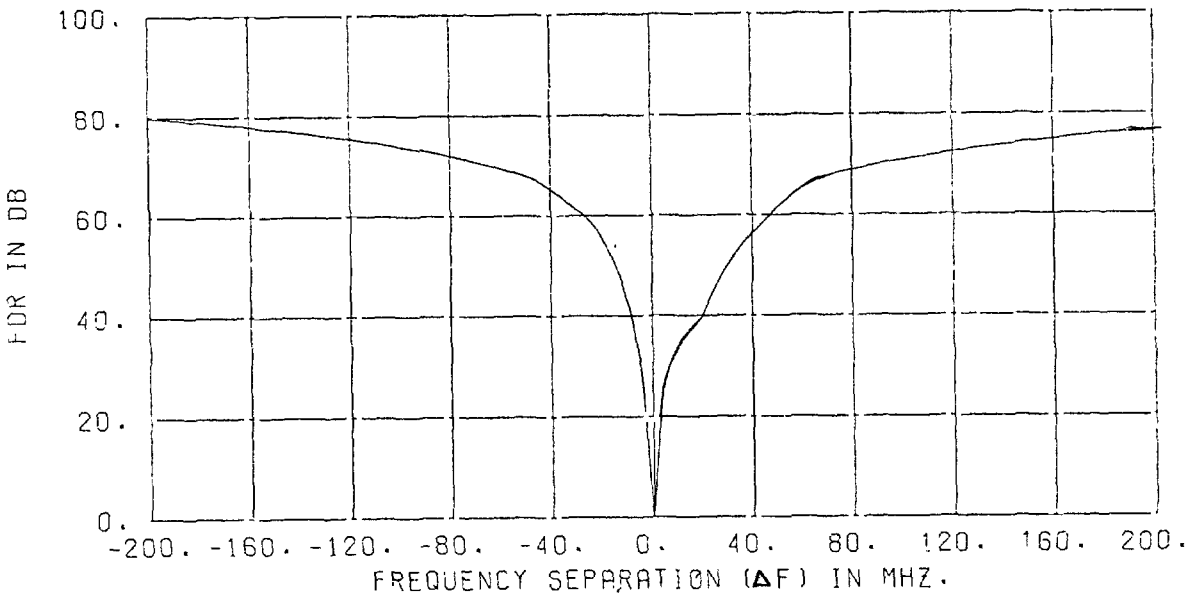

Figure C-11. FDR for Category 3 Transmitter Vs. Category A Receiver.

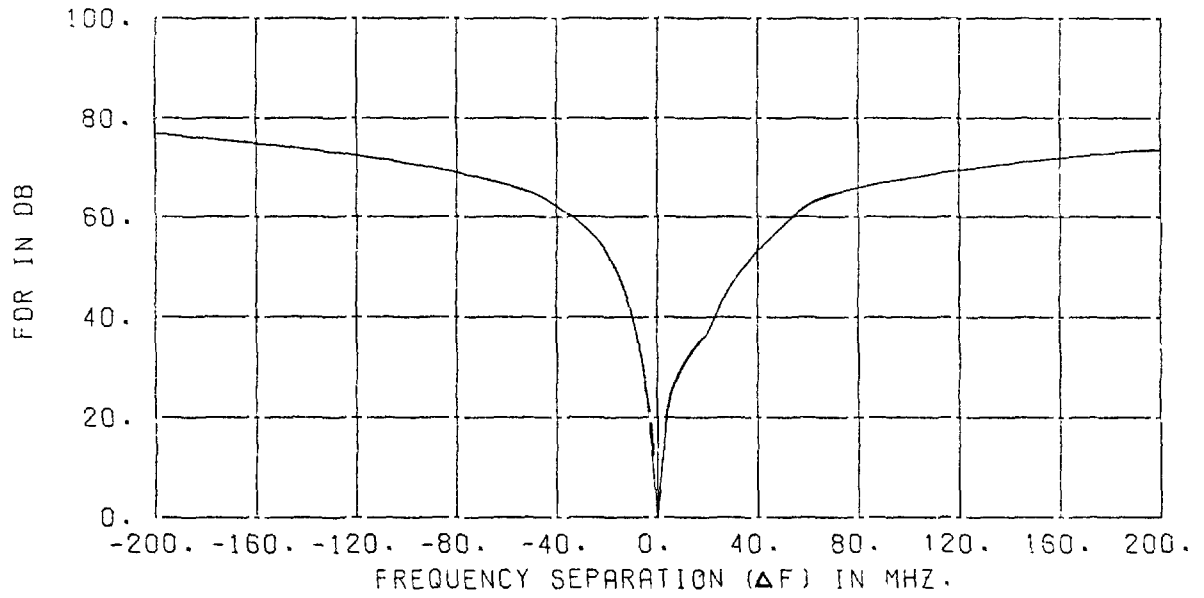

Figure C-12. FDR for Category 3 Transmitter Vs. Category B Receiver.

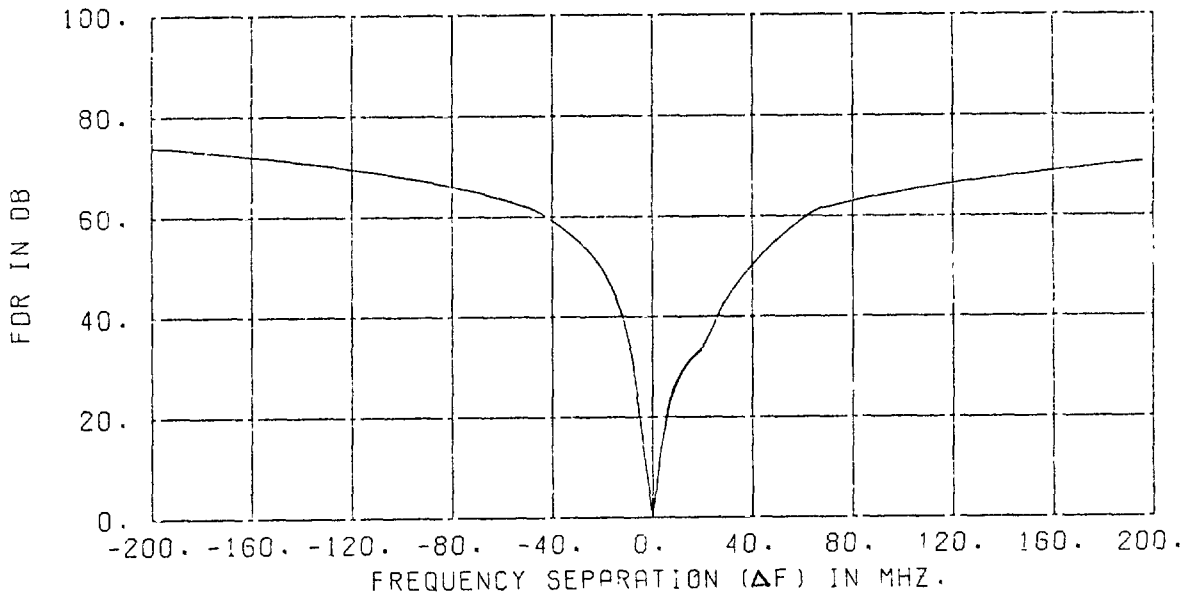

Figure C-13. FDR for Category 3 Transmitter Vs. Category C Receiver

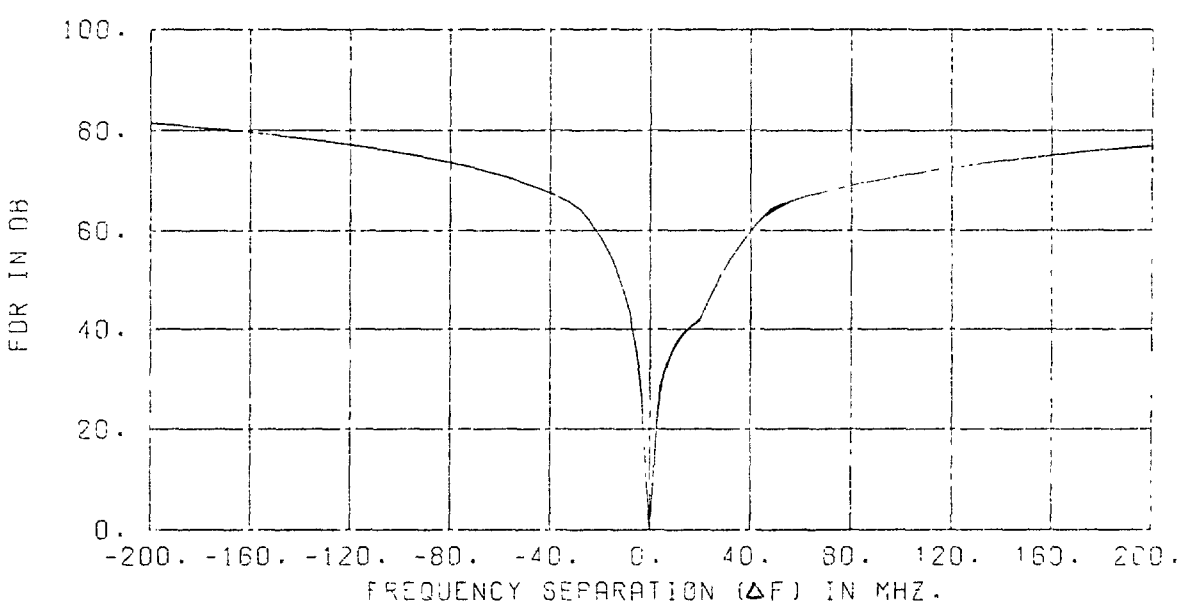

Figure C-14. FDR for Category 4 Transmitter Vs. Category A Receiver.

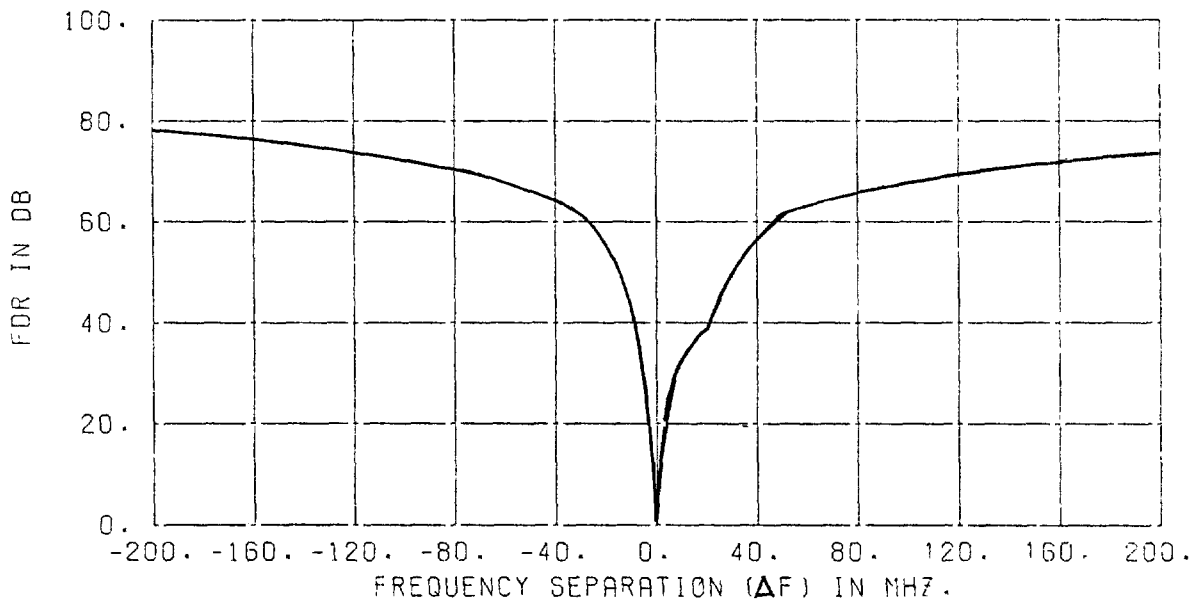

Figure C-15. FDR for Category 4 Transmitter Vs. Category B Receiver.

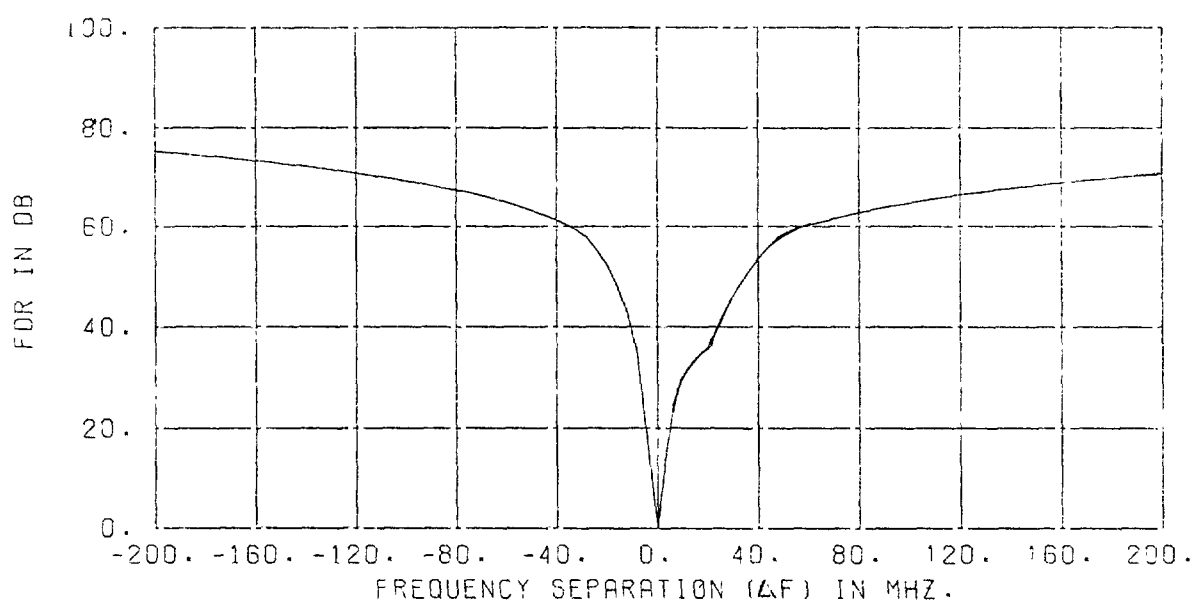

Figure C-16. FDR for Category 4 Transmitter Vs. Category C Receiver.

Therefore, the FDR for positive values of ΔF correspond to the transmitter being tuned higher than the receiver frequency.

The OTR factor was computed using Equation C-5 to take into account the category A receiver bandwidth being less than the category 1 and 2 transmitter emission bandwidths. The FDR curves that appear in Figures C-5 and C-8 were shifted up about 6.0 and 2.0 dB, respectively, to take the OTR factor into account.

Emission Spectrum Effect on FDR

The relative width of the category 1 through 4 emission spectra are reflected in the FDR curves. The narrowest emission spectra, associated with category 4 transmitters, caused the category 4 transmitter FDR curves (Figures C-14 through C-16) to have steeper slopes in the $\Delta F = 0$ region than other transmitter category FDR curves (Figures C-5 through C-13). This indicated that the FDR curve is highly dependent on transmitter emission spectra shape and relatively independent of IF selectivity curve shape.

SUMMARY OF FDR MODELING

Since FDR is emission spectrum dependent, the error in FDR predictions are dominated by the error between measured and modeled emission spectra. FDR curves were computed using the Ontario ASR-5 and Longbeach ASR-5 radar measured emission spectra (Figure B-12, B-13), and the measure IF selectivity of the Los Alamitos AN/CPN-4 radar (Figure C-17). The resulting FDR curves are shown in Figure C-18 and C-19 superimposed on the corresponding transmitter/receiver category FDR curves computed from modeled emission spectra and IF selectivities.

The difference between the FDR curves, FP-FM, were computed for every 10 MHz. These differences were used to compute the average absolute difference and standard deviation indicated in Table C-2, for the $-\Delta F$ and $+\Delta F$ regions of FDR curves. The agreement of the average absolute error and standard deviation values for category 2 radars, shown in Table C-2, agree to within 0.2 dB of those for the category 2 emission spectrum errors shown in Table B-3. This confirms that the FDR error approximately equals the emission spectrum modeling error.

Uncertainty in the exact frequency separation can also contribute to error in the FDR prediction. Radar frequency

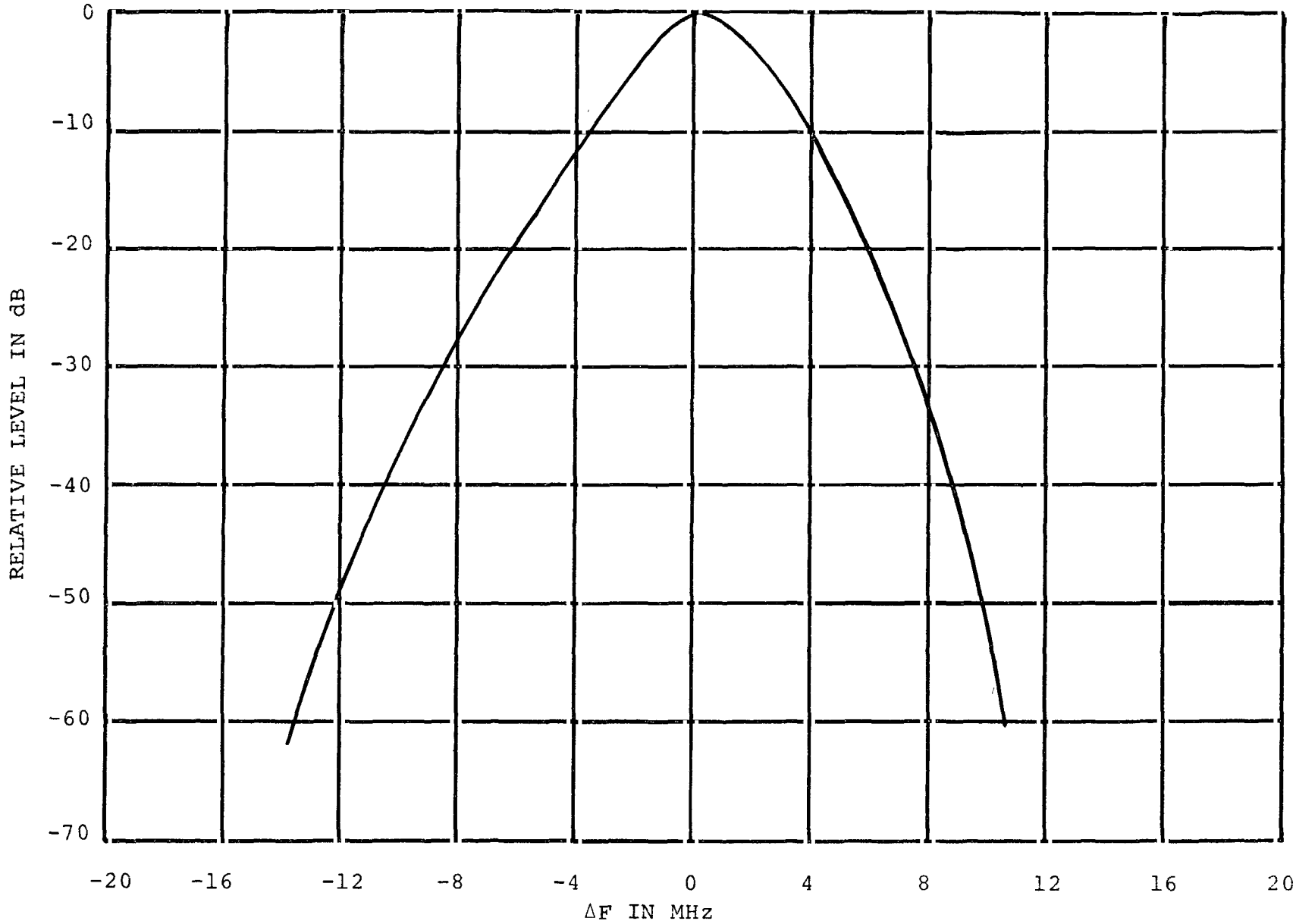

Figure C-17. Measured IF Selectivity of Los Alamitos AN/CPN-4 Radar

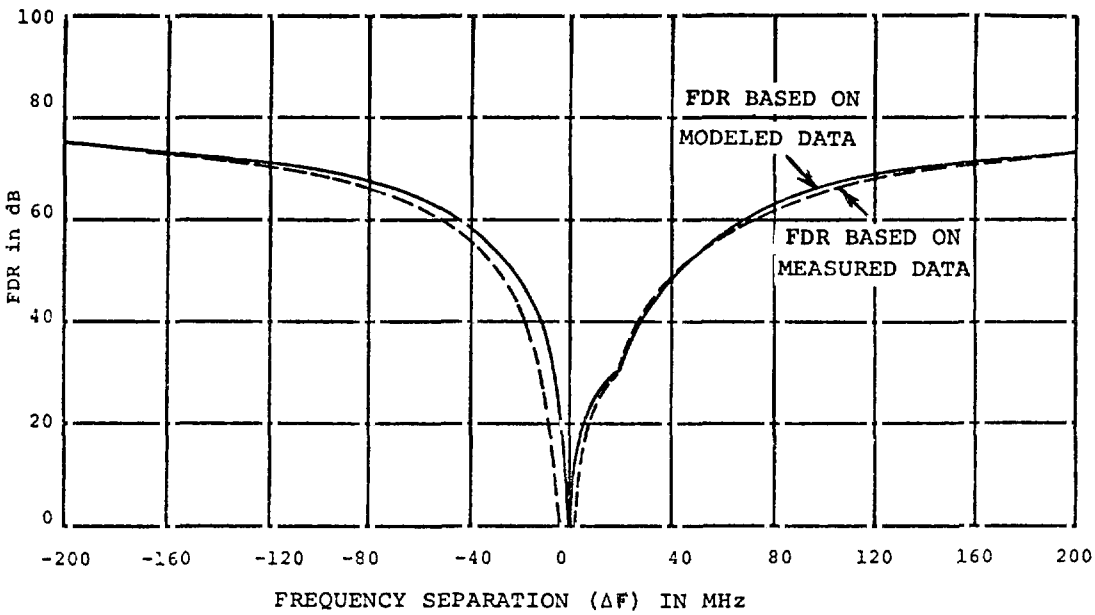

Figure C-18. FDR for Ontario Transmitter Vs. Los Alamitos Receiver.

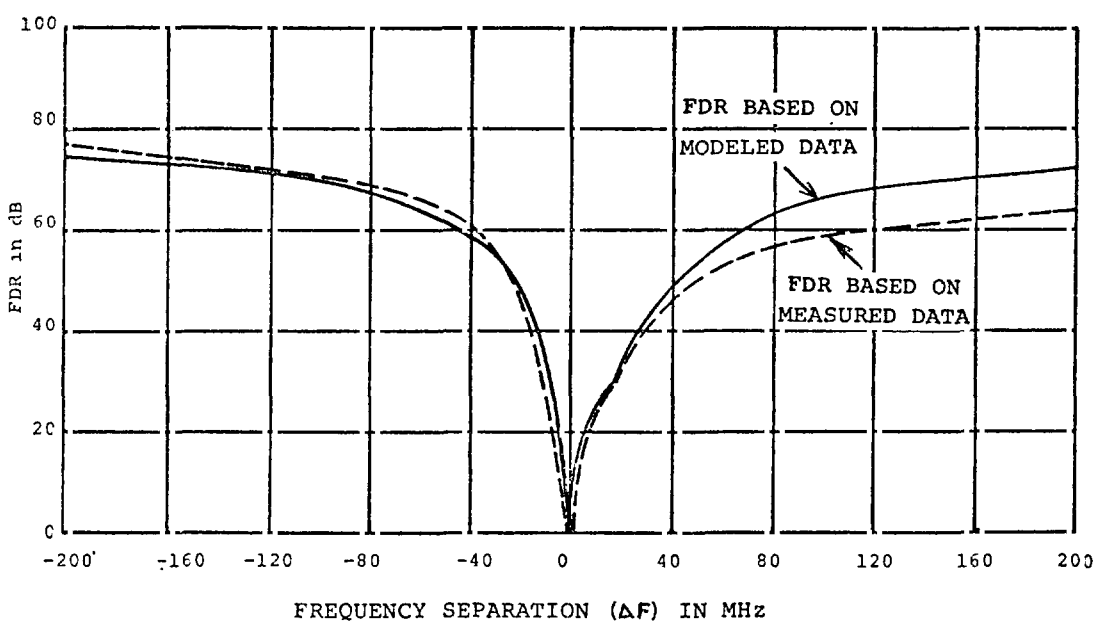

Figure C-19. FDR for Long Beach Transmitter Vs. Los Alamitos Receiver.

TABLE C-2

COMPARISON OF FDR CURVES COMPUTED
FROM MODELED AND MEASURED DATA

STATISTICAL COMPARISON CRITERIA \ SIDE OF FDR CURVE	$-\Delta F$	$+\Delta F$
MEAN $\overline{X} = \frac{\Sigma \lvert FP-FM \rvert}{N}$ (dB)	1.4	3.8
STANDARD DEV. BETWEEN PRED. AND MEAS. $= \left[\frac{\Sigma (FP-FM)^2}{N} \right]^{1/2}$ (dB)	3.3	5.4

FP = Computed FDR Based on Modeled Emission Spectra and IF Selectivity Curves

FM = Computed FDR Based on Measured Emission Spectra and IF Selectivity Curves

N = Total Number of Comparisons (Frequency Points)

measurements in the Los Angeles and San Francisco area indicate that radars are not always operated exactly at their assigned frequency. The error contribution to FDR predictions due to the uncertainty of frequency separation between transmitter (interferer) and receiver (victim) can be significant for frequency separations less than 10 MHz.

APPENDIX D

PROPAGATION LOSS

INTRODUCTION

The prediction of the propagation loss between interfering transmitters and victim receivers is an important step in an EMC analysis because it affects the level of interference at the victim receiver. In order for a propagation model to give accurate predictions, it must consider the environment in which the system operates and all possible modes of propagation.

This appendix discusses the capability and inadequacies of the propagation models used in the Los Angeles and San Francisco area radar-to-radar interference investigations. The propagation losses predicted by the models are compared with measured propagation losses. The appendix also discusses factors that contributed to the differences between predicted and measured loss, and proposes methods in which the factors can be included in the prediction of propagation loss.

PROPAGATION LOSS PROGRAMS AND MODELS

The area and point-to-point version of the propagation loss model, founded on the 1968 Computer Method by Longley and Rice (Reference 14), was employed in this investigation. The model was derived from well established propagation theory with adjustments based on extensive transmission loss measurements over various terrains in unpopulated areas. The following is a brief description of the two versions of the program and how they were applied in the Los Angeles and San Francisco area radar-to-radar interference investigation.

Point-to-Point Model

The point-to-point batch program is normally used to compute basic propagation loss when the specific coordinates of antenna locations are known. The program automatically addresses a terrain data base, extracts the appropriate terrain profile, computes geometric terrain parameters, and selects the lowest loss propagation mode for calculation of propagation loss. One critical parameter in any model that predicts propagation loss over irregular terrain is that which characterizes the terrain roughness. The point-to-point model employs an "interdecile" range parameter, $\Delta h(d)$. Using the least squares method, a straight line is fitted to the terrain

profile, and the cumulative distribution of terrain heights above and below this line are computed. The difference between the 90 and 10 percentile (i.e., the interdecile range) of the cumulative distribution defines $\Delta h(d)$.

Area Model

The area version of the model is normally used to compute basic median propagation loss when the particular path or specific antenna locations are not known. The terrain parameter, $\Delta h(d)$, for the point-to-point model is deterministic and computed from a single path. However, the area prediction model uses $\Delta h(d)$ as a statistical parameter to characterize terrain roughness of many paths in a general area. The $\Delta h(d)$ in this case is the median distribution value of $\Delta h(d)$'s associated with many point-to-point paths. The $\Delta h(d)$ parameter for the area model is usually estimated from Table D-1 or a map of $\Delta h(d)$ contours.

TABLE D-1

Propagation Roughness Factors

Type of Terrain	Δh(meters)
Water or very smooth terrain	0-1
Smooth terrain	10-20
Slightly rolling terrain	40-60
Hilly terrain	80-150
Rugged mountains	200-500

The area model also requires the user to specify one of the three following antenna siting factors:

1. Random . . . . 0 meters
2. Fair . . . . . 5 meters
3. Good . . . . . 10 meters

to account for the antenna's terrain elevation effects on propagation loss. The siting factor is defined as the median difference by which the effective antenna height above the ground exceeds the structural antenna height. The effective

antenna height is the antenna height above its effective reflecting plane or its surrounding average terrain level. If random siting is specified, the program sets the effective antenna height equal to the antenna structural height. For antenna locations near and on hilltops, fair and good siting respectively, whould be specified. In this case, the effective antenna height computed exceeds the structural height by an amount whose median value depends on the structural antenna height and the parameter $\Delta h(d)$.

APPLICATION OF PROPAGATION MODELS

Both the point-to-point and area versions of the propagation programs were employed in this investigation. The point-to-point propagation program was used to predict propagation loss between 253 radar pair combinations in the Los Angeles area and 210 radar pair combinations in the San Francisco area. These loss predictions were used in the INR calculations for all radar pair combinations.

The area model was also used to predict propagation loss over those radar-to-radar paths (21) in which propagation loss measurements were made. This allowed the point-to-point and area model prediction accuracies to be compared. Because of the subjectivity involved in selecting the antenna siting factor associated with the area model, the area model loss predictions were made with both random and fair antenna siting factors specified. To take advantage of the known terrain profile between radars and increase prediction accuracy, the $\Delta h(d)$s computed by the point-to-point model were used in the area model predictions.

Propagation Model Mode Selection Deficiencies

The accuracy of the point-to-point propagation loss prediction depends on the resolution of the topographical terrain data file and the model's interpretation of it. The terrain data file includes data points every 30 seconds of arc which corresponds to a distance of 0.5 nautical miles. Although this resolution is adequate for many applications involving relatively smooth terrain, it can give large errors for propagation loss predictions over rough terrain. The propagation program interprets the elevation of the terrain data point that falls horizontally closest to the specified antenna coordinates as the antenna site elevation. This interpretation can result in a propagation mode selection error when the closest terrain data point to the antenna site is at a lower elevation than the actual antenna site elevation. The problem manifested itself in the Los Angeles investigation

for the propagation prediction between the San Pedro and Los Angeles airport radars. For this path, the model placed the San Pedro radar on the other side of San Pedro Hill from the Los Angeles Airport radars; however, the antenna site is actually located on the top of the hill. The program consequently interpreted the terrain profiles as a knife edge path and computed 153 dB propagation loss. When the program was manually instructed to use the correct line-of-sight path, it computed a loss of 133 dB. This program deficiency was corrected for the San Francisco area investigation by providing the user with an option to specify the antenna site elevation.

The point-to-point program also incorrectly interpreted three single knife edge propagation paths as being double knife edge. This situation occurred when adjacent terrain data points were located at approximately equal terrain elevations on opposite sides of a common horizon peak. The program incorrectly identified the mountain or hill as having a flat top between the two data points and selected double knife edge as the mode for predicting propagation loss. The 6 to 11 dB loss prediction error that resulted from this incorrect program mode selection was corrected by manually rerunning the program with the sum of the distances between the radars and their horizons set equal to the total great circle distance between the two radars.

The terrain profile computer printouts and propagation mode selection for each path investigated in the Los Angeles and San Francisco area were examined to insure that the proper propagation mode was selected by the model.

BASIC PROPAGATION LOSS MEASUREMENT PROCEDURE

The following is a discussion of the RSMS van antenna systems used during the measurements to determine the propagation path loss between radars in the Los Angeles and San Francisco area, and the procedure used to calculate the basic propagation loss for validation of the previously mentioned propagation models. A detailed description of the RSMS van instrumentation and software programs (Single Frequency Scan and Frequency Tracking Scan) used to determine the propagation loss are discussed in Appendix G.

RSMS Van Antennas

In a free space propagation coupling environment, the power level received at the input of a measurement receiver,

after normalization of the receiver antenna gain, is independent of the receiving system antenna pattern. However, in a multi-pathing and ducting environment, the power level received is very much affected by the receiving system antenna pattern. In fact, in a multipathing and ducting environment, the propagation loss and receiving antenna pattern are virtually inseparable. The RSMS van does not have an antenna system which approximates the cosecant squared elevation pattern of the normal search radar, or the ability to adjust the height of a directional antenna to the height of the actual radar antenna. It is generally believed that if there is any major flaw in the procedures used to determine the propagation loss between radars, it is in the receiving antenna system used. Because of this, a discussion of the RSMS van antenna systems used to determine the propagation path loss between radars is imperative.

Three types of RSMS van antennas were employed to measure propagation loss:

1. A right-hand circular polarized one meter diameter parabolic reflector.

2. A right-hand circular polarized cavity back spiral.

3. A +45 degree slant polarized omni-directional antenna.

Both the dish (parabolic reflector) and nondirectional antennas (cavity and omni) were used to measure propagation loss over all paths when the nondirectional antennas provided sufficient sensitivity. However, for certain propagation conditions, only the data measured with the dish or nondirectional antennas were used to determine propagation loss. The following is a discussion of the selected RSMS van antenna used for particular propagation conditions.

Dish. The dish (parabolic reflector) was used to measure loss over those paths in which multipath was primarily taking place in the azimuthal plane. The 8 degree pencil beam of the dish approximates the radar's azimuthal antenna pattern response to azimuthal multipath closer than the nondirectional antennas.

Nondirectional Antennas. The cavity and omni antennas were used, when they provided sufficient measurement sensitivity, to measure propagation loss during superrefraction conditions. During superrefraction conditions and for paths over water, multipathing primarily occurs in the elevation plane. The wide elevation beam width of the nondirectional antennas approximate the radar cosecant squared elevation antenna pattern closer than the dish's 8 degree beamwidth. In addition,

combining the ducting data measured with the nondirectional and dish antennas would unrealistically increase the signal variation due to ducting from 40 to 60 dB. The majority of this 20 dB increase is believed to be due to the different response of the nondirectional and dish antenna pattern to multipath.

The capability to adjust the cavity antenna height was used to measure propagation loss as a function of antenna height. The cavity was also used over those paths in which it was critical to measurement accuracy to match the measurement receiving antenna height to the radar antenna height.

Calculation of Basic Propagation Loss

The received power level measured by the RSMS van was used to compute the basic transmission loss (LM) by:

$$LM = P_T + G_T - L_T - L_I + G_V + L_C - P_R \qquad \text{(D-1)}$$

where:

P_T = transmitter power, in dBm

G_T = transmitter antenna gain, in dBi

L_T = radar transmitting antenna gain reduction due to the upward tilt angle of the transmitting antenna, in positive dB

L_I = transmitter waveguide and coupling loss, in positive dB

G_V = the RSMS van receiving antenna gain, in dBi

L_C = receiving antenna cable calibration correction factor, in dB

P_R = measured receive power, in dBm

The values for the transmitter power (P_T) were obtained from radar site personnel and confirmed by on-site observation of the radar transmitter power meter. These values were used instead of the GMF transmitter power values indicated in Tables 4-2 and 5-2 to minimize error in the propagation loss calculations. The transmitter antenna gain values (G_T) were obtained from the GMF and confirmed by phone contact with site personnel.

The transmitter antenna tilt angles shown in Tables 4-2 and 5-2 were obtained by phone contact with radar site personnel and subsequently confirmed by on-site observation. The radar antenna gain reduction (L_T) due to antenna tilt angle was determined by one of two techniques. For radars having a cosecant-squared elevation antenna pattern, the gain reductions were determined from the ASR elevation pattern shown in Figure A-2 of Appendix A. For radars having a pencil beam antenna, such as the WSR-57, the gain reduction was computed from the Bassel functions that define the antenna pattern of a circular aperture antenna with cosine-squared aperture illumination (Reference 53). This function was then checked against the known 3 dB beamwidth and sidelobe specification of the antenna for accuracy.

A 2 dB insertion loss (L_I) was included for all radars to account for the transmitter waveguide and rotary coupler loss and is based on measurements performed by the FAA (Reference 31) on an ASR-4 radar.

The calibrated antenna gain (G_V) of the RSMS van dish, cavity, and omni antennas are 20, 3, and 0 dB, respectively. These values include the 3 dB polarization mismatch loss for reception of a vertical and horizontal polarized signal.

A correction factor (L_C) of 2 dB was included for those measurements performed with the dish and omni antennas. This correction factor was not required for measurements performed with the cavity antenna because noise diodes located on the van antenna tower were used to calibrate out the cable loss.

PROPAGATION LOSS MEASUREMENTS

Propagation loss measurements between radars in the Los Angeles and San Francisco area were measured with the RSMS van intermittently during 1975. The measurements were conducted over 13 paths in the Los Angeles area and 8 paths in the San Francisco area.

Propagation Measurements over Nonducting Paths in Los Angeles Area

The results of propagation loss measurements over 13 nonducting paths in the Los Angeles area are shown in the next to last column of Table D-2. The predicted propagation loss for the point-to-point model and the area model with both random and fair antenna siting specified are also shown in the Table. The difference (LP-LM) between the loss predictions and measurements are shown adjacent to the model prediction columns.

The measured propagation loss shown in the Table for each path represents the statistical reduction of numerous half-hour measurements at different RSMS van locations around each radar antenna site. The measurements were conducted at more than one position to average out the effect of signal level variation due to multipathing. Signal level changes due to short term fading during half-hour propagation measurement was less than 4.0 dB. The median value of this signal level variation was used in determining the measured losses shown in Table D-2.

Long Beach to Los Alamitos Propagation Measurements. To investigate the effect of the antenna height difference between the cavity and dish antenna on measured propagation loss, the loss was measured as a function of cavity antenna height at Los Alamitos (Figure D-1) and Long Beach (Figure D-2). The table in the upper right hand corner of Figure D-1 and D-2 indicates the antenna height corresponding to the time reference scale on the abscissa. The propagation loss measured from 10.5 to 25 feet antenna height at Los Alamitos resulted in a 4.0 dB difference, and at Long Beach a 11.0 dB difference. These changes in propagation loss with antenna height (antenna height gain) exceeded that predicted by the propagation model. This is believed to be due to the fact that the model did not take into account the reduction in shadowing by trees and buildings. The propagation loss difference for 10.5 and 25 feet antenna heights at Long Beach was 7 dB greater than the change at Los Alamitos, because the Los Alamitos radar antenna is located in an open airfield and the Long Beach radar antenna in an area surrounded by trees and buildings. Figure D-3 illustrates the geometry of the clutter relative to the paths between the transmitting and receiving antenna for various receiver antenna heights. The two ray paths (indicated by solid lines) from the Long Beach radar antenna to the two antenna measurement height extremes at Los Alamitos do not pass through the trees; however, the propagation ray paths (indicated by dotted lines) from the Los Alamitos radar antenna to the lower measurement antenna height at Long Beach, does pass through the trees and buildings resulting in increased signal attenuation.

The propagation loss measured on the Long Beach end of the Long Beach/Los Alamitos path was 157 dB with the cavity, and 176 dB with the dish. Eleven of this 19 dB variation in measured propagation loss was due to the difference between the dish antenna height (14 feet) and the cavity antenna height (25 feet) as indicated in Figure D-3. The remaining 8.0 dB of the 19 dB difference between using the cavity and dish at Long Beach, is attributed to the difference in weighting of the diffused signal energy through the trees by the different beamwidths associated with the cavity and dish

TABLE D-2

COMPARISON OF PREDICTED AND MEASURED PROPAGATION LOSS BETWEEN LOS ANGELES RADARS

FROM	TO	DIST. (kM)	POINT-TO-POINT LOSS 50/50 (dB)		AREA LOSS RANDOM SITING 50/50 (dB)		AREA LOSS FAIR SITING 50/50 (dB)		MEAS. EQUIV. LOSS LM (dB)	CHARACTERISTICS OF PATH
			PREDICTED (LP)	LP-LM	PREDICTED (LP)	LP-LM	PREDICTED (LP)	LP-LM		
LOS ANGELES ASR-4	LOS ALAMITOS AN/CPN-4	37.3	179	7	166	-6	162	-10	172	ROUNDED EARTH (BUILDINGS)
LOS ANGELES ASR-7	LOS ALAMITOS AN/CPN-4	36.5	176	-9	165	-20	161	-24	185	ROUNDED EARTH (BUILDING)
BURBANK ASR-6	LOS ALAMITOS AN/CPN-4	54.1	186	1	183	-2	177	-8	185	KNIFE EDGE
EL TORO ASR-5	LOS ALAMITOS AN/CPN-4	34.2	142	-16	166	8	155	-3	158	LINE-OF-SIGHT
ONTARIO ASR-5	LOS ALAMITOS AN/CPN-4	51.4	183	-1	161	-23	150	-34	184	KNIFE EDGE
NORTON AN/MPN-13	LOS ALAMITOS AN/CPN-4	82.5	198	6	202	10	199	7	192	KNIFE EDGE
SAN PEDRO AN/FPS-90	LOS ALAMITOS AN/CPN-4	27.0	137	-14	176	25	166	15	151	LINE-OF-SIGHT

TABLE D-2 (Continued)

FROM	TO	DIST. (kM)	POINT-TO-POINT LOSS 50/50 (dB)		AREA LOSS RANDOM SITING 50/50 (dB)		AREA LOSS FAIR SITING 50/50 (dB)		MEAS. EQUIV. LOSS LM (dB)	CHARACTERISTICS OF PATH
			PREDICTED (LP)	LP-LM	PREDICTED (LP)	LP-LM	PREDICTED (LP)	LP-LM		
LONG BEACH ASR-5	LOS ALAMITOS AN/CPN-4	8.9	130	-19	138	-11	131	-18	149	LINE-OF-SIGHT (BUILDINGS)
LOS ALAMITOS AN/CPN-4	LONG BEACH ASR-5	8.9	130	-27	138	-19	131	-26	157	LINE-OF-SIGHT (BUILDINGS)
EL TORO ASR-5	LONG BEACH ASR-5	43.1	144 143*	-24	174 172*	6	167	-1	168	LINE-OF-SIGHT
BURBANK ASR-6	LONG BEACH ASR-5	47.1	182 181*	-7	181 178*	-10	172 171*	-19	191	KNIFE EDGE (BUILDING)
LONG BEACH ASR-5	BURBANK ASR-6	47.1	184 181*	-3	181 178*	-7	172 171*	-13	185	KNIFE EDGE (BUILDING)
EL TORO ASR-5	BURBANK ASR-6	84.4	154 151*	-22	199 196*	23	197 195*	21	176	KNIFE EDGE
LOS ANGELES ASR-4	LOS ANGELES ASR-7	2.4	119	-5	114	-10	111	-13	124	LINE-OF-SIGHT (BUILDINGS)

*Predicted Propagation Loss For Radar Antenna Height if Different than Predicted for Van Dish Antenna Height.

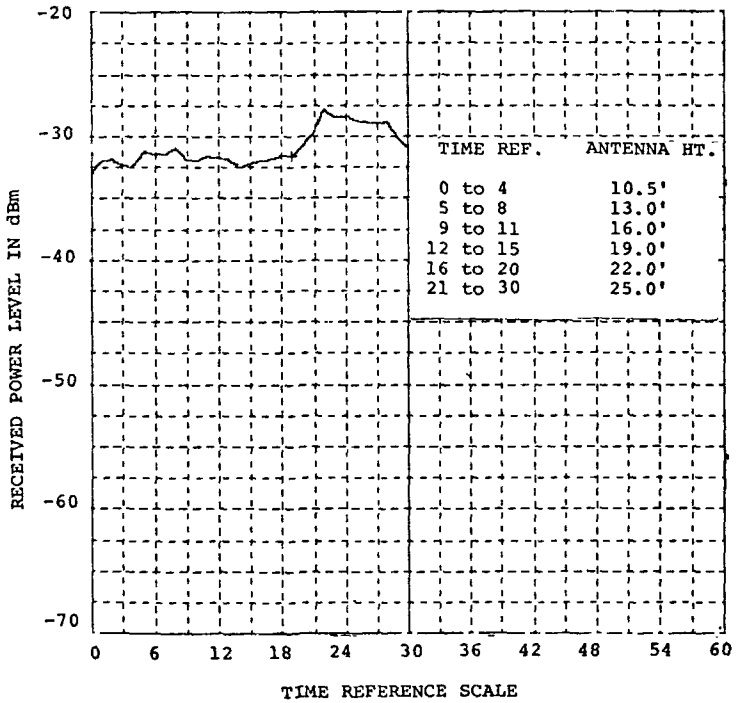

Figure D-1. Measured Propagation Loss at Los Alamitos from Long Beach as a Function of Measurement Antenna Height.

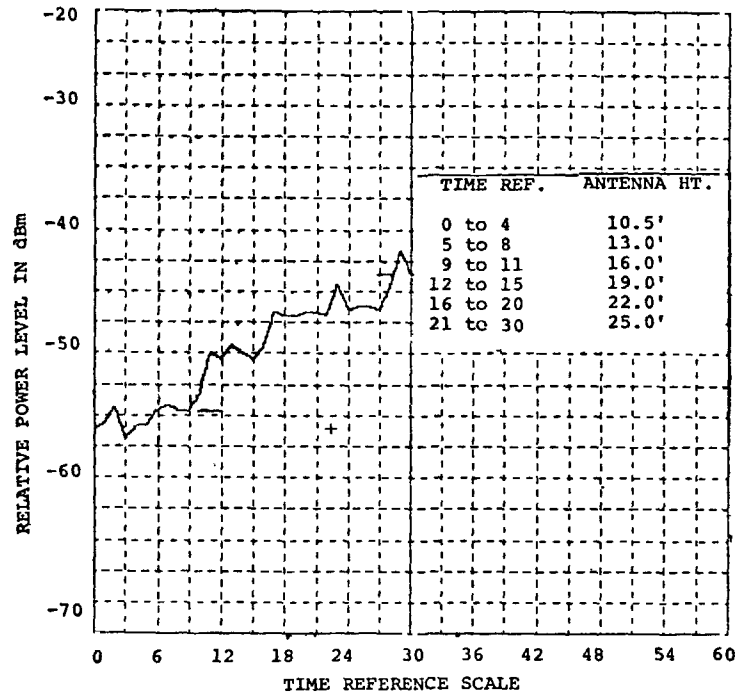

Figure D-2. Measured Propagation Loss at Long Beach from Los Alamitos as a Function of Measurement Antenna Height

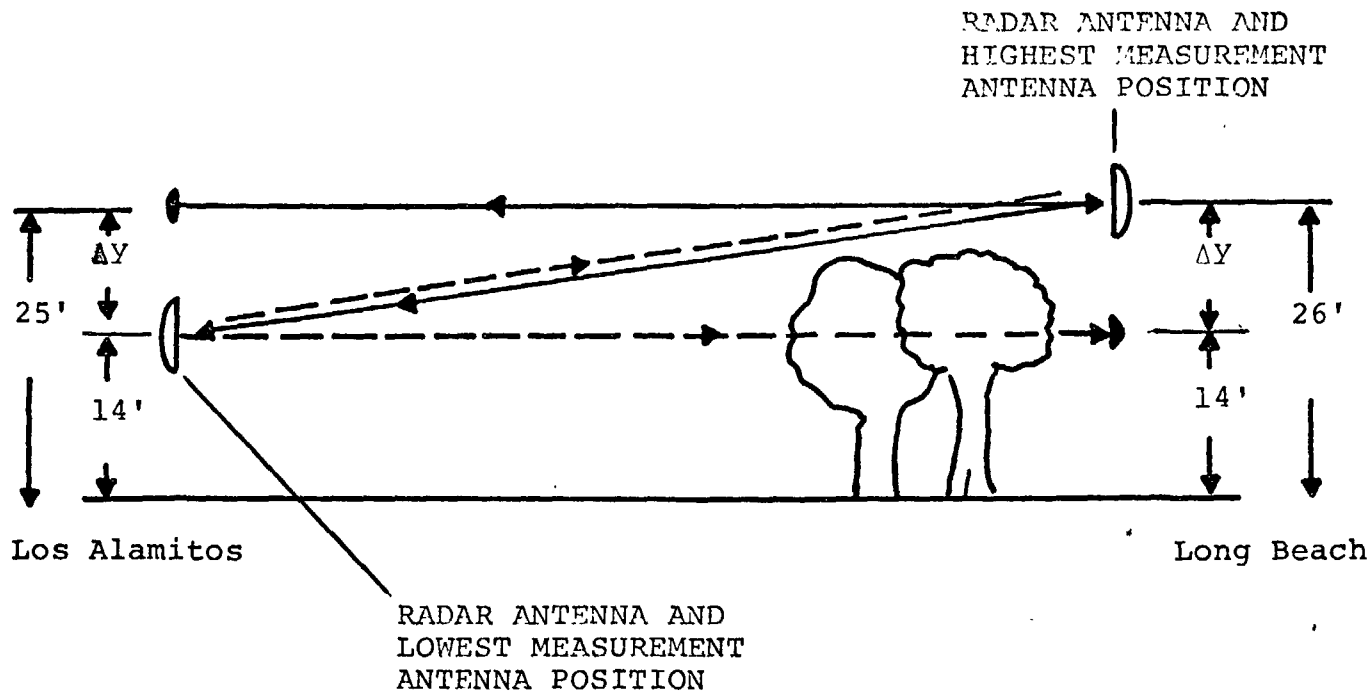

NOTE: Δy is height range that measurement antenna was varied

Figure D-3 Propagation Loss Geometry Associated with Measured Propagation Loss vs. Antenna Height at Los Alamitos and Long Beach

antennas. The 75 degree beamwidth of the cavity antenna captures more multipath energy than the dish's 8 degree beamwidth.

To preclude propagation loss measurement error due to differences between the radar and receiving measurement antenna height, the cavity antenna was used at the Long Beach end of the path. It was the only RSMS van antenna that could be matched to the radar antenna height. The dish was used on the Los Alamitos end of the path because the dish height is approximately equal to the Los Alamitos radar antenna.

The long term propagation loss measured on the Los Alamitos end of the path (see Table D-2) was 149 dB; however, on the Long Beach end of the path it was 157 dB. This 8 dB difference is attributed to two reasons. The azimuthal distribution of multipath signal phase and amplitude arriving at the measurement receiving antenna was different at the two radar site locations. In addition, the cavity and dish's antenna response to a multipath environment are different because they have different antenna patterns.

To investigate the multipath environment between Long Beach and Los Alamitos, the RSMS van dish antenna pattern was measured at Los Alamitos using the Long Beach radar as a signal source. This involved tuning the RSMS receiver to the Long Beach radar frequency and rotating the RSMS van antenna 360 degrees. The resulting antenna pattern, shown in Figure D-4, was compared with the RSMS van dish free space antenna pattern to determine the level of the antenna response to multipath signals as a function of azimuth. The peak of the pattern corresponds to the Long Beach radar azimuth. The second peak labeled Screen corresponds to the azimuth of an 18 by 100 yard metal screen on the outside edge of the Los Alamitos airfield periphery. A geometrical analysis revealed that the screen's vertical plane orientation was such that equal incident and reflection angles occurred for multipath signals between Long Beach and Los Alamitos. However, the angle between the direct and reflected path at the two radar sites was greater than the radar azimuth antenna beamwidths. Therefore, the direct energy from the radar and reflected energy from the screen incident on the measurement receiving antenna was at least 20 dB different for the instant that radar and measurement antenna mainbeam coupling occurred. This analysis indicated the difference in loss measured on the two ends of this path was not due to the screen, as originally suspected, but due to the effect of multipath within plus or minus 10 degrees of the direct path.

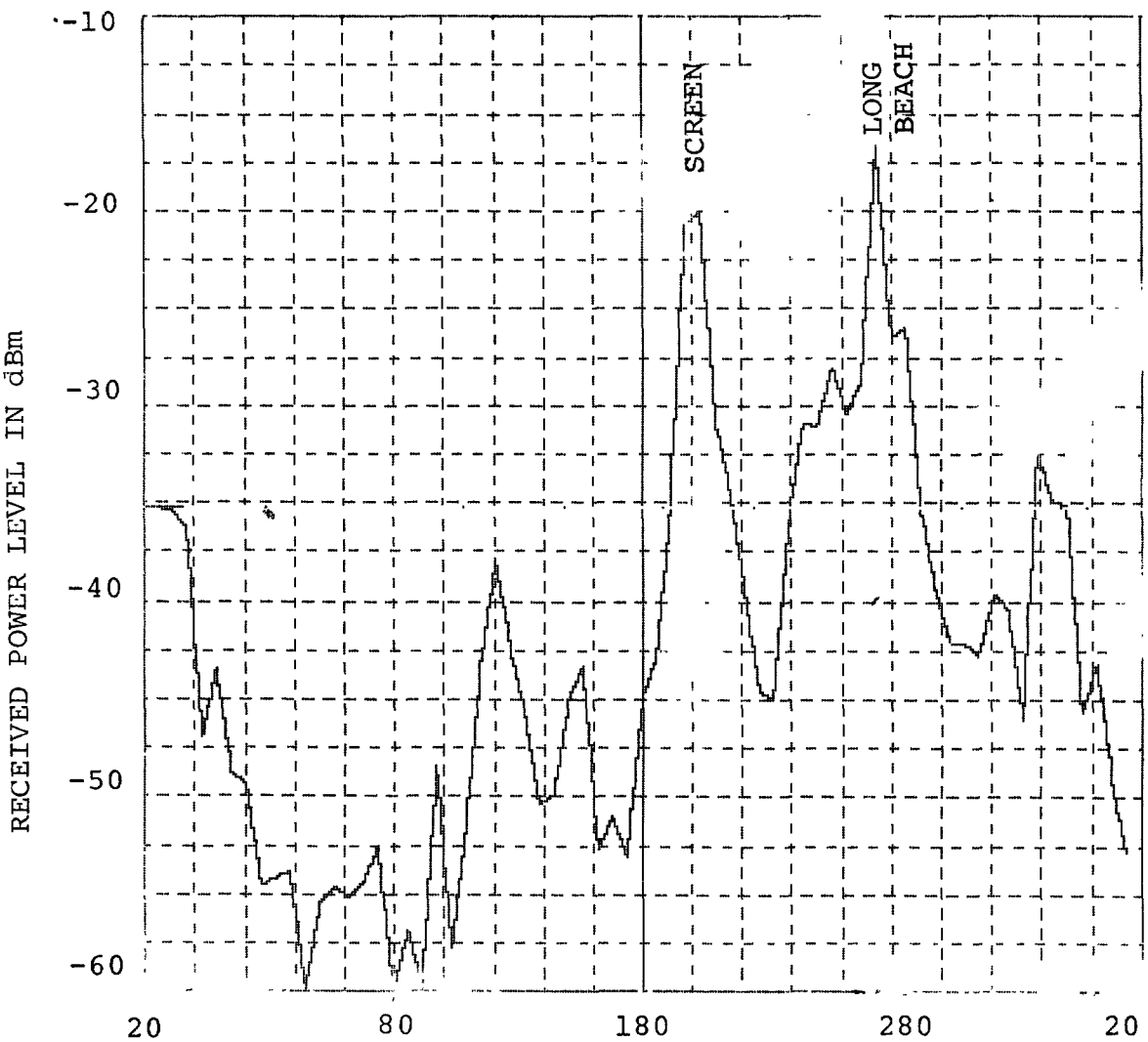

Figure D-4 RSMS Van Parabolic Antenna Pattern at Los Alamitos Using Long Beach as Signal Source.

Long Beach to Burbank Propagation Measurements. The RSMS van dish antenna was used as the receiving antenna on both ends of the Long Beach to Burbank path to measure propagation loss, because only the dish antenna provided sufficient measurement sensitivity. The loss measured on the Long Beach end of the path was 191 dB and on the Burbank end 185 dB. However, the point-to-point propagation model predicted that the loss should be 2 dB less on the Long Beach end of the path because the Burbank radar is 36 feet (62-26) higher than the Long Beach radar antenna. This total 8 dB difference between expected and measured propagation loss is attributed to the fact that the van dish was at a lower height than the radar antenna. This increased the measured loss more on the Long Beach end of the path because the Long Beach radar site is surrounded by close-in buildings and trees, while the Burbank site is located in an open area. The van dish height was well below the tops of trees and buildings at the Long Beach radar site.

San Pedro to Los Alamitos and Long Beach Propagation Measurements. The propagation loss from San Pedro to other radars was difficult to measure because of the nonperiodic scan of the AN/FPS-90 height finding radar antenna. However, the power level from San Pedro was measured at Long Beach and Los Alamitos over a continuous ten-hour period. A one-hour sample of each site measurement is shown in Figure D-5 and D-6. The sawtooth pattern is caused by the irregular azimuthal rotation of the AN/FPS-90 height finding radar antenna. The measured equivalent propagation loss for these paths, that appears in Table D-2, was computed using the height finder's mainbeam antenna gain of 39 dB and the maximum power received during the 10 hour propagation loss measurement period.

Propagation Measurements Over Nonducting Paths in San Francisco Area

The results of the propagation loss measurements over 6 nonducting paths in the San Francisco area are shown in the next to last column of Table D-3. All paths were identified as line-of-sight by the point-to-point propagation model except from Mather-to-Travis which was identified as a forward scatter path.

Propagation measurement data from the Mt. Tamalpais and Almaden AN/FPS-90 height finding radars were obtained by coordinating with the ADC personnel to have the radar's antenna nod in the direction of the measurement van for a one-half hour period. This insured mainbeam coupling of the height finding radars with the measurement van antenna. The propagation loss measurements from the Sacramento WSR-57 to the Travis AN/FPN-55 radar were conducted with the WSR-57 radar antenna

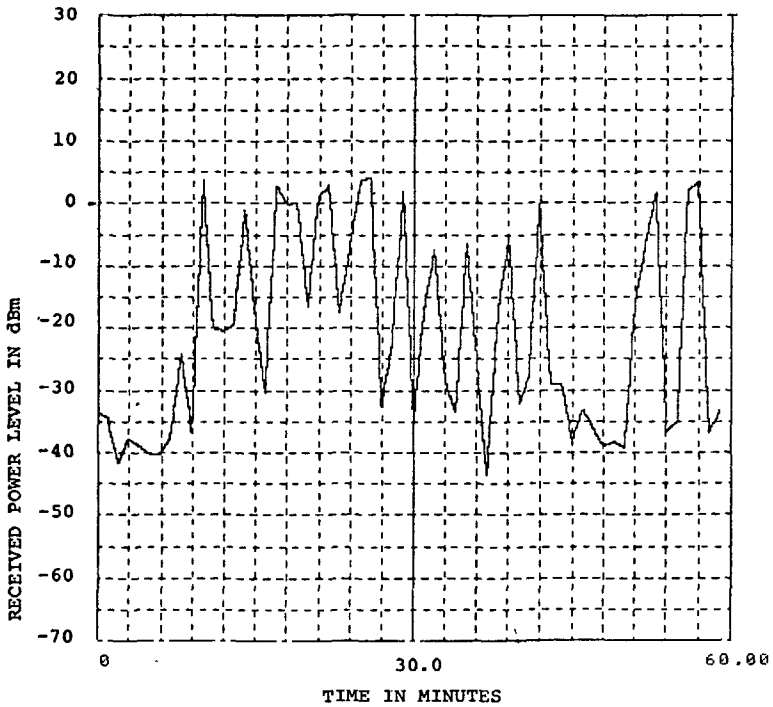

Figure D-5. Measured Power Level at Long Beach from San Pedro AN/FPS-90 using RSMS Parabolic Dish as Receiving Antenna

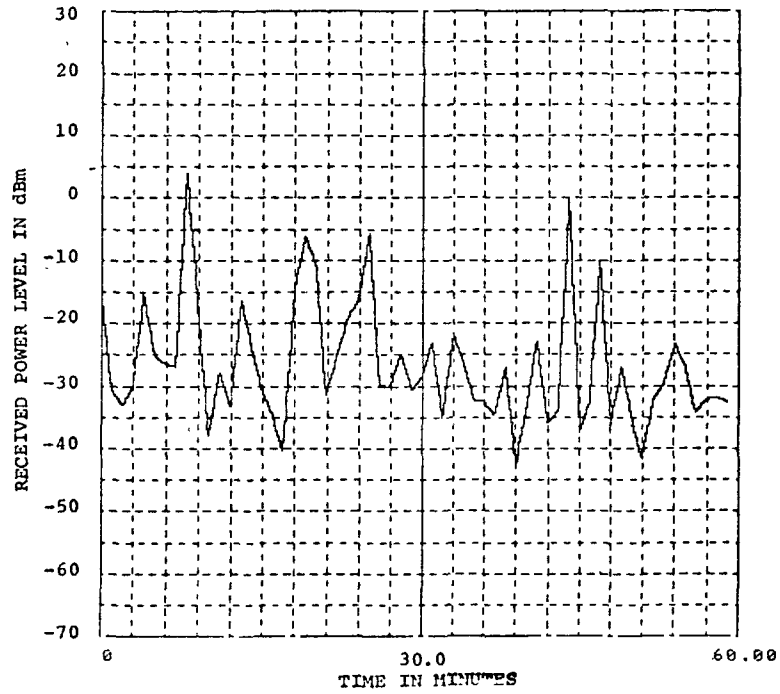

Figure D-6. Measured Power Level at Los Alamitos from San Pedro AN/FPS-90 using RSMS Parabolic Dish as Receiving Antenna

TABLE D-3

COMPARISON OF PREDICTED AND MEASURED PROPAGATION LOSS BETWEEN SAN FRANCISCO RADARS

FROM	TO	DIST. (kM)	CORRECTED POINT-TO-POINT LOSS 50/50 (dB)		AREA LOSS RANDOM SITING 50/50 (dB)		AREA LOSS FAIR SITING 50/50 (dB)		MEAS. EQUIV. LOSS-LM (dB)	CHARACTERISTICS OF PATH
			PREDICTED (LP)	LP-LM	PREDICTED (LP)	LP-LM	PREDICTED (LP)	LP-LM		
ALMADEN AN/FPS-90	MOUNTAIN VIEW ASR-5	31.2	143	2	205	64	196	55	141	LINE-OF-SIGHT
MT. TAMALPAIS AN/FPS-90	MOUNTAIN VIEW ASR-5	75.3	151	-9	197	37	193	33	160	LINE-OF-SIGHT
OAKLAND ASR-7	ALAMEDA AN/MPN-11	12.6	136	-12	135	-13	135	-13	148	LINE-OF-SIGHT (EXCEPT SHIPS)
MT. TAMALPAIS AN/FPS-90	ALAMEDA AN/MPN-11	28.1	142	3	195	56	183	44	139	LINE-OF-SIGHT
MATHER AN/MPN-13	TRAVIS AN/FPN-47	63.9	179	6	190	17	184	11	173	FORWARD SCATTER
SACRAMENTAL WSR-57	TRAVIS AN/FPN-47	51.4	148	-8	162	6	161	5	156	LINE-OF-SIGHT

rotating in azimuth at 1.0 degree elevation. The gain reduction due to the 1^{o} elevation tilt of the WSR-57's pencil beam antenna was accounted for in determining the measured propagation loss.

The propagation loss from the Mt. Tamalpais AN/FPS-90 to the Mountain View ASR-5 and Alameda AN/MPN-11 radars were both measured over a half-hour period. The signal level varied 10 dB more than the normal short term fading observed on nonducting paths. The 14 dB signal level variation over these two paths may have been due in part to ducting. A large percentage of each path transverses the San Francisco Bay, but the average altitude of the path was 1500 feet higher than paths in which 35 dB signal level variations due to ducting occurred. Since insufficient data was taken to positively identify the occurrence of ducting from Mt. Tamalpais, the measured and predicted losses for these two paths are recorded in the nonducting path (Table D-3).

Propagation Measurements Over Los Angeles and San Francisco Ducting Paths

A high degree of ducting occurred over the Miramar to Los Alamitos path in the Los Angeles area, and over the Oakland to Mt. View, and Alameda to Mountain View, paths in the San Francisco Bay area. The statistics of the signal level variation for each path is indicated in Table D-4 along with the point-to-point model propagation loss predictions. The accumulative probability distribution of the measured propagation loss versus time for the three paths are shown in Figures D-7, D-8, and D-9. These curves and the statistics shown in Table D-4 were derived from data measured over a 7-hour period of time and do not necessarily represent typical signal variations for every day of the year. Variations in signal level not only occur as a result of meteorological changes through the day, but from season-to-season.

Many researchers have investigated the ducting phenomenon in the California area. Bean (Reference 54) noted that during the summer months at San Diego and Oakland that an elevated duct is observed about 50 percent of the time. Rosenthal (Reference 60, 61) and Crain (Reference 62) states that much of the coastal area of California is usually in a moist marine layer capped by a dry inversion layer. The inversion layer produces ducting conditions throughout the year and is most frequent in the summer months. Meterological parameters were measured by NELC (Reference 43) over a 5-year period, for all seasons and times of the day, in the off-shore San Diego area. These studies indicated that radar range enhancement occurs 30% of the time. Bean and Cahoon (Reference 55) report rapid horizontal changes in refractive index associated with land-sea

TABLE D-4 COMPARISON OF PREDICTED AND MEASURED PROPAGATION LOSS FOR PATHS IN WHICH DUCTING OCCURRED

FROM	TO	DIST (KM)	POINT-TO-POINT PREDICTED LOSS (dB)	MEASURED LOSS (dB)			
				MEDIAN	MINIMUM	MAXIMUM	STANDARD DEVIATION
MIRAMAR ASR-5	LOS ALAMITOS AN/CPN-4	132.0	202	183	163	196	9.0
OAKLAND ASR-7	MOUNTAIN VIEW ASR-5	36.1	180	151	142	175	8.0
ALAMEDA AN/MPN-11	MOUNTAIN VIEW ASR-5	7.6	185	185	160	203	11.0

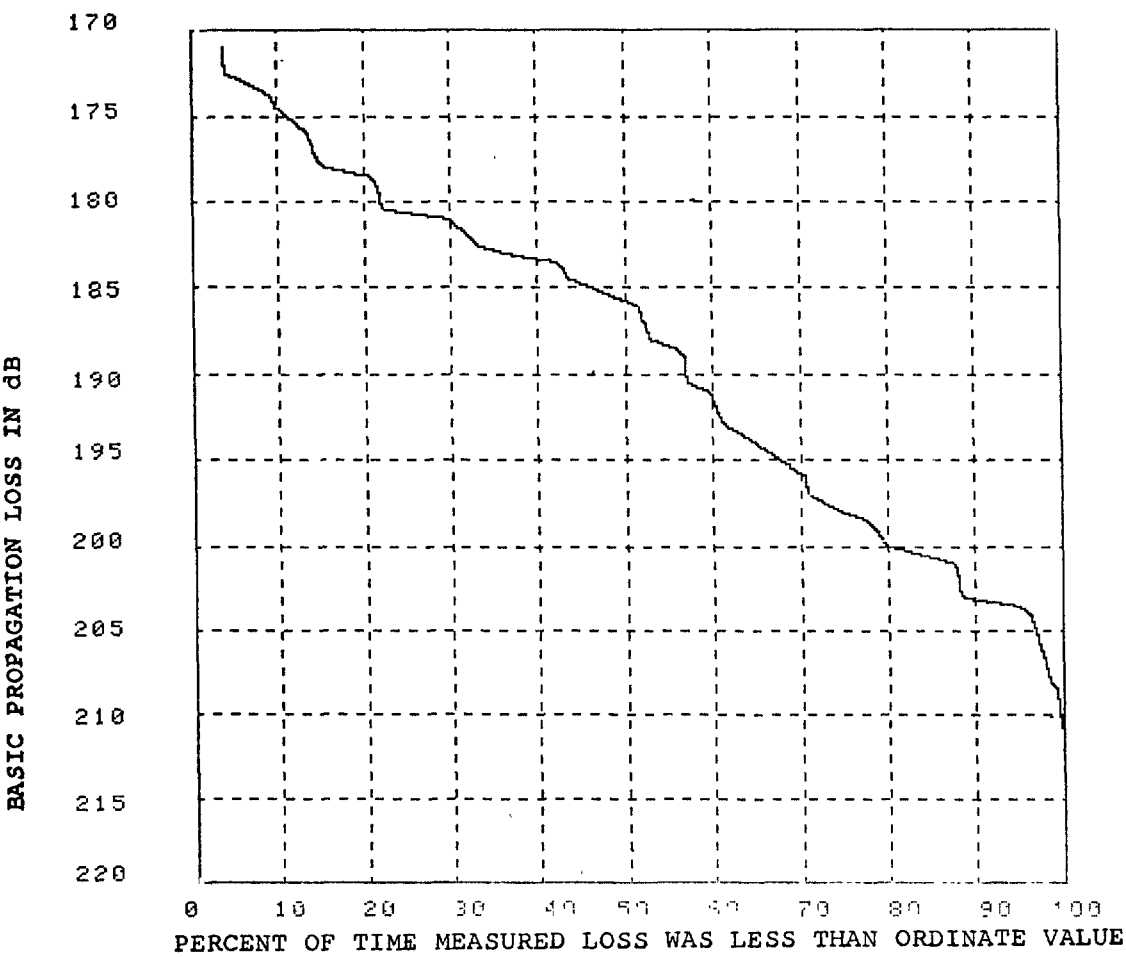

Figure D-7. Cumulative Probability Distribution of Measured Propagation Loss from Miramar ASR-5 to Los Alamitos AN/CPN-4.

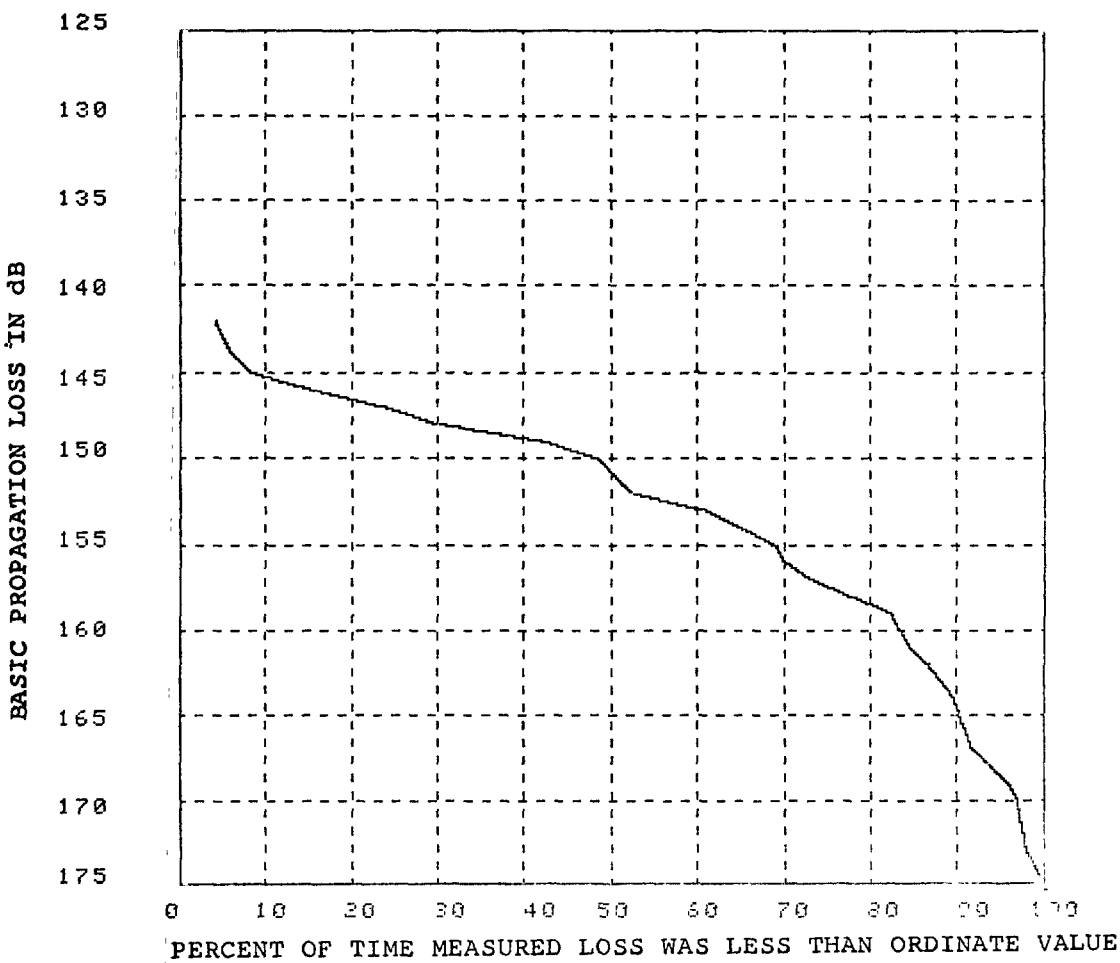

Figure D-8. Cumulative Probability Distribution of Measured Propagation Loss from Oakland ASR-7 to Mountain View ASR-5.

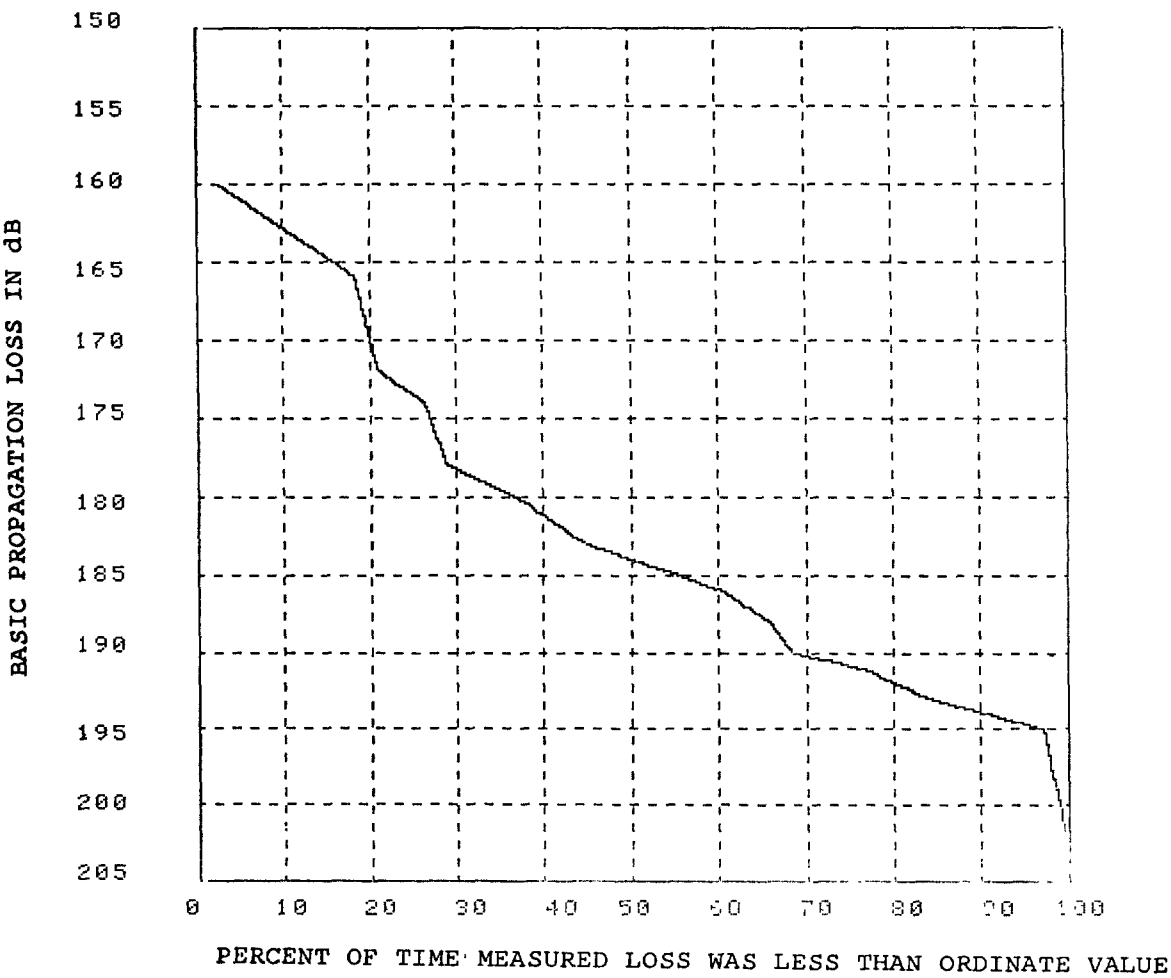

Figure D-9. Cumulative Probability Distribution of Measured Propagation Loss from Alameda AN/MPN-11 to Mountain View ASR-5

breezes, storms, and frontal passages.

Two thirds of the path from the Miramar ASR-5 to Los Alamitos AN/CPN-4 radar transverses the coastal region of the Pacific Ocean. The van dish was used to measure propagation loss over this path because it was the only RSMS antenna that could provide the required system sensitivity. The propagation loss was measured from 1015 to 1415 hundred hours on January 21, 1975, and from 1900 to 2100 on January 23, 1975. Two one-hour segments of the 6-hour period of measurements is shown in Figures D-10 and D-11. The data in Figure D-10 was measured at 1116 hours and the data in Figure D-11 at 1954 hours. The ducting appeared to be more extreme in the morning hours than in the evening. Other researchers have noted large diurnal variations due to land-sea breeze circulation. In the Los Angeles area, Neiburger (Reference 56) noted that the inversion layer undergoes significant changes in elevation, with a maximum about 0800 hours and a minimum in the evening. Edlinger (Reference 57) also reported rapid changes in the marine layer with time of day.

The two ducting paths in the San Francisco area transverse the San Francisco Bay, perpendicular to the San Mateo Bridge, Dumbarten Bridge, and numerous power lines. The RSMS van omni antenna was used to measure propagation loss because it approximates the radars cosencant-squared elevation antenna pattern closer than the dish. The loss between Oakland and Mountain View was measured from 2300 hours on November 13 to 0600 hours on November 14, and between Alameda and Mountain View intermittently on November 13 and 14. A one-hour segment of each path's measurements, in which the most extreme ducting occurred, is shown in Figures D-12 and D-13. Since all three radars have an elevation above mean sea level of less than 36 feet, the propagation paths are close to the surface of the bay and results in low grazing angles. The grazing angle of the path has a significant effect on the intensity of ducting and radio holes. The degree that radio rays are bent by atmospheric layers depend not only on the change in refractive index but also on the angle between the rays and the horizontal stratified refractive index. Significant ducting and radio holes generally occur only with elevation or grazing angles less than 3 degrees. Reber (Reference 58) observed that ray bending is reduced by about half when the elevation angle is increased from 0 to 1.4 degrees. Rogers (Reference 59) noted on a slant path that attenuation of the signal is much less frequent as the elevation angle is increased.

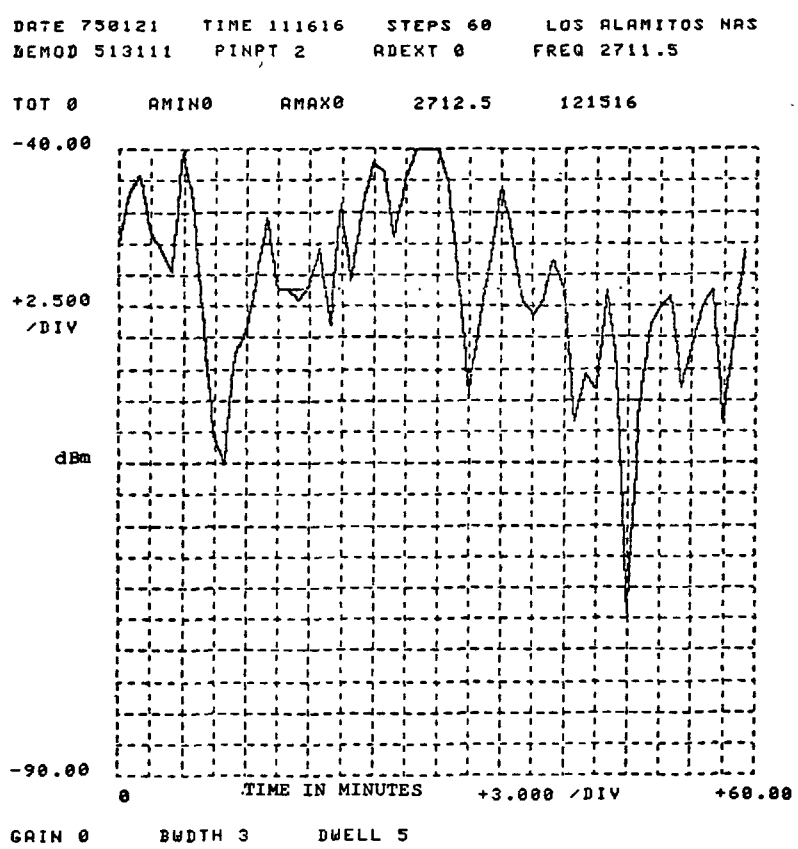

Figure D-10 Received Power Level from Miramar ASR-5 to Los Alamitos AN/CPN-4 during Morning Ducting Conditions

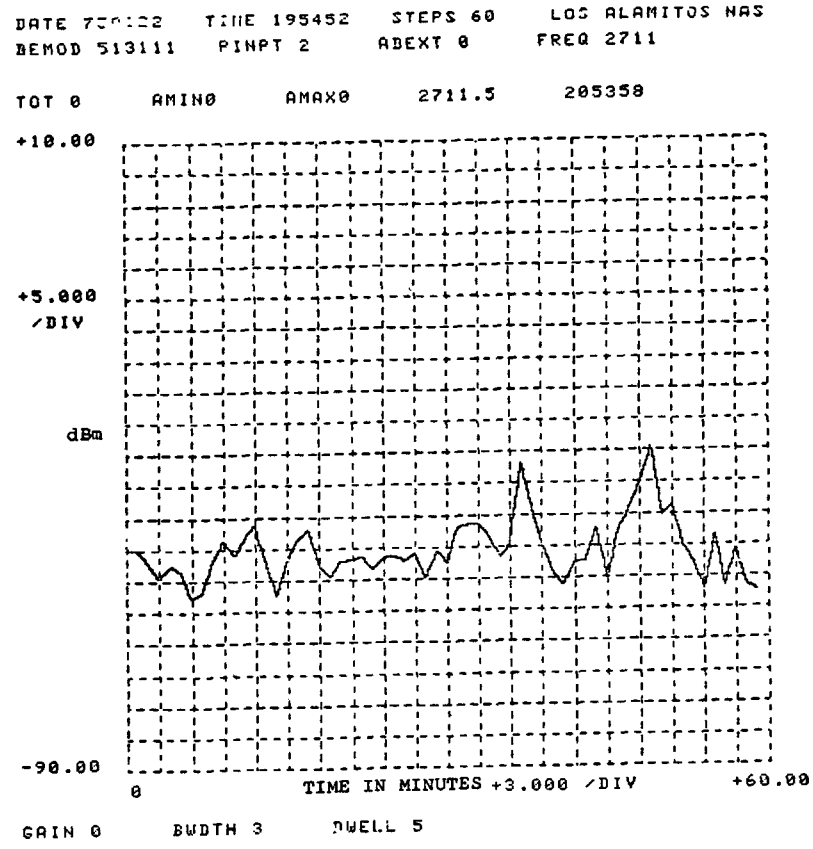

Figure D-11 Received Power Level from Miramar ASR-5 to Los Alamitos AN/CPN-4 during Evening Ducting Conditions

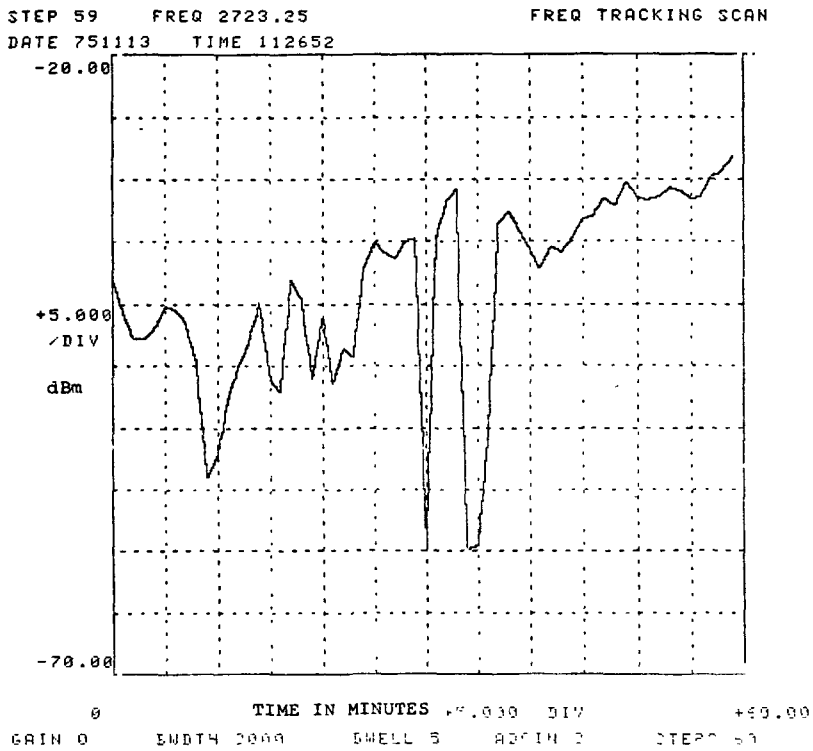

Figure D-12 Received Power Level from Oakland ASR-7 to Mountain View ASR-5 during Ducting Conditions

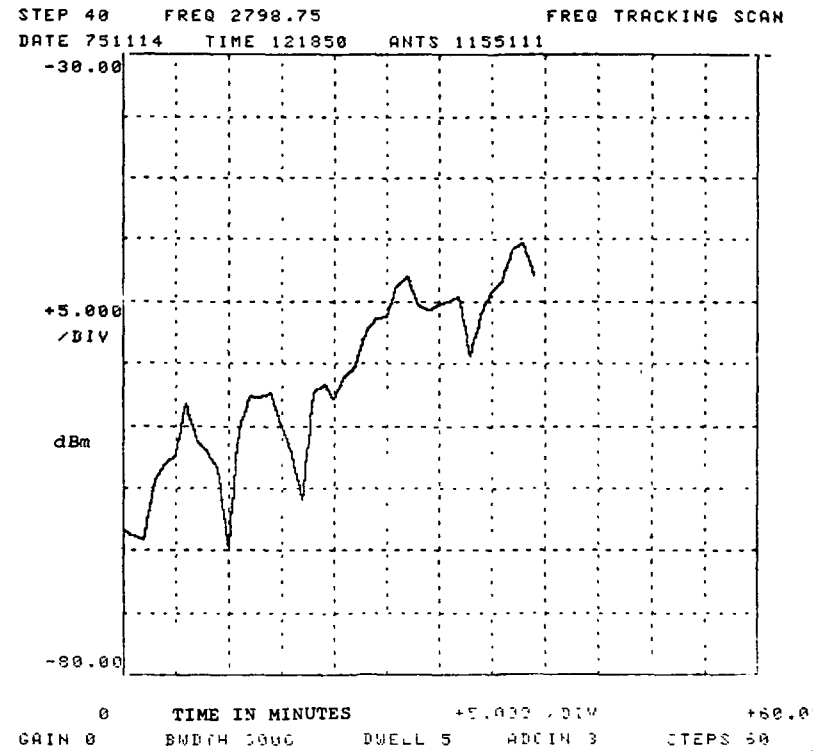

Figure D-13 Received Power Level from Alameda AN/MPN-11 to Mountain View ASR-5 during Ducting Conditions

COMPARISON OF PREDICTED AND MEASURED PROPAGATION LOSS

One of the objectives of the Los Angeles and San Francisco area investigation was to determine the error contribution by the various models used to predict interference. To accomplish this, point-to-point and area type propagation model predictions were compared statistically with measured propagation losses. The difference between predicted and measured propagation loss over ducting paths were not included in this statistical analysis.

Los Angeles Nonducting Paths

The differences, LP-LM, between predicted and measured propagation loss for each Los Angeles area nonducting path are shown in Table D-2. The propagation loss predicted for the measurement receiving antenna height, instead of the receiving site radar antenna height, were used to compute LP-LM. The LP-LM values in Table D-2 were used to compute the statistical comparison results indicated in Table D-5. The mean of the differences between each model prediction and the measured loss are presented. A minus sign indicates that the propagation model's predictions were less than the measured losses.

The standard deviation of the difference between predicted and measured about the mean difference is an indication of how repeatable the absolute difference between the predicted and measured losses were from path-to-path. The absolute mean and standard deviation of the predicted about the measured loss are indicators of the over-all disagreement between predicted and measured losses regardless of sign. The mean of the differences were less for the area than the point-to-point prediction model; however, the standard deviation of the difference about its mean, range, absolute mean, and standard deviation between predicted measured loss were lower for the point-to-point model.

San Francisco Nonducting Paths

The results of statistical comparisons between predicted and measured propagation loss in the Los Angeles area and information gained in a subsequent literature search were used to make more accurate propagation loss predictions in the San Francisco area. Since measured propagation loss over Los Angeles paths were typically greater than predicted, additional loss was added to the point-to-point model propagation loss predictions to take into account attenuation due to man-made structures and foliage. This involved using a 24000:1

TABLE D-5

COMPARISON OF PREDICTED AND MEASURED PROPAGATION LOSS OVER 14 LOS ANGELES AREA PATHS.

STATISTICAL COMPARISON CRITERIA / PROPAGATION MODEL	POINT-TO-POINT PREDICTION 50/50	AREA PREDICTION, RANDOM ANTENNA SITING 50/50	AREA PREDICTION FAIR ANTENNA SITING 50/50
MEAN $\bar{X} = \frac{\Sigma(LP-LM)}{N}$ (dB)	-10	-3	-9
STANDARD DEV. ABOUT MEAN, $\sigma_{\bar{x}} = \left[\frac{\Sigma(LP-LM-\bar{X})^2}{N-1}\right]^{1/2}$ (dB)	11	15	16
EXTREMES OF DIFFERENCES BETWEEN PREDICTED AND MEASURED (dB)	-27 to 7	-23 to 25	- 34 to 21
ABSOLUTE MEAN $= \frac{\Sigma\|LP-LM\|}{N}$ (dB)	12	13	15
STANDARD DEV. BETWEEN PRED. AND MEASURED $= \left[\frac{\Sigma(LP-LM)^2}{N-1}\right]^{1/2}$ (dB)	15	16	17

LP = PREDICTED PROPAGATION LOSS

LM = MEASURED PROPAGATION LOSS

N = TOTAL NUMBER OF PROPAGATION PATHS

U.S. Geological Survey Map to identify the degree of building congestion that propagation paths passed through, and matching it to the environmental description indicated in Table D-7. Table D-7 lists the measured propagation loss below free space, reported by Turin (Reference 35), for various degrees of building congestion in the San Francisco area. For paths other than line-of-sight, the median propagation loss below free space in Table D-7, that corresponded to the selected environmental description, were added to the point-to-point propagation loss prediction. For line-of-sight paths, the loss selected from Table D-7 was simply added to free space loss to predict propagation loss. There are two reasons why it is believed adding attenuation to free space instead of model predicted loss for line-of-sight paths gives more accurate results:

(1) The paths used to compute the medium propagation losses in Table D-7 would have been line-of-sight if buildings were not present.

(2) The loss below free space predicted by the propagation point-to-point model for line-of-sight paths were in part derived empirically from measurements in unpopulated areas.

The corrected point-to-point model and uncorrected area model propagation loss predictions are indicated for San Francisco nonducting paths in Table D-3. The differences, LP-LM, between predicted and measured propagation loss indicated in Table D-3 were used to compute the statistical results shown in Table D-6. The mean and standard deviation of the difference is 19 dB less for the corrected point-to-point model than the area propagation model prediction. The main reason for this difference is not because a 12 dB building and attenuation factor was not added to the area model prediction , but partly because 5 of the 6 San Francisco paths were line-of-sight. The area model with random and fair antenna siting specified predicts too high of a loss for line-of-sight paths.

Comparison of Predictions Accuracies for Los Angeles and San Francisco Paths

The results of comparing the point-to-point model propagation loss predictions with measurements for the Los Angeles and San Francisco area paths are illustrated by the histograms in Figure D-14 and D-15 respectively. The mean of the difference between predicted and measured loss is only -3 dB for the San Francisco point-to-point model predictions which included added attenuation for man-made clutter. This is a 7 dB

TABLE D-6

COMPARISON OF PREDICTED AND MEASURED PROPAGATION LOSS OVER 7 SAN FRANCISCO AREA PATHS.

STATISTICAL COMPARISON CRITERIA \ PROPAGATION MODEL	CORRECTED POINT-TO-POINT PREDICTION 50/50	AREA PREDICTION, RANDOM ANTENNA SITING 50/50	AREA PREDICTION FAIR ANTENNA SITING 50/50
MEAN $\bar{X} = \frac{\Sigma(LP-LM)}{N}$ (dB)	-3	28	23
STANDARD DEV. ABOUT MEAN, $\sigma_{\bar{x}} = \left[\frac{\Sigma(LP-LM-\bar{X})^2}{N-1}\right]^{1/2}$ (dB)	7	30	26
EXTREMES OF DIFFERENCES BETWEEN PREDICTED AND MEASURED (dB)	-12 to 6	-13 to 64	-13 to 55
ABSOLUTE MEAN $= \frac{\Sigma\lvert LP-LM\rvert}{N}$ (dB)	7	32	27
STANDARD DEV. BETWEEN PRED. AND MEASURED $= \left[\frac{\Sigma(LP-LM)^2}{N-1}\right]^{1/2}$ (dB)	8	43	36

LP = PREDICTED PROPAGATION LOSS

LM = MEASURED PROPAGATION LOSS

N = TOTAL NUMBER OF PROPAGATION PATHS

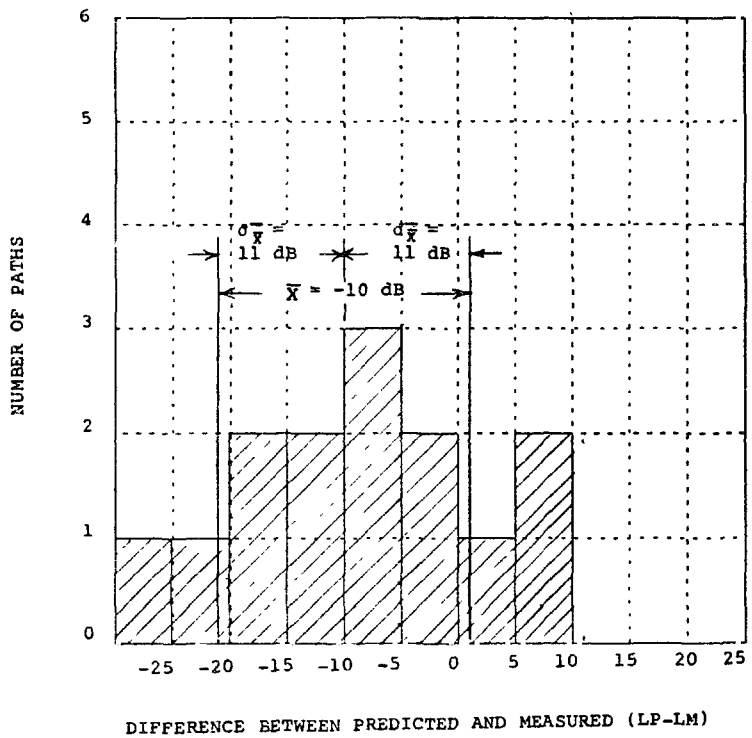

Figure D-14. Histogram of Differences Between Predicted and Measured Propagation Loss for Los Angeles Paths

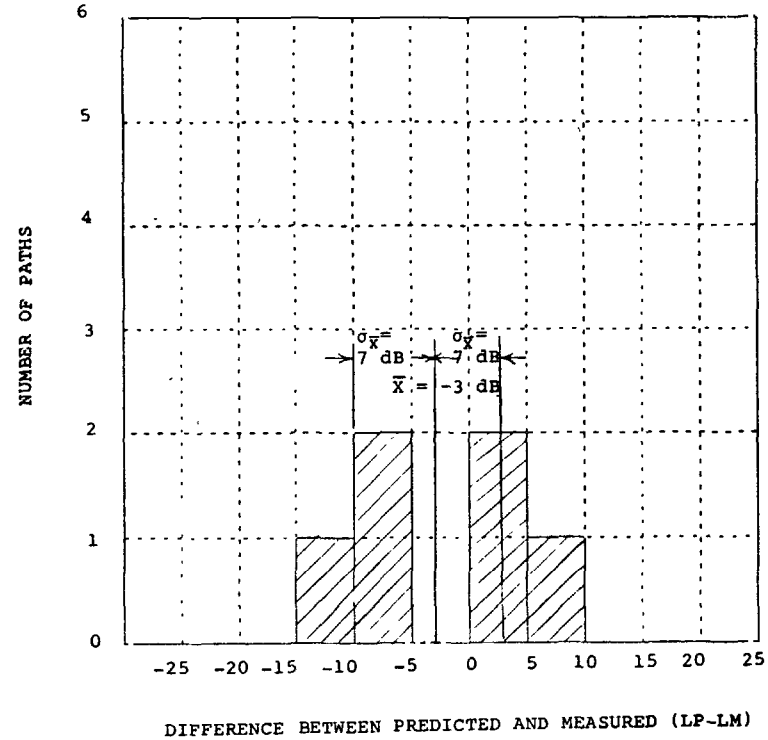

Figure D-15. Histogram of Differences Between Predicted and Measured Propagation Loss for San Francisco Paths

better than the -10 dB mean computed for Los Angeles paths point-to-point prediction that did not include additional attenuation for man-made clutter. The standard deviation of the difference about the mean is also 4 dB less for San Francisco predictions.

Eighty-three percent of the San Francisco paths used in this analysis were line-of-sight; however, only 41.6% of the Los Angeles paths analyzed were line-of-sight. This fact is not attributed to the improvement in prediction accuracy for San Francisco paths, because the greatest differences between predicted and measured loss for the Los Angeles paths analyzed were line-of-sight. There is reason to believe that adding attenuation to the point-to-point model loss to account for foliage and man-made obstacles will also result in more accurate predictions for diffraction and forward scatter paths, if the geometry and location of the propagation ray through the man-made clutter is considered.

Comparison of Predicted and Measured Propagation for Ducting Paths

The results of the comparison between predicted and measured propagation loss for Los Angeles and San Francisco areas ducting paths are shown in Table D-4. The point-to-point model propagation loss prediction does not take into account ducting. Measured propagation loss from Miramar to Los Alamitos and from Oakland to Mountain View is less than predicted. However, the point-to-point propagation loss prediction from Alameda to Mountain View equaled the median value of the measured propagation loss over this forward scatter path. It is not uncommon to encounter radio holes or strong fading and signal enhancement during superrefraction conditions. Bean (Reference 52) reported observing prolonged fadeouts, often reaching 20 dB and lasting from one minute to several hours, during periods of superrefraction. At the same time, propagation losses less than normal were observed. Barris and Capps (Reference 63) also noted that superrefractive layer on a path from San Nicolas Island to Luguna Peak tended to produce large fades. In a series of measurements at about 4 GHz, Ikegarmi (Reference 64) noted that, if the transmitter is located in a duct, strong signal levels and blind regions extend over receiver locations within and near the duct.

FACTORS CONTRIBUTING TO DIFFERENCES BETWEEN PREDICTED AND MEASURED PROPAGATION LOSS

Differences between propagation loss predictions and

measurements occurred in many cases because the propagation model and terrain data base did not account for all environmental factors that affect propagation loss. The following is a discussion of suspected factors that caused the differences between predicted and measured propagation losses and methods to account for these factors in propagation loss predictions.

Man-made Clutter

Two Los Angeles area paths over which propagation loss measurements were conducted, and man-made obstacles were suspected to have caused a definite increase in propagation loss, included the Los Alamitos AN/CPN-4 to Long Beach ASR-5 path and the Los Angeles ASR-4 to Los Angeles ASR-7 path. The uncorrected point-to-point model propagation loss (130 dB) from Los Alamitos to Long Beach was 27 dB less than measured (157 dB) as shown in Table D-2. This path included two multistory buildings, a large number of 1-story houses, supermarkets, gas stations, and trees. The location of the two multistory buildings are shown superimposed in the terrain profiles in Figure D-16.

The Los Angeles ASR-4 to ASR-7 path includes the edge of one 3-story building (PANAM terminal) and the center of one four-story building. Because of the relative absence of foliage and the fact that this is a short (2.4 KM) line-of-sight path, the majority of the 5 dB difference between the point-to-point predicted value (119 dB) and the measured value (124 dB) is attributed to the building factor.

Attenuation was added to the point-to-point model loss predictions for San Francisco paths to account for increased attenuation due to man-made obstacles. The amount of attenuation added was based on the degree of man-made obstacle congestion anticipated for each path. However, 12 dB greater attenuation occurred over the Oakland ASR-7 to Alameda AN/MPN-11 path than anticipated. It is believed that the additional attenuation was caused by 3 aircraft carriers which were docked at the Alameda Naval Air Station, and blocked the otherwise line-of-sight path.

Since the most accurate propagation loss predictions are made by models that use the topographical data file, one might be tempted to include man-made obstacles in the topographical file. There are three reasons why this may not be practical either on a case-by-case basis or in general.

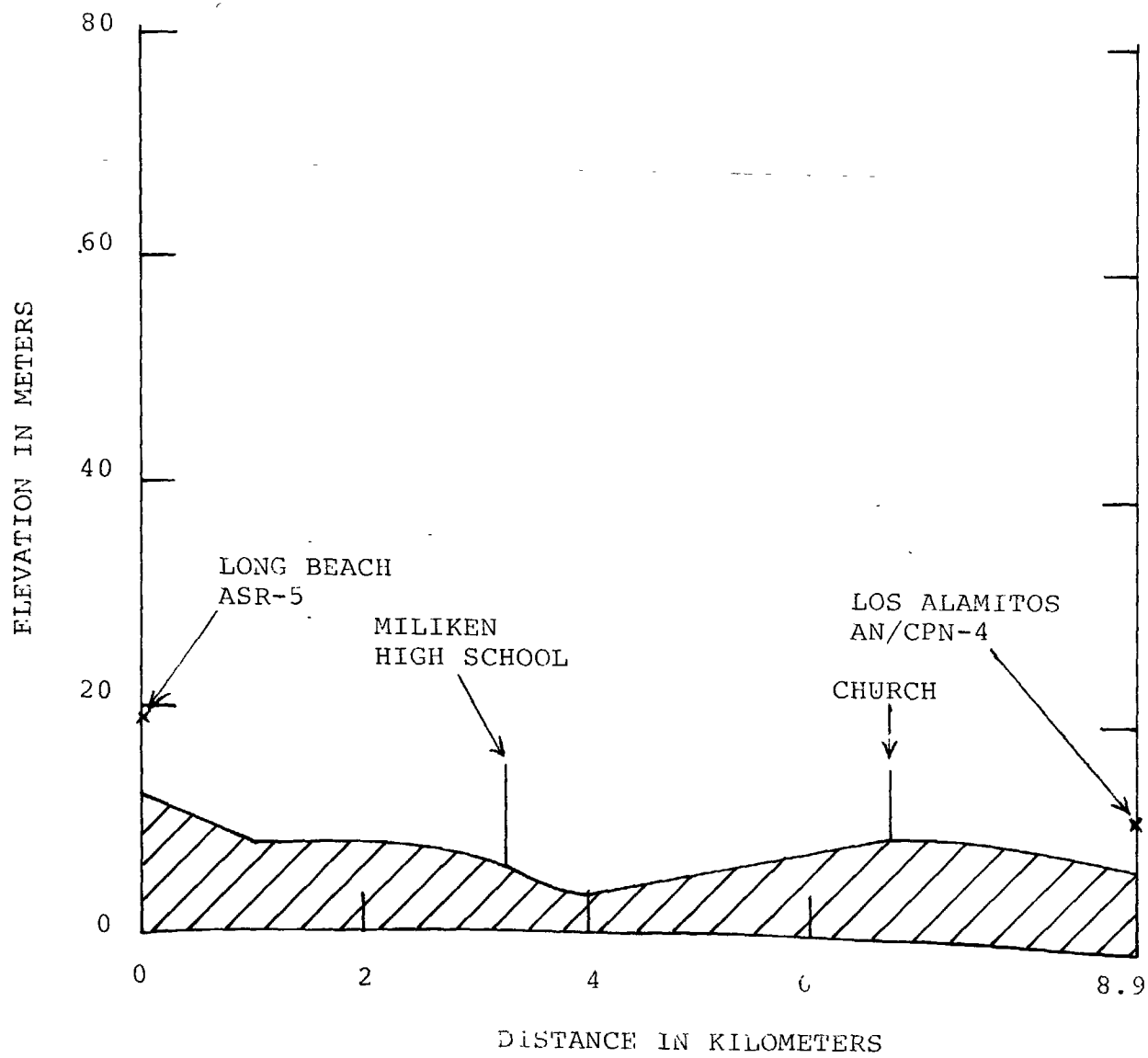

Figure D-16. Terrain Profile and Multistory Buildings Between Long Beach and Los Alamitos

(1) The propagation model interprets obstacles in the topographical file as being completely absorbing. All buildings do not have infinite attenuation and are not completely absorbing.

(2) The task of determining the building profile through urban and suburban areas would be very time consuming and would require constant updating.

(3) The propagation loss through urban and suburban areas is caused not only by attenuation through the buildings but by the many multipaths caused by signal reflection and diffraction from the buildings. The current propagation prediction models that use the topographical file only consider terrain profile in the vertical plane between two points and consequently would not consider multipath effects due to building reflections and diffractions.

It is believed that the most practical approach is to employ empirical results in selecting a man-made obstacle attenuation factor for addition to the propagation model loss prediction. The result of the propagation loss measured by other investigators for various degrees of built-up area will be summarized. The results are statistical at best; however, there is some consistency among investigators in characterizing the propagation loss in these complex environments. Propagation loss test results reported by some investigators are not applicable because they included both terrain irregularities and man-made environmental clutter into the measurements. Because the point-to-point model takes into account terrain irregularities, only the results of those measurements that were performed on flat terrain or over line-of-sight paths will be presented.

Okumura (Reference 33) has reported results of extensive propagation tests in land mobile service bands including 1920 MHz. The tests were conducted in and around Tokyo and included various situations of environmental clutter. The man-made clutter environments were classified into the following three groups according to the degree of congestion:

(a) Open Area - open space where there are no obstacles in the propagation path.

(b) Suburban Area - village or highway scattered with trees and houses but not very congested.

(c) Urban Area - built-up city or large town crowded with large buildings and two-or-more storied houses, or in a larger village closely interspersed with houses and thickly grown trees.

The correction factor curves presented by Okumura indicate that a suburban and urban area have 19 dB and 33 dB, respectively, greater loss than an open area at 2800 MHz. For locations midway between suburban and open areas, 5 dB greater loss than the open area results. The propagation loss differences between the area classifications defined above were found to be independent of base station antenna height and distance between the transmitter and receiver. Okumura found the location variability (standard deviation) of loss was 12 dB for suburban areas and 11 dB for urban areas 2800 MHz. The variability of loss is greater for suburban areas because the man-made clutter is less homogeneous in a suburban than an urban area.

Propagation loss measurement for various degrees of building congestion in the San Francisco area were reported by Turin (Reference 35). The environmental description, geometry of the test set-up, and measured median loss below free space with standard deviation, are indicated in Table D-7. These measurements were made to support development of a statistical urban propagation model for evaluating mobile radio location performance. The paths described would have been line-of-sight if man-made obstacles were not present. Therefore, the propagation losses below free space, shown in Table D-7, can be attributed mostly to the building factor. The measurement results shown in the table were made at 1280 MHz but are reported to be very close to values obtained at 2920 MHz.

The geometry of base station antenna height (30-1000 meters) and the mobile antenna height (0-10 meters) used in Okumura's and Turin's measurements are similar to the height relationship between a height finding radar, usually located on a hill, and a GCA or ASR radar, usually located in a valley. It is also similar to the geometry of one end of a knife edge diffraction or forward scatter path.

The relation to the vertical angle of arrival (that is, the elevation angle that the base station antenna forms with the mobile station) does not appear to be critical to attenuation for angles less than 1 degree, which correspond to the geometry of most radar-to-radar paths. However, measurement in Italy (Reference 71) and Tokyo by Okumura, indicate as much as 25 dB change can result for elevation changes from 1 to 4 degrees. The height gain varies considerably from open to suburban and urban areas, depending on the agerage height of surrounding houses and buildings. Since an antenna height gain factor is taken into account by the point-to-point model for terrain in the absence of man-made clutter, the question arises as to what antenna

TABLE D-7

PROPAGATION LOSS BELOW FREE SPACE DUE TO VARIOUS URBAN ENVIRONMENTS

ENVIRONMENTAL DESCRIPTION	LOSS BELOW FREE SPACE (dB)
WORST CASE - MODERN METROPOLIS Transmitter on 120 foot high roof, reception area 1 mile away and consisting of densely packed skyscrapers (up to about 50 stories high).	μ = 51 dB σ = 8 dB
DOWNTOWN DISTRIBUTION OF MEDIUM SIZED CITY Transmitter on roof of building located on 1300 foot hill, reception area 5.5 miles away and consisting of clustered sky scrapers up to 40 stories, interspersed with 2-3 story metal frame buildings	μ = 18 dB σ = 8 dB
DOWNTOWN AREA OF SMALL-TO-MEDIAN SIZED TOWN Transmitter located on roof of building located on roof of building located on 1300 foot hill, reception area 1.5 miles away and consisting of a few 10-20 story buildings, many 2-5 story metal frame buildings, and some small 1-2 story wood frame buildings	μ = 12 dB σ = 7 dB
ENVIRONMENTAL DESCRIPTION PRIVATE-RESIDENCE SUBURBS OF MOST TOWNS AND CITIES Transmitter on roof of building located on 1300 foot hill, reception area 1-1.5 miles away consisting of 1-2 story wood-frame housed, trees, supermarkets, etc.	μ = 12 dB σ = 5 dB

NOTE: (1) The receiver for above measurement was located at street level
(2) μ average of Log Normal distribution
(3) σ standard deviation of Log Normal distribution

height gain should be employed. Okumura presents measured based station and mobile antenna height gain curves for distances between transmitter and receiver ranging from 30 to 1000 meters. These measurements were conducted over smooth terrain. It is proposed that the difference between the height gain measured by Okumura and the point-to-point model height gain for the same type of path be used to represent the additional height gain due to man-made clutter. This difference would then be added to the point-to-point model height gain.

The results of measurements by Turin were employed in the San Francisco area propagation loss predictions with a fair amount of success. It resulted in a 7 dB improvement over the Los Angeles prediction. The average difference between predicted and measured loss for San Francisco was only -3 dB.

Foliage

The propagation loss measurements in man-made clutter environments, referenced in the preceding section, included sparse foliage. This section references attenuation measurements caused by dense homogenious foliage in the absence of man-made clutter, that results in blockage to otherwise line-of-sight paths. The measured propagation loss on the Long Beach end of the Los Alamitos to Long Beach path was affected by the grove of trees surrounding the Long Beach radar antenna. The trees and buildings surrounding Long Beach are suspected to have caused the 19 dB difference (Table D-2) between propagation loss measured with the RSMS cavity-back spiral and parobolic dish antenna, on the Long Beach end of the path. In summary, it was deduced that the trees and buildings caused an 11 dB (see Figure D-2) difference in antenna height gain between the dish height (14 feet) and highest height (25 feet) of the cavity antenna. However, the antenna height gain difference predicted by the point-to-point propagation model for these two antenna heights was insignificant. The remaining 8 dB difference was found by comparing the measured propagation loss of the cavity and dish antenna at the same height of 14 feet, which was well below tree-top level (Figure D-3). The 8 dB difference was attributed to the difference in weighting of the diffused signal energy through the trees by the different beamwidths associated with the cavity and dish antennas. The diffused signal energy, often called leakage field, as reported by Head (Reference 36), occurs when the receiving antenna is within 100 feet or less of the trees. Head reported that the receiving antenna did not exhibit any clear maximum and minimum response as the antenna was rotated. In many instances, it was not possible

to identify the direction toward the transmitter from the orientation of the receiving antenna. The measurement by Head was performed with horizontal polarization, the same linear polarization as Los Alamitos transmits, and at a frequency of 488 MHz. There is no reason to believe the direction of the signal energy under these conditions would be any less diffused at 2800 MHz.

Precise propagation loss prediction due to trees are difficult because of variations in tree type, heights, shape, and distribution. In addition, foliage density which changes with seasons of the year also affect attenuation. However, some success has been obtained by hypothesizing the trees as diffracting objects with an effective height. An experimental study of propagation behind a grove of live-Oak and Hackberry trees for several frequencies, including 2950 MHz, was reported by La Grone (Reference 37). Receiver antenna height-gain measurements were made at several distances behind the grove of trees for horizontal polarized waves. The results were compared with theoretical curves for propagation over a smooth spherical earth and diffractions over a single knife edge. At frequencies of 2950 MHz and distances between the receiving antenna and the trees, greater than five times the tree height, and antenna heights from 15 to 20 feet, the measurement agreed to within 4 dB of single knife edge diffraction theory. For receiver antenna heights from 20 to 60 feet, the measurements agree with theory to within 2 dB. The measured data matched the theoretical curve for single knife edge diffraction closer than smooth earth diffraction curves.

In another experimental study by La Grone (Reference 38), measurements at two locations were performed at 2000 MHz and vertical polarization for very low angles over wooded areas. The elevation angle of the transmitter from a fixed receiving antenna location was varied. The measurement location involved different degrees of shadowing because of the transmitting and receiving antenna geometry relative to the trees. At one site, the propagation path was almost parallel to the tree tops and at the other site, paths at angles greater than 20 degrees in respect to tree tops. For example, a path from the receiver to the transmitter, one degree below the line-of-sight, passed through approximately one thousand feet of oak and ceder trees while a similar path at the other site passed through only 87 feet of pine forest. The measured propagation loss as a function of elevation angle agreed to within 4 dB of a theoretical knife edge diffraction curve for the site in which the propagation path was not near parallel to tree-top level. However, the measured loss for the site with propagation paths, nearly parallel to tree-top

level, followed the smooth earth diffraction curve to within 6 dB and differed from the single knife edge diffraction curve by as much as 12 dB.

La Grone, in Reference 37, reported disagreement between signal attenuation measured and predicted by diffraction theory, for distances between the receiving antenna and forest edge of less than 5 times the tree height. Similar results have been reported by other researchers. Head (Reference 35) reported that attenuation due to the trees was substantially less than predicted by smooth sphere diffraction when the receiving antenna was very close (within 100 feet or less) to the obstructing mass of trees. Head measured field strengths at 483 MHz and horizontal polarization for cases in which the receiving antenna was within 10 feet of the nearest edge of the woods. The signal in this region is sometimes referred to as leakage fields. An examination of eight observations by Head in this field region, at receiving antenna distances ranging from 12.0 to 22.5 miles from the transmitter, indicated that the average signal level below the calculated smooth earth field to be more or less independent of distance. For these eight points, the average depression of the field below the smooth-earth field was approximately 30 dB with a standard deviation of 3.3 dB. Head presents a simple model in Reference 35 that hypothesizes a continuous relationship between the leakage and smooth earth diffraction fields, as a function of distance along a profile consisting of trees and clearings. Head also presents curves for both lowest and highest attenuation, corresponding to favorable and unfavorable sequence of woods and clearings, as a function of percent forest cover. It should be pointed out that Head's model was developed for television field strength predictions in which the transmitter was located 620 feet high. The measured leakage field under these conditions arrive at the receiving antenna principally through the tops of the woods and does not typify every radar-to-radar interference path involving foliage.

The measured data reported by Saxton and Lane (Reference 39) indicated a signal attenuation of about 0.4 dB/meter at 2800 MHz when both transmitting and receiving antenna are well below trees in full leaf.

Propagation loss due to foliage changes seasonally in most areas. Mobile communication signal measurements by Reudink and Wasowietz (Reference 40) were performed on the same streets in summer and winter in suburban Holmdel, New Jersey. The average signal strength in the summer, when the trees were in full leaf, was about 10 dB and 15 dB lower than the corresponding location in winter for frequencies of 836 MHz and 11.2 GHz respectively.

In summary, determining foliage propagation loss would require on-site observation of the geometry of the receiving antenna, relative to surrounding trees. The most suitable propagation foliage loss models; single knife edge diffraction, smooth earth diffraction, or signal loss as a function of tree depth, would then be chosen to predict the increase in propagation loss due to foliage. This value would then be added to the point-to-point model loss prediction.

Mountain Multipath

The RAPIT point-to-point propagation models consider only the terrain profile in the vertical plane defined by the great circle path between the transmitter and receiver. However, other propagation paths due to reflection and diffraction through mountainous or hilly terrain can sometimes result in the same or less loss.

The reason that the propagation loss for the Norton to Los Alamitos, March to Los Alamitos, and San Pedro to Burbank paths was less than predicted, is attributed to lower loss paths not considered by the propagation model.

The measured propagation loss (Table D-2) from Norton to Los Alamitos was 6 dB less than predicted by the point-to-point model. The measurement of the Norton antenna pattern at Los Alamitos using the AN/CPN-4 as the receiving antenna, (figure 28A in Appendix A) indicates a broadening of the radar antenna beamwidth. The broadened beamwidth indicates the presence of a number of multipaths in a 10 degree region around Norton's bearing, caused by diffraction and reflection in the Chino Hills located between the two radar sites.

The fact that March was erroneously predicted as not being an interferer to Los Alamitos (INR = -17.6 dB) is also attributed to the lower than predicted propagation loss and interferer antenna beam spreading, caused by miltipathing through the Chino Hills.

A large percentage of the interference traces observed on the Burbank ASR-6 PPI display, due to the San Pedro AN/FPS-90 radar, occurred in the 270 to 90 degree sector of the display. The fact that this sector corresponds to the San Gabriel Mountain on the far side of Burbank from San Pedro, and that San Pedro's bearing is 165^{o}, indicated a high probability that the interference was arriving by mountain reflections. The terrain profile for the point-to-point path is shown extended beyond the Burbank site in Figure D-17 to indicate the San Gabriel mountain on the far side of Burbank from San Pedro.

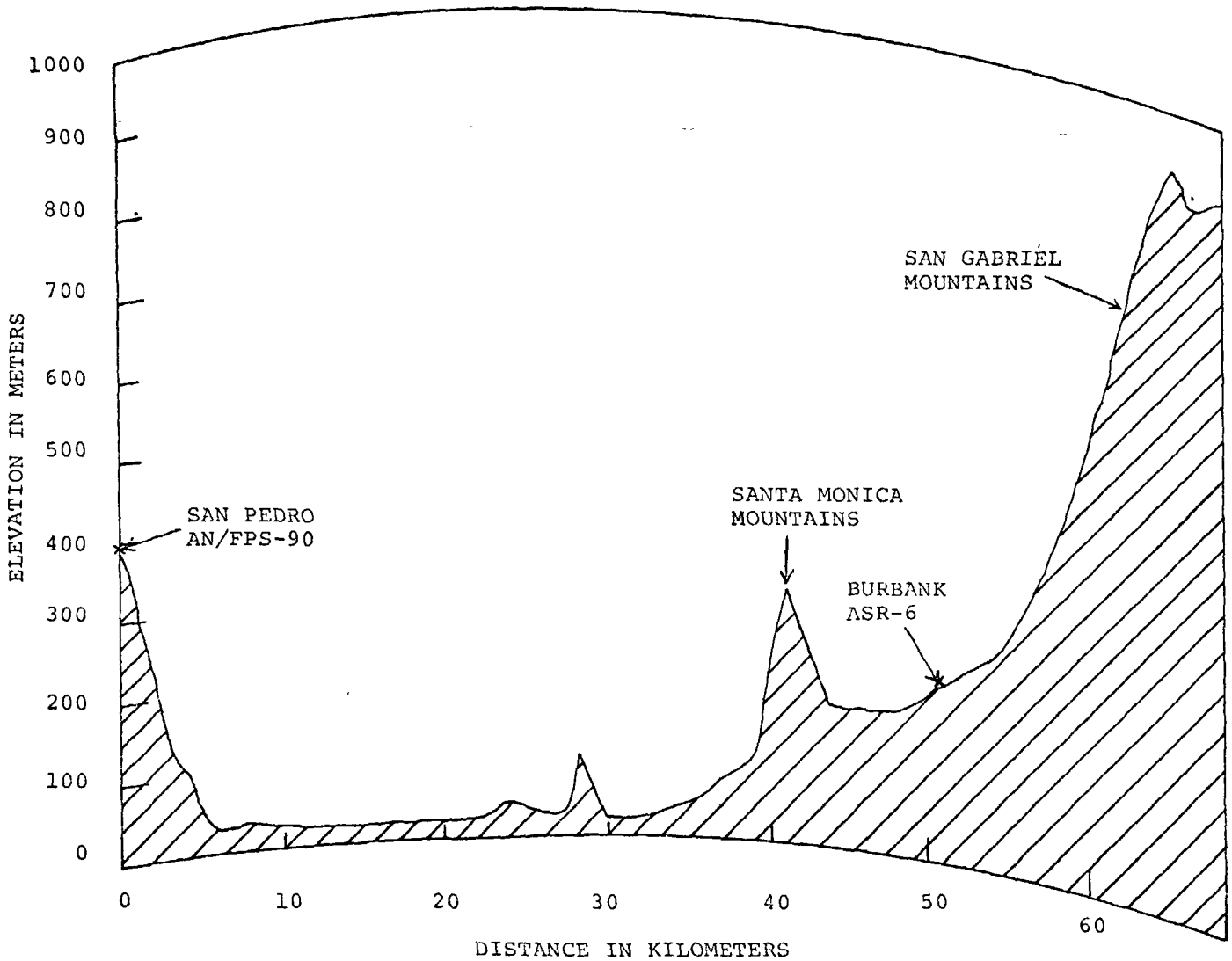

Figure D-17. Terrain Profile Between San Pedro AN/FPS-90 Radar and San Gabriel Mountains Including Burbank ASR-6 Radar.

To evaluate the relative level between the mountain reflected and direct signal, the RSMS van dish antenna was rotated at the Burbank radar antenna site. Because of the nonperiodic antenna scan of the AN/FPS-90 height finding radar antenna at San Pedro, the L-Band ARSR, located at the same site, was used as a signal source for this measurement. The van dish antenna has an 18 degree beamwidth, 22 dB sidelobe level, and a front-to-back ratio of 24 dB at the ARSR frequency (near 1300 MHz). The measured signal level as a function of bearing from Burbank is shown in Figure D-18. This level represents the envelope of the signal peaks received for three complete scans of the RSMS van dish. The combination of the three 360 degree van dish scans at 1.0 degree/second and the ARSR rotation rate of 5 RPM resulted in envelope points about every 4.0 degrees of bearing. The signal level, indicated in Figure D-18, from the mountain reflection bearings is only 6 dB less than the signal level received at San Pedro's bearing. It should also be noted that the signal level in the 40 degree region around San Pedro's bearing is within 8 dB of the peak received signal, indicating possible additional multipathing near the direct path. The multipath environment that the Burbank radar antenna sees may be slightly different than that measured with the RSMS van dish. The Burbank radar antenna is 46 feet higher than the van dish and was located about 0.2 miles from the RSMS van measurement location. This may be the reason that the interference occurred more often from the mountain region than the direct path bearing, which contradicts the fact that the measured miltipath signal level at the van location (Figure D-18) was 6 dB less than the direct signal.

Multipathing due to reflection from the San Gabriel mountains also took place between Burbank and Long Beach and is described in detail in Appendix A.

The following discussion suggests possible ways in which the mountain multipath may be taken into account to more accurately predict propagation loss. Mountain multipath can be categorized into two types:

a. Isolated multipath - multipath signals caused primarily by mountain reflections that arrive from vastly different directions from the direct path.

b. Direct multipath - multipaths that occur at azimuths around the direct path bearings caused primarily by mountain or hill diffraction.

In addition to stretching pulse width, the isolated type multipath can cause additional interference pulses when the difference in distance between the direct and reflected path

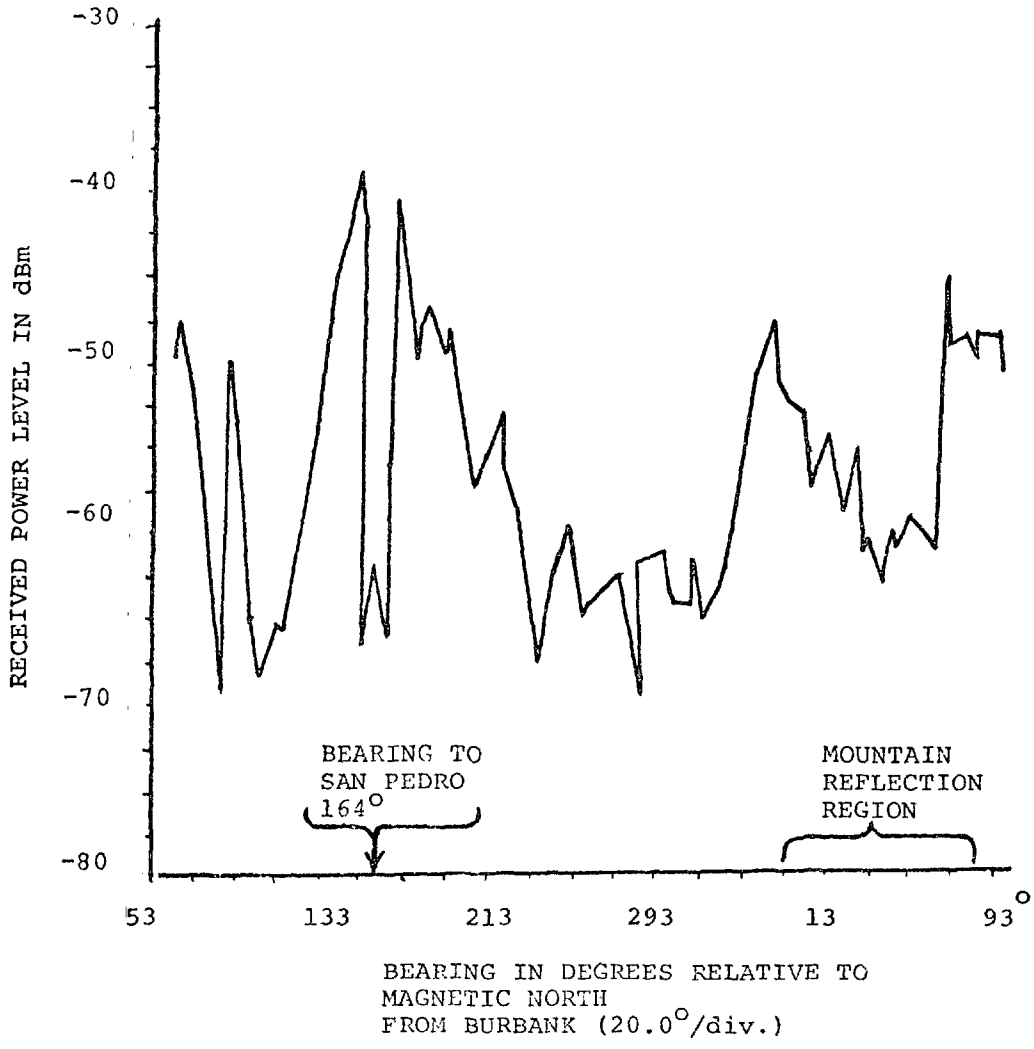

Figure D-18. Multipath Signal Level Environment at Burbank due to ARSR Radar at San Pedro

exceeds the distance (0.3 km) that a signal can travel in one pulse width. A first step for determining the propagation loss associated with strong isolated multipaths outside of the direct path region (mountain reflection type observed at Burbank) would be to first identify the common reflection region between the two radars. This would involve examining the terrain profile and topography in the general area between and around the two sites. Those mountains or hills would be considered that are illuminated by the most direct energy from the transmitter and whose orientation results is near equal angles of incidence and reflected energy from the transmitter to the receiver. Those mountain surfaces which satisfy these conditions and are also in line-of-sight with the receiver location would be used to hypothetically define a multipath between transmitter and receiver. The point-to-point model would then be used to determine the magnitude of incidence energy on various points of the reflection region. If the reflection region is in line-of-sight with the transmitter and extends beyond the transmitter antenna beamwidth, the transmitting antenna pattern effect on the distribution of the incident energy would also be taken into account. The rigorous determination of the reflection from a rough surface is a difficult problem; however, there is a good deal of measured data available on the subject. Measurements have shown that the reflection coefficient of rough terrain is in the range of 0.2 to 0.4 (Reference 41 and 42). The difference between the incident and reflection energy is an additional loss that would be included in the total path loss prediction. The next step would be to apply the point-to-point model a second time from the reflection region to the receiving antenna. The final step, if the reflection region is in line-of-sight with the receiving antenna and subtends an angle greater than its beamwidth, would be to consider the weighting of reflection region energy distribution by the receiving antenna pattern. In summary, the three losses, model loss prediction from transmitter to reflection region, loss due to diffuse reflection, model loss prediction from reflection region to receiver, and antenna pattern weighting loss would be added to obtain the total propagation loss for the multipath.

The second type of multipath arrives at azimuths close to the direct path bearing, and can cause beam spreading of the interferer radar antenna pattern that the victim radar sees. To determine terrain situations in which this can occur, the following technique is proposed. The first step would be to detect multipaths in the region around the direct path that could possible result in lower or about the same loss as the direct path. This would involve examining terrain profiles in planes perpendicular and near perpendicular to the direct path. Once the potential low loss multipath is identified, its associated terrain profile in the

non-vertical plane, defined by the receiver point, transmitter point, and common off-set horizon point between the two sites, would be used in the point-to-point model to predict the propagation loss of the multipath. Other possible low loss paths and their non-vertical terrain profile parameters would also be identified and used in the point-to-point model to predict their loss. Figure D-19 indicates these oblique (non-vertical) terrain profile planes associated with multipath over a mountain ridge. The predicted low of the multipath and special weighting of the transmitter and receiver antenna patterns would then be used to predict the degree of beam spreading.

Ducting

The measured propagation loss for the Miramar to Los Alamitos ocean path and the Oakland to Mountain View bay path were as much as 39 dB below the predicted loss. The large difference between measured and predicted propagation loss occurred because the propagation model did not account for the superrefraction conditions that can occur for paths over water.

Evaporation of moisture from water creates a refractive index gradient at low heights that can refract microwave energy downward to create a "guiding" effect or duct. Propagation of electromagnetic waves in such a duct can vary from a near lossless situation, to signal enhancement, depending on the frequency and intensity of the evaporation duct. The intensity of the evaporation duct is most often described in terms of "duct height" which is defined as the height in which the modified refractivity is minimized.

The mechanism of propagation within a duct has been explained in terms of mode theory by several investigators including Chang (Reference 65), Joseph and Smith (Reference 66), Ring (Reference 67), Sodha (Reference 68), and others. Jeske and Brocks (Reference 69) explain duct propagation in terms of the mode theory of Booker and Walkinshaw. They found a high correlation between measured field strengths and the width of a surface evaporative duct at cm wavelengths. Joseph and Smith solved the wave equation by mode theory to include a number of trapped modes. Similarly, Chang, who explains radio observations by "Whispering Gallery" modes, calculates the received field for antennas above, within, and below the duct. He concludes that when both antennas are above or within the duct, the received field is 10 to 20 dB above free space. When one or both terminals are below the duct, the field is 10 to 25 dB below free space, even at distances up to 1200 km. He carefully points out, however, that ray theory

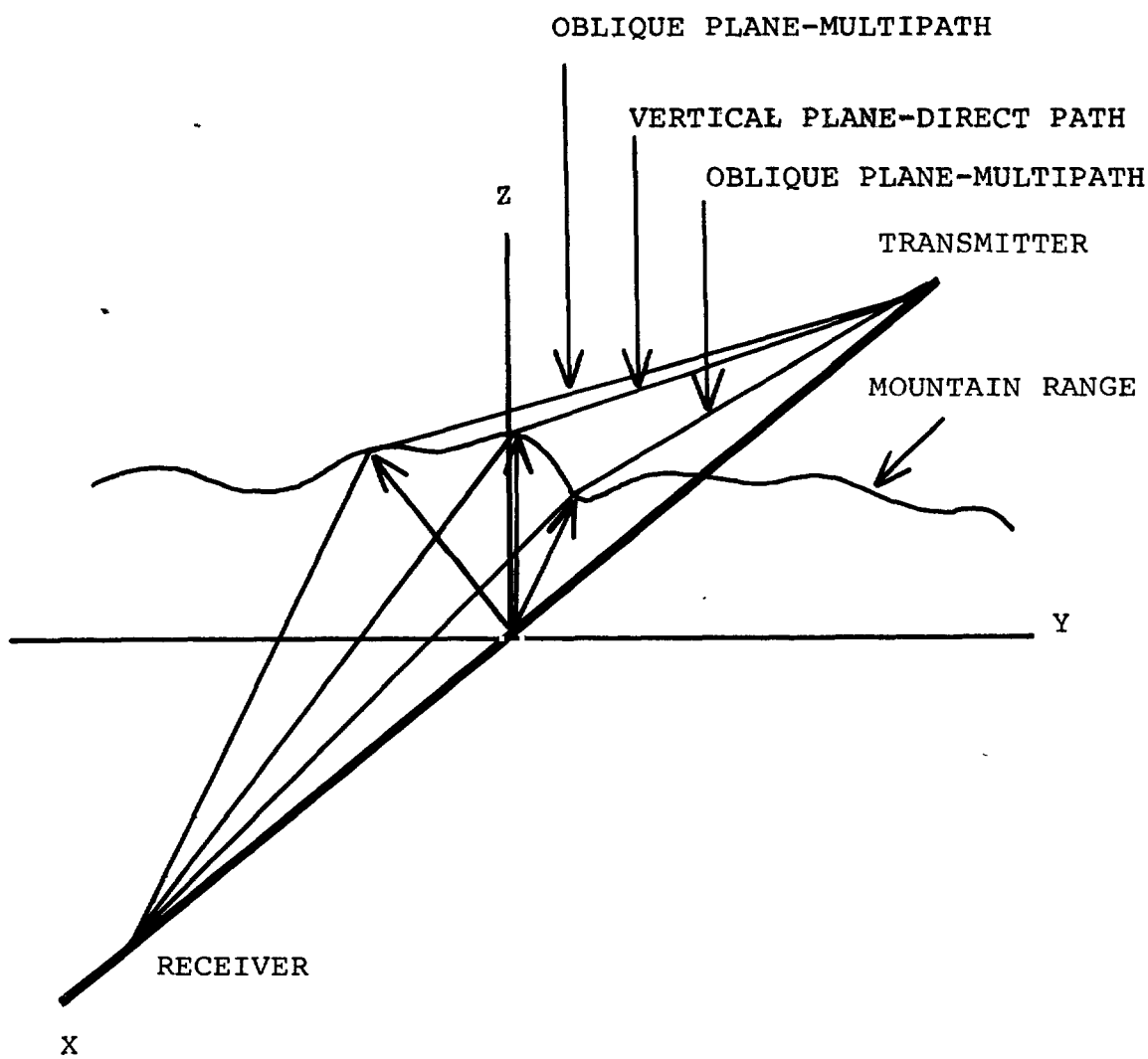

Figure D-19. Geometry of Multipath Signals over Mountain Ridge

neglects the energy leakage through the layer, which may be quite significant.

NELC (Naval Electronics Laboratory Center) has developed a tropospheric waveguide computer program (Reference 43) to solve the model equation for various duct height profiles at 3.3 GHz. The propagation loss as a function of transmitter and receiver height and range can be calculated using this program. Measurements of meteorological parameters over a five-year period, for all seasons and times of the day, were made in the off-shore San Diego area. Calculations by the program using this data base indicated that radar range enhancement occurs 30% of the time over ocean paths in the San Diego area.

SUMMARY OF PROPAGATION LOSS MEASUREMENTS AND MODELING

It was evident that measured propagation loss is affected by receiving antenna beamwidth due to spatially weighting of incident multipath signals by the receiving antenna pattern, and that antenna height has more impact on measurement in some environments than predicted by the propagation model. In addition, the displacement of the physical location of the receiving antenna by several feet can result in large variation in the received signal level. For these reasons and in the interest of obtaining more accurate measurements, it is recommended that future propagation loss measurements be performed, if possible, using the radar antenna.

The point-to-point model can sometimes select the incorrect mode of propagation due to misinterpretation of the terrain data file. However, overall the point-to-point model provided more accurate predictions, over the 20 paths analyzed, than the area model.

It is believed that the difference between the predicted and measured propagation loss for Los Angeles paths occurred because the propagation model did not consider the following factors:

1. Increased attenuation due to man-made clutter
2. Increased attenuation due to foliage
3. Multipath due to mountains
4. Sporadic attenuation during supperrefractive conditions

It is recommended that the point-to-point propagation loss

prediction be amended on a case-by-case basis to take these factors into account. The results of measurements by other investigators on the increase in attenuation due to urban and suburban environments presented in this appendix can be used to arrive at a suitable correction factor for various degrees of buulding congestion. The simple diffraction and attenuation models discussed in this appendix, to account for attenuation due to foliage, agree well with measurements and can also be used as a correction factor to the point-to-point propagation model predictions.

The empirical result of loss measurements in man-made clutter environments by Turin were incorporated in the San Francisco loss predictions. The difference between the San Francisco loss predictions and measurements on the average was -3 dB, a 7 dB improvement over Los Angeles predictions.

A combination of contour map and terrain profile analysis with repeated application of the point-to-point model is proposed to identify mountain propagation paths with the same or less loss than the direct path. Two techniques are presented in this appendix to help predict the temporal and special effect of multipath on interference. The first technique can be employed to predict the type of mountain terrain that can cause antenna beam spreading and to what degree. The second technique may be useful for predicting the angle of arrival and magnitude of multipath signal caused by mountain reflections significantly displaced from the direct path region.

The decrease in propagation loss due to ducting can be predicted from well established models identified in this appendix. Sufficient measured data is available for the California area to predict how often and to what degree ducting occurs.

The addition of correction factors to the point-to-point propagation model will no doubt still result in prediction errors. The subjectivity of choosing the most suitable correction factor for a given environment and the fact that some of these correction factors are based upon average values of empirical measurements, indicates that discrepancies between predicted and measured values will exist. However, the average absolute propagation prediction error should approach 5 dB.

APPENDIX E

DETAILED MEASUREMENTS

INTRODUCTION

Part of the Los Angeles and San Francisco area measurement program involved making detailed measurements at several radar sites. These measurements were made using the RSMS van instrumentation with the objective of determining what caused:

1. The absence of predicted interference,
2. The presence of unpredicted interference,
3. The interference having a different form on the PPI scope than predicted.

These detailed measurements involved measuring:

1. Interferer emission spectrum,
2. Interferer antenna pattern at victim radar site,
3. Propagation loss between victim and interferer,
4. Victim radar antenna pattern.

A limited number of measurements were also made connecting the RSMS 8580 receiver to the victim radar IF preamplifier output with the victim radar transmitter turned off. This permitted peak power measurements at the victim radar IF preamplifier output, and positive identification of the interferer using the AS-330 pulse train separator. The measured peak power level at the IF preamplifier output was then converted to a RF input level using a measured transfer function. A more expanded discussion of the detailed measurement plan is given in Appendix F.

The measured data referenced in this Appendix is contained in Appendices A through D. The following is a discussion of the detailed measurements conducted in the Los Angeles and San Francisco areas.

LOS ALAMITOS AN/CPN-4 VICTIM RADAR MEASUREMENTS

The nominal characteristics of the Los Alamitos AN/CPN-4 radar are given in Table 4-2. Closed system measurements made on the radar indicated that the nonsynchronous MDS INR was 6 dB for the normal channel and 7 dB for the MTI channel with the integrator off. A steady level of interference could be observed at an INR of 10 dB for both the normal and MTI mode. The receiver inherent noise level (N_j) is -102 dBm.

The RSMS van dish antenna was approximately the same height as the AN/CPN-4 antenna height. Therefore, the measurements made at this site using the RSMS van dish should be fairly representative of what the AN/CPN-4 antenna received. Possible objects causing reflections at the site are discussed in Appendix D.

The predicted interferers for the Los Alamitos AN/CPN-4 radar were:

Radar	Interferer Freq. (MHz)	Victim Freq. (MHz)	INR
San Pedro AN/FPS-90	2835	2801	25.5
Long Beach ASR-5	2777	2801	26.2

San Pedro AN/FPS-90. Interference from the San Pedro height finder was observed on the PPI scope of the AN/CPN-4 at Los Alamitos. The interference observed on the PPI scope varied from interference occurring in a 5° sector when the height finder was not nodding in the direction of Los Alamitos to interference approximately covering 3/4 of the PPI display when the AN/FPS-90 radar was nodding in the direction of Los Alamitos. Because of the random scanning of the AN/FPS-90 mainbeam, it was very difficult to determine the propagation loss from the height finder. However, the RSMS van was used to measure the peak power level received at Los Alamitos from the height finder for a period of several hours. Figure D-6 shows a sample of the measured data taken using the RSMS van dish which has a 20 dB gain. Figure D-6 shows a maximum received peak power level of +4 dBm. It is not positively known that this +4 dBm level occurred when the height finder was nodding in the direction of Los Alamitos. However, these types of measurements were made over a 12-hour period, and +4 dBm was the maximum peak received power. Correcting the +4 dBm level for the gain of the van dish gives a peak power level at the AN/CPN-4 antenna of -16 dBm (P_r). The INR at the AN/CPN-4 IF output caused by the San Pedro AN/FPS-90 can then be determined by:

$$INR_{ij} = P_r + G_{rj} - FDR_{ij} - N_j \qquad \text{(E-1)}$$

It is shown in Appendix C that the FDR is emission spectrum limited. The measured emission spectrum of the San Pedro AN/FPS-90 is shown in Figure B-19, and indicates an FDR of approximately 45 dB at the operating frequency (2801 MHz) of the Los Alamitos AN/CPN-4 radar. The predicted FDR was 53 dB (Figure C-12). Using a mainbeam gain of +24 dBi (corrected for antenna tilt angle, 7 dB) and receiver noise level (N_j) of -102 dBm, the calculated INR using equation E-1 for coupling from the San Pedro radar would be +65 dB. The calculated INR of +65 dB indicates why a majority of the PPI scope was covered by interference from the height finder when the AN/FPS-90 was nodding in the direction of Los Alamitos. When the height finder was not nodding in the direction of Los Alamitos, the INR should be approximately 49 dB less (mainbeam-to-median backlobe ratio of height finder antenna) which would give an INR of 16 dB and still cause interference on the PPI display.

INR measurements made using the 8580 receiver and tapping off the AN/CPN-4 IF preamplifier output, yielded measured INR's between 15 dB and 48 dB which is in close agreement to the previously discussed INR range.

Predicted interference to the Los Alamitos AN/CPN-4 from the San Pedro AN/FPS-90 for antenna coupling of the victim mainbeam with the backlobe of the height finder, using the PPI simulation model, is shown in Figure E-1. The actual observed interference agreed fairly well with the predicted interference for antenna coupling of the victim mainbeam with the backlobe of the height finder.

Long Beach ASR-5. Interference from the Long Beach ASR-5 was not observed on the Los Alamitos AN/CPN-4 PPI display. The Long Beach ASR-5 emission spectrum was measured at Long Beach to determine the FDR factor. The Long Beach ASR-5 emission spectrum is shown in Figure B-13, and indicates an FDR factor of 53 dB at the Los Alamitos AN/CPN-4 operating frequency of 2801 MHz. The predicted FDR was 47 dB (Figure C-9). The predicted propagation loss was 19 dB less than the measured propagation loss (149 dB, Table D-2). The median backlobe level of the Long Beach ASR-5 was measured to be -11.8 dBi (Table A-1). Also a comparison of Figures A-6 (line-of-sight antenna pattern) and Figure A-24 (Long Beach ASR-5 environmental antenna pattern measured at Los Alamitos) shows that the backlobe level of the Long Beach ASR-5 antenna radiation is attenuated by the foreground clutter at the Long Beach radar site. This additional attenuation of the Long Beach ASR-5 backlobe level

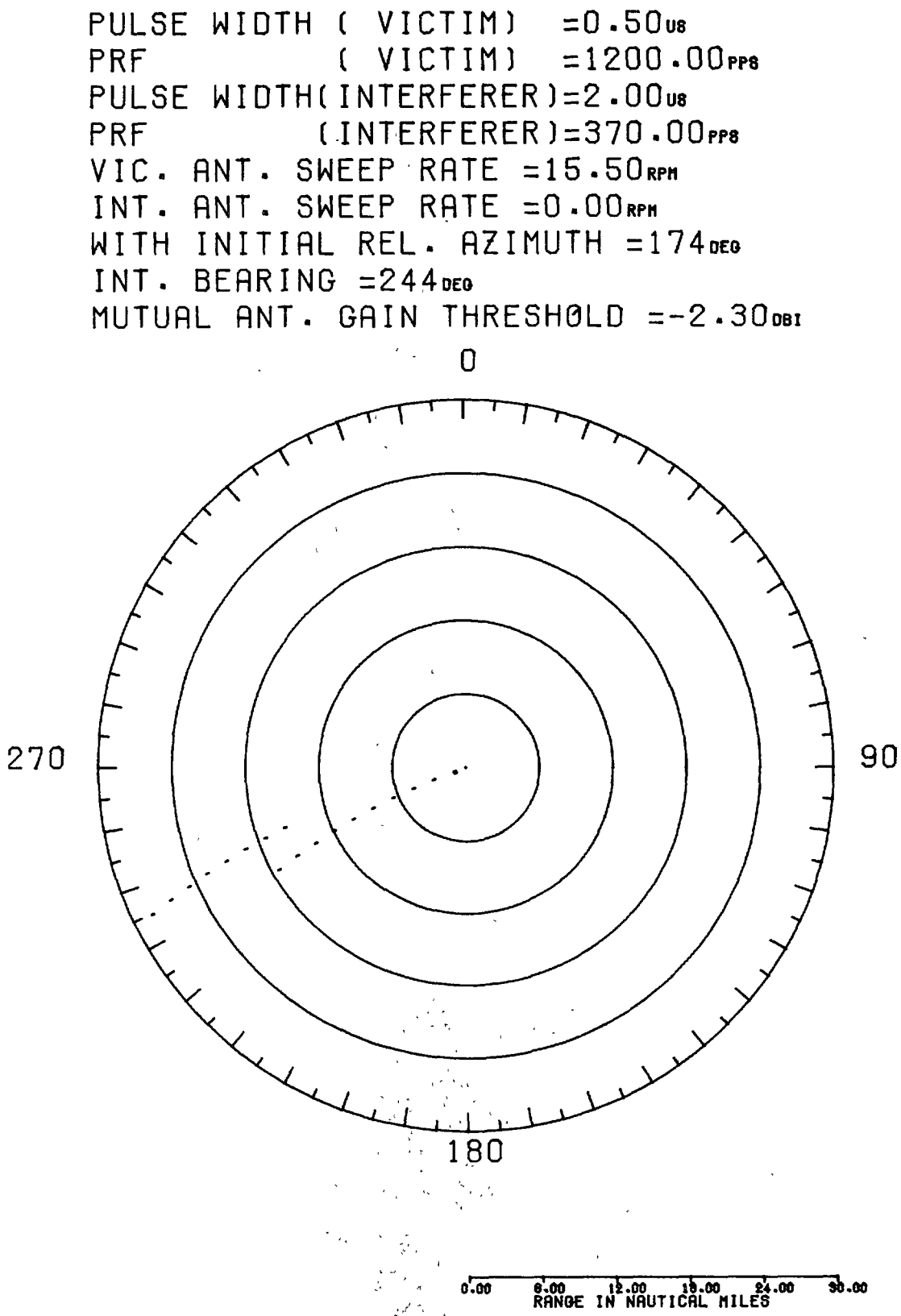

Figure E-1. Simulated PPI Display of Los Alamitos AN/CPN-4 with San Pedro AN/FPS-90 Interference

was found to be approximately 5.6 dB and is discussed in Appendix A. Taking into account the additional attenuation of the Long Beach antenna radiation backlobe and using the measured FDR (Long Beach emission spectrum), propagation loss and Long Beach antenna backlobe level, the measured INR is -0.7 dB using Equation 3-1 as compared to the predicted INR of 26.2 dB. An INR of approximately -0.7 dB would not cause interference on the AN/CPN-4 PPI display. Predicted interference to the Los Alamitos AN/CPN-4 from the Long Beach ASR-5 is shown in Figure E-2 using the PPI simulation model. There was actually no observed interference from Long Beach on the PPI display of the Los Alamitos AN/CPN-4 radar.

Ontario ASR-5. Interference was observed on the Los Alamitos AN/CPN-4 PPI display from the Ontario ASR-5. Interference from the Ontario ASR-5 radar was not predicted since the predicted INR was -4.6 dB for antenna coupling of the mainbeam of the victim to backlobe of the interferer. The emission spectrum of the Ontario ASR-5 radar is shown in Figure B-12. The figure shows that the predicted FDR should be within a few dB of the actual FDR. The measured propagation loss was found to be 184 dB (Table D-2) as compared to 183 predicted. Therefore, some other factor other than error in the predicted FDR and propagation loss had to contribute to the occurrence of interference from the Ontario ASR-5 radar to the Los Alamitos AN/CPN-4 radar. Figures A-25 through A-27 show environmental antenna patterns of the Ontario ASR-5 radar measured at Los Alamitos. The higher antenna sidelobe and broadened beamwidth shown in these figures indicates the presence of multipathing caused by diffraction and reflection in the Chino Hills between the two radar sites. The broadened beamwidth and higher sidelobe level of the Ontario antenna pattern, as seen by the Los Alamitos radar, increased the probability of equivalent mainbeam-to-mainbeam coupling.

INR measurements made using the 8580 receiver and tapping off the AN/CPN-4 IF preamplifier output, yielded measured INR's between 15 dB and 24 dB.

Norton AFB AN/MPN-13. Interference was observed on the Los Alamitos radar from the Norton AFB AN/MPN-13 radar. Interference from the Norton AFB AN/MPN-13 was not predicted since the predicted INR was -8.9 dB. Since the Norton radar is operating cochannel with the Los Alamitos AN/CPN-4 (Transmitting frequency 2800 MHz, Figure B-11) the FDR rejection is 0 dB. The measured propagation loss was found to be 192 dB (Table D-2) as compared to 198 dB predicted. Therefore, the measured propagation loss was 6 dB less than predicted. However, the 6 dB less propagation loss does not account for the occurrence of interference from the Norton AFB AN/MPN-13 radar.

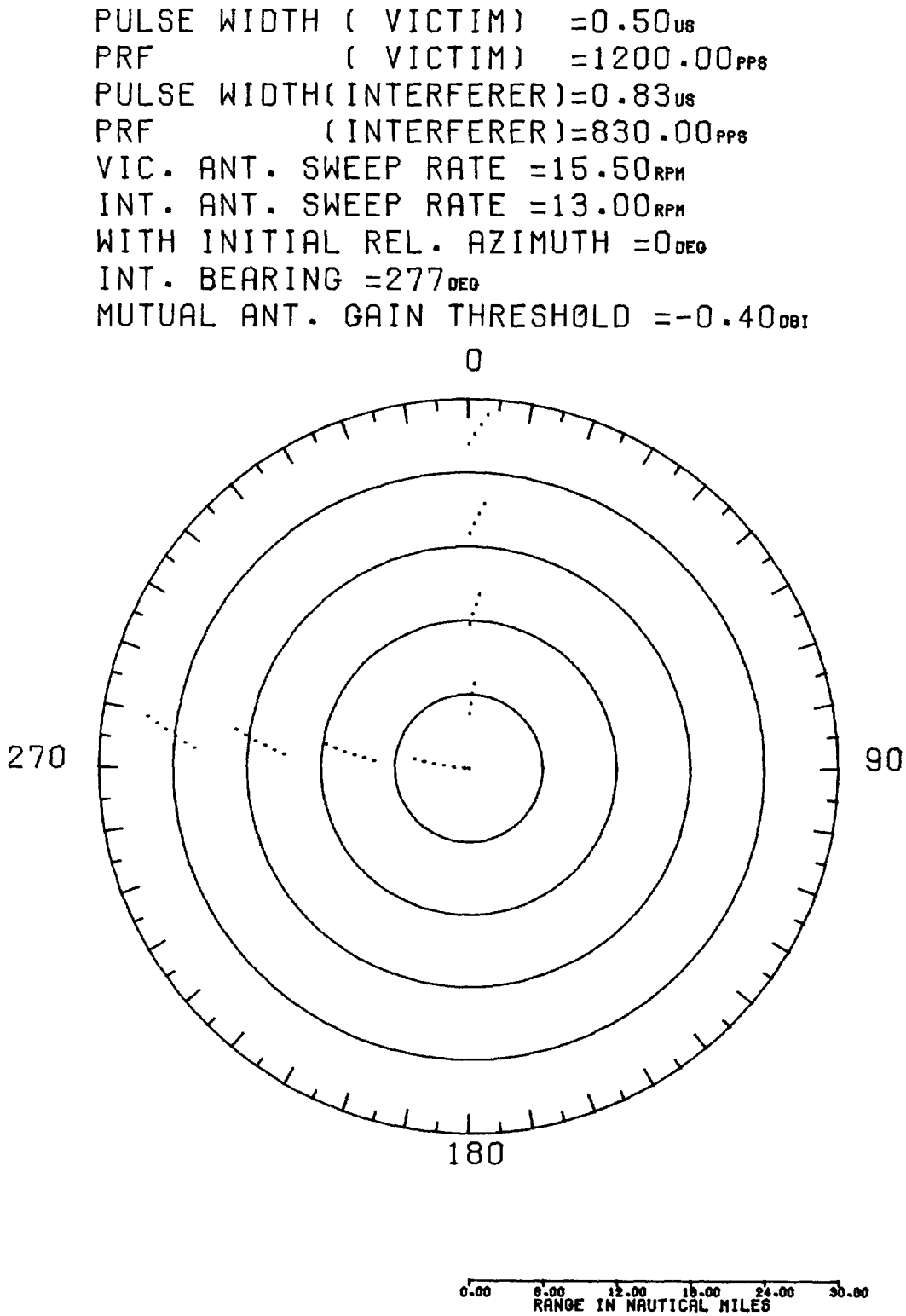

Figure E-2. Simulated PPI Display of Los Alamitos AN/CPN-4 with Long Beach ASR-5 Interference

Figure A-28 indicates that multipath phenomena also caused the occurrence of interference from the Norton radar. The broadening of Norton's antenna beam as seen by Los Alamitos (Figure A-28), and the 6 dB lower than predicted propagation loss, caused by mountain diffraction and reflection in the Chino Hills, resulted in interference from the Norton AN/MPN-13 radar which was not predicted.

March AFB AN/MPN-13. Interference from the March AFB AN/MPN-13 was also observed on the Los Alamitos AN/CPN-4 radar. The predicted INR from the March radar was -17.6 dB. The March radar also operates on approximately the same frequency (Transmitter frequency 2800 MHz, Figure B-10) as the Norton AN/MPN-13 radar and is also cochannel with the Los Alamitos AN/CPN-4 radar. Propagation measurements from the March AFB AN/MPN-13 could not be measured since the received power level at the RSMS van 8580 receiver input was below the receiver noise level. The RSMS van has approximately 25 dB less sensitivity than the AN/CPN-4 radar due to a higher inherent noise level and 11 dB less antenna gain. Interference from the March AN/MPN-13 radar was identified by tapping off the AN/CPN-4 IF preamplifier output and connecting it up to the RSMS van 8580 receiver. Interfering signals from the Norton AFB AN/MPN-13 were identified by requesting the Norton radar to operate in their stagger mode (3 x 365 = 1095), and the March radar with stagger off (1095 PRF). The AS-330 pulse train separator was then used to differentiate between the two radars.

LONG BEACH ASR-5 VICTIM RADAR MEASUREMENTS

The nominal characteristics of the Long Beach ASR-5 radar are given in Table 4-2. Closed system measurements made on the radar indicated that the nonsynchronous MDS INR was 6 dB for normal channel and 5 dB for the MTI channel with the integrator off. With the integrator on, the MDS INR was 6 dB for the MTI channel. An INR of 10 dB would cause a steady level of interference on both the normal and MTI channels even with the integrator on. The receiver inherent noise level (N_j) is -106 dBm.

The ASR-5 radar site at Long Beach is a cluttered site, and an ideal location for the RSMS van was very difficult to find. The ASR-5 radar at Long Beach has an antenna height of 26 feet. The RSMS van dish height is only 14 feet. The RSMS van cavity back spiral antennas mounted on a tower have the capability of reaching a height of 25 feet. However, the cavity back spiral antennas are not directional antennas

and reflections of the ASR-5 antenna platform and reflector could cause erroneous propagation loss measurements.

The predicted interferers for the Long Beach ASR-5 radar operating on the high channel were:

Radar	Interferer Freq. (MHz)	Victim Freq. (MHz)	INR
San Pedro AN/FPS-90	2835	2777	27.1
Burbank ASR-6	2788	2777	11.8
Los Alamitos AN/CPN-4	2801	2777	50.7

San Pedro AN/FPS-90. Interference from the San Pedro AN/FPS-90 height finding radar was observed on the PPI scope of the ASR-5 at Long Beach. The interference varied from covering a 40° sector of the PPI when the height finder's vertically nodding antenna was pointed in azimuth at Long Beach, to a 3° sector when the antenna was not pointed at Long Beach. Because of the random scanning of the AN/FPS-90 antenna, it was difficult to measure propagation loss between San Pedro and Long Beach. However, the RSMS van with a 20 dB gain dish was used to monitor the power level received at Long Beach from the height finder over a period of several hours. A one-hour sample of this measured data, shown in Figure D-5, indicates a maximum received peak power level of +4 dBm. Since the 4 dBm level was also the maximum peak power measured over a 12-hour period, it is likely that it occurred when the San Pedro antenna was nodding at the Long Beach radar. Correcting the +4 dBm level for the gain of the van dish gives a peak power level at the ASR-5 antenna of -16 dBm (Pr). The INR at the Long Beach ASR-5 IF output caused by the San Pedro AN/FPS-90 can be determined by Equation E-1. It is shown in Appendix C that the FDR is emission spectrum limited. The measured emission spectrum of the San Pedro AN/FPS-90, as shown in Figure B-19, indicates an FDR of approximately 51 dB at the operating frequency (2777 MHz) of the Long Beach ASR-5 (the predicted FDR was 61 dB, Figure C-13). Using Equation E-1 and a mainbeam gain of +27 dBi (correcting for antenna tilt angle, 7 dB) and receiver noise level of -106 dBm, the calculated INR for coupling from the San Pedro radar would be +66 dB indicates why a majority of the PPI display was covered by interference from the height finder when the AN/FPS-90 was nodding in the direction of Long Beach. When the height finder was not nodding in the direction of Long Beach, the INR should be approximately 49 dB less (mainbeam-to-median backlobe ratio of height finder

antenna) which would give an INR of 17 dB, and still cause interference on the PPI display.

INR measurements made using the 8580 receiver and tapping off the ASR-5 IF preamplifier output, yielded measured INR's between +18 dB and +35 dB. During these detailed measurements, the height finder did not nod at Long Beach. Therefore, we did not measure an INR as high as +66 dB. Predicted interference to the Long Beach ASR-5 radar for mainbeam of the victim coupling with the backlobe of the height finder using the PPI simulation model is shown in Figure E-3.

Burbank ASR-6. Interference was observed on the Long Beach ASR-5 PPI display from the Burbank ASR-6 radar. The interference from the Burbank radar appeared on the PPI display approximately 1 out of 5 scans, and covered approximately a 3° sector at the bearing of the Burbank radar (320°). The measured propagation loss from Burbank to Long Beach was found to be 191 dB (Table D-2), and the predicted propagation loss was 181 dB. However, the propagation loss measurements were made with the RSMS van dish which was about 12 feet lower than the ASR-5 antenna height. Because of foreground clutter, measurements made with the dish may be a few dB low. Propagation loss measurements from Burbank to Long Beach could not be made with the cavity back spiral antenna to determine the propagation loss as a function of antenna height because of the inability to discriminate against the Long Beach ASR-5 emissions. The measured propagation loss from Long Beach to Burbank was found to be 185 dB (Table D-2). This difference in nonreciprocity is discussed in detail in Appendix D. An estimate of the additional propagation loss due to the difference in antenna height at Long Beach was 3 dB. Therefore, a good estimate of the actual propagation loss from Burbank to Long Beach would be 188 dB. An approximate FDR was taken from Figure B-14, and found to be 27 dB. The average antenna backlobe level of the Burbank radar was found to be -11.9 dBi (Table A-1). Using Equation 3-1 and the measured data, the calculated INR would be -8.9 dB. One major factor contributing to the big difference between measured and predicted INR levels was the FDR factor. A frequency separation of 5 MHz (Long Beach frequency 2780 MHz and Burbank frequency 2785 MHz) was used for the INR prediction. Due to the fact that the ASR'S usually do not operate at the edge of their 10 MHz band, the actual frequency separation was 11 MHz (Long Beach frequency 2777 MHz and Burbank frequency 2788 MHz). This made a difference in the emission spectrum level of approximately 10 dB because of the sharp fall-off of the emission spectrum for small ΔF. Measurements indicate that the INR for mainbeam-to-backlobe coupling was -8.9 dB which indicated that interference from the

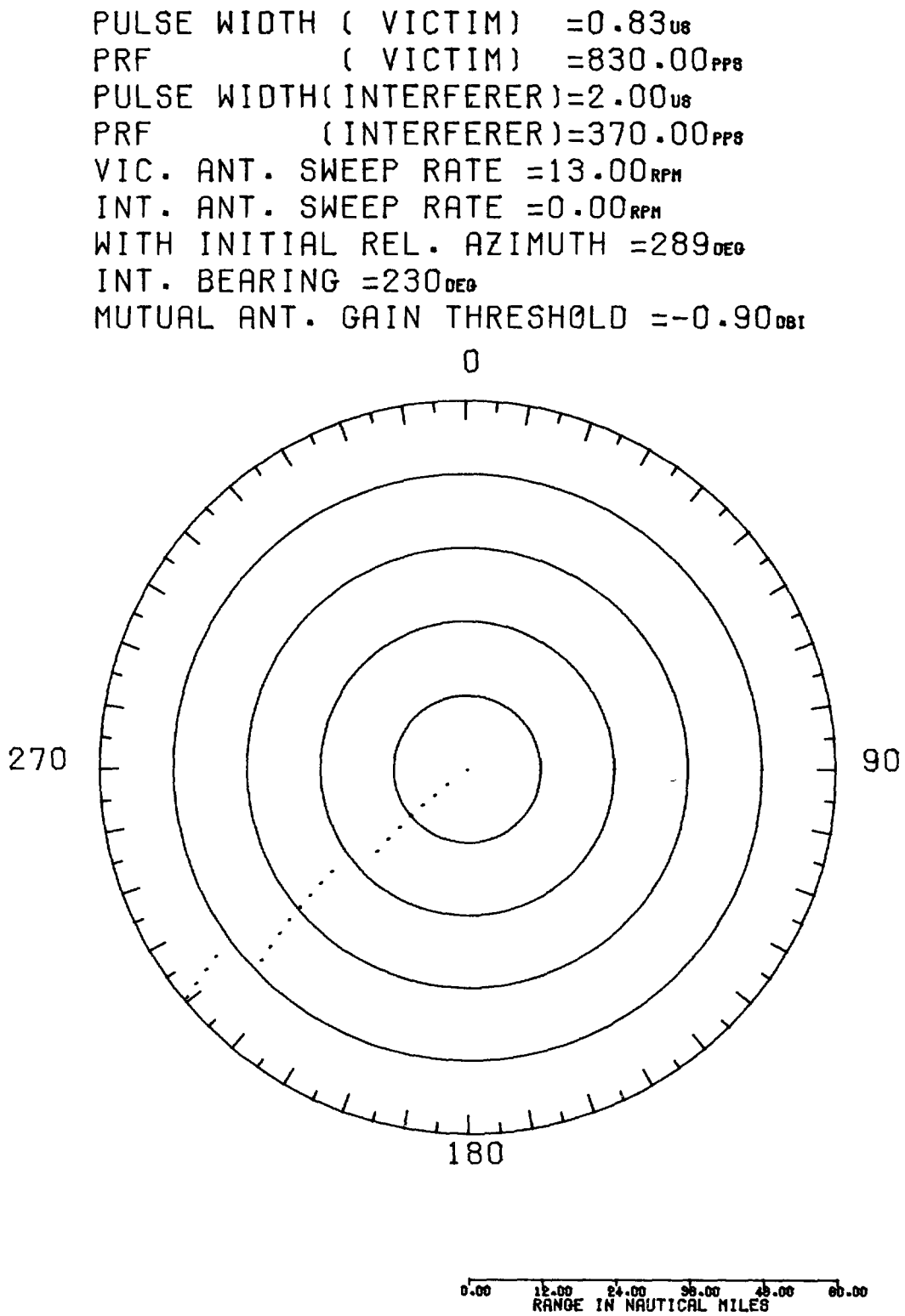

Figure F-3. Simulated PPI Display of Long Beach ASR-5 with San Pedro AN/FPS-90 Interference

Burbank ASR-6 should not appear on the PPI display at Long Beach. However, interference from the Burbank ASR-6 was observed approximately 1 out of 5 scans. An explanation of the possible cause of the interference is given in Appendix A. Figure A-32 shows that a multipath phenomena was occurring due to a mountain range between the two radars and a high mountain range in back of the Burbank ASR-6 radar. INR measurements made using the 8580 receiver and tapping off the ASR-5 IF preamplifier output, yielded measured INR's between +26 dB and +35 dB. This indicates that the interference was occurring when interfering signal levels were received due to the multipath phenomena. Figure E-4 shows the form of the predicted interference using the PPI simulation program.

Los Alamitos AN/CPN-4. Interference was observed on the Long Beach ASR-5 PPI display from the Los Alamitos AN/CPN-4 radar. The interference from the Los Alamitos radar was very infrequent and only appeared at the bearing of the Los Alamitos radar (97°). Since the FDR is emission spectrum limited, the FDR can be determined from Figure B-6. The FDR (emission spectrum level at 2777 MHz) is approximately 38 dB. The average backlobe level of the Los Alamitos antenna was found to be -8.4 dB (Table A-1). The measured propagation loss from Los Alamitos to Long Beach was 157 dB (Table D-2) using the van cavity back spiral antennas at a height of 25 feet (approximate height of Long Beach ASR-5 antenna). When the van dish was used at a height of 14 feet, the measured propagation loss was 176 dB. Using the cavity back spiral antennas and raising the tower from 14 feet to 25 feet, the propagation loss decreased by 11 dB. The Long Beach ASR-5 radar site was a cluttered site which caused the signal energy from the Los Alamitos radar to be scattered. This was evident from the smeared appearance of the interference on the Long Beach ASR-5 PPI display. Because of this signal scattering phenomena and antenna beamdwith difference associated with the measurement antennas and actual radar antenna, it is very difficult to actually determine what the propagation loss was between the two radars without using the radar antenna to measure the propagation loss. The subject of propagation loss between these two antennas is discussed in more detail in Appendix D. Another factor which may have contributed to the absence of the frequency of predicted interference from the Los Alamitos radar was additional attenuation of the Los Alamitos antenna backlobe radiation due to foreground clutter. Also, the Los Alamitos AN/CPN-4 radar had been realigned between the time the emission spectrum was measured and the time the measurements were made at Long Beach. The actual operating frequency of the Los Alamitos AN/CPN-4 was changed from 2807 MHz to 2801 MHz. This realignment could have also changed the emission spectrum shape. Considering these factors, it is very difficult to assess

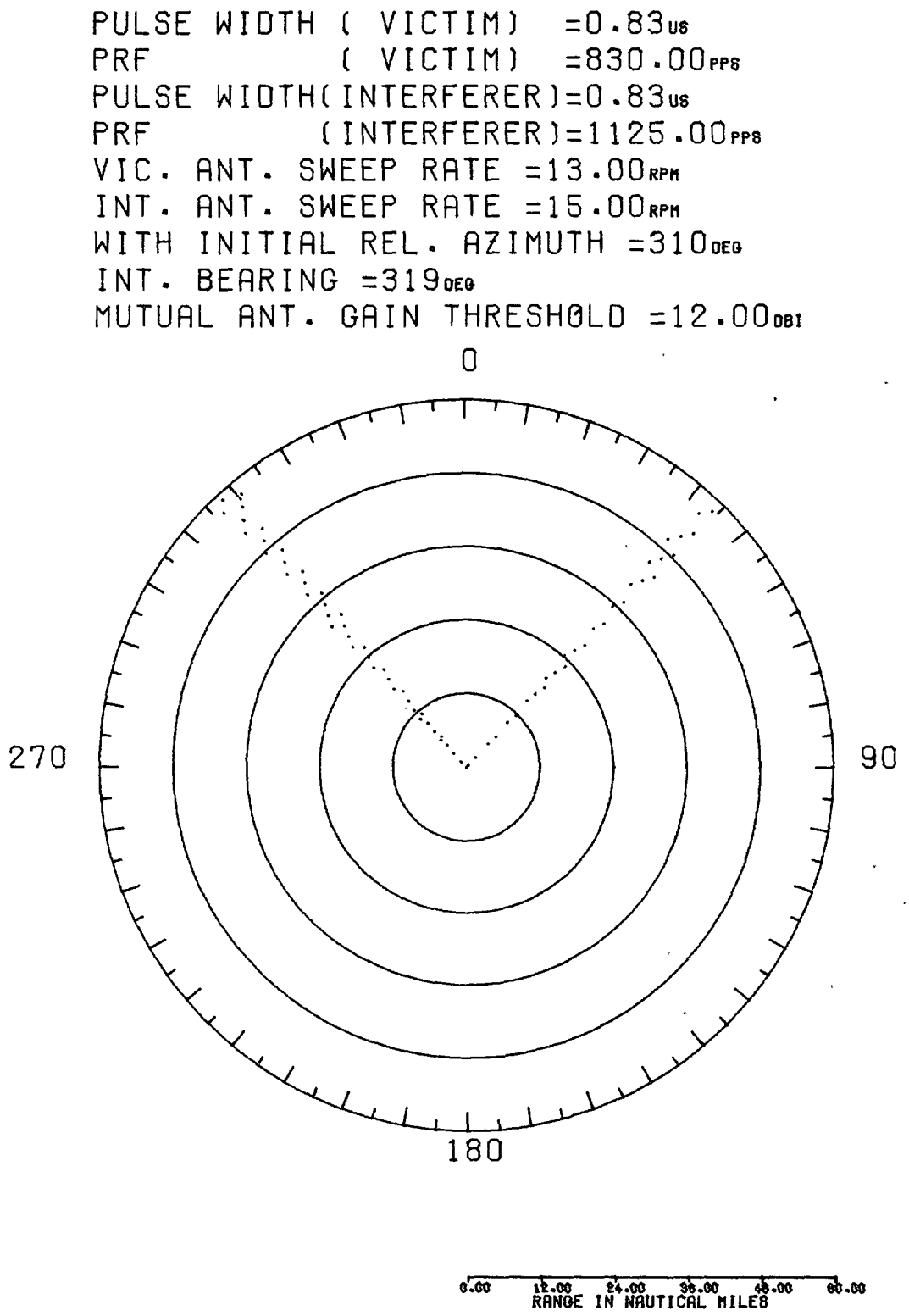

Figure E-4. Simulated PPI Display of Long Beach ASR-5 with Burbank ASR-6 Interference

actually why the form of interference from the AN/CPN-4 was not the same as predicted without making additional measurements. Figure E-5 shows the form of the predicted interference using the PPI simulation program. As seen in Figure E-5, the predicted interference was extremely pessimistic when compared to the observed interference. It was concluded that buildings and trees along the propagation path caused the interfering signal to be diffused causing a significant increase in propagation loss.

MOUNTAIN VIEW ASR-5 VICTIM RADAR MEASUREMENTS

The ASR-5 radar site at Mountain View is an uncluttered site located at the southern tip of the San Francisco Bay. The Mountain View radar site was chosen as a detailed measurement site with the major objective of obtaining propagation path loss data on ducting phenomena which occurs in the bay area. Propagation path loss data was obtained for predicted interfering radars, and also radars which were not predicted as potential interferers.

The ASR-5 radar at Mountain View has an antenna height of 26 feet. Both the RSMS van dish (height 14 feet) and omni antenna (height 30 feet) were used to measure the power received from the other radars in the bay area. Emission spectra of the predicted interferers were also measured.

The nominal characteristics of the Mountain View ASR-5 radar are given in Table 5-2. The predicted interferers for the Mountain View ASR-5 radar were:

Radar	Interference Freq. (MHz)	Victim Freq. (MHz)	INR (dB)
Almaden AN/FPS-90	2778	2758	32
Almaden AN/MPS-14	2793	2758	22
Mt. Tamalpais AN/FPS-90	2737	2754	23

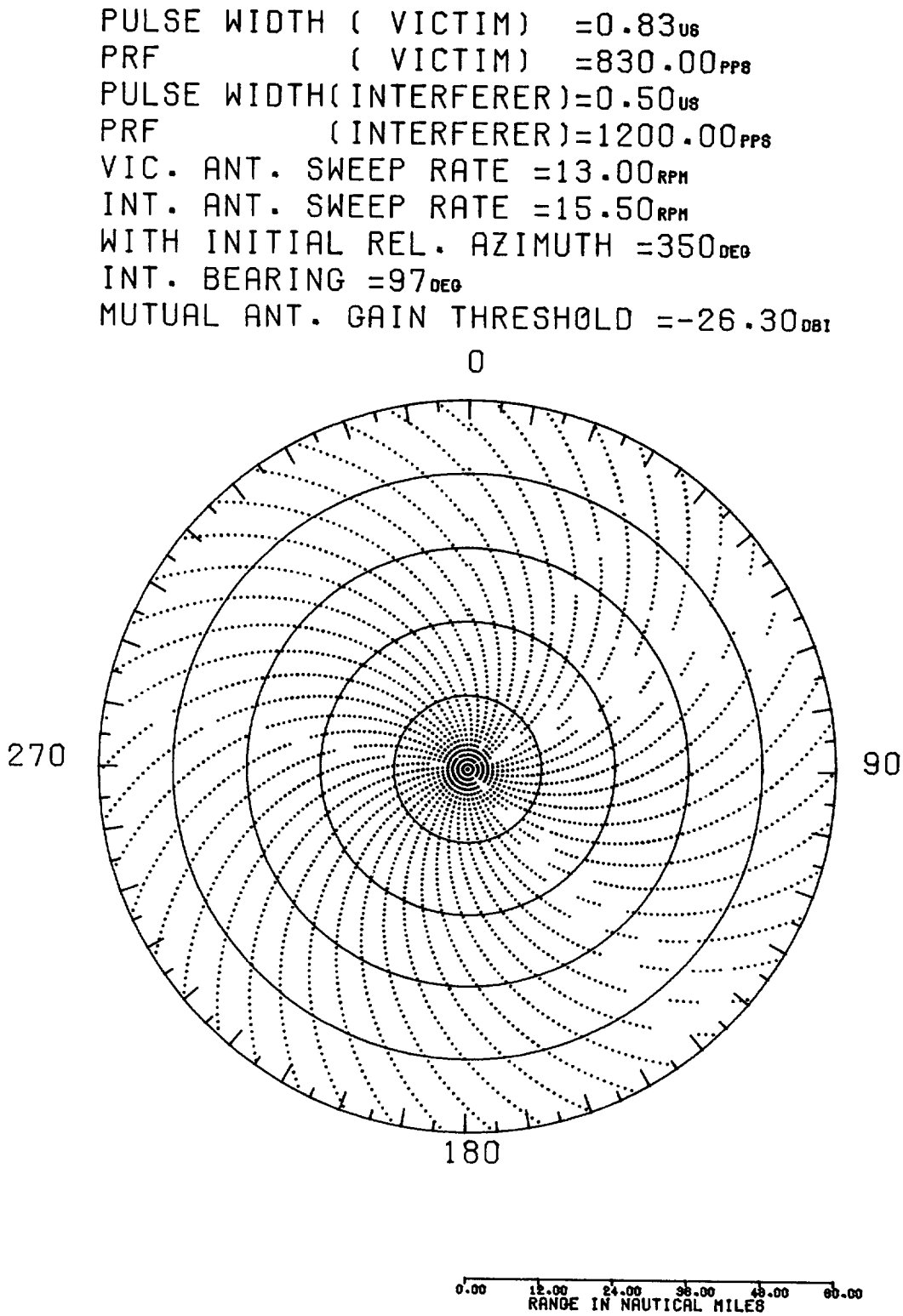

Figure E-5. Simulated PPI Display of Long Beach ASR-5 with Los Alamitos AN/CPN-4 Interference

Almaden AN/FPS-90. Interference from the Almaden AN/FPS-90 radar was observed on both channels of the Mountain View ASR-5 radar. The interference from the Almaden AN/FPS-90 radar covered 3° to 40° sectors of the victim radar PPI scope. For approximately twenty minutes, the Mountain View ASR-5 transmitter was turned off, and the pulse train separator (AS-330) was used to identify the PRF of signals processed by the radar receiver. The pulse train separator locked on to the PRF (275) of the Almaden radar. Due to the ability to coordinate with the ADC personnel at Almaden, propagation path loss measurements from the height finding radar were made by having the height finding radar nod in the direction of Mountain View for a one-half hour period. The measured propagation path loss from Almaden to Mountain View was found to be 141 dB (Table D-3) which was only two dB off from the predicted propagation loss of 143 dB. Using the measured emission spectrum to determine the FDR factor, Figure B-17 shows the emission spectrum to be down 36 dB from the fundamental frequency at 2758 MHz. The predicted FDR was 37 dB (Figure C-13). The backlobe antenna gain of the Almaden AN/FPS-90 radar could not be measured. Using a nominal antenna backlobe gain of -13 dBi for the Almaden radar, the measured propagation loss and FDR, and the nominal characteristics of the Mountain View ASR-5, the calculated INR is 35 dB using Equation 3-1. The actual predicted INR was 32 dB.

Predicted interference, using the PPI Simulation model, to the Mountain View ASR-5 from the Almaden AN/FPS-90 is shown in Figure 5-6. The actual observed interference varied from a 3° to 40° wedge of interference on the victim PPI display. Several runs of the PPI Simulation model need to be made to simulate this dynamic nature of the interference on the victim PPI display.

Almaden AN/MPS-14. ADC personnel at Almaden alternate the operation of the AN/MPS-14 and AN/FPS-90 on a monthly basis. Because of this operating procedure verification of interference from the Almaden AN/MPS-14 radar could not be made.

Mt. Tamalpais AN/FPS-90. Interference from the Mt. Tamalpais AN/FPS-90 radar was observed on both channels of the Mountain View ASR-5 radar. Positive identification of the interference was made using the pulse train separator when the victim radar transmitter was turned off. The interference from the Mt. Tamalpais AN/FPS-90 appeared on the victim PPI display about one out of every four scans as interference wedges of 3° to 30°. Propagation measurements from the Mt. Tamalpais radar were also made by having the height finding radar nod in the direction of Mountain View for a one-half hour period. As mentioned in Appendix D, the path from Mt. Tamalpais to Mountain View is across the San Francisco Bay. The measurements showed a 14 dB variation in the measured propagation loss from Mt. Tamalpais

to Mountain View over the measurement period of one-half hour. Due to the inability to coordinate several hours of propagation measurements with ADC personnel, verification of the path as a ducting path could not positively be made. The measured propagation loss from Mt. Tamalpais varied from 155 dB to 169 dB with an average propagation path loss of 160 dB (Table D-3). The predicted propagation path loss was 151 dB. Using the measured emission spectrum to determine the FDR factor, Figure B-18 shows the emission spectrum to be down 32 dB from the fundamental frequency at 2754 MHz. The predicted FDR was 40 dB (Figure C-13). The backlobe antenna gain of the Mt. Tamalpais AN/FPS-90 radar could not be measured. Using a nominal antenna backlobe gain of -13 dBi for the Mt. Tamalpais radar, the measured propagation loss and FDR, and the nominal characteristics of the Mountain View ASR-5, the calculated INR is 22 dB using Equation 3-1. The actual predicted INR was 23 dB. Figure 5-6 shows the predicted form of the interference from the Mt. Tamalpais AN/FPS-90 radar to the Mountain View ASR-5.

TRAVIS AFB AN/FPN-55 VICTIM RADAR MEASUREMENTS

The AN/FPN-55 radar site at Travis AFB is an uncluttered site, and the RSMS van was able to locate approximately 30 feet from the radar antenna. The AN/FPN-55 radar at Travis AFB has an antenna height of 26 feet. Only the RSMS van dish (height 14 feet) was used to make measurements at the Travis AFB radar site. The directional discrimination of the RSMS van dish was required to suppress the AN/FPN-55 signal since the operating frequency of the victim radar and potential interfering radar were only separated by 4 MHz. In order to obtain enough suppression of the Travis AFB AN/FPN-55 radar signal, both RF and video blanking were required. The RF blanking was achieved by using a pin diode modulator and the AN/FPN-55 radar STC pretrigged to turn off the modulator during the transmission of the AN/FPN-55 pulse. The video blanking was achieved using the AS-330 pulse train separator. The radar characteristics of the AN/FPN-55 are given in Table 5-2. The predicted interferers for the Travis AFB AN/FPN-55 radar were:

Radar	Interferer Freq. (MHz)	Victim Freq. (MHz)	INR (dB)
Mather AFB AN/MPN-13	2797	2801	26

Mather AFB AN/MPN-13. Interference from the Mather AFB AN/MPN-13 radar was not periodic as predicted, and actually only appeared on the victim PPI display four times during a 20-minute period. Due to a tight time schedule during the San Francisco area investigation, the emission spectrum and antenna pattern of the Mather AFB AN/MPN-13 were not measured. The measured propagation path loss from Mather AFB to Travis AFB was found to be 173 dB (Table D-3). The predicted propagation path loss was 179 dB. Measurements at Travis also showed that there was a 4 MHz frequency separation in the operating frequency of the two radars. Both the Travis AFB AN/FPN-55 radar and the Mather AFB AN/MPN-13 radar are assigned to operate on 2800 MHz. Measurements of the Travis AFB radar receiver RF frequency response were not made to determine if the maximum signal response occurred at 2801 MHz. However, a 4 MHz frequency separation could result in 17 dB of FDR (Figure C-10). Another factor contributing to lighter interference than predicted was the antenna tilt angle of the victim radar.

Air Force radar personnel at Travis AFB said the tilt angle of the AN/FPN-55 radar antenna was set at 4.25° rather than the nominal 3.5° antenna tilt angle. The different antenna tilt angle could also result in a 2 dB error in the victim radar mainbeam gain (Figure A-2) used to calculate the INR. It was also discovered that the AN/FPN-55 radar receiver had an 8 dB noise figure. The initial INR calculation was based on a 4 dB noise figure since the AN/FPN-55 radar receiver was reported to be identical to the ASR-5 radar. Although measurements of the interferer emission spectrum and antenna pattern were not made, the above factors could have contributed in a 17 dB difference between the predicted and actual INR resulting in lighter interference than predicted. The predicted form of the Mather AFB AN/MPN-13 interference on the Travis AFB AN/FPN-55 radar PPI display is shown in Figure 5-11.

APPENDIX F

LOS ANGELES AND SAN FRANCISCO AREA MEASUREMENT PLAN

INTRODUCTION

This appendix discusses the measurement plan used in the 2.7 to 2.9 GHz Spectrum Resource Assessment of the Los Angeles and San Francisco areas. A description of the RSMS van measurement system and application programs associated with the measurement plan is given in Appendix G. The major objective of the measurements was the validation of radar-to-radar interference prediction techniques including the radar performance degradation model. This required on-site verification of predicted interference situations, and the use of the RSMS van to determine the accuracy of the various input component models (i.e., propagation, emission spectrum, antenna pattern, and frequency-dependent-rejection). Measurements results were also to be compared with the radar performance degradation model.

MEASUREMENT PLAN

The 2.7-2.9 GHz test plan was divided into the following three measurement areas:

A. Preliminary radar site visits where video tape recordings (VTR) and photographs of PPI display were taken.

B. Detailed open system measurements at 2 radar sites which involves measuring emission spectrums, antenna patterns and received power from potential interferers. The open system measurements also included video tape recordings of the PPI display with the RF input power level of the interfering signal being recorded on the VTR.

C. Closed system measurements to determine the effect which various radar fixes (e.g., MTI, STC, integrator, etc.) have on the processing of interfering signals of various signal levels and PRF's. Video tape recordings will be used to document this set of experiments. These measurements were made on the radar spare channel during normal operation of radar and air traffic control.

PRELIMINARY RADAR SITE VISITS

The purpose of these measurements was to verify predicted interference situations to the extent that the live environment conditions and parameters used to predict the interference exist. This set of measurements was shallow in depth with the main objective to compare predicted interference with the live environment conditions for 12 victim radar sites.

Preliminary observations of potential victim radars were conducted with the victim radars in regular operational configuration. The AS-330 Pulse Train Separator was used as an aid in identifying the interfering radars. The AS-330 was set up for three PRF's of potential interferer radars, using a small audio oscillator and a pulse-forming circuit or a normal pulse generator. The local radar was set for non-stagger operation so that the de-stagger circuits would not alter the sequence of the received interference pulses, and the AS-330 was connected to one of the radar's video outputs. Although the video channel contained mostly pulses with the PRF of the local radar, the AS-330 sorted out the pulses belonging to the interfering radars with the PRF's set up previous to the measurements. The only output used from the AS-330 was the indicator lights on the AS-330 front panel. The AS-330 was positioned so that the video tape recordings made of the interference also included the indicator lights of the AS-330. Interferers were also identified by the relative bearing to the victim radar when possible. Also, the RSMS van WB scan program was used to verify the operational frequencies of the victim radar and potential interferer radars during these measurements. Without this capability, positive verification of proper operating frequency of the predicted interferers would not have been possible.

DETAILED RADAR MEASUREMENTS

The purpose of these sets of measurements was to determine why there was disagreement between predicted and observed interference at the visited preliminary radar sites. The preliminary radar observations resulted in two radar sites being selected for more detailed measurements. The following set of measurements were made at the victim radar site using the RSMS van, and involved:

a. Locating the RSMS van as close as possible to the victim radar site.

b. Scanning the 2.7 to 2.9 GHz band to identify all significant emitters, and verifying the operation of all predicted interferers.

c. Measuring the power received from each predicted and unpredicted interferer for a period of at least one half hour to determine propagation path loss. The right hand circular CBS was used when possible. If the dish was required, approximate dish azimuth and elevation angles were obtained from RAPIT (Propagation Model) bearing and radio horizon elevation data.

d. Measuring the interfer antenna patterns at victim radar site.

e. Measuring the victim radar antenna pattern.

Measurements made at the predicted and unpredicted interferer sites using the RSMS van included:

a. Measuring the emission spectrum of the interferer radar to levels of 60-80 dB down from the peak.

b. Measuring interferer antenna patterns.

Arrangements were also made during the detailed measurement program to shut the victim radar transmitters down, so that no pulses would be received from its own transmitter. Thus isolated, the interfering radar pulses could be studied more carefully. With this arrangement, all of the traces on the PPI display were caused by interference. For this experiment, the RSMS van was connected to the radar as shown in Figure F-1. The RSMS van was tuned to 30 MHz and measured the peak power delivered to the 8580 every second. The operator in the RSMS van watched a TV monitor showing the interference traces on the PPI display. Whenever a pulse of interest shows up, the operator read the power measured by the 8580 into the intercom to the radar PPI display, where the audio was picked up by the video tape recording equipment.

In addition to measuring the peak input power, the 8580 generated a log video signal which was fed back to the radar building for further analysis. The AS-330 pulse train separator was driven from this signal to indicate the PRF of the interfering signal, similar to the technique used in the preliminary radar measurements. Thus, a peak power measurement was tied to a given interferer. The peak power measured by the 8580 was a measurement of the peak power at the input

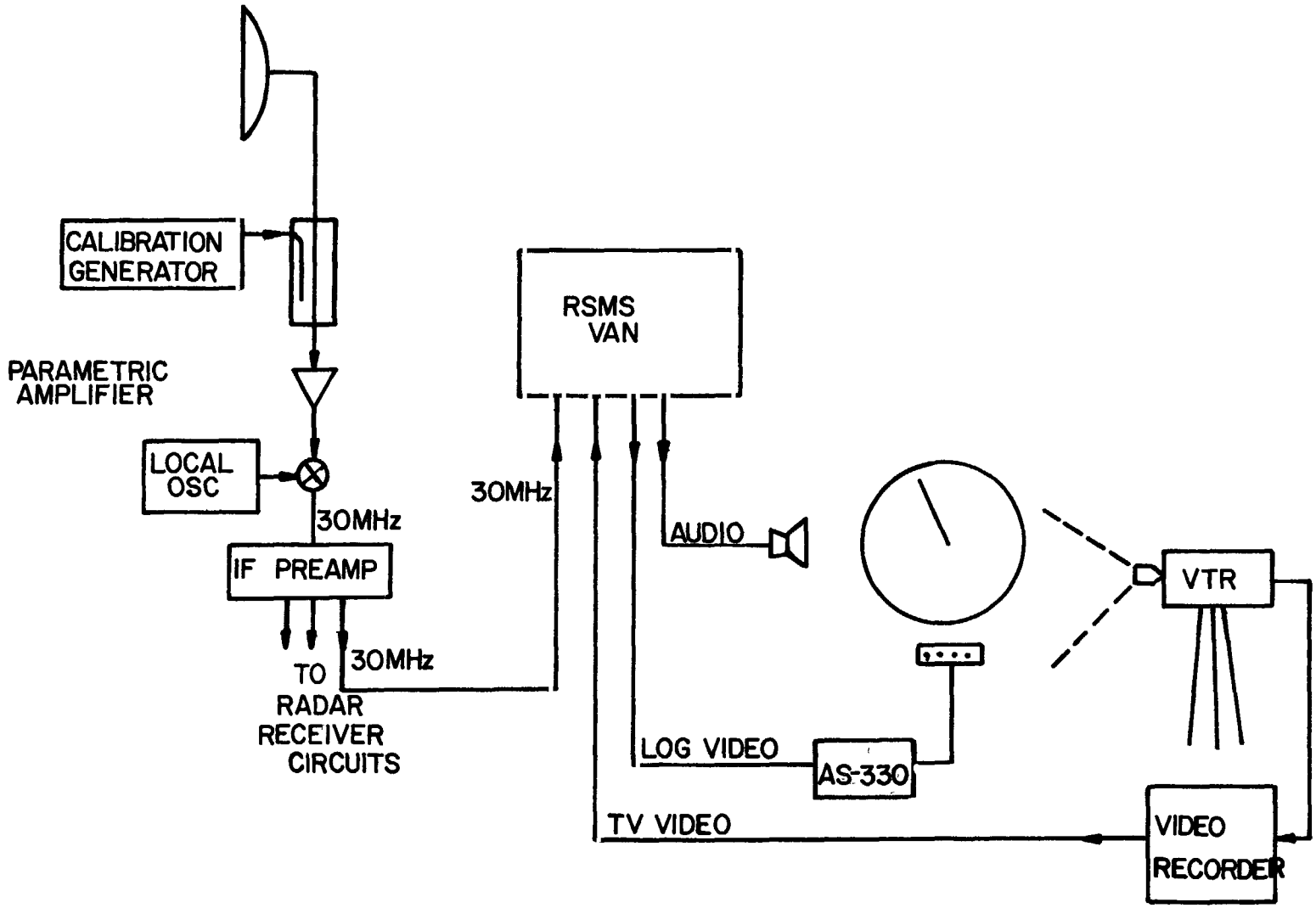

Figure F-1. Detailed Radar Measurement Configuration.

of the 8580, which was related to the peak power seen by the radar receiver. This relationship was established by injecting a calibration signal at the input of the radar receiver through a waveguide coupler of known loss characteristics and measuring this signal with the 8580. This measurement was made at different input amplitudes to obtain a transfer characteristic for the radar receiver front end characteristics, including noise and saturation.

CLOSED SYSTEM MEASUREMENTS

Closed system measurements were made on an analog radar (ASR-4,5,6) and a digital radar (ASR-7). The measurements were made on the space channel of the radar while the radar and air traffic control was normally operating. The objective of these sets of measurements was to determine the synchronous and nonsynchronous pulse PPI MDS level for several operational modes of the radars, and what radar fixes need to be modeled in order to accurately predict the pattern of the interference as it appears on the PPI scope. Video tape recordings of the PPI display and A-scope were made for the various radar-operating modes during these measurements. The result of these measurements will be given in a subsequent report.

APPENDIX G

RSMS VAN MEASUREMENTS

INTRODUCTION

This appendix describes some of the RSMS measurement procedures used during the Los Angeles and San Francisco area radar-to-radar interference measurements. It is included here to aid in interpreting the measured data. The appendix includes a compendium of the RSMS van measurement system and application programs related to radar measurements. Additional information may be found in the RSMS Operations Manual or by contacting RSMS personnel in Boulder, Colorado.

RSMS VAN SYSTEM DESCRIPTION

The RSMS was used in many different modes during this measurement program. Most of the measurements were made with the HP 8580 receiver and 8500 computer systems connected as shown in Figure G-1. Two sets of RHCP receiving antennas were used for these measurements - 4 fixed cavity-backed spiral antennas on the tower and the dish antenna on the roof of the van. These antennas can be connected to the input of the RSMS, where signals are attenuated, if necessary, by an RF attenuator, and then, filtered and amplified by YIG-tuned preselectors and a preamplifier. The signal is then further processed by a mixer, several IF's and log detector. The output of the log detector is a DC-coupled signal proportional to the logarithm of the envelope of the input signal which is processed in several further ways. For many of the measurements, a pulse blanking capability is used to pass only the radar pulses belonging to the desired radar. The peak amplitude of selected radar pulses is held in a peak hold circuit, and digitized. Once digitized, the peak amplitude information is processed by the 8580 computer which has several calibration algorithms, and special software application programs. The specific application program information may be displayed as part of a graph, recorded on magnetic tape or cassette, or copied with the Versatec plotter.

Antennas

Two sets of right-hand circular polarization antennas were used in these measurements. A set of 4 cavity-backed spiral antennas (CBS) on the tower were used more-or-less as

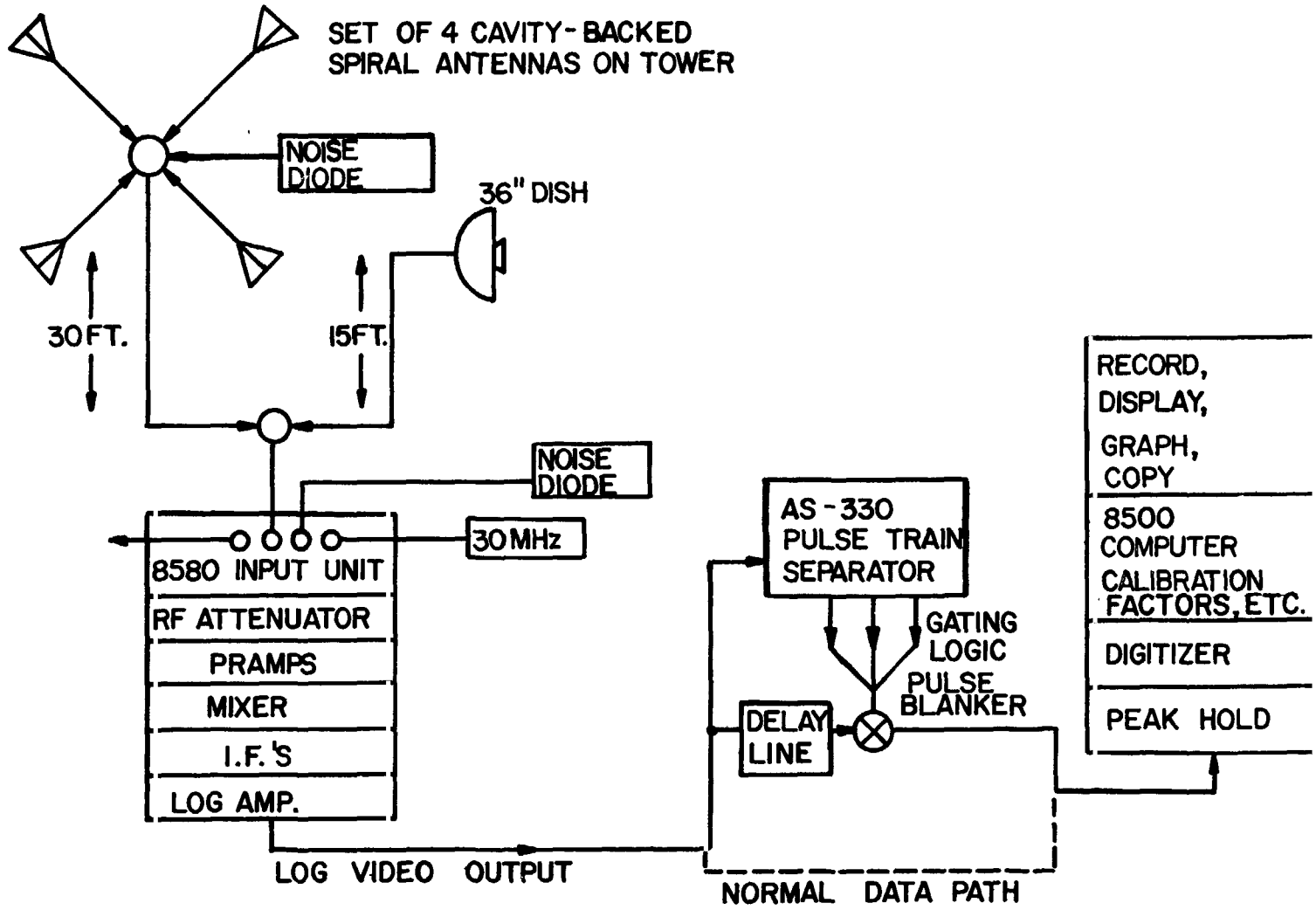

Figure G-1. RSMS System Block Diagram.

omnidirectional antennas. These antennas have a 70-90° beamwidth, 2 dB gain for a linearly polarized signal, and gave relatively good coverage between the 4 of them which were aimed 90° apart. A 36-inch diameter dish was also used. This antenna could be pointed in different directions, with an 8° beamwidth and a 20 dB gain for a linearly polarized signal at 2800 MHz.

Noise Diodes and Calibration

Broadband noise diodes are used to calibrate the system in terms of absolute amplitude at various points in the system. In general, the particular noise diode is used which is closest to the measurement point of interest. When the CBS antennas are used for measurements, the noise diode in the tower associated with those antennas is used for system calibration. This assures the maximum likelihood that the calibration procedure will account for all of the various effects on signal gain which are seen by the signal itself. By using the noise diode in the tower, for example, one corrects for the approximately 4 dB of transmission line and relay switching loss which attenuate the signal received by the CBS antennas, as well as calibration errors within the 8580. The diode at the front panel could also be used as a reference point, but this diode would only correct for calibration errors within the 8580. The 36-inch dish antenna does not have a noise diode associated with it, which means that it cannot be calibrated exactly. Instead, one can use either the front panel noise diode or the CBS noise diode, assuming that the CBS noise diode compensates for 4 dB line loss and the front panel noise diode compensates for 0 dB line loss. The measured line loss to the dish is around 2 dB at 2800 MHz, so that either diode is about equally poor, one giving answers 2 dB too high, the other giving answers 2 dB too low.

In addition to the noise diode calibration procedure, there is a 30 MHz system linearization procedure which tests the system under different conditions and generates a calibration curve for the log amplifier. The log amplifier calibration curve is different, however, depending on whether the peak-hold hardware is used (see below). If the peak-hold hardware is used for the measurements, one gets more linear system dynamic range if the system is calibrated using the peak-hold hardware. Figure G-2 shows the system dynamic range using peak-hold for measurements and for calibration. This shows that the linear dynamic range using peak-hold calibration is about 50 dB, before the cumulated error exceeds 3 dB.

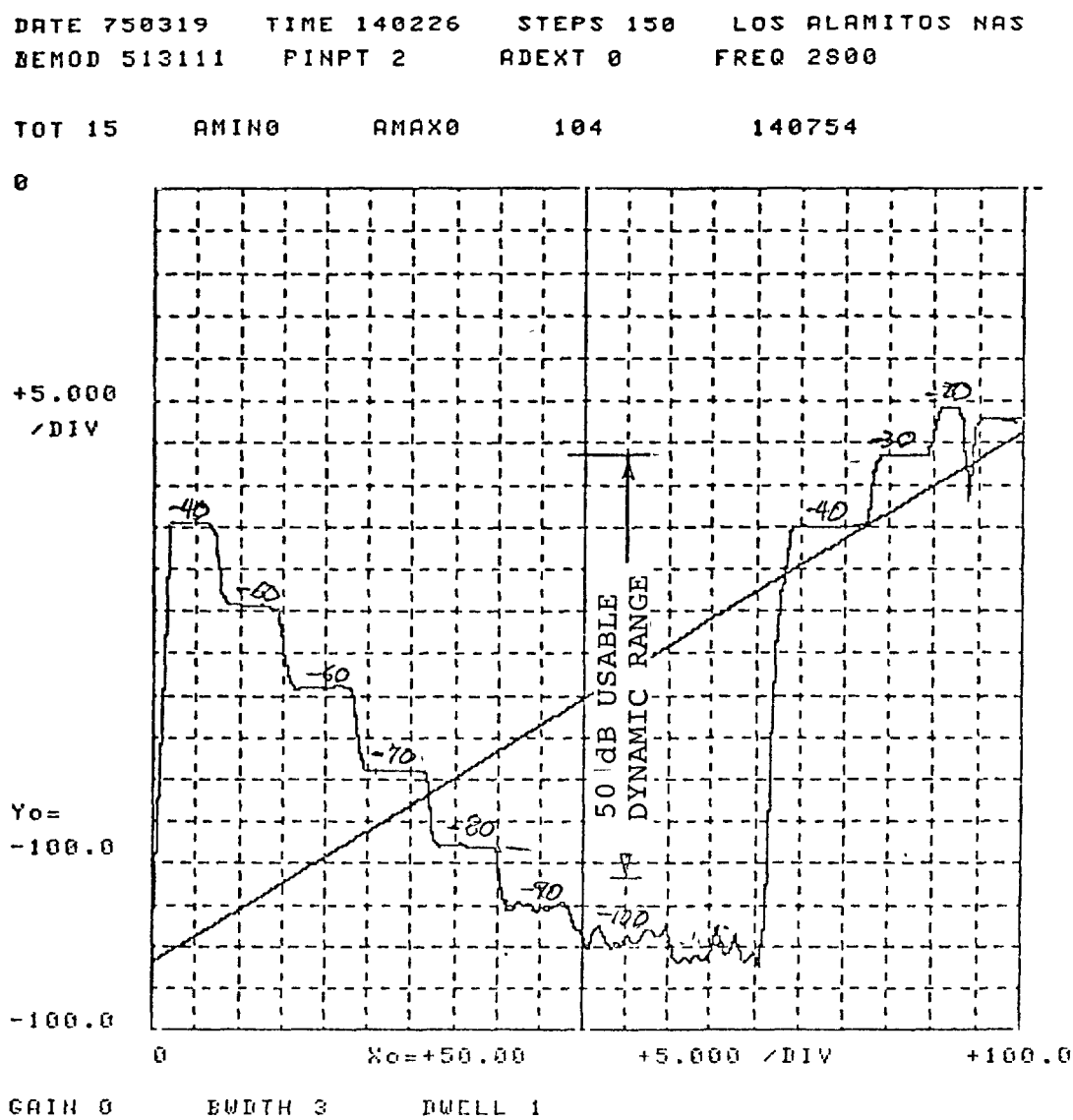

Figure G-2. RSMS system dynamic range at 2800 MHz.

Pulse Blanking and AS-330 Pulse Train Separator

Since radar signals are very low duty, there is the possibility of separating out only the signals of interest by turning on the measurement system only during the instant the signal of interest occurs. This process is accomplished with the pulse-blanking equipment shown in Figure G-1. The pulse-blanking card acts as a high-speed switch, connecting the log detector to the peak hold only during the instant when the desired radar pulses are present. The AS-330 pulse train separator contains 3 independent PRF filter channels that can be set up for up to 3 separate radars. These PRF filters generate TTL-level switching signals whenever pulses of the corresponding PRF occur. These switching signals control the pulse-blanking card in an additive mode or in a subtractive mode. A series of switches controls which mode is used; the modes may be mixed. The switches on the pulse-blanking card are each associated with a single PRF filter. When the switch is in the additive position, the pulses recognized by that PRF filter are passed through the pulse-blanking card to be measured. Several PRF filters can be switched to the additive mode at the same time, which will cause pulses belonging to several PRF's to be measured. The system can also be used in the subtractive mode. When a PRF filter is switched to the subtractive mode, those pulses belonging to the given PRF are subtracted from the total number of pulses transmitted through the pulse-blanker card. The pulse-train-separator card has been quite effective in the additive mode, suppressing unwanted radars by as much as 40-50 dB, as shown in Figure G-3. The subtractive blanking mode is not as effective, typically suppressing unwanted radars by 5 dB. This is because the PRF filters are typically "too choosy", and do not recognize all of the pulses belonging to a given PRF. Thus, in the subtractive mode, not all of the unwanted pulses are removed from the total number of pulses. In the additive mode, it is not crucial that all of the pulses be recognized, because the peak-hold hardware keeps only the largest amplitude pulse anyway, and chances are good that a typical sample contains 10-20 pulses which are all near the peak amplitude. It is very unlikely that all of these pulses would be missed by the PRF filter. For calibration, the pulse blanker is turned on all the time and a normal KALIB is run through the pulse-blanker card. Pulse blanking can be used with most of the Radar Measurement Programs.

Application Programs

The following is a brief description of several RSMS van application programs used during the Los Angeles and

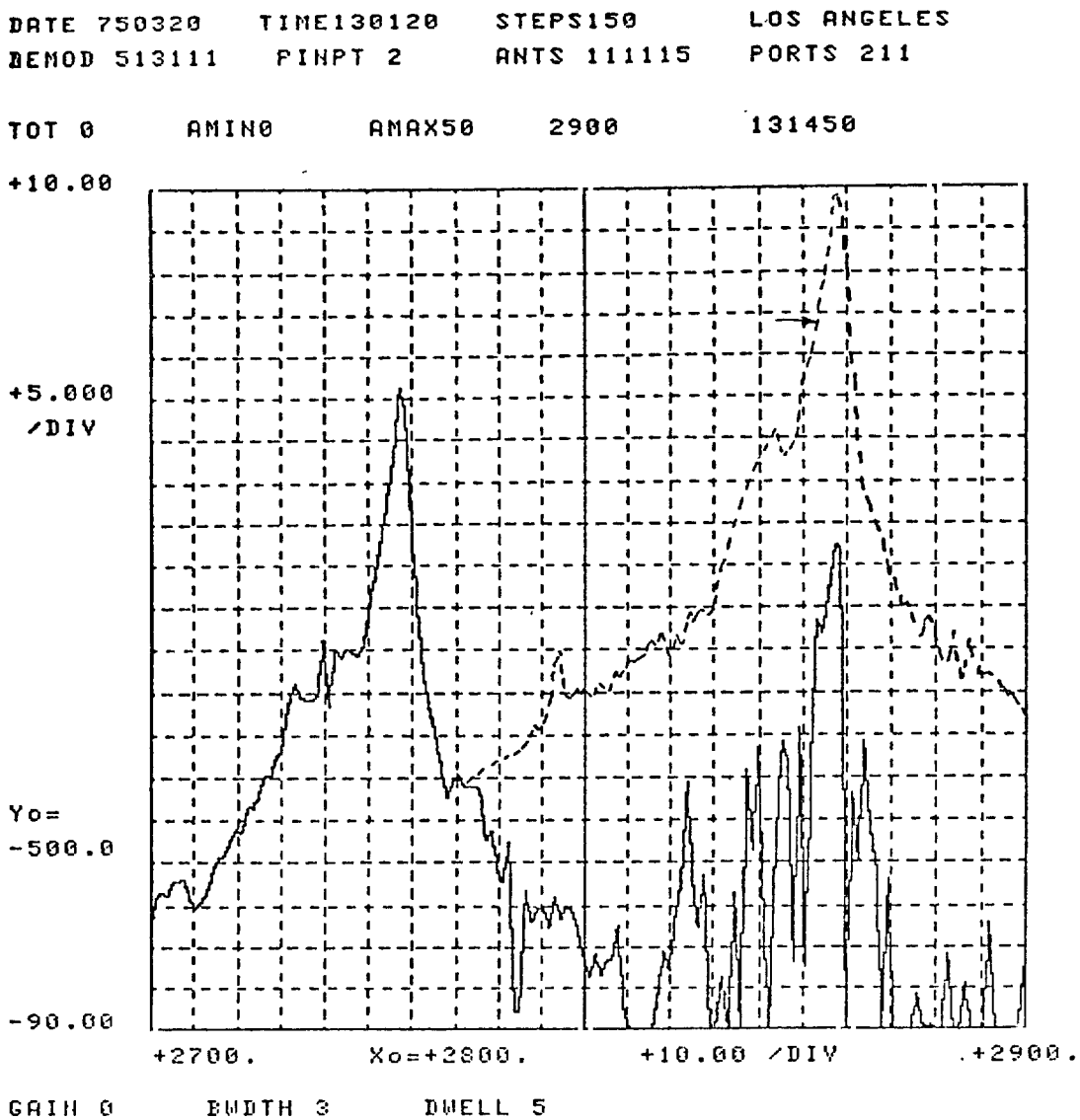

Figure G-3. Pulse blanker operational efficiency--dotted line shows radar subtracted by blanking.

San Francisco area radar-to-radar interference investigation.

Wide-Band Scan - Radar Band Occupancy and Emission Spectra

The Wide-band (WB) scan allows a specification of many operating parameters, including frequency range, number of frequency steps within the specified range, dwell time on each frequency step, bandwidth, RF attenuation, IF attenuation, peak hold, and receiving antenna. The program makes a measurement of peak amplitude received at each frequency, starting at the lower end of the frequency range and continuing until the upper end of the frequency range is reached. At each frequency, the system waits for a specified dwell time (typically 5 seconds) continually measuring the peak amplitude of the signal and updating its measurement when a still stronger pulse occurs. If the dwell time is chosen somewhat larger than the rotation period of the radar antenna, one is assured that the measurement at each will contain the instant when the radar antenna was aimed directly at the RSMS van. This situation will give the largest peak power reading, which is the power recorded for that frequency. As the measurements are made, the measured data is graphed. The operator may add or subtract attenuation in 10 dB steps whenever action is required to keep the signal within the linear dynamic range of the system. The system corrects for input attenuation so that the graphed data is continuous and appears to have been measured with a system with very large dynamic range. For many of the measurements made with this program, a 200 MHz frequency range is specified (usually 2700-2900 MHz), with 150 steps within this range. This means that a measurement is made every 200/150 = 1.33 MHz, which compares with measurement bandwidth of 1.5 MHz. Therefore, WB SCAN is typically operated with frequency steps slightly less than the measurement bandwidth.

As mentioned previously, WB SCAN is used for measuring the emission spectra of a particular radar, as well as for measuring general spectrum occupancy in the radar bands. The chief difference between these two applications is in the efforts made to select one radar only from out of several radars that might be received in the frequency band. For the general band occupancy measurement, WB SCAN is used with the CBS antennas, often making a band scan with each of the four CBS antennas to get an omnidirectional composite of band occupancy (Figure G-4A). When making a measurement of the emission spectra of a particular radar (Figure G-4B), several techniques are used to assure that only the desired radar is measured. First, the dish antenna is often used for these measurements. The extra gain of the dish gives

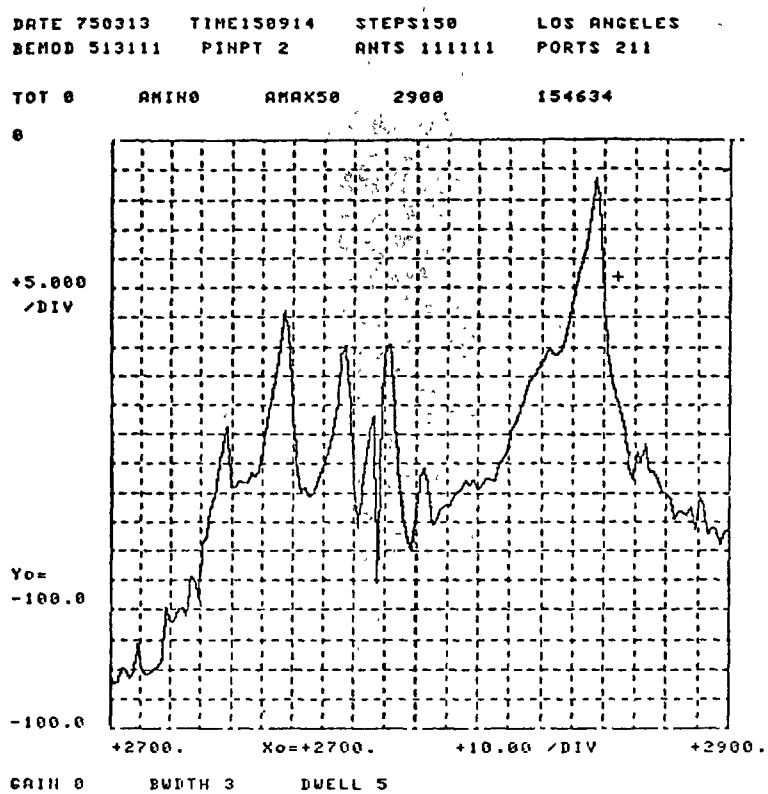

Figure G-4A. WB SCAN measurement of radar spectrum occupancy.

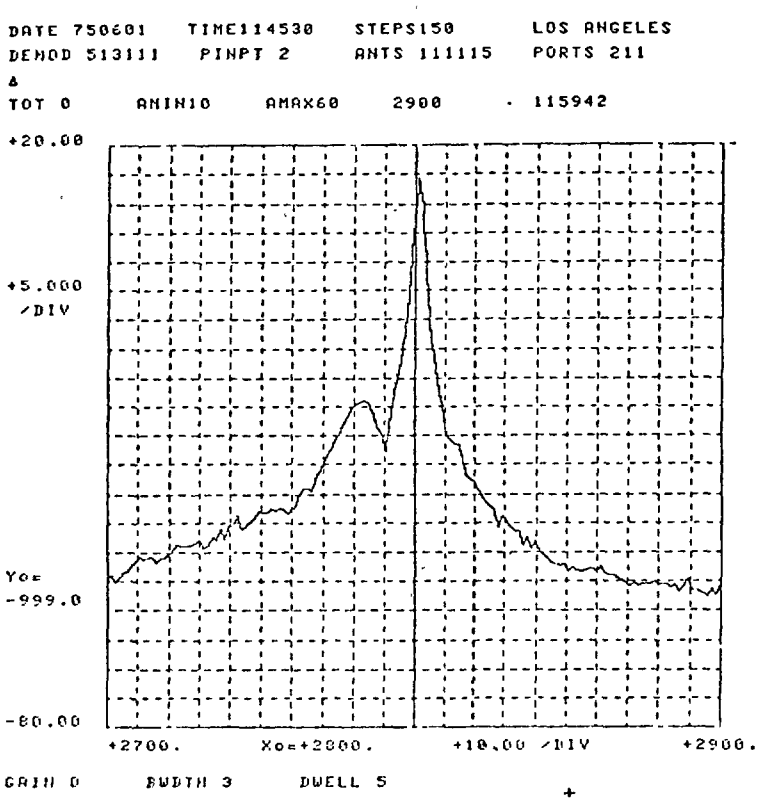

Figure G-4B. WB SCAN measurement of single radar emission spectra.

considerable angular discrimination against other radars, in addition to giving the extra system gain necessary to measure further down on the skirts of the radar spectra. The pulse blanker capability may be used, generally in an additional mode with the AS-330 set to the PRF of the desired radar. Finally, for some of the radar emission spectra, the RSMS van was moved line-of-sight to the radar and measurements were made with sufficient input attenuation that other radars in the band were generally not seen by the RSMS.

In order to assure that the 8580 receiver IF bandwidth would not distort the WB SCAN and emission spectrum measurements when operating in the peak hold mode, the receiver IF bandwidth was set to meet the inequality (Reference 44)

$$\frac{(B_r\ T_i)^2}{4} < 1$$

where: B_r = 8580 receiver IF bandwidth

T_i = Largest pulse width measured

Single Frequency Scan. Propagation Loss and Direction of Arrival.

The Single Frequency Scan (SFS) program is a close relative of WB SCAN. The main difference is that SFS does not change in frequency as it measures, but stays at the same frequency. The same input parameters can be specified as for WB SCAN except that frequency range is replaced by a single frequency. The program plots peak received amplitude at the single selected frequency versus time. Dwell time is the amount of time spent collecting data for each measurement point, and "steps" gives the number of measurement points across the graph. The scale across the graph can be any arbitrary scale, typically 0 to 150 or -200° to 200° or 200° to -200°.

SFS is used for a variety of propagation loss measurements, using the CBS or the dish antennas. Since dwell is usually set at 5 sec (the typical rotation time of radars in this band), one gets one measurement point every 5 seconds and a typical graph might take 5-15 minutes. Measurements were made of distance-gain curves using SFS with the RSMS van driving along the runway at Los Alamitos. Some propagation measurements were made with SFS alongside the Long Beach ASR-5 at a frequency quite close to the ASR-5 frequency.

SFS was chosen over other propagation measurement programs because the 1 measurement/5 seconds characteristic gave less chance for local radar signals to get through the pulse-blanking equipment. Another use of SFS involved measuring amplitude as a function of direction of arrival. For this measurement, the graph scale is set up to match the -200° to +200° headings on the dish azimuthal rotation limits. By proper choice of steps and dwell, the graphing can be made to track the 1°/second rotation of the dish, and the graph gives a read-out of received amplitude versus heading (Figure G-5).

Frequency Tracking Scan (FTS). Propagation Loss Measurements.

For long-term propagation measurements, the FTS program offers some benefits over SFS. FTS is similar to SFS except that FTS has some capability to continually track the slowly drifting frequency of a desired signal. Thus, use of FTS assures that any change in received amplitude is not caused by transmitter frequency drift. When a graph is completed, the graph is copied on the Versatec and a new graph is started on the system. FTS was often used to gather data on a radar overnight. In this mode a new graph was copied each hour and 8-12 hours of data were obtained without operator intervention. FTS tracks frequency by tuning over a small range on either side of the nominal frequency and keeping track of what frequency gives the highest received signal amplitude. The highest amplitude is graphed and the corresponding frequency is used as the nominal frequency for the next set of measurements. SFS scans $\pm$2.5 MHz on either side of the nominal frequency in 0.5 MHz steps. With a 5 second dwell at each measurement frequency, the total set of 11 measurements requires almost exactly 1 minute. Thus each measurement point on the graph requires about 1 minute, and a 60-step graph requires 1 hour. Height-gain curves for potentially interfering radars were measured at Long Beach using FTS, while the RSMS tower was raised such that the receiving antenna increased in height in 3-foot steps, from waiting to several minutes at each height (Figure G-6).

Radar Antenna Patterns

The RSMS has a capability to make measurements of radar antenna patterns which is particularly flexible because of the large amount of mathematical and statistical work that can be done on the raw data before it is plotted. Nevertheless, the RSMS system has the same constraints as any system that measures antenna patterns and some effort should be made to account for the effect of reflections from the ground and

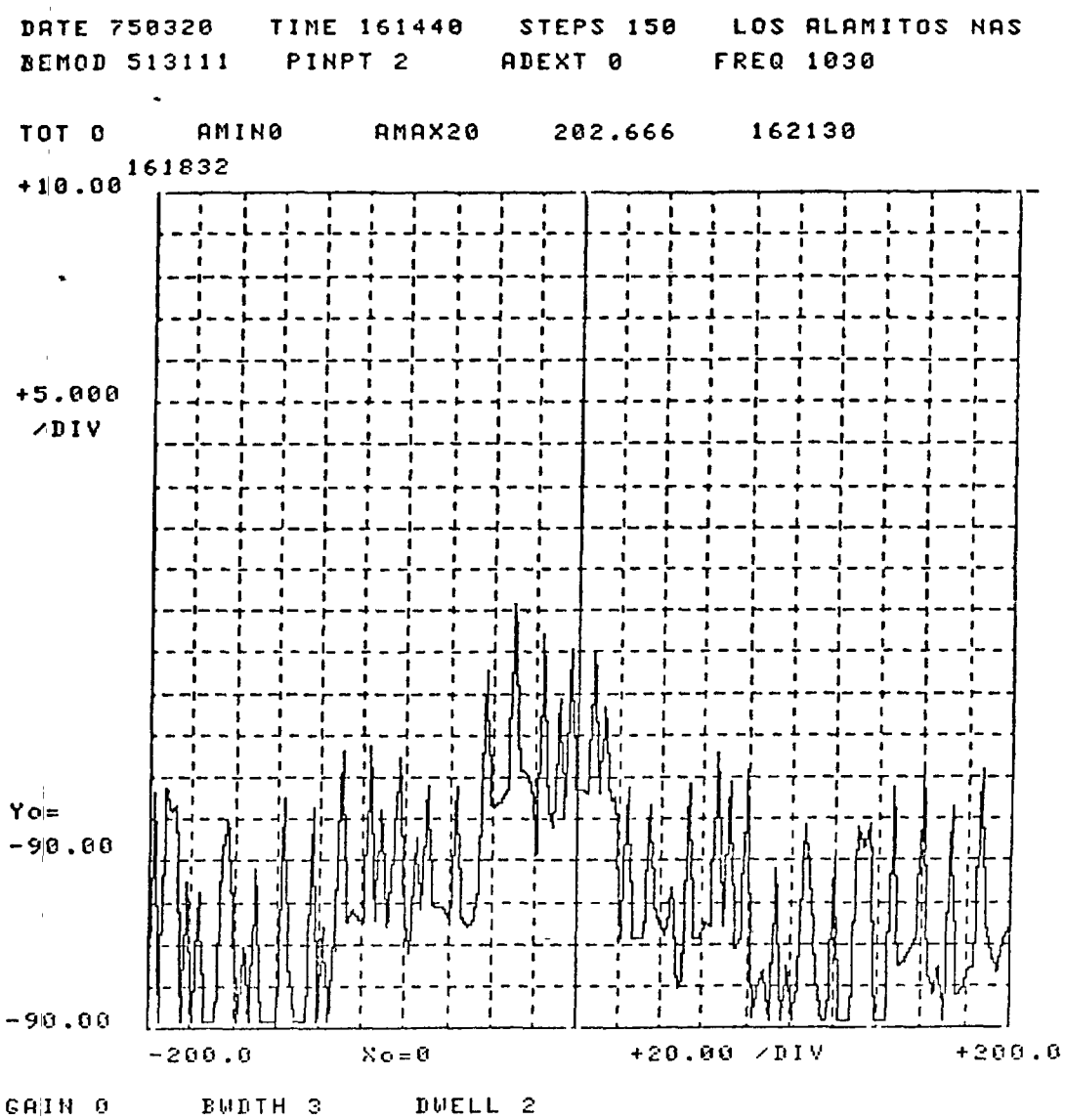

Figure G-5. Single frequency scan, used with rotating dish (dBm vs. azimuth).

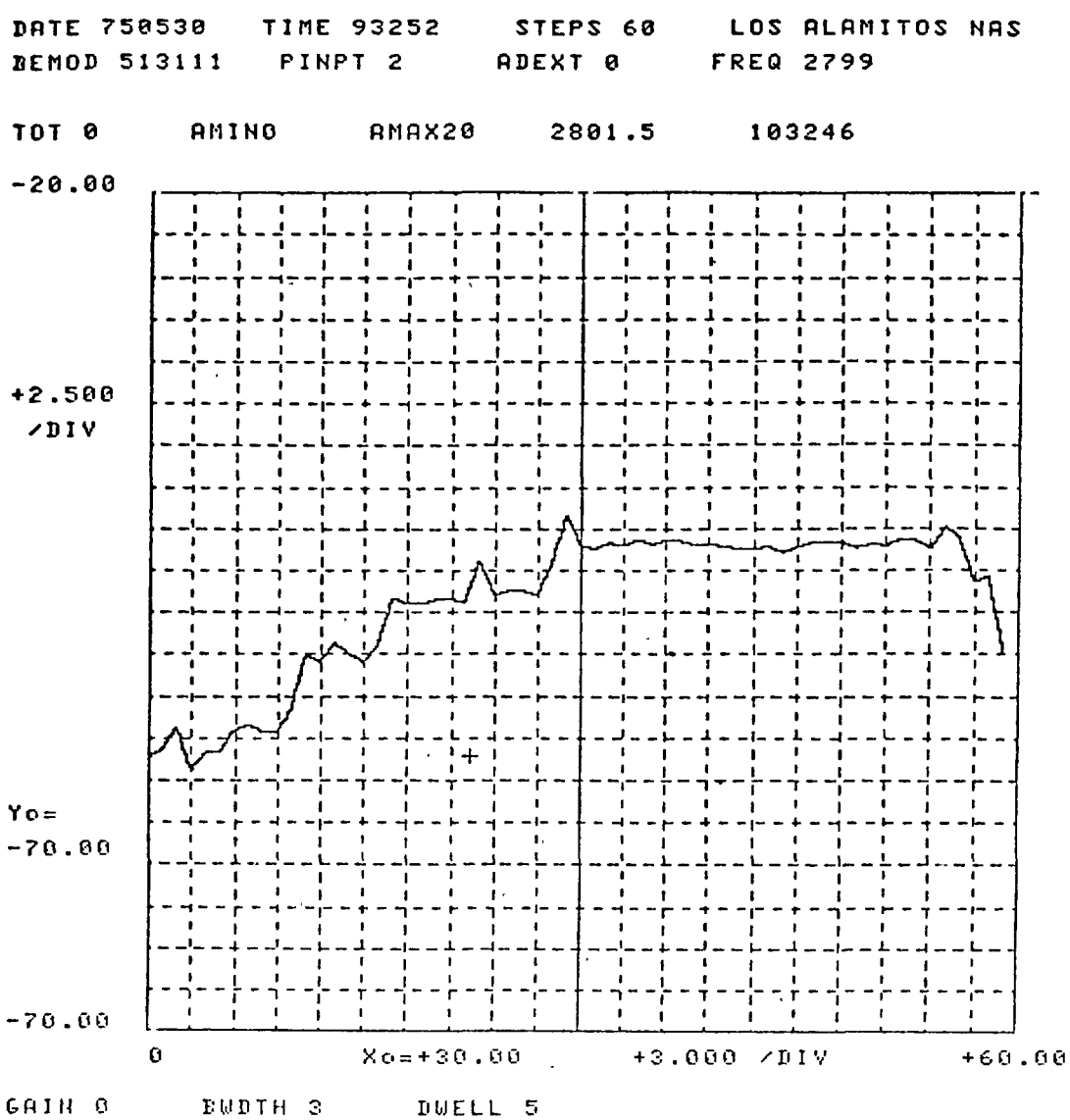

Figure G-6. Frequency tracking scan. First half showing height/gain, second half long-term propagation.

other structures. Two types of antenna pattern measurements were made. For one type of pattern we are concerned with what the victim radar saw as an interferer antenna pattern, knowing that this pattern would likely be not line-of-sight and badly distorted by all sorts of propagation phenomena. For these patterns, we try to duplicate the performance of the victim radar as closely as possible. Occasionally, we were actually able to use the victim radar antenna itself, but usually we had to make measurements with dish or CBS antennas on the RSMS van. In general, the CBS antennas could be positioned closer to the victim radar antenna and at about the same height. However, the dish antenna more closely matched the performance of the radar antenna, as well as offering better gain for the desired radar and more rejection of the local radar. The other type of radar antenna pattern measurement is an attempt to measure the free-space pattern of the radar antenna. For these measurements, great care is taken to locate the RSMS van so that it is line-of-sight to the radar with open fields behind the radar to eliminate reflections from the ground between the radar and the RSMS van, several things were done. The spacing between the radar and the van was considered carefully so the dish would be in the proper zone, away from the possibility of deep nulls. In addition, the dish was often aimed up slightly to minimize gain in the direction of the ground reflection, though this was probably not too effectively done because of uncertainty about the position of the null, the levelness of the van, etc. In order to minimize the distortion of the antenna pattern measurements due to receiver dynamic range, variable attenuators are used to set the measured radar peak received power level at the 8580 RF input to approximately -30 dBm. This permits only a 3 dB compression of the antenna pattern over a 50 dB range (Figure G-2). However, in some cases, where good radar siting exists, the lower level of the cumulative antenna distribution may be distorted due to insufficient 8580 receiver linear dynamic range.

Once the receiving antenna position was judged satisfactory, the radar antenna pattern program was run. This program allows complete specification of 8580 operating parameters in the first section of the program. The second section of the program makes 500 measurements over a specified period of time, minimum time about 4 seconds. The third section of the program analyzes and plots the data. The pattern program assumes a continuously rotating radar antenna, where the peak signal received by the RSMS antenna occurs when the radar antenna points at the RSMS antenna. The program also assumes that the set of 500 measurements has been taken in such a way that the highest amplitude received in the first

250 measurements occurred when the radar antenna pointed to the RSMS van and the highest amplitude in the second set of 250 measurements occurred when the antenna had made one more complete rotation. This means that the elapsed time for the burst of 500 measurements should be about 20% greater than the rotation time of the antenna and that the burst of measurements should be started slightly before the mainbeam points at the RSMS van. After all 500 measurements are made, the analysis of the measurements begins. Various correction factors are added to the measurements to give readings in dBm. The highest amplitude in the first set of 250 measurements is labeled "0°"; the highest amplitude measured in the second group of 250 measurements is labeled "360°"; and all the rest of the measurement points are assigned a rotation angle by linear interpolation between these two fixed points. If desired, the antenna patterns are plotted with the 0° reading normalized to 0 dB, with the rest of the pattern plotted in dB below mainbeam. For better plotting resolution, the pattern is actually plotted in two graphs - one graph between -20° and 180°, the other graph between 180° and 380°. These two graphs are intended to be pasted together to get a single graph of the antenna pattern. (Figure G-7).

Along with the antenna pattern, other information is written on the graph, including time, date, frequency, peak received power, antenna rotation period, and some statistical averages. The statistical averages describe the antenna pattern in terms of average dB below the mainbeam gain. The "Complete Average" is the level of the antenna pattern in dB below mainbeam gain, averaging between 0° and 360°. The "Sidelobe Average" is a similar average, except that the pattern is averaged only from 3° to 25° on either side of the mainbeam. The "Backlobe Average" is another similar average, including only the backlobe region of the pattern not within 25° of the mainbeam.

Instead of working with the amplitude as a function of rotation angle, for some applications it is easier to work with a statistical antenna pattern (Figure G-8). For this function, the statistics of the antenna pattern are summarized in a graph which plots amplitude in dB below mainbeam gain versus percentage of the pattern which exceed this amplitude. This kind of a pattern serves as a sort of figure-of-merit for the antenna and indicates how much of the time the sidelobes and backlobes of the antenna are likely to cause interference to (or receive interference from) another radar. The analysis of this data involves merely sorting the measured points of the pattern (0 to 360°) into amplitude bins with 1 dB resolution and plotting a cumulative distribution of the number of measurements within each bin.

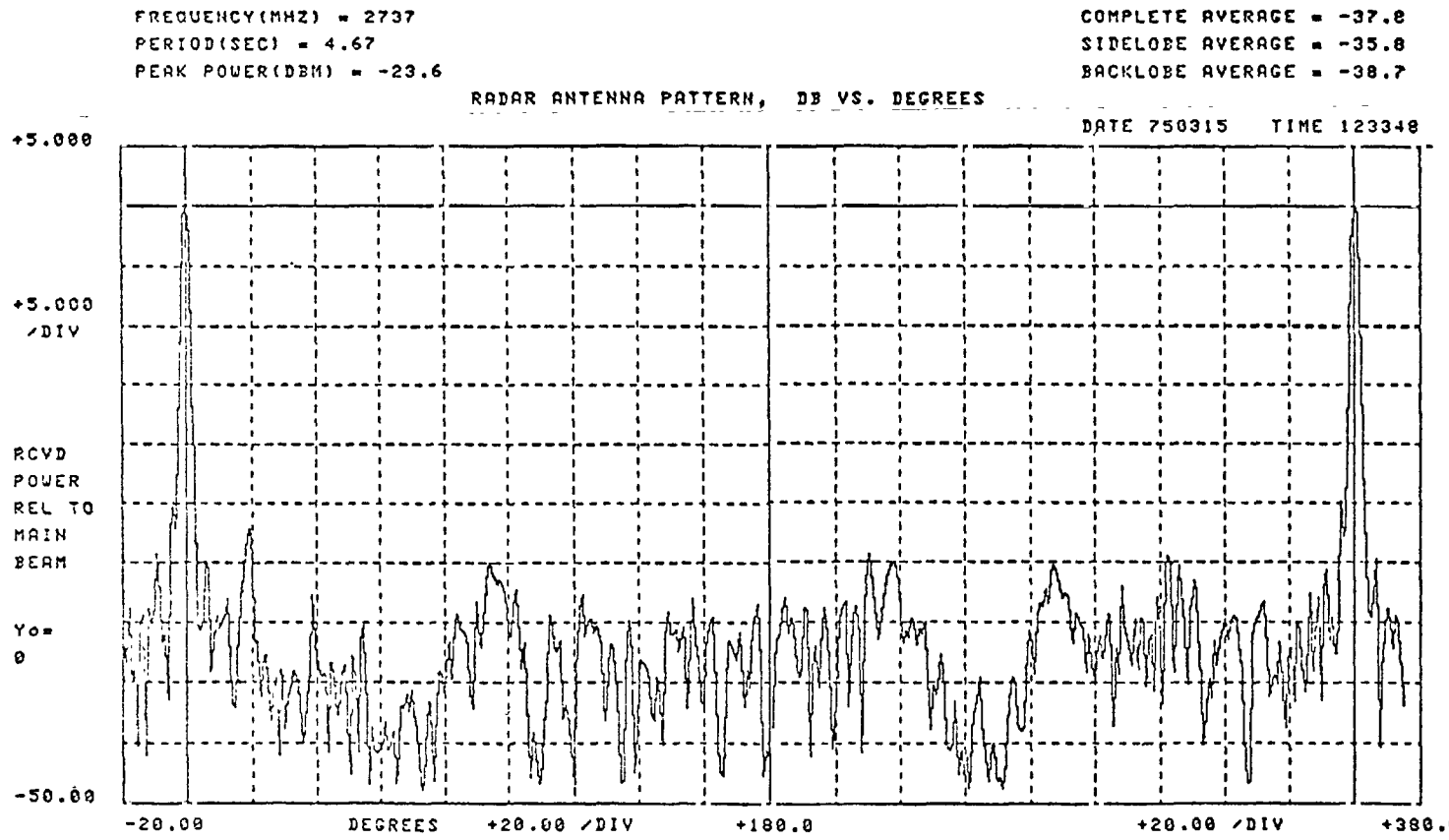

Figure G-7. Radar antenna pattern.

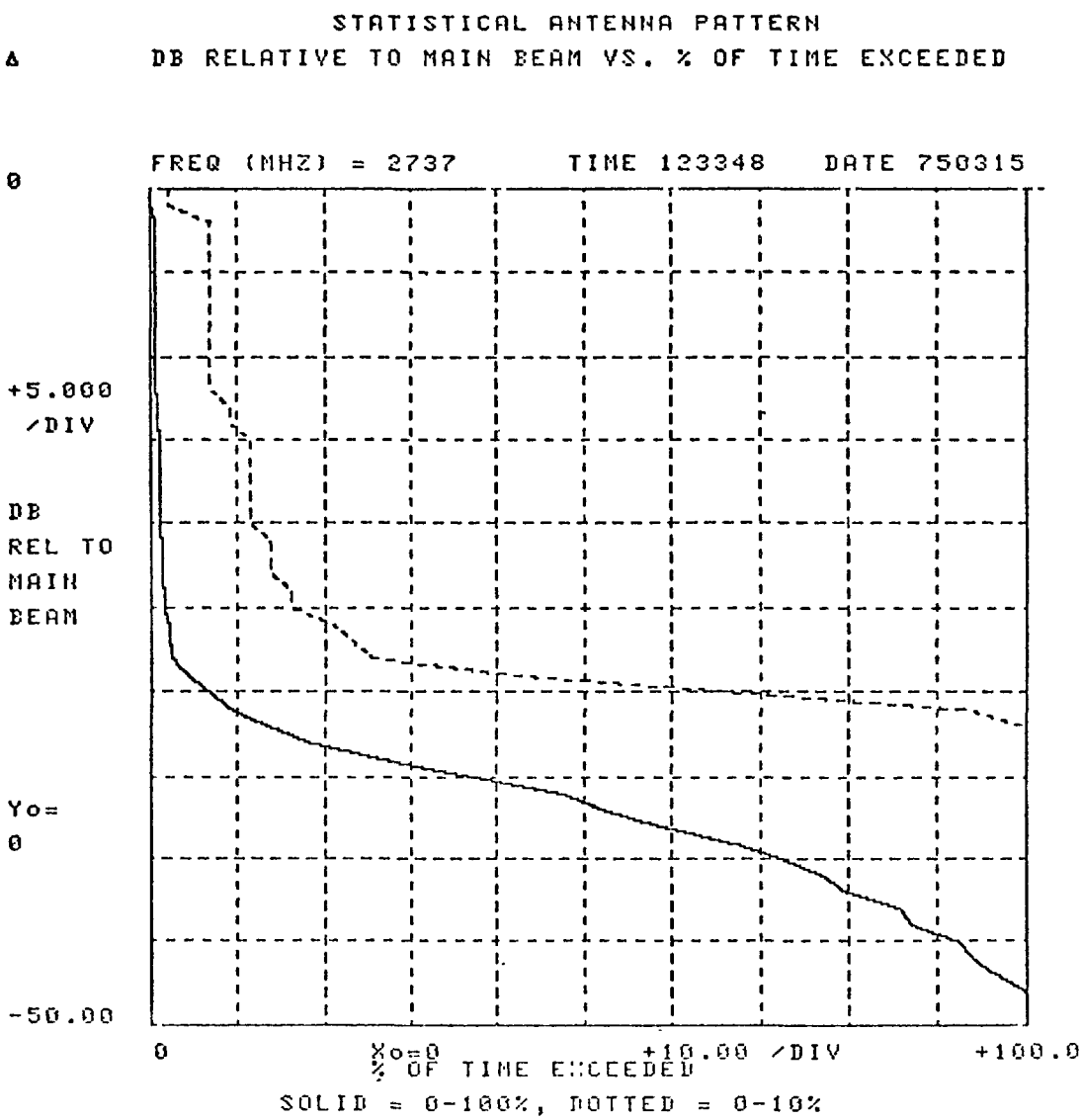

Figure G-8. Statistical radar antenna pattern.

In the cases where antenna pattern measurements were made through another radar antenna, the programs were run as normal except that the RSMS was connected to the 30 MHz IF of the radar system and tuned to 30 MHz. The radar transmitter was turned off and the radar system was pointed towards the interfering radar of interest. The rest of the measurement is made routinely. One problem with this type of measurement is that there is no easy way to attenuate the interfering radar signal if transfer curve data show that the interfering signal may be saturating in the radar receiver.

REFERENCES

1. Letter dated 20 December 1973 from Mr. W. Dean, Jr. (OTP Assistant Director for Frequency Management) to to Mr. S. I. Cohn (OT Chief of Spectrum Management Support Division).

2. E. J. Haakinson, H. G. Kimball, Spectrum Resource Assessment for the 1535-1660 MHz Band - Phase II Analysis, OT/TM-74-165, March 1974.

3. G. F. Hurt, Spectrum Resource Assessment for the 960-1300 MHz Band, Phase II Analysis, May 1975.

4. W. E. Frazier, E. L. McHugh, Spectrum Resource Assessment for the 4990-5250 MHz Bands, Phase II Analysis, OT/TM 75-191.

5. R. Mayher, R. Parlow, Spectrum Resource Assessment in the 7.25-8.40 GHz Band - Phase II Analysis, OT/TM-73-155, December 1973.

6. R. Hinkle, R. Mayher, Spectrum Resource Assessment in the 2.7-2.9 GHz Band, Phase I - Background and study definition Report N. 2/73 - P1, April 1975.

7. Summary Minutes First OTP Meeting on 2700-2900 MHz Spectrum Resource and Allocation Provision, 27 October 1972.

8. Summary Minutes Second OTP Meeting on 2700-2900 MHz Spectrum Resource and Allocation Provision, 13 December 1972.

9. Long range plan for fixed and transportable radars in the 2700-2900 MHz and 3500-2700 MHz Bands, SPS Ad Hoc Committee, 9 October 1974.

10. Letter dated May 28, 1974 from Mr. John P. Kemper (FAA Western Region Frequency Coordinator) to Mr. Robert L. Hinkle.

11. Letter dated 18 April 1974 from Mr. E. E. Angle (DOD Western Area Frequency Coordinator) to Mr. Robert L. Hinkle.

12. Farber, Leonard, "A Computer Graphic Display of Pulsed Interference on a PPI Scope," ECAC-TN-74-17, July 1974.

13. Interference Notebook, Rome Air Development Center, RADC-TR-66-1, July 1967.

14. Longley, A. G., Rice, R. L., Prediction of Tropospheric Radio Transmission Loss Over Irregular Terrain, A Computer Model, ESSA Tech Report ERL-79-ITS 67.

15. "Search Radar PPI Display Operation Performance," CALSPAN Prepared for EGAC/IITRI, August 1974.

16. "Development of Terminal Radar Interference Threshold Criteria," FAA Research and Technology Resume, July 17, 1973.

17. Hollis, J. S., et al, Microwave Antenna Measurements, Scientific-Atlanta, Inc., Atlanta, Georgia, July 1969.

18. Guccione, S., Ricker III, H., A Median Gain Model for Rotating Radar Antennas, ECAC-TN-74-07, February 1974.

19. Bailey, Norman T. J., The Elements of Stoehostic Processes, John Wiley and Sons, Inc., 1964.

20. Jakes, Jr., William C., Microwave Mobile Communications, John Wiley and Sons, New York, 1974.

21. Katz, L., Singer, A. M., "An Empirical Estimate of the Contribution of Terrain Reflections to Interfering Signal Distributions," Title 106, ECAC, February 1964.

22. Skolnik, M. I., "Introduction to Radar System," McGraw-Hill, New York, 1962.

23. Mason, S. J. and Zimmerman, H. J., "Electronic Circuits, Signals, and Systems," pp. 237-242, John Wiley & Sons, Inc., New York, 1960.

24. Newhouse, Paul D., "Simple Realistic Model for Radar Emission Spectra, ECAC Radar Analysis Bulletin.

25. Ablumavage, M., "The Current State of Several Techniques for the Measurement of Radar Emission Characteristics," ECAC-TN-005-43, ECAC, Annapolis, Maryland, October 1965.

26. Electronic Designers' Handbook, Londee, Davise, Alhect, McGraw-Hill, 1957.

27. Maiuzzo, Michael A., "Analysis of Factors Affecting Electromagnetic Compatibility of Radars Operating in the 2700 to 2900 MHz Band," FAA Report No. FAA-RD-71-91, July 1972.

28. Fleck, R., "Procedures for Computing Separation Criteria and Off-Frequency Rejection in Electromagnetic Compatibility Problems," ECAC-ESD-TR-67-5, March 1967.

29. Harris, Robert, "OFR and F-D analysis with Program OFRCAL," ECAC-TN-71-25, September 1971.

30. White, D. R. J., "Electromagnetic Interference Handbook," Vol. 5, 1972

31. Offi, Domenick L., Herget, William F., "Preliminary Measurements of ASR-5 RF System Insertion Loss and VSWR," FAA Data Report, Project No. 241-021-06X, May 1968.

32. Langley, A. G., Reasoner, R. K., Fuller, V. L., "Measured and Predicted Long-Term Distribution of Tropospheric Transmission Loss," O. T. Technical Report, TRER 16, July 1971.

33. Okumura, Y., Ohmori, E. Kawano, T., And Fukuda, K., "Field Strength and its Variability in VHF and UHF Land Mobile Service," Rev. Elec. Comm. Lab., 16, September-October 1970, page 825.

34. Reudink, D. U., "Comparison of Radio Transmission at X-Band Frequencies in Suburban and Urban Areas," IEEE Trans. Ant. Prop., AP-20, July 1972.

35. Turin, George L. et al, "A Statistical Model of Urban Multipath Propagation," IEEE Transaction on Vehicular Technology, Vol. VT-21, No. 1, February 1972.

36. Head, Howard T., "The Influence of Trees on Television Field Strengths at Ultra-High Frequencies," Proceeding of the IRE, June 1960.

37. La Grone, A. H., Marting, P. E., and Chapman, C. W., "Height Gain Measurements at VHF and UHF Behind a Grove of Trees," IRE Trans. Ant. Prop., 9, 1961, pp. 487-491.

38. La Grone, A. H., Chapman, C. W., "Some Effect of Trees on Low Angle Radio Propagation at a Wavelength of 10.4 CM," University of Texas, ERD-TN-60-766 AFRD-Detachment No. 2. July 1960.

39. Saxton, J. A., Lane, I. A., "VHF and UHF Reception Effects of Trees and Other Obstacles," Wireless World, Vol. 61, pp. 229-232, May 1955.

40. Letter dated 20 December, 1973 from Mr. W. Dean, Jr. (OTP Assistant Director for Frequency Management) to Mr. S. I. Cohn (OT Chief of Spectrum Management Support Division).

41. Bachynski, M. P., "Microwave Propagation over Rough Surfaces," RCA Rev., Vol. 20, pp. 308-335, June 1959.

42. Sherwood, E. M., Ginzton, E. L., "Reflection Coefficient of Irregular Terrain at 10 Cm," Proc. IRE, Vol. 43, pp 877-878, July 1955.

43. Hitney, Herbert, V., "Radar Detection Range Under Atmospheric Ducting Conditions," IEEE International Radar Conversence Record IEEE Aerospace and Electronic System Society, April 1975.

44. Newhouse, Paul D., "Peak Output Power in Victim Receivers," ECAC Radar Analysis Bulletin No. 2, 7 May 1969.

45. Edwards, Robert, Telephone conversations, Raytheon Microwave and Power Tube Division, July-August 1975.

46. Newhouse, Paul D., Telephone conversations, IIT Research Institute, ECAC, July 1975.

47. Katz, L., "PPI Interference Prediction", IEEE EMC Proceedings, Oct 1963.

48. Letter dated 23 June 1975 from Mr. William B. Hawthorne (FAA IRAC Representative) to Mr. Robert Hinkle (OT, Spectrum Management Support Division).

49. Letter dated 21 May 1975 from Mr. H. W. Holsopple (Navy member, Spectrum Planning Subcommittee) to the Chairman of the Spectrum Planning Subcommittee.

50. Letter dated 10 September 1975 from USAF Colonel William S. O' Gwynn (PRCCT, Command and Control Division, Directorate of Command Control and Communications) to Robert Hinkle (OT, Spectrum Management Support Division).

51. Letter datted 12 February 1975 from Mr. John P. Kemper (FAA Western Region Frequency Coordinator) to Mr. Robert Hinkle.

52. Bean, B. R., Prolonged space-wave fadeouts at 1046 Mc observed in Cheyenne Mountain propagation program, Proc. IRE 42, 848-853, 1954.

53. Silver, S., "Microwave Antenna Theory and Design," MIT Radiation Laboratory Series, Vol. 12, McGraw-Hill Inc., New York.

54. Bean, B. R., Climatology of ground-based radio ducts, NBS 63D, 1959.

55. Bean, B. R., and B. A. Cahoon, Effect of atmospheric horizontal inhomogeneity upon ray tracing, J. Res. NBS 63D, 287-292, 1959.

56. Neiburger, M., Temperature changes during formation and dissipation of West Coast stratus, J. Meteorol. 1, 29-41, 1944.

57. Edinger, J. G., Changes in the depth of the marine layer over the Los Angeles basin, J. Meteorol. 16, 219-226, 1959.

58. Reber, G., Tropospheric refraction near Hawaii, IRE Trans. AP-3, 143-144, 1955.

59. Rogers, R. R., Radar-derived statistics on slant path attenuation at 10 GHz, Radio Sci. 7, 631-643, 1972.

60. Rosenthal, J., PMR refractive support to Fleet Range users in a highly refractive environment. Proc. Com. Third Fleet's Navy Conf., Refractive Effects on EM Propagation, San Diego, Calif., 1973.

61. Rosenthal, J., Point Mugu forecaster handbook, Tech. Publication PMR-TP-72-1, Pacific Missile Range, Pt. Mugu, Calif. 93042, 1972.

62. Crain, C. M., Refractometer measured tropospheric index-of-refraction profiles, Vols. I and II, Univ. of Texas, EERL Rept. 6-02, 1953.

63. Barsis, A. P., and F. M. Capps, Effect of superrefractive layers on tropospheric signal characteristics in the Pacific Coast region, IRE WESCON Conv. Record, 116-133, 1957.

64. Ikegami, F., Influence of an atmospheric duct on microwave fading, IRE Trans. AP-7, 252-257, 1959.

65. Chang, H-T., The effect of tropospheric layer structures on long-range VHF radio propagation, IEEE Trans. Ant. Prop. AP-19, 751-756, 1971.

66. Joseph, R. I., and G. D. Smith, Propagation in an evaporation duct; results in some simple analytic models, Radio Sci. 7, 433-441, 1972.

67. Ring, R. M., A theoretical study of tropospheric radiowave propagation, AFCRL-67-0112, Office of Aerospace Research, USAF, Bedford, Mass. 01730. (Also AFCRL-63-713), 1967.

68. Sodha, M. S., A. K. Ghatak, D. P. Tewari, and P. K. Dubey, Focusing of waves in ducts, Radio Sci. 7, 1005-1010, 1972.

69. Jeske, H., and K. Brocks, Comparison of experiment on duct propagation above the sea with the mode theory of Booker and Walkinsaw, Radio Sci. 1, 891-895, 1966.

70. Guinard, N. W., J. Ransome, D. Randall, C. Purves, and P. Watkins, Propagation through an elevated duct. Tradewinds III, IRE Trans. AP-12, 479-490, 1964.

71. CCIR Doc., Results of Propagation Measurements in Large Cities, Doc. V/99-E, Pg. 21, Jan. 1966 (Italy).

FORM OT-29
(3-73)

U S DEPARTMENT OF COMMERCE
OFFICE OF TELECOMMUNICATIONS

BIBLIOGRAPHIC DATA SHEET

	1. PUBLICATION OR REPORT NO. OT REPORT 76-97	2. Gov't Accession No.
3. Recipient's Accession No.		
4. TITLE AND SUBTITLE SPECTRUM RESOURCE ASSESSMENT IN THE 2.7 to 2.9 GHz BAND Phase II. Measurements and Model Validation Report No. 1		5. Publication Date
		6. Performing Organization Code 901
7. AUTHOR(S) Robert L. Hinkle, Robert M. Pratt, Robert J. Matheson		9. Project/Task/Work Unit No. 9016512 1/73
8. PERFORMING ORGANIZATION NAME AND ADDRESS Office of Telecommunications 179 Admiral Cochrane Drive Annapolis, Maryland 21401		10. Contract/Grant No.
11. Sponsoring Organization Name and Address Office of Telecommunications Policy (OTP) 1800 G St NW Washington, DC		12. Type of Report and Period Covered
		13.

14. SUPPLEMENTARY NOTES

15. ABSTRACT *(A 200-word or less factual summary of most significant information. If document includes a significant bibliography or literature survey, mention it here.)*

The Office of Telecommunications (OT) undertook a detailed program to measure and analyze spectrum utilization in the 2.7 to 2.9 GHz band in the Los Angeles and San Francisco areas in support of an Office of Telecommunications Policy (OTP) Spectrum Resource Assessment task. The measurement program consisted of on-site visits to compare predicted and actual PPI interference patterns, and utilization of the Radio Spectrum Measurement System (RSMS) van to validate the component models used in predicting radar-to-radar interference.

16. Key words *(Alphabetical order, separated by semicolons)*

Radar, Interference, Measurements, Model Validation

17. AVAILABILITY STATEMENT ☐ UNLIMITED ☒ FOR OFFICIAL DISTRIBUTION	18. Security Class *(This report)* Unclassified	20. Number of pages
	19. Security Class *(This page)* Unclassified	21. Price

USCOMM-DC 29716-P73